SYNTHESIS OF "CLICKABLE" SBA-15 AND MCM-41 MESOPOROUS MATERIALS AND THEIR APPLICATIONS IN CATALYSIS AND BIO-CATALYSIS

THESIS SUBMITTED TO THE

UNIVERSITY OF PUNE

FOR THE DEGREE OF

DOCTOR OF PHILOSOPHY

IN

CHEMISTRY

BY

BHARMANA MALVI

RESEARCH SUPERVISOR

DR. SAYAM SEN GUPTA

CHEMICAL ENGINEERING AND PROCESS DEVELOPMENT DIVISION
NATIONAL CHEMICAL LABORATORY
PUNE-411008
INDIA

OCTOBER 2012

सीएसआयआर-राष्ट्रीय रासायनिक प्रयोगशाला
(वैज्ञानिक तथा औद्योगिक अनुसंधान परिषद)
डॉ. होमी भाभा मार्ग, पुणे - 411 008. भारत
CSIR-NATIONAL CHEMICAL LABORATORY
(Council of Scientific & Industrial Research)
Dr. Homi Bhabha Road, Pune - 411 008. India.

CERTIFICATE

This is to certify that the work incorporated in the thesis entitled: **"Synthesis of "Clickable" SBA-15 and MCM-41 Mesoporous Materials and their Applications in Catalysis and Bio-catalysis"**, submitted by Mr. Bharmana Malvi, for the Degree of *Doctor of Philosophy,* has been carried out by him under my supervision at Chemical Engineering and Process Development Division, National Chemical Laboratory, Pune-411008, India. All the materials from other sources have been duly acknowledged in the thesis.

Sayam Sen Gupta

Research Guide

(Dr. Sayam Sen Gupta)

Communication Channels	☎	FAX	WEBSITE
	NCL Level DID : 2590	Director's Office : +91-20-25902601	www.ncl-india.org
	NCL Board No. : +91-20-25902000	COA's Office : +91-20-25902660	
	EPABX : +91-20-25893300 +91-20-25893400	COS&P's Office : +91-20-25902664	

DECLARATION

I hereby declare that the thesis entitled **"Synthesis of "Clickable" SBA-15 and MCM-41 Mesoporous Materials and their Applications in Catalysis and Bio-catalysis",** submitted for the ***Degree of Doctor of Philosophy*** to the University of Pune, has been carried out by me at Chemical Engineering and Process Development Division, National Chemical Laboratory, Pune-411008, India, under the supervision of Dr. Sayam Sen Gupta. The work is original and has not been submitted in part or full by me for any other degree or diploma to this or any other University.

Bharmana Malvi

Dedicated

To

My Beloved Parents, Teachers

and

My Lovely wife Neeta

Acknowledgement

It is my great pleasure to express my heartfelt gratitude to my research supervisor, Dr. Sayam Sen Gupta, Scientist, National Chemical Laboratory, Pune, for his invaluable guidance, constant support, numerous discussion and constructive suggestions throughout the course of this investigation. His wide knowledge, logical way of thinking, understanding, and guidance has provided a good basis for the present thesis. I will be remaining ever grateful to him for teaching me scientific and non-scientific lessons. I take this opportunity to salute his supporting attitude that has always led me to think and work independently, and follow them in the proper perspectives. My deepest regards and reverence are always due for his wonderful personality. I sincerely thank for the care and affection that I received from him and his family in the entire period.

I would like to thank the Council of Scientific and Industrial Research for award of research fellowship. I am thankful to Dr. S. Sivaram, Ex-Director, Dr. R. V. Chaudhari, Ex-Deputy Director, Dr. B. D. Kulkarni, Ex-Deputy Director, Dr. S. Pal, Director and Dr. V. V.Ranade, Deputy Director, National Chemical Laboratory to carry out my research work and extending all possible infrastructural facilities for completion of my research work.

My heartfelt thanks to all the scientific members of our CEPD Division, especially, Dr. A. Kulkarni, Dr. (Mrs.) M. Gadgil, Dr. V. Panchagnula, Dr. Kelkar, Dr. A. Orpe and Mrs. S. Shingote for their helping hands and fruitful discussions. I need to express my thanks to the support group (Patane kaka, Kamble kaka, Subbi, Ravi & Radha) and all the staff members of our division, especially Mr. Raheja for his valuable cooperation and help and an exceptionally healthy working atmosphere. Special thanks to Dr. Hotha, Dr. Satyanarayana, Dr. (Ms.) Nandini Devi, Dr. B. L. V. Prasad, Dr. C.S. Gopinath and Dr. (Mrs.) S. Umbarkar from NCL for their help and scientific discussions. I would like to acknowledge Dr. R. Banerjee and his research group and Dr. Mayadevi for help with gas adsorption-desorption studies. Special thanks to Dr. Nandini devi and her research group for the help provided for powder XRD instrumentation. I shall also acknowledge the help from Mrs. D. Dhoble, Mrs. P. Purohit and Mr. S. Jha for help regarding FT-IR, UV-Vis spectroscopy and TGA analysis. I would like to thank Dr. S. Bhatt and his research group for help with confocal instrumentation. I need to also acknowledge to Dr. Ajithkumar and his research group from NMR division and Mr. A. Gaikwad, Mr. R. Gholap, Mr. Ketan, Mr. Naren, Mr. Anuj, Mr. Pandiraj and Mr. Pankaj from Centre for Materials characterization for their help in characterizations with NMR, SEM and TEM.

I would like to thank all my colleagues and labmates (past and present) for their helpful hand and cheerful attitude that had made my working very easy and enjoyable. I should mention my seniors Bibhas, Shashi, and Amit for their support and help. I shall specially thank present labmates Mrityunjoy, Anal, Debasis, Chaka, Sushma, Munmun, Soumen, Neha, Vinita, Kundan, Santanu and Hasan for their presence in all aspects of my Ph.D. career. Special thanks goes to my senior Bibhas for giving me first lessons in the research laboratory, synthesis of mesoporous materials and for scientific discussions. Special thanks also goes to Dr. Basab Dhar, Pull Officer for his scientific contributions to my research work. I would like to thank Varsha, Anandita, Rajeesh, Suyana and Yudhajit for their help and support during their stay at NCL. I would like to acknowledge the friendship of Anand, Jeetu, Shivaji, Deepika, Ajeet, Nivedita, Roopa, Kaushal, Umesh, Atul, Praddep, Mangesh, Prakash, Abhijeet, Kiran, Ankush, Deepak, Asif, Shiva, Lalita, Nitin, Shinde, Pippalad, Kausik, Nandu, Dev, Mohan, Latif, Ajay, JP, Kapil and many more in NCL, who made my stay more colorful.

It gives me great pleasure to thank my old friends Anand, Mahesh, Deepak, Sachin, Amit and others from whom I have received unfailing support and encouragement during many years of studies. I have to acknowledge especially my teachers in B.Sc. and M.Sc. class who really nourished my interest in Chemistry. It gives me great pleasure to thank my parents and family members and relatives for their love, unfailing support, tremendous patience, trust and encouragement that they have shown to me.

Nothing appropriate can describe the love and support of my dearest wife Neeta, whose constant encouragement and admiration sets new horizons for me to reach, in every facet of my life. It's being the most colorful and glorious time of my life ever since our relation bloomed and that strengthens me every day to achieve desired goals with better ease and confidence.

Bharmana Malvi

Table of Contents

LIST OF FIGURES

LIST OF SCHEMES

LIST OF TABLES

List of Abbreviations

AzPTES	3-azidopropyltriethoxysilane
BET	Braunauer-Emmett-Teller
BJH	Barrett-Joyner-Halenda
CP-MAS	Cross-Polarization Magic Angle Spinning
CLSM	Confocal laser scanning microscopy
CuAAC	Cu (I) catalyzed azide-alkyne cycloaddition
CTAB	Cetyltrimethyl ammonium bromide
DFT	Density Functional Theory
FSM-16	Folded Sheet Material
FTIR	Fourier Transform Infrared
GC	Gas Chromatography
HRTEM	High Resolution Transmission Electron Microscopy
ICP	Inductively Coupled Plasma
LC-MS	Liquid Chromatography-Mass Spectrometer
MCM	Mobil's Composition Material
NMR	Nuclear Magnetic Resonance
P123	Pluronic P123 Triblock Co-polymer
PEO-PPO-PEO	Polyethylene oxide-polypropylene oxide-polyethylene oxide
SBA	Santa Barbara Amorphous
SEM	Scanning Electron Microscopy
TEOS	Tetraethyl orthosilicate
TEM	Transmission Electron Microscopy
TMOS	Tetramethyl orthosilicate
UV-Vis	Ultraviolet-Visible
XRD	X-Ray Diffraction

Abstract of the thesis

Mesoporous silica materials represent a unique class of silica based materials which possess high specific surface area, large pore volume, uniform pore size (between 2-50 nm), high hydrothermal stability and rich surface chemistry. Their surface can be easily functionalized by organic molecules and these hybrid materials promise great opportunities for generation of new functional materials with improved and tailored properties for applications in various fields including adsorption, separation, energy storage, sensors, catalysis and biotechnology. Therefore, surface functionalization of these materials with organic molecules has emerged as one of the most important research areas in the field of advanced functional materials. In particular, mesoporous siliceous matrices like SBA-15 and MCM-41 are ideal candidates for functionalization due to their large surface area (~1000 m^2/g), large and tunable pore sizes (2-50 nm), hydrothermal stability and thicker walls that can be easily functionalized using simple silanol chemistry. SBA-15 and MCM-41 have been functionalized by various organic functional groups. These include amines, thiols, carboxylic acid, sulfonic acid, vinyl and nitrogen based heterocycles. The recent discovery of the Cu(I)-catalyzed 1,3-dipolar cycloaddition of organic azides to alkynes has provided the most powerful "click chemistry" tool for conjugation between appropriately functionalized binding partners via an 1,2,3-triazole linkage. The favorable thermodynamics, exceptionally high yields, ease and compatibility with a broad repertoire of functional groups has led to numerous applications of Cu(I)-catalyzed azide-alkyne click chemistry (CuAAC) reaction in various fields of organic, medicinal, polymer, materials and biological chemistry. CuAAC has been successfully used to functionalize metal nanoparticles, single-walled carbon nanotubes, powdered silica, and mesoporous silicon rugate filters. Therefore, synthesis of azide containing silica mesoporous materials would be very useful in the development of functional materials. The presence of an organic azide on mesoporous materials such as SBA-15 and MCM-41 gives a handle to anchor various moieties such as enzymes and catalysts via this chemoselective ligation.

In the present work, azide functionalized SBA-15 and MCM-41 mesoporous materials have been synthesized by both grafting and co-condensation methods followed by the evaluation of the ability of these azide functionalized mesoporous

materials to undergo Cu(I)-catalyzed azide alkyne cycloaddition (CuAAC) reaction with various organic molecules bearing alkyne functionality. Hybrid mesoporous materials synthesized by this methodology have been used for various applications such as organocatalysis, immobilization of enzymes and development of sensors. The thesis is presented in five chapters; a brief summary of each chapter is given below.

Chapter 1 provides general introduction to the mesoporous materials including synthetic strategies for mesoporous materials, mechanism of formation of mesoporous materials and different approaches for the synthesis of hybrid organic-inorganic mesoporous materials by incorporation of functional organic groups onto surface of these materials. Basic principles of various analytical techniques used for the characterization of mesoporous materials are also described. A brief introduction to click chemistry is also provided.

Chapter 2 describes synthesis and characterization of "clickable" SBA-15 and MCM-41 mesoporous materials. This chapter is divided into two parts. Part A describes synthesis and characterization of azide functionalized SBA-15 by both post synthetic grafting and one-pot co-condensation method. 3-azidopropyltriethoxysilane was used to introduce azides onto the surface of SBA-15. The efficiency of the azide functionalized SBA-15 to undergo Cu(I)-catalyzed azide-alkyne click chemistry reaction was evaluated by using various organic substrates containing alkyne functionality. These materials have been characterized by various techniques such as powder XRD, SEM, TEM, nitrogen adsorption-desorption studies, IR and solid state NMR spectroscopy. This methodology was used to incorporate mannose on the surface of SBA-15. Incubation of mannose labeled SBA-15 with fluorescein labeled concanavalin-A led to the formation of fluorescent silica-protein hybrid material.

Part B discusses synthesis and characterization of azide functionalized MCM-41 by one-pot co-condensation method. The density of azido-propyl groups incorpoarated on the surface of MCM-41 was varied by varing the mole% of organo-azide silica precusor during synthesis of MCM-41 from 0.2% to 10%. The efficiency of the azide functionalized MCM-41 to undergo Cu(I)-catalyzed azide-alkyne click chemistry reaction was evaluated by using various organic substrates containing alkyne functionality. Synthesis of site dense to site isolated azides on the surface of MCM-41 was established by fluorescnce spectroscopy of pyrene functionalized

MCM-41 materials. These materials have been characterized by various techniques such as powder XRD, SEM, TEM, nitrogen adsorption-desorption studies, IR and solid state NMR spectroscopy. Further, site dense to site isolated proline anchored on MCM-41 via CuAAC reaction was used for aldol condensation reaction. Increase in rate of aldol condensation reaction was observed for the site isolated proline catalyst anchored on MCM-41.

Chapter 3 describes the synthesis of mesoporous silica nanoparticles (MSNs) based hybrid material (Fe-MSN) that mimics the enzyme HRP and functions as a biosensor at physiological pH. This hybrid material contains a robust small molecule peroxidase mimic [Fe^{III}(biuret-amide)] developed in our group that is covalently attached to azide containing MSN particles by Cu(I) catalyzed azide alkyne cycloaddition reaction (CuAAC). These hybrid MSN particles have been used as biosensor for the quantitative detection of H_2O_2 and glucose in a one-pot method. The synthesized Fe-MSN nanoparticles were characterized by several techniques such as FT-IR, EPR, ICP and nitrogen adsorption-desorption experiments.

Chapter 4 describes synthesis of hierarchical mesoporous silica based hybrid material and its application as a support for the immobilization of trypsin in a “ship-in-a-bottle” approach. Enzyme adsorbed onto an azide functionalized mesoporous spherical SBA-15 with pores larger than the diameter of the enzyme were capped with alkyne functionalized mesoporous silica nanoparticles (MSNs) by covalent linkage using efficient CuAAC reaction. The mesoporous silica nanoparticles (MSNs) have pores that are large enough to allow small molecules such as reactants and products to diffuse in and out of SBA-15 but do not allow enzyme to leach out of SBA-15. Hence, in this hierarchical silica mesoporous hybrid material, the pores of MSNs on the surface of spherical SBA-15 act as windows for enzyme and effectively stops the enzyme from leaching. The bio-orthogonal nature of CuAAC ensures that the efficient capping of organoazide groups on spherical SBA-15 particles and can be carried out with alkyne functionalized MSN without loss of activity of the enzyme. Transmission electron microscopy, nitrogen adsorption, FT-IR spectroscopy, TGA and confocal laser scanning microscopy (CLSM) analysis unambiguously establish the formation of enzyme encapsulated hierarchical mesoporous material. The encapsulated trypsin functions as an efficient biocatalyst over 10 cycles without loss activity.

Chapter 5 provides overall conclusion of the work done. As a whole this thesis describes the synthesis of azide functionalized SBA-15 and MCM-41 mesoporous materials by both grafting and co-condensation methods followed by the evaluation of the ability of these azide functionalized mesoporous materials to undergo Cu(I)-catalyzed azide alkyne cycloaddition (CuAAC) reaction with various organic molecules bearing alkyne functionality. Using this methodology, several hybrid SBA-15 and MCM-41 type materials were synthesized. The application of these materials as catalysts and biosensors has also been evaluated in this.

CHAPTER 1

Introduction and Literature Survey

1.1 Introduction

Nanoporous materials, an important class of nanostructured materials that possess high specific surface area, large pore volume, uniform pore size and rich surface chemistry, has witnessed an exponential growth in research and development in the last two decades.[1, 2] These materials present great promise and opportunities for generation of new functional materials with improved and tailored properties for applications in various fields including adsorption, separation, energy storage, sensors, catalysis and biotechnology.[2, 3] Inorganic or hybrid organic-inorganic nanoporous materials present paramount advantages to facilitate integration and miniaturization of the devices (nanotechnologies), thus affording a direct connection between the inorganic, organic, and biological worlds. The ability to assemble and organize inorganic, organic and biological components in a single material represents an exciting direction for developing novel multifunctional materials presenting a wide range of novel properties.[1] Synthesis of well-ordered functional nanoporous materials is one of the possible routes towards the development of future catalysts, controlled release and delivery devices, optical devices, biocatalysts and bio-sensors. In this direction mesoporous silica materials show a great promise because of their desired properties such as tunable large pores, high surface area, easy functionalization and high hydrothermal stability of their pore walls among others.[4-6] In this thesis, we describe the functionalization of SBA-15 and MCM-41 silica mesoporous materials with organic functionality bearing azide groups. The ability of azide groups on mesoporous silica to undergo very efficient Cu(I)-catalyzed azide alkyne cycloaddition (CuAAC) reaction with organic alkynes is exploited to synthesize novel catalysts, sensors and biocatalysts.[7, 8] We set the stage for the thesis in this chapter by introducing synthesis of organic-inorganic hybrid mesoporous materials, mechanism of formation of mesoporous materials and various analytical techniques used for characterization of mesoporous materials. A brief introduction to “click chemistry”, which is used as a tool in this thesis to synthesize novel functional mesoporous materials, is provided. Finally, this chapter also outlines the motivation of our work and objective of this thesis.

1.2 Mesoporous materials

Nature has been building nanoporous materials for ages. Many living organisms produce nanoporous siliceous structures. For example, plants produce phytoliths, sponges produce spicules and diatoms produce cell walls made-up of silica.[9] Diatoms cell walls represent an outstanding example of nanostructured material in the nature (Fig. 1.1a). Each diatom species constructs a uniquely structured cell wall composed of silica, which is often ornately and intricately shaped with fine features on the nanometer scale.[10] Even, the ability of diatoms to manipulate silicon at the nanoscale level exceeds that of progress made by human in nanotechnology. The patterned silica cell wall of diatoms are synthesized intracellularly by condensation of silicic acid present in water over polyamines or phosphoproteins as templates.[11, 12]

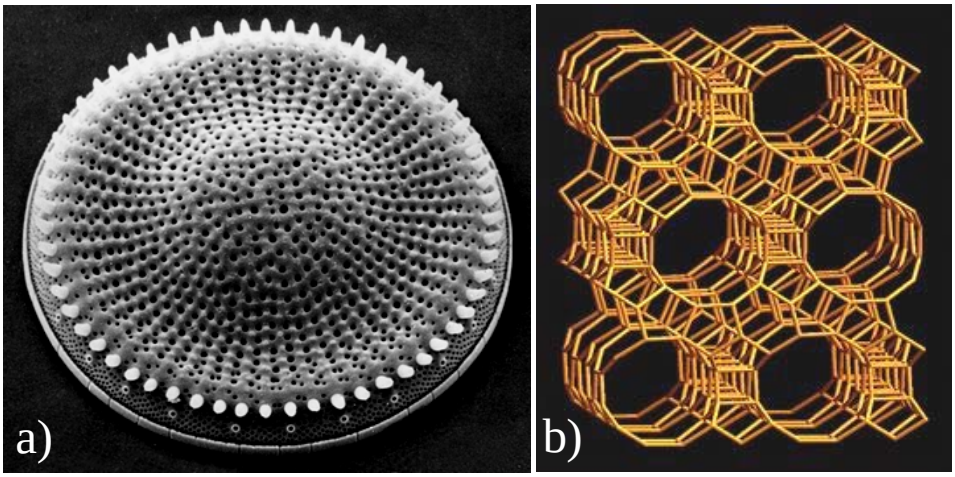

Figure 1.1: a) SEM image of hierarchical porous structure of cell walls of Diatoms (SEM photo by the late F.E. Round, courtesy of D.G. Mann, Royal Botanic Garden Edinburgh, with permission) b) structure of zeolite beta

Zeolites represent another naturally occurring and commercially important nanoporous material (Fig. 1.2b). These are alumino-silicates and are formed naturally where volcanic rock of specific chemical composition is immersed in water so as to leach away some of the components. The composition and pore size depend upon the kind of rock minerals involved. Synthetic zeolites are formed by template directed condensation of alumino-silicates. In the synthesis of zeolites, small organic molecules such as tetra ethyl ammonium hydroxide are used as structure directing templates, over which alumino-silicates condenses and crystallizes to produce highly

ordered crystalline solid material. Finally, removal of template gives ordered porous material.[13] These porous materials have found many applications in materials science including their usage as catalysts, catalyst supports and adsorbents.

According to the IUPAC definition, porous materials are divided into three types based on their pore diameters (d), microporous: d < 2 nm, mesoporous: d = 2-50 nm and macroporous: d >50 nm.[14] It should be noted that the word 'nanoporous' is commonly used to cover porous materials with pore size nanometer to several nanometers. Microporous materials such as zeolites have their pore diameters in the range of 0.2-1.0 nm and are attractive as heterogeneous catalysts or catalysts support due to properties such as well-defined crystalline structure, high internal surface area, uniform pore sizes, good thermal stability and highly acidic sites in the protonated form.[15, 16] The applications of zeolites are limited by the relatively small pore sizes and therefore can only be used in the applications involving small molecules. Because of this limitation of zeolites, there has been a continuous demand for synthesis of mesoporous materials that have physical properties similar to zeolites but with well defined larger pore diameters. These materials could then be potentially used as catalysts in processes such as heavy oil cracking and catalytic conversion for large molecules. They can also be used as separation media or as hosts for bulky molecules for advanced materials applications such as biosensors and biocatalysis.[15] Thus, mesoporous materials with large pore diameters and well-defined pore structure remain an active area of research. In this context, the discovery of mesoporous silica molecular sieves opened up new possibilities in many areas of chemistry and material science.[17-20] The first synthesis of an ordered mesoporous material was described in the patent literature in 1969.[21] However, due to a lack of proper analysis, the remarkable features of this product were not recognized.[22] The breakthrough came in 1992 with the discovery of M41S family of mesoporous materials.[17, 18] These new silicate materials, with well defined pore sizes of about 2-10 nm, have broken the pore-size constraint (< 2 nm) of microporous zeolites. For synthesizing these highly ordered M41S mesoporous materials, Mobil scientists employed long chain alkyl quaternary ammonium halides surfactant molecules [$C_nH_{2n+1}(CH_3)_2NX$, X = Cl, Br and n = 8-16] as the structure-directing agent instead of using small organic molecules as in the case of zeolites.[18] The most well-known representatives of this class of materials include the silica solids MCM-41 (with a hexagonal arrangement of the

mesopores, MCM stands for Mobil Composition of Matter), MCM-48 (with a cubic arrangement of the mesopores), and MCM-50 (with a laminar structure) (Fig. 1.2). The discovery of the M41S series of ordered mesoporous materials has drawn great interest because they are promising as catalysts in their own right and also proved to be useful as catalyst support, separation medium and host material for inclusion compounds. They also possess extremely high surface areas (> 1000 mg^{-1}), high pore volumes and well ordered pore structures with narrow pore size distributions. One drawback associated with MCM-type materials is their rather limited hydrothermal stability, which is a result of the very thin amorphous pore walls. The weak hydrothermal stability of these materials greatly limits their extensive utilization in the applications such as heterogeneous catalysis, where these materials need to be recycled several times. In 1998, Stucky and co-workers discovered another mesoporous materials, designated as SBA-15 (SBA stands for Santa Barbara Amorphous) consisting of thermally stable thick walls and hexagonal mesopores (4-10 nm) which overcame the weak hydrothermal stability encountered by M41S materials.[19, 20] For the synthesis of SBA-15 a non-ionic triblock co-polymer, poly (ethylene oxide)–poly (propylene oxide)–poly (ethylene oxide) (PEO–PPO–PEO) was used as templating agent. Since the discovery of SBA-15, this material has been extensively studied and used for various applications. The remarkable interest in SBA-15 arises from several features that makes SBA-15 very exciting. These includes tailored pore size, high degree of structural ordering, ease of synthesis, thicker pore walls, higher hydrothermal stability in comparison to M41S and substantial amount of silanol groups that allows incorporation of high amount of organic groups on its surface. Also it should be noted that the polymer employed to obtain SBA-15, poly (ethylene oxide)–poly (propylene oxide)–poly (ethylene oxide) (PEO–PPO–PEO), is cheap and biodegradable.[19] Subsequently, Stucky and co-workers reported synthesis of many other mesoporous materials from the SBA family with various mesophases using non-ionic triblock, star diblock and oligomeric surfactants.[20]

Further this new approach of template directed synthesis of mesoporous silica materials was expanded successfully towards the synthesis of other non-silica mesoporous materials, such as various metal oxides,[23-26] metal sulfides,[27, 28] phosphates,[29] and metals.[30, 31] A variety of lyotropic liquid-crystalline surfactants and phase-separated block copolymers were used as templates for the assembly of the

inorganic frameworks. These inorganic materials formed as disordered, hexagonal, cubic or lamellar structures with a high control of the pore diameter that could be tuned between 2–100 nm.

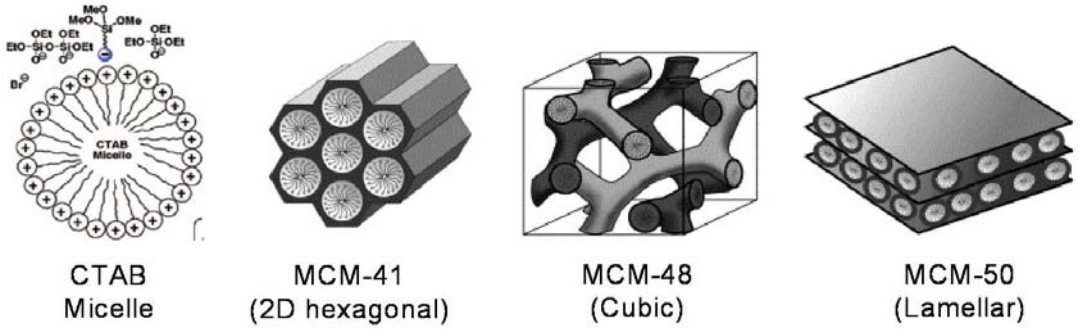

Figure 1.2: Structures of M41S materials.[5]

1.3 Syntheses of mesoporous materials

Syntheses of mesoporous materials involve the use of supramolecular aggregates of surfactants as structure-directing agents (SDAs). These SDAs, in the form of a liquid-crystalline phase, lead to the assembly of an ordered mesostructured composite during the condensation of the silica precursor's .The dimensions of these mesopores can be tailored through choice of surfactant, auxiliary chemicals, and reaction conditions.[5] Generally, mesoporous materials are prepared by typical sol-gel process under "hydrothermal" conditions. The general synthetic procedure involves several steps (Fig. 1.3): formation of silica mesostructure under synthesis conditions by mixing silica precursor and organic template, hydrothermal treatment, separation, drying and template removal. First, a homogeneous solution is obtained by dissolving the surfactant(s) in the solvent, water water being the most commonly used solvent. Silicate precursors (e.g. TEOS or TMOS) are then added into the solution where they undergo acid or base catalyzed hydrolysis and condensation and transformed in to a sol of silicate oligomers. The interaction between oligomers and surfactant micelles results in cooperative assembly and aggregation and finally precipitates to form a gel.[32] During this step, microphase separation and continuous condensation of silicate oligomers occur. Then the solution containing mesostructured material is further subjected to hydrothermal treatment to induce the complete condensation and solidification, and to further improve the organization.[33] The resultant product is cooled down to room temperature, filtered, washed, and dried. The mesoporous material is finally obtained after removal of the organic template. Ordered

mesoporous silicates are generally synthesized under basic or acidic conditions.[34, 35] Some of the important factors involved in the synthesis of mesoporous materials are discussed below.

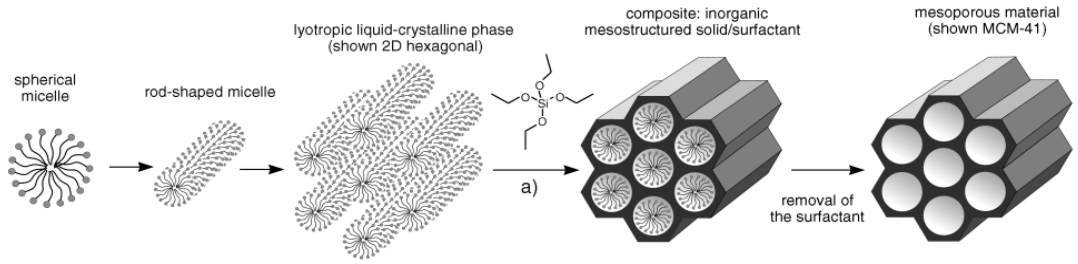

Figure 1.3: Surfactant templated method for the formation of ordered mesoporous silica materials[5]

1.3.1 Synthesis under basic conditions

Well known M41S family of mesoporous materials were synthesized under basic conditions.[18] Under basic conditions, between pH 9.5-12.5, hydrolysis and condensation of silicate species is reversible. Therefore, a wide variety of silica precursors such as silica gels, colloidal sols, sodium silicates, silica aerogels, or TEOS can be used for the preparation of ordered mesoporous silica. Hydrothermal treatment is necessary to prepare ordered mesoporous silicates. TEOS is the most convenient and efficient silicate precursor in the laboratory.[36] Base catalysis leads to fast polymerization and condensation of silicates, yielding 3D silicate networks. Sodium hydroxide, potassium hydroxide, ammonia, tetramethylammonium hydroxide and tetraethylammonium hydroxide can be used as a base.[4]

1.3.2 Synthesis under acidic conditions

Huo et al. were first to synthesize highly ordered mesoporous material SBA-15 under strongly acidic conditions by using cetyltriethylammonium bromide as a template.[36] Subsequently large pore mesoporous materials SBA-15 and SBA-16 were synthesized under strong acid conditions using triblock copolymers as templates.[19, 20] The synthesis of mesoporous silica is accelerated by lowering the pH values of the solution. A high concentration of acid leads to a fast precipitation rate. Strong acids such as HCl, HNO_3, HBr, HI, and H_2SO_4 can be used as catalysts. Acidic synthesis is also suitable for the formation of mesoporous silicates with diverse morphologies, such as “single crystals”, thin films, fibers, spheres, etc.[37] This is

possible because, linear silicate oligomers are the main products from hydrolysis of silicates under acidic condition that favor formation of regular morphologies. The addition of inorganic salts like KCl, NaCl, Na_2SO_4, and K_2SO_4 can accelerate the synthesis, while the organic solvent additives reduce the formation rate in acidic, non-ionic surfactant systems.[37-39] Yu et al. have reported the synthesis of high quality SBA-15 at low temperature and low triblock copolymer P123 concentration by addition of inorganic salts.[38, 39]

1.3.3 Hydrothermal treatment

Hydrothermal treatment is one of the most efficient methods to improve mesoscopic regularity of these materials.[40, 41] After completion of the reaction in solution, the mesostructures undergo reorganization, growth, and crystallization during hydrothermal treatment. Generally a long treatment is necessary which varies from days to weeks. The time for hydrothermal treatment can be significantly shortened up to 2 h or even lower by using microwave treatment.[42, 43] The temperature during hydrothermal treatment can be kept between 80 and 150^oC. Higher temperatures would result in degradation of the surfactant which directs the formation of mesoporous material. In general, higher hydrothermal temperature is required when cationic quaternary ammonium salts are used as templates. The ordered microdomains of the surfactants, and their strong interactions with silica species perhaps require high hydrothermal treatment to undergo reorganization, growth and crystallization.

1.3.4 Separation and drying

As-synthesized mesoporous material can be obtained by either filtration or centrifugation from the mother liquor. Mesoporous materials which have good crystallinity and particle size of about 0.1mm can be easily filtered. Isolated material is further washed with suitable solvent (generally either water or alcohol is used). The washing step is critical for basic synthesis since residual NaOH can cause destruction of mesostructures during the calcination step. However, washing is not needed in acidic synthesis, since the volatile nature of HCl can be removed completely together with the template during calcination.[44] The drying process for an as-synthesized mesostructured material is usually carried out at room temperature.

1.3.5 Template removal

As-synthesized material is then subjected to template removal in order to obtained the porous material. Generally calcination or solvent extraction methods are used for the removal of template. Calcination temperatures should be lower than temperature at which the mesoporous materials remain stable. Organic surfactants can be totally decomposed or oxidized with oxygen or air atmosphere. Higher calcination temperatures would lead to higher cross-linking degrees of mesoporous materials which may result in formation of reduced surface areas, pore volumes and surface hydroxyl groups. But these materials exhibit higher hydrothermal stability due to higher degree of cross-linking.[45] The temperature ramp should be slow enough to avoid structural damage caused by local overheating. Typically heating the as-synthesized sample with slow heating rate of 1-2 °C/min to 550 °C and keeping this temperature for 5-6 h removes the template completely. The principle drawback of calcination process is that the surfactants cannot be recovered and that the density of surface hydroxyl groups is reduced due to crosslinking. On the other hand, solvent extraction method does not affect the frame work and porosities of the mesoporous materials.[46] Ethanol or THF can be used for template extraction. Small amount of HCl is typically added to the extracting solvent to improve the cross-linkage of framework. [44] However, extraction process is limited by the fact that surfactants cannot be removed completely.

1.4 Mechanism for the formation of mesoporous materials

A large number of studies have been carried out to investigate the formation and assembly of mesostructures on the basis of surfactant self assembly and its interactions with inorganic species. Two mechanisms are widely accepted: true liquid-crystal templating (TLCT) mechanism and cooperative liquid-crystal template mechanism which are discussed in short below.

1.4.1 True liquid-crystal templating mechanism

In true liquid-crystal templating mechanism, the concentration of the surfactant is so high that under the synthesis conditions (pH and temperature) a lyotropic liquid crystalline phase is formed without requiring the presence of silica precursor (TEOS/ TMOS). The mechanism involves the following five steps

(Fig. 1.4, path a): First, surfactant molecules assemble to form micelles in the solution which then further organize to form cylindrical rods of micelles. In the next step cylindrical micelles rods stack into a regular array leads to the formation of micelle liquid crystals. Then the condensation of inorganic silica precursor over the micelle liquid crystals leads to formation of mesostructure composite. Finally, removal of the surfactant micelle templates gives the mesoporous silica structures.[5, 4, 47]

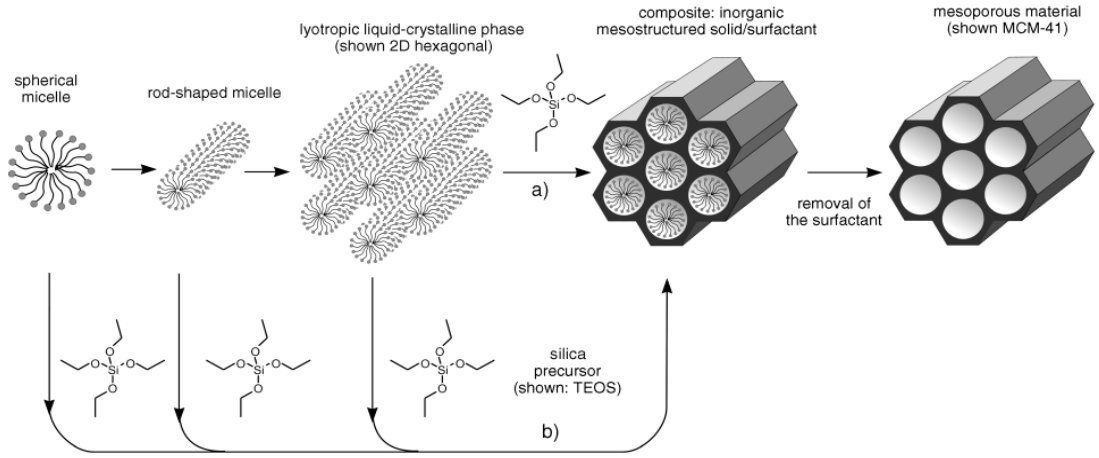

Figure 1.4: Formation of mesoporous materials by structure directing agents[5]

1.4.2 Cooperative liquid-crystal template mechanism

In cooperative liquid-crystal template mechanism, the lyotropic liquid crystalline phase is formed at lower concentrations of surfactant molecules by the cooperative self assembly of the surfactants and inorganic silica precursor. Here, the formation of spherical micelles to regular array of micellar liquid crystals is combined into a single concerted process leading to a regular array of surfactant-silica assemblies (Fig. 1.4, path b). Further condensation of inorganic silica precursor over the micelle liquid crystals leads to formation of mesostructure composite. Finally, removal of the surfactant micelle templates gives the mesoporous silica structures. As predicated by this model, the resulting liquid crystal structures can be reshaped by changing the reaction conditions during the synthesis of the materials. This can be achieved by varying the value of ionic strength, the type of silicate precursors or co-surfactants, the number of ionic charges on the silicate precursors and the concentration of surfactants.[18-20, 48]

A fundamental condition required for the formation of mesostructure by employing structure directing agents is that an attractive interaction between the

structure directing template and the silica precursor occurs to ensure inclusion of structure director without phase separation. Stucky and co-workers have proposed four general synthetic routes that are listed below (Fig. 1.5):[36, 49]

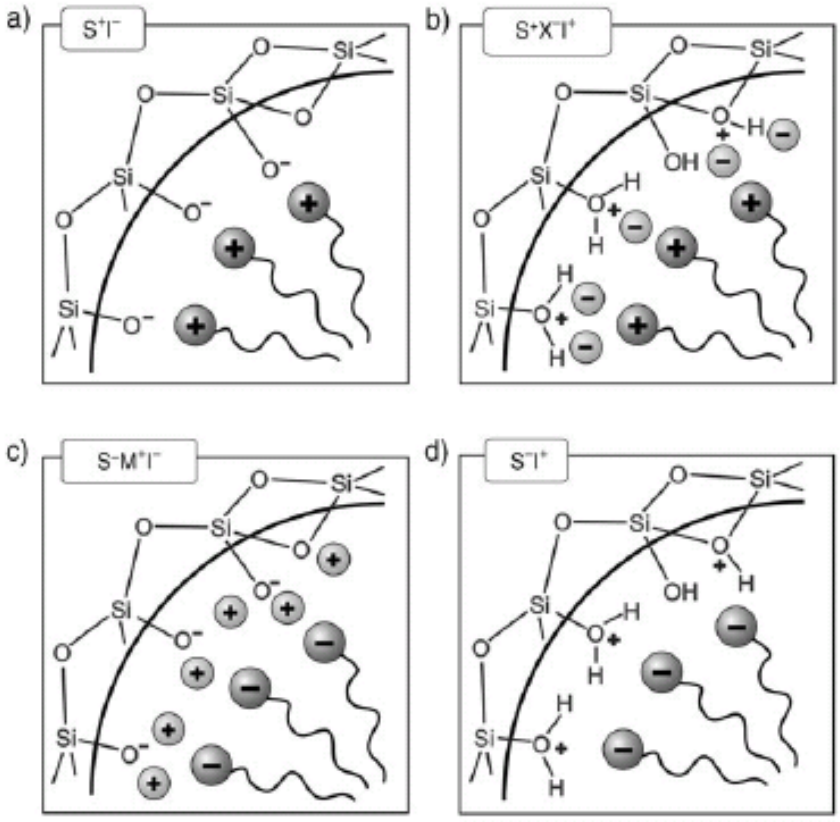

Figure 1.5: Interactions between the inorganic species and the head groups of the surfactant[5]

a) S^+I^-: The reaction takes place under basic condition (silica is negatively charged) and quaternary ammonium surfactants are used as template.

b) $S^+X^-I^+$: The reaction takes place in acidic condition (below the isoelectronic point of the Si-OH bearing inorganic species; pH=2) where the silica species are positively charged and they interact with the cationic surfactant via a mediator ion X^- (typically halide).

c) $S^-M^+I^-$: Here negatively charged surfactants (e.g. long chain alkyl phosphates) are used as the template. It is possible to work in a basic media. The mediator ion (M^+) must be added to ensure interaction between the negatively charged silica and surfactant.

d) S^-I^+: Mediator ion is not required in acidic media. Thus, the dominating interaction in this pathway is of electrostatic nature. Moreover, it is still possible for the attractive interactions to be mediated through hydrogen bonds. This is the case when non-ionic surfactants are used.

1.5 Hybrid organic - inorganic mesoporous materials

The applications of pure inorganic siliceous mesoporous materials are limited since only silanol groups are present on their surface. However, their range of applications can be increased several folds by tailoring the properties of these materials by incorporation of organic functional groups. The enormous functional variation of organic chemistry combined with the advantages of a thermally stable and robust inorganic solid matrix affords possibilities in creating a wide range of novel materials for various applications. Thus, these surface functionalized mesoporous materials have found wide spread applications in catalysis,[50-52] separation,[53, 54] decontamination,[55] drug delivery[56] and sensor design.[57] Mesoporous materials have been functionalized by various organic functional groups which include amines,[58, 59] thiols,[60] carboxylic acid,[61] sulfonic acid,[62] vinyl[63] and nitrogen based heterocycles.[55] These functional groups present on the surface of mesoporous material have been used to anchor various synthetic catalysts, biomolecules and polymers to generate novel functional materials.

In general, formulation of siliceous materials with covalently linked organic functional groups can be designed using two different synthetic strategies. These are post-synthesis modification (also known as grafting) and direct synthesis or co-condensation, as discussed below.

1.5.1 Post-synthetic functionalization of silica (Grafting)

Grafting is the post-synthesis modification of a pre-fabricated mesoporous support by attachment of functional molecules to the surface of the mesopores, usually after surfactant removal. In other words, it is the subsequent modification of the pore surface of a purely inorganic silica material by organic group. Mesoporous silicates possess surface silanol (Si-OH) groups that can be present in high concentration like amorphous silica. It acts as a convenient point for grafting reaction. Surface modification with organic groups is most commonly carried out by silylation,

although modification of silanol groups is also possible by esterification. In principle, functionalization with a variety of organic groups can be realized in this way by variation of the organic residue R in $(RO)_3SiR$ (Fig. 1.6). This method of modification has the advantage that under the synthetic conditions the mesostructure of the starting silica phase is usually retained, whereas the lining of the walls is accompanied by a reduction in the porosity of the hybrid material. If the organo silanes react preferentially at the pore openings during the initial stages of the synthetic process, the diffusion of further molecules into the center of the pores is prevented. Such blocking can in turn lead to a non homogeneous distribution of the organic groups within the pores, i.e. organic functional groups inside the pore is less than on the outer surface. If a high surface coverage with functional groups is desired, it is necessary to maintain a large number of surface silanol groups after removal of the surfactant. Surfactant removal is carried out either by calcination or by appropriate solvent extraction methods. Calcination promotes condensation of unreacted silanol groups, and many surface silanol groups are lost at typical calcination temperatures (400-550 ^{o}C). To minimize the loss of surface silanols, post-extraction thermal treatments can be used to increase the surface reactivity for silylation and strengthen the walls through additional condensation.

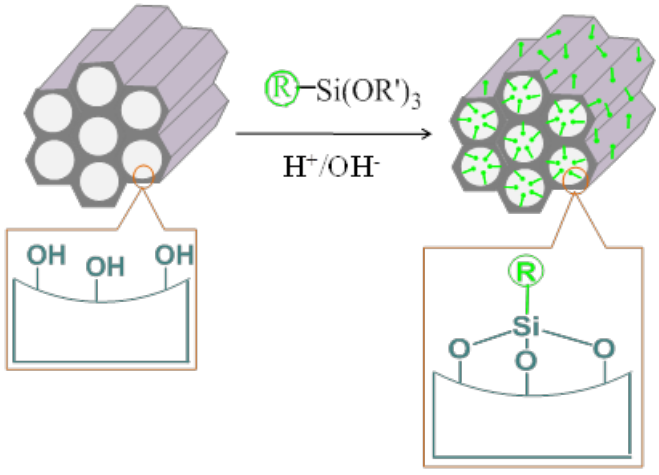

Figure 1.6: Functionalization of mesoporous materials by grafting method[5]

1.5.2 Co-Condensation method for synthesis of hybrid mesoporous material

This is another method to synthesize organically functionalized mesoporous silica material. This is also called a “one pot” co-condesation synthesis. It is possible to prepare mesostructured silica phases by the co-condensation of tetraalkoxysilanes

[$(RO)_4Si$ (TEOS or TMOS)] with terminal trialkoxyorganosilanes of the type $(R'O)_3SiR$ in the presence of structure-directing agents leading to materials with organic functional groups anchored covalently to the pore walls (Fig. 1.7). Since the organic functionalities are direct components of the silica matrix, pore blocking is not a problem in the co-condensation method. Furthermore, the organic units are generally more homogeneously distributed than in materials synthesized with the grafting process. However, the disadvantage of this method is that increasing the concentration of $(R'O)_3SiR$ can lead to the formation of disordered mesoscopic structure or even loss of order in the final material. Moreover, an increase in the concentration of organic functional group leads to the reduction of pore volume and specific surface area. It should be noted that the care must be taken not to destroy the organic functionality during the removal of surfactant. Hence, solvent extraction methods are commonly used for template removal.

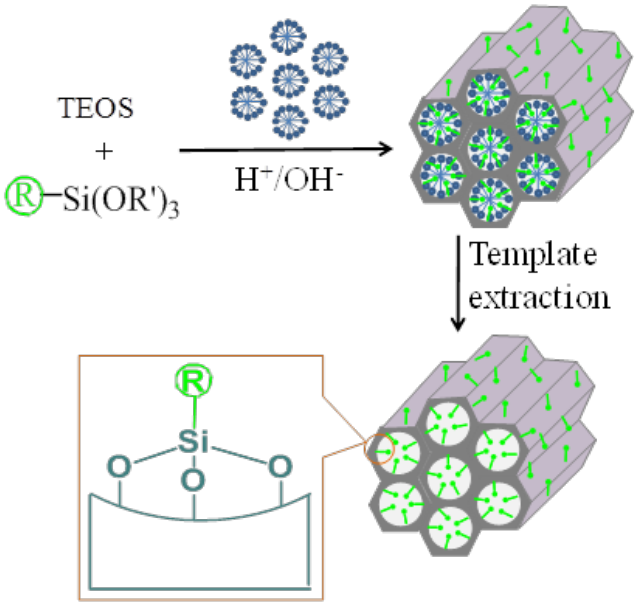

Figure 1.7: Functionalization of mesoporous materials by co-condensation method [64]

Mesoporous materials have been functionalized with a variety of organic functional groups by both grafting and co-condensations methods as presented in the table 1.1.

Table 1.1: Mesoporous materials functionalized with various organic functional groups

Functional group	Method	Mesophase	Author, year, reference
3-aminopropyl-, 2-cyanoethyl-	Co-condensation	HMS	Macquirrie, 1996,[65]
Phenyl-, n-octyl-	Co-condensation	MCM-41	Mann, 1996,[66]
3-aminopropyl-, allyl-, 3-imidazole-, 3-mercaptopropyl-, 3-(2,3-epoxypropoxy)propyl-,	Co-condensation	MCM-41	Mann, 1997,[67]
vinyl-	Co-condensation	MCM-41	Stein, 1997,[68]
3-mercaptopropyl-	Co-condensation	HMS	Jacobs, 1998,[69]
methyl-	Co-condensation	MCM-41	Corma, 1998,[70]
Methyl-, ethyl-, vinyl n-octyl-, phenyl	Co-condensation	SBA-3	Babonneau, 1999,[71]
3-chloropropyl-	Co-condensation	HMS	Macquirrie, 1999,[72]
3-chloropropyl-	Co-condensation	MCM-41	Tatsumi, 2000,[73]
coumarin-	Grafting	MCM-41	Mal, 2003,[74 , 75]
coumarin-	Co-condensation	MCM-41	Mal, 2003,[75]

1.6 Click chemistry

In 2001 Sharpless and co-workers coined the prototypical concept of click chemistry.[76] Click chemistry enables a modular approach to generate novel products by utilizing a collection of reliable chemical reactions.[76] Those reactions thus give products stereo-selectively in high yields, produce inoffensive byproducts, are insensitive to oxygen and water, utilize readily available starting materials and have a thermodynamic driving force of at least 20 kcal mol^{-1}. Preferably, the reactions should be conducted in benign solvents such as water and products of the reaction should be purified by non-chromatographic techniques such as re-crystalization or distillation.

Based on these characteristics, Sharpless and co-workers classified following reactions under click chemistry category: 1) cycloaddition reactions of unsaturated species, such as 1,3-dipolar cycloaddition reactions, and hetero Diels -Alder reactions; 2) nucleophilic substitution chemistry, particularly ring-opening reactions of strained heterocyclic systems such as epoxides, aziridines, aziridinium ions, and episulfonium ions; 3) carbonyl chemistry of the "non-aldol" type; such as formation of ureas, thioureas, aromatic heterocycles, oxime ethers, hydrazones, and amides and 5) additions to carbon - carbon multiple bonds, especially oxidative reactions such as epoxidation, dihydroxylation, aziridination, and sulfenyl halide addition, but also Michael additions of Nu-H reactants.[76] Recently, addition of thiols to alkenes (also called as thiol-ene coupling, TEC) has also been classified as click chemistry reaction.[77, 78] Of all the click reaction reported so far, the most widely studied and used is Huisgen [3 + 2] cycloaddition between a terminal alkyne and an azide to yield substituted 1,2,3-triazoles, **1** (Scheme 1.1).[7, 79] This reaction has been termed the "cream of the crop" of click reactions[76] and has found application in various fields of research as diverse as organic synthesis, polymer and material science, medicinal chemistry, molecular biology, and biotechnology.[8, 80-83] The great success of this reaction as a ligation tool-relies on the efficiency and selectivity (regio- and chemo-), the ready occurrence of the process under aerobic conditions, and compatibility with a broad repertoire of functional groups. The formation of a robust linker such as the 1,4-disubstituted 1,2,3-triazole ring which displays biological and pharmacological activities of its own, is an added advantage of the synthetic utility of the CuAAC reaction in the discovery of novel drugs.[80]

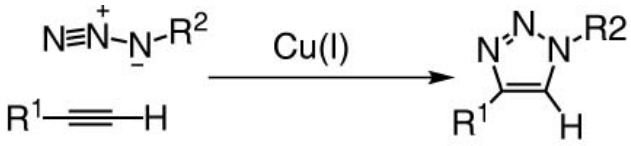

Scheme 1.1: CuAAC reaction between an alkyl azide and alkyne

1.6.1 Mechanism of CuAAC reaction

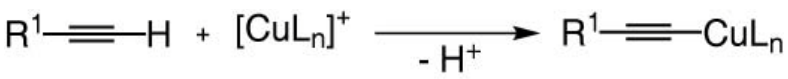

Scheme 1.2: Proposed catalytic first step of the CuAAC reaction based on DFT calculations[7]

The active Cu(I) catalyst required for the CuAAC reaction can be generated from Cu(I) salts or from Cu(II) salts by using sodium ascorbate as the reducing agent. Based on DFT calculations, Sharpless and co-workers proposed the mechanism involving formation of copper(I) acetylide.[7] The copper(I) acetylide formed likely through a π-alkyne copper complex intermediate (Scheme 1.2), was calculated to be exothermic by 11.7 kcal mol^{-1}.[7] A careful kinetic investigation of the copper (I)-catalyzed reactions between an alkyne and organic azide under various conditions revealed a second-order dependence on Cu(I).[84-86] More recently DFT calculations based on the requirement of two copper atoms in the transition state complex showed a significant reduction in the value of activation energy.[87, 88] This probably suggests the involvement of two Cu atoms in the CuAAc reaction mechanism. Further, the detailed structural investigation of phenylethylcopper(I) $[(PhCCCu)_2]_n$ by powder X-ray diffraction shows formation of ladderane structure in which the phenylethyl residues are linked to two copper(I) atoms that are ideally positioned to take part in the CuAAC reaction.[89-91] Heaney et al. prepared dinuclear copper(I) ladderane complexes of various alkynes by different methods including the reaction conditions used for CuAAC reaction i. e. reduction of copper(II) sulphate with sodium ascorbate in 1:1 *t*-BuOH/H_2O.[90] These alkyne copper(I) derivatives were then used in catalytic amounts with appropriate alkyne and organic azide for carrying out CuAAC reaction in *t*-BuOH/H_2O to obtain CuAAC derivatives in excellent yields.[90] Based on these experiments Heaney et al. concluded that the isolated dinuclear copper(I) ladderane complexes act as efficient catalysts under mild reaction conditions that were originally used by Sharpless et al. All these observations lead to a minor change to the mechanism of click reaction that was originally proposed by Sharpless et al.[7] In this revised mechanism, sodium ascorbate reduces copper(II) to copper (I) which then deprotonates the alkyne to form copper(I) complex of the alkyne. This is then

followed by a collapse to the true dinuclear Cu(I) ladderane complexes as shown in the scheme 1.3.

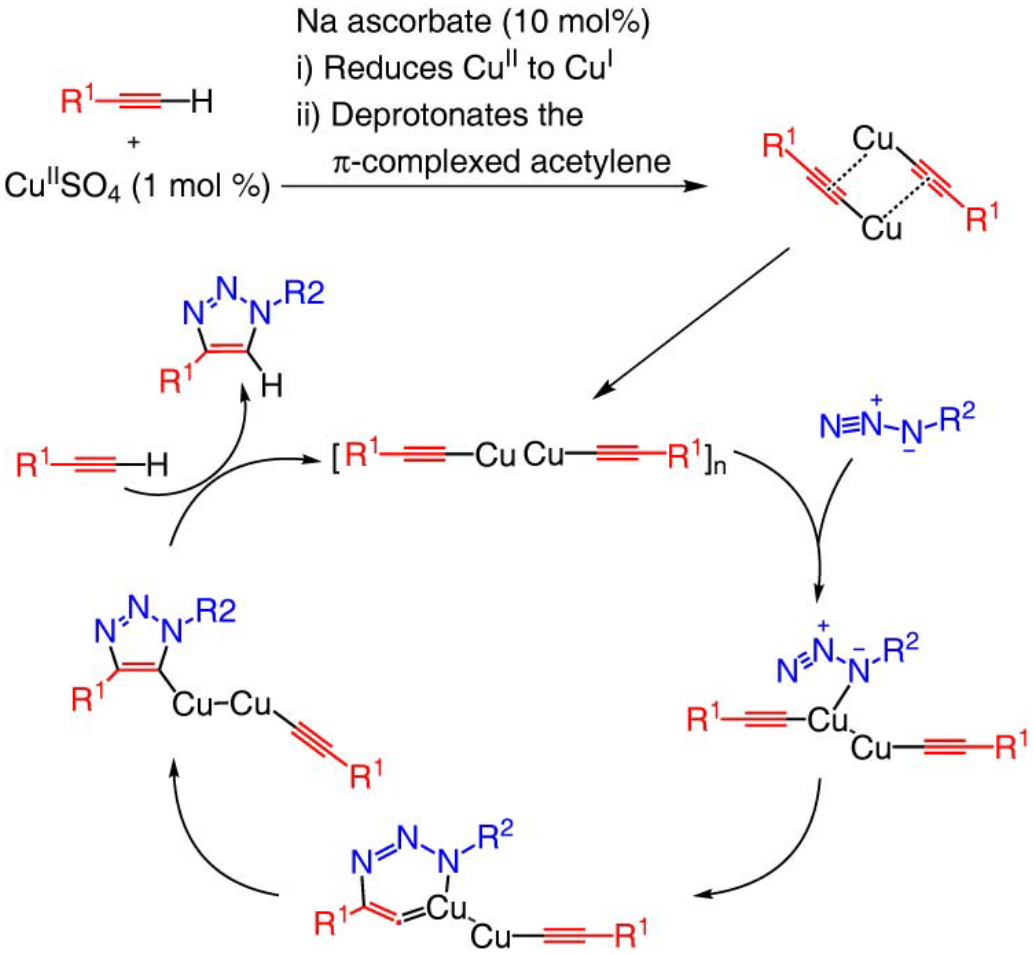

Scheme 1.3: Mechanism of the CuAAC reaction with dinuclear Cu^{I} ladderane complexes.[90]

1.6.2 Applications of CuAAC reaction

CuAAC reactions have found enormous applications in organic synthesis, biology and materials chemistry. Some of important applications are discussed below.[8, 81, 92]

The CuAAC reaction has provided a unique tool for easy access to functionalized surfaces of reliable and reproducible surface densities. CuAAC has shown to be a versatile tool for the functionalization of nanomaterials. Androv and co-workers have reported functionalization of carbon nanotubes with polymers by CuAAC. Functionalization of nanotubes with polymers promotes colloidal dispersion of the resulting nanotubes in organic solvents.[93] Gold surfaces, silcon wafers and glass

slides have been functionalized with self-assembled monolayers by CuAAC.[94-97] A wide variety of synthetic and biological molecules have been attached on SAMs for a wide range of applications in molecular electronics, catalysis and bio-sensors.

Applications of CuAAC in bioconjugation have been reported by Finn and co-workers.[98, 99] Free amines from lysine residues or thiols from cysteine residues present on the outer surface of cowpea mosaic virus particles were used to functionalize the virus with azide or alkyne functionality, via peptide coupling or thio-ether linkage. This virus resembles a cage-like molecule, formed from 60 identical copies of a two-protein asymmetric unit, which surrounds the genetic information in the core. The virus was then conjugated with various molecules such as fluorescein, sugars, peptides, poly(ethylene oxide) polymers, and the iron carrier protein transferring via CuAAC reaction. Further, CuAAC reactions have found enormous applications in bioconjugation, particularly it has been proved to be very fruitful in the field of activity based protein profiling (ABPP).[100-103]

CuAAC reaction has been widely used in the separation chemistry for the preparation of stationary phase.[92] Finn et al. have used CuAAC in the affinity chromatography with agarose bead support and used for separation of biomolecules based on affinity chromatography technique.[104] Frechet at al. have prepared HPLC packing using CuAAC modified acrylate polymer beads as support and used in the separation of variety of proteins and peptides.[105] Liang and co-workers have used CuAAC as tool for immobilization of various organic molecules ranging from long chain alkyl groups, hydroxyl groups, sugars and cyclodextrins on the HPLC silica beads for the generation of various type of stationary phases such as reverse phase and hydrophilic interaction chromatography (HILIC).[106-110] These stationary phases exhibited excellent chromatographic properties and used successfully for the separation of non-polar and polar compounds. Polar compounds such as bases, nucleosides, sugars and sugar derivatives were well retained and separated, which was mostly attributed to the hydrogen bonding interactions between polar compounds and exposed polar groups on the surface of stationary phase. Recently, Marra et al. reported synthesis of galactose and lactose sugar-based silica gel stationary phases by CuAAC. This sugar based stationary phases showed potency for the separation of very polar compounds (e.g. amino acids). Further sugar anomers were completely separated with high chromatographic efficiencies.[111] CuAAC has also been used for

the modification of solid surfaces with chiral functional groups such as β-cyclodextrin, cinchona, chiral amino-acids and their derivatives for usage in chiral analysis and separation.[112-114]

1.7 Physico-chemical characterization

The inorganic–organic hybrid mesoporous materials can be characterized by various techniques, which provide important information about different physico-chemical properties of these materials. In this section, a brief introduction to the theory and principle of various characterization techniques employed in the present study are discussed.

1.7.1 Powder X-ray diffraction

Powder X-ray diffraction is the most commonly used tool to identify and measure the uniqueness of structure, phase purity, degree of crystallinity and unit cell parameters of crystallite materials. The mesoporous materials exhibit characteristic high intensity peaks in the low angle region between $2\theta = 0.5\text{-}10^{o}$. The XRD patterns are recorded by the measurements of the angles at which the X-ray beams are diffracted by the sample. The relation between the distance between two *hkl* planes *(d)* and angle of diffraction (2θ) is given by Bragg's equation as follows (Eq. 1.1):

$$n\lambda = 2d \sin\theta \qquad \text{(Eq. 1.1)}$$

Where λ = wavelength of X-rays, n= an integer known as the order of reflection (*h, k,* and *l* represent Miller indices of respective planes).[115] From the diffraction patterns, the uniqueness of mesoporous structures, phase purity, degree of crystallinity, and unit cell parameters of the semi crystalline hybrid materials can be determined.[116] The identification of phase is based on a comparison of a set of reflections of the sample with that of pure reference phases distributed by International Center for Diffraction Data (ICDD). Unit cell parameter (a_o) of a cubic lattice can be determined by the following equation: $a_o = d_{hkl}(h^2 + k^2 + l^2)^{1/2}$, where d = distance between two consecutive parallel planes having Miller indices *h, k,* and *l*.[115] The unit cell dimensions determined by XRD are also used to calculate the wall thickness of mesoporous materials in combination with pore size data determined from gas adsorption-desorption studies.

1.7.2 Scanning electron microscopy

Scanning electron microscopy (SEM) is an important technique for characterization of size and morphology of mesoporous materials. This technique provides not only topographical information like optical microscopes do, but also information on the chemical composition near the surface. SEM creates the magnified image by using electrons instead of light waves. It generates very detailed three-dimensional image at much higher magnification than is possible with an optical microscope. A scanning electron microscope can generate an electron beam scanning back and forth over a solid sample. The interaction between the beam and the sample produces different types of signals providing detailed information about the surface structure and morphology of the sample. When an electron from the beam encounters a nucleus in the sample, the resultant Coulombic attraction leads to a deflection in the electron's path, known as Rutherford elastic scattering. A fraction of these electrons will be completely backscattered, reemerging from the incident surface of the sample. Since the scattering angle depends on the atomic number of the nucleus, the primary electrons arriving at a given detector position can be used to produce images containing topological and compositional information.[117], [118] The high-energy incident electrons can also interact with the loosely bound conduction band electrons in the sample. However, the amount of energy given to these secondary electrons as a result of the interactions is small, and so they have a very limited range in the sample. Hence, only those secondary electrons that are produced within a very short distance from the surface are able to escape from the sample. As a result, high resolution topographical images can be obtained in this detection mode.[119] SEM is non-destructive to samples although some electron beam damage is possible. SEM scans over a sample surface with a probe of electrons (5-50 kV) and detects the yield of either secondary or back-scattered electrons as a function of the position of the primary beam. Magnification of 10-500,000 times is possible with a resolution of about 1 nm. Sample requirements are minimal; they should be vacuum compatible and invariably be coated with a conducting film to avoid sample charging during the measurement.

1.7.3 Transmission electron microscopy

Transmission electron microscopy (TEM) is a major analytical tool in a range of scientific fields including materials and biological sciences. TEM is typically used for high resolution imaging of thin sections of solid samples for nanostructural and compositional analysis. The technique involves: (i) irradiation of a very thin sample by a high energy electron beam, which is diffracted by the lattice of a crystalline or semi crystalline material and propagated along different directions. (ii) imaging and angular distribution analysis of the forward-scattered electron (unlike SEM where backscattered electrons are detected), and (iii) energy analysis of the emitted X-rays. [120] A beam of accelerated electrons can interact with an object in a conventional transmission electron microscope in one of two ways. Usually elastic scattering takes place, whereby the electrons change their path in the specimen without a loss of energy. Inelastic scattering can also occur, resulting in a loss of energy due to an interaction of the impinging electrons with the orbital electrons surrounding the nucleus of each atom in the object. Those electrons, which are not or hardly scattered, contribute positively to the image. However, considerably deflected electrons are prevented from doing so by apertures in the optical path. As a result, differences in light intensity (contrast) are created in the final image, which relate to areas in the object with different scattering potentials. As the atomic number increases, their scattering efficiency will also increase. Hence, heavy metals can form images with good contrast. The imaging system consists of an objective lens and one or more projector lenses. The chief lens in transmission microscopes is the objective. It determines the degree of resolution in the image. It forms the initial enlarged image of the illuminated portion of the specimen in a plane that is suitable for further enlargement by the projector lens. The projector lens, as it implies, serves to project the final magnified image on the screen or photographic emulsion. The great depth of focus provides the high magnification of the sample. The topographic information obtained by TEM in the vicinity of atomic resolution can be utilized for structural characterization and identification of various phases of mesoporous materials, viz., hexagonal, cubic or lamellar.[121, 122] TEM also provides real space image on the atomic distribution in the bulk and surface of a nanocrystal.[123] The modern TEM machines can achieve resolution below 0.5 angstroms (50 pm) at magnifications above 50 million times.[124]

1.7.4 Gas adsorption-desorption studies

Gas adsorption-desorption studies is one of the widely used technique for evaluating the surface area, pore size, pore volume and pore size distribution of porous solid materials.[125] In this technique, the amount of gas adsorbed by a solid is measured, which in turn is directly related to the porous properties and pore structure of the material.[126] Depending on the nature of the adsorbent solid and information required, various gases like Nitrogen (N_2), Carbon dioxide (CO_2) and Argon (Ar) are used as adsorbates. The volume of gas adsorbed by the solid is measured over a wide range of relative pressures, and a plot of the volume adsorbed with varying relative pressure (p/p_o) is called the adsorption isotherm. N_2 adsorption isotherm at sub-atmospheric pressures and -196 ºC is routinely used for determining pore information and pore size distributions in microporous, mesoporous and macroporous range.[126] Surface area is determined from the Brauner-Emmett-Teller (BET) equation (Eq. 1.2), based on monolayer adsorption of gases.[14, 127]

$$\frac{p}{v\,(p_o - p)} = \frac{1}{v_m\,c} + \frac{c-1}{v_m\,c} X \frac{p}{p_o} \qquad \text{(Eq. 1.2)}$$

where, v = volume of N_2 adsorbed by the sample under pressure p, p_o = saturated vapor pressure at the same temperature, v_m = volume of N_2 adsorbed when the surface is covered with monolayer, and c = BET constant for a given adsorbate.

The equation suggests that the plot of $p/v(p_o - p)$ versus p_o/p should be linear, and from the intercept $1/v_m c$ and slope $(c-1)/v_m c$, the values of v_m and c can be determined. Thus the specific surface area (S) of a sample can be determined as follows (Eq. 1.3):

$$S = \frac{N_o v_m A}{22414\,m} \qquad \text{(Eq. 1.3)}$$

where N_o = Avogadro number, m = mass of solid adsorbent, A = cross-section of the gas molecules (16.2 $Å^2$ for N_2), and S is expressed in $cm^2\,g^{-1}$ unit.

Several computational procedures are available for the derivation of pore size distribution of mesoporous samples from physisorption isotherms. Most popular

among them is the Barrett-Joyner-Halenda (BJH) model, which is based on speculative emptying of the pores by a stepwise reduction of p/p_o, and allowance being made for the contraction of the multilayer in those pores already emptied by the condensate. The mesopores size distribution is usually expressed as a plot of dV_p/dr_p versus r_p, where V_p = mesopore volume, and r_p = pore radius. It is assumed that the mesopores volume is completely filled at high p/p_o.

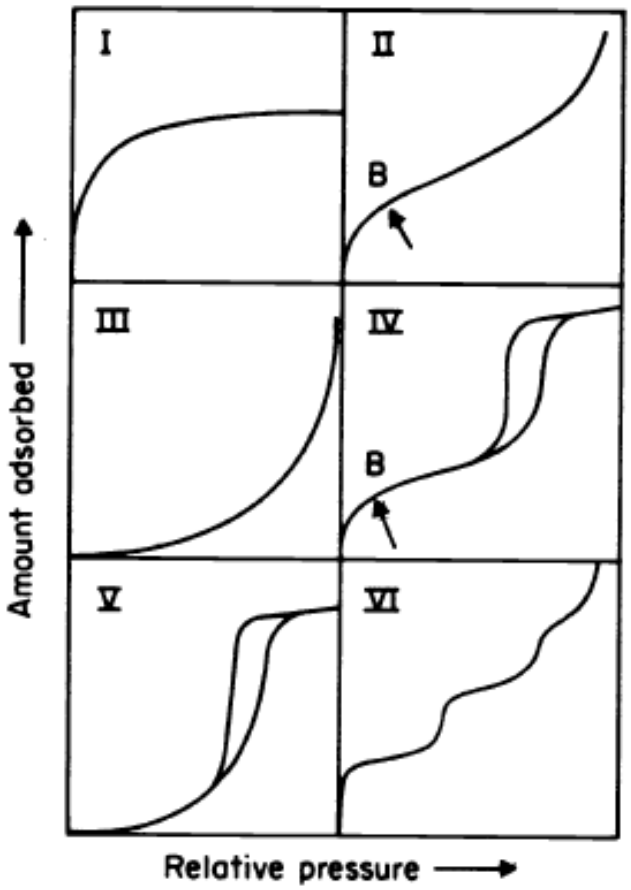

Figure 1.8: Types of physisorption isotherms.[14]

The physisorption isotherms have been classified into six distinct types by IUPAC (Fig 8)[14] : Type I reversible isotherms exhibited by microporous solids; Type II reversible isotherms exhibited by nonporous and macroporous solids; Type III isotherm, which is rarely seen for example nitrogen on polyethylene, in such type of isotherms adsobate-adsorbate interactions play an important role; Type IV isotherm with hysteresis loop, exhibited by mesoporous solids; Type V isotherm which is rarely seen and arises due to weak adsorbent-adsorbate interactions. Type VI isotherm arising from stepwise multilayer adsorption on a uniform nonporous solid. The

different isotherms are shown in Figure 1.7. The hysteresis loop exhibited in the type IV isotherm is classified in to 4 distinct types: H1, usually exhibited by pores with regular shape and narrow pore size distribution; H2, usually associated with pores with narrow necks and wide bodies; H3, usually associated with plate like particles; H4, usually associated with slit-like pores.[14] The shapes of the different hysteresis loops are shown in Fig. 9.

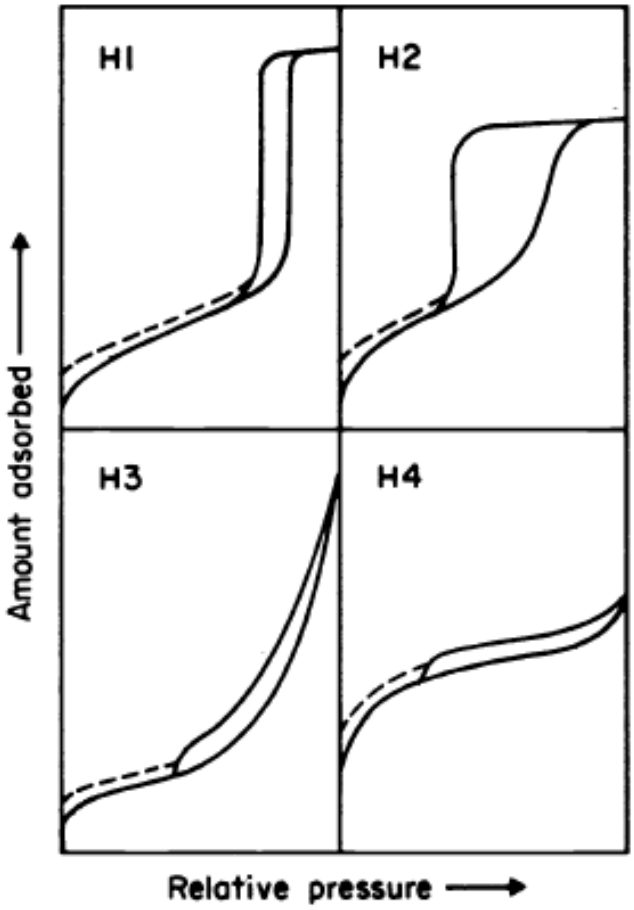

Figure 1.9: Types of hysteresis loops.[14]

1.7.5 Thermogravimetric analysis

Thermogravimetric analysis or TGA is a technique in which the weight loss of a sample is studied with increasing temperature. It is a highly sensitive technique, which provides information about the weight percentage of moisture, volatiles, solvent, organic /inorganic contents, etc in a samples. It is done by placing the sample in a weighing balance and heating the sample at a controlled rate. The weight loss is studied in various ambient atmospheres like nitrogen or air. TGA is widely used for

studying the weight percentage of templates in mesoporous material synthesis and to estimate the organic /inorganic contents in modified mesoporous materials.[128]

1.7.6 Fourier transform infrared spectroscopy

Fourier transform infrared (FTIR) spectroscopy deals with the vibration of chemical bonds in a molecule at various frequencies depending on the elements and types of bonds. After absorbing electromagnetic radiation the frequency of vibration of a bond increases leading to transition between ground state and several excited states. These absorption frequencies represent excitations of vibrations of the chemical bonds and thus are specific to the type of bond and the group of atoms involved in the vibration. The energy corresponding to these transitions corresponds to the infrared region (4000–400 cm^{-1}) of the electromagnetic spectrum. The term Fourier transform (FT) refers to a recent development in the manner in which the data are collected and converted from an interference pattern to an infrared absorption spectrum that is like a molecular "fingerprint".[129] In the case of porous silicates, the FTIR spectra in the 400–1300 cm^{-1} region provides information about the structural details, for example, peaks at 466, 800, 1070 and 1220 cm^{-1} are typical of Si-O-Si bands that are associated with formation of silica framework. Whereas the bands in the 3000–4000 cm^{-1} region allows to determine different organic functional groups present on the surface of the materials, Bronsted and Lewis acid sites and silanol groups.[130, 131]

1.7.7 Cross-polarization magic angle spinning NMR spectroscopy

Nuclear magnetic resonance (NMR) spectroscopy is one of the most powerful tools to investigate structure and dynamics of a molecular system in liquid phase. Atomic nuclei consisting of odd number of protons and/or neutrons possessing a nuclear spin $I \neq 0$ and consequently a magnetic moment $\mu = \gamma\hbar I$ (γ = gyromagnetic ratio), when placed in a magnetic field of strength B_o, Zeeman interaction results in quantized orientations of the nuclear magnetic moments. The nucleus can adopt $2I + 1$ Eigen states with energies $E(m) = -m\gamma\hbar B_o$, where m = (I, I–1,…., –I). Transitions between neighbouring energy states ($\Delta m = \pm 1$) can be induced by electromagnetic radiation (energy $E = h\nu$) of frequency $\nu_o = \gamma B_o/2\pi$. The chemical shift interaction arises from secondary local magnetic fields induced by the interaction of the electrons surrounding the nucleus. The induced local field opposes B_o and hence shields the

nucleus under observation. The shielding is spatially anisotropic due to the nonspherical electron distribution around the nucleus.

In solid-state NMR, the line shape is determined by dipolar and quadrupolar interactions. The lines are usually broader because the rigid structure of the solid phase prevents the averaging of the dipolar interaction by motions. Since, the first order quadrupolar and dipolar interactions are proportional to $(3\cos^2\theta - 1)$, where, θ is the angle between an internuclear vector and the magnetic field, these interactions can be removed, to a first order approximation, by spinning the sample around the so-called magic angle θ with respect to the external magnetic field, for which $3\cos^2\beta - 1 = 0$, i.e. $\beta = 54.74°$. This technique is known as Magic Angle Spinning (MAS).[132, 133]

Cross-polarization (CP) involves indirect excitation of the less abundant nucleus through magnetization transfer from an abundant spin system (*e.g.* ^{1}H) *i.e.*, to increase the signal to noise ratio (SNR) of the spectra of nuclei with low natural abundance (*e.g.* ^{13}C, ^{29}Si, ^{31}P *etc*.), and to monitor the spatial proximity of nuclei.[134, 135] CP technique does not affect the line width of the spectra, but is applied to improve the sensitivity.

1.8 Motivation and objective of the present work

As described in the previous section, discovery of the Cu(I)-catalyzed 1,3-dipolar cycloaddition of organic azides to alkynes (CuAAC) has provided the most powerful "click chemistry" tool for conjugation between appropriately functionalized binding partners via an 1,2,3-triazole linkage.[7] The favorable thermodynamics, exceptionally high yields, ease and compatibility with a broad repertoire of functional groups has led to numerous applications of Cu(I)-catalyzed azide-alkyne click chemistry (CuAAC) reaction in various fields of organic, medicinal, polymer, materials and biological chemistry.[136] CuAAC has been successfully used to functionalize metal nanoparticles,[137] single-walled carbon nanotubes,[137] powdered silica,[106, 112] and mesoporous silicon rugate filters.[138] Therefore, synthesis of azide containing silica mesoporous materials would be very useful in the development of functional materials. The presence of an organic azide on mesoporous materials such as SBA-15 and MCM-41 gives a handle to anchor various moieties such as enzymes and catalysts via this chemoselective ligation. In this context, the present thesis describes the syntheses of azide functionalized mesoporous materials with different

pore sizes and morphologies and their reactivity with various organic and inorganic substrates bearing alkyne functionality using CuAAC reaction. Hybrid mesoporous materials synthesized by this methodology have been used for various applications such as organocatalysis, immobilization of enzymes and development of sensors. By keeping the above objectives in mind, the following specific work was selected for the present thesis:

1. Synthesis and characterization of azide containing mesoporous materials (SBA-15, MCM-41) via both one-pot co-condensation and post-synthetic grafting.
2. Evaluation of the effeiciency of these azide functionalized mesoporous materials to undergo CuAAC reaction with various organic moieties bearing alkyne functionality.
3. Attachment of organocatalyst proline onto azide fnctionalized MCM-41 by CuAAC reaction and its application in asymmetric aldol condensation reaction.
4. Development of biosensor for detection of hydrogen peroxide and glucose by anchoring a small molecule peroxidase mimic [Fe^{III}(biuret-amide)] onto MCM-41 (mesoporous silica nanoparticles, MSNs).
5. Encapsulation of enzyme trypsin into the mesopores of spherical SBA-15 by a "ship-in-a-bottle" approach and evaluation of the efficacy of the encapsulated enzyme as bio-catalyst.

1.9 Outline of the thesis

Thesis is divided into five chapters with proper references at the end of each chapter. Thesis includes syntheses of azide functionalized MCM-41 and SBA-15 mesoporous materials, their reactivity with various organic substrates bearing alkyne functionality using CuAAC reaction, aldol condensation reaction by site isolated proline anchored on MCM-41, development of biosensor for detection of hydrogen peroxide and glucose by [Fe^{III}(biuret-amide)] anchored on MCM-41 and encapsulation of enzyme, trypsin into the mesopores of spherical SBA-15.

Chapter 1: A comprehensive review of literature on silica mesoporous materials: method of synthesis, hybrid inorganic-organic mesoporous materials,

methods of surface modification with organic functional groups and characterization techniques of mesoporous materials is provided. A brief introduction to Cu(I) catalyzed azide-alkyne click chemistry (CuAAC) is discussed.

Chapter 2: This chapter is divided into two parts as described below. First part of the chapter discusses synthesis and characterization of azide functionalized SBA-15 by both post synthetic grafting and one-pot co-condensation method. The efficiency of the azide functionalized SBA-15 to undergo CuAAC was evaluated by using various organic substrates containing alkyne functionality. These materials have been characterized by various techniques such as powder XRD, SEM, TEM, nitrogen adsorption-desorption studies, IR and ^{13}C and ^{29}Si solid state NMR spectroscopy etc. This methodology was used to incorporate mannose on the surface of SBA-15. Incubation of mannose labeled SBA-15 with fluorescein labeled concanavalin-A led to the formation of fluorescent silica-protein hybrid material.

Second part of this chapter describes the synthesis and characterization of azide functionalized MCM-41 by one-pot co-condensation method. The density of azido-propyl groups incorpoarated on the surface of MCM-41 was varied by varing the mole% of AzPTES during synthesis of MCM-41 from 0.2% to 10%. The efficiency of the azide functionalized MCM-41 to undergo Cu(I)-catalized azide-alkyne click chemistry reaction was evaluated by using various organic substrates containing alkyne functionality. Synthesis of site dense to site isolated organo azides on the surface of MCM-41 was established by fluorescence spectroscopy of pyrene clicked on these materials.[139] Further, site dense to site isolated proline anchored on MCM-41 via CuAAC reaction was used for the aldol condensation reaction. Increase in rate of aldol reaction was observed for the site isolated proline catalyst anchored on MCM-41.

Chapter 3: This chapter discusses the synthesis of mesoporous silica nanoparticles (MSNs) based hybrid material (Fe-MSN) that mimics the enzyme HRP and functions as a biosensor at physiological pH. This hybrid material contains a robust small molecule peroxidase mimic [Fe^{III}(biuret-amide)] developed in our group[140] that is covalently attached to azide containing MSN particles (CuAAC). These hybrid MSN particles have been used as biosensor for the quantitative detection of H_2O_2 and glucose in a one-pot method. The synthesized Fe-MSN nanoparticles

were characterized by several techniques such as FT-IR, EPR, ICP and nitrogen adsorption-desorption experiments

Chapter 4: This chapter describes the synthesis of hierarchical mesoporous silica based hybrid material and its application as a support for the immobilization of trypsin in a "ship-in-a-bottle" approach. Enzyme adsorbed into the pores of an azide functionalized mesoporous spherical SBA-15 (diameter 5-8 μm) with pores larger than the diameter of the enzyme were capped with alkyne functionalized mesoporous silica nanoparticles (MSNs; diameter ~100 nm) by covalent linkage using efficient CuAAC. The mesoporous silica nanoparticles (MSNs) have pores that are large enough to allow small molecules such as reactants and products to diffuse in and out of SBA-15 but do not allow enzyme to leach out of SBA-15. Hence, in this hierarchical silica mesoporous hybrid material, the pores of MSNs on the surface of spherical SBA-15 act as windows for enzyme and effectively stops the enzyme from leaching. These materials have been characterized by various analytical techniques such as powder XRD, SEM, TEM, FT-IR, confocal laser scanning microscopy (CLSM) and nitrogen adsorption-desorption experiments. The efficacy of the encapsulated enzyme as bio-catalyst was shown by the hydrolysis of BAPNA as substrate over 10 catalytic cycles.

Chapter 5: This chapter presents an overall summary of the work done and describes the major findings of the studies. Future directions based on the work reported in the thesis are also discussed.

1.10 References

1. G. J. D. Soler-illia, C. Sanchez, B. Lebeau and J. Patarin, *Chem. Rev.*, 2002, **102**, 4093-4138.
2. G. Q. Lu and X. S. Zhao, *Nanoporous materials, science and engineering, vol. 4, Imperial College Press, London, 2004.*
3. T. J. Barton, L. M. Bull, W. G. Klemperer, D. A. Loy, B. McEnaney, M. Misono, P. A. Monson, G. Pez, G. W. Scherer, J. C. Vartuli and O. M. Yaghi, *Chem. Mater.*, 1999, **11**, 2633-2656.
4. Y. Wan and Zhao, *Chem. Rev.*, 2007, **107**, 2821-2860.
5. Frank Hoffmann, Maximilian Cornelius, Jürgen Morell and M. Fröba, *Angew. Chem. Int. Ed.*, 2006, **45**, 3216-3251.

6. A. Stein, B. J. Melde and R. C. Schroden, *Adv. Mater.*, 2000, **12**, 1403-1419.
7. V. V. Rostovtsev, L. G. Green, V. V. Fokin and K. B. Sharpless, *Angew. Chem. Int. Ed.*, 2002, **41**, 2596-2599.
8. J.-F. Lutz, *Angew. Chem. Int. Ed.*, 2007, **46**, 1018-1025.
9. M. A. Brzezinski, *Proc. Natl. Acad. Sci.U. S. A.*, 2008, **105**, 1391-1392.
10. M. Hildebrand, *J. Nanosci. Nanotechnol.*, 2005, **5**, 146-157.
11. E. Brunner, K. Lutz and M. Sumper, *Phys. Chem. Chem. Phys.*, 2004, **6**, 854-857.
12. G. Pohnert, *Angew. Chem. Int. Ed.*, 2002, **41**, 3167-3169.
13. U. Lohse, B. Altrichter, R. Fricke, W. Pilz, E. Schreier, C. Garkisch and K. Jancke, *J. Chem. Soc. , Faraday Transactions*, 1997, **93**, 505-512.
14. K.S.W. Sing, D.H. Everett, R.A.W. Haul, L. Moscou, R.A. Pierotti, J. Rouquerol and T. Siemieniewska, *Pure and applied chemistry*, 1985, **57**, 603-619.
15. J. Cejka and S. Mintova, *Catalysis Reviews*, 2007, **49**, 457-509.
16. J. Cejka, A. Vondrova, B. Wichterlova, G. Vorbeck and R. Fricke, *Zeolites*, 1994, **14**, 147-153.
17. C. T. Kresge, M. E. Leonowicz, W. J. Roth, J. C. Vartuli and J. S. Beck, *Nature*, 1992, **359**, 710-712.
18. J. S. Beck, J. C. Vartuli, W. J. Roth, M. E. Leonowicz, C. T. Kresge, K. D. Schmitt, C. T. W. Chu, D. H. Olson and E. W. Sheppard, *J. Am. Chem. Soc.*, 1992, **114**, 10834-10843.
19. D. Zhao, J. Feng, Q. Huo, N. Melosh, G. H. Fredrickson, B. F. Chmelka and G. D. Stucky, *Science*, 1998, **279**, 548-552.
20. D. Zhao, Q. Huo, J. Feng, B. F. Chmelka and G. D. Stucky, *J. Am. Chem. Soc.*, 1998, **120**, 6024-6036.
21. V. Chiola, J. E. Ritsko and C. D. Vanderpol, *US Patent*, 1971, No. 3 556725.
22. F. Di Renzo, H. l. n. Cambon and R. Dutartre, *Micro. Mater.*, 1997, **10**, 283-286.
23. D. M. Antonelli and J. Y. Ying, *Current Opinion in Colloid & Interface Science*, 1996, **1**, 523-529.
24. Z.-R. Tian, W. Tong, J.-Y. Wang, N.-G. Duan, V. V. Krishnan and S. L. Suib, *Science*, 1997, **276**, 926-930.
25. X. He and D. Antonelli, *Angew. Chem. Int. Ed.*, 2002, **41**, 214-229.

26. P. Yang, D. Zhao, D. I. Margolese, B. F. Chmelka and G. D. Stucky, Chem. Mater., 1999, **11**, 2813-2826.
27. P. V. Braun, P. Osenar and S. I. Stupp, *Nature*, 1996, **380**, 325-328.
28. P. Yang, D. Zhao, D. I. Margolese, B. F. Chmelka and G. D. Stucky, *Nature*, 1998, **396**, 152-155.
29. U. Ciesla, S. Schacht, G. D. Stucky, K. K. Unger and F. Schüth, *Angew. Chem. Int. Ed.*, 1996, **35**, 541-543.
30. G. S. Attard, P. N. Bartlett, N. R. B. Coleman, J. M. Elliott, J. R. Owen and J. H. Wang, *Science*, 1997, **278**, 838-840.
31. G. S. Attard, J. M. Corker, C. G. Göltner, S. Henke and R. H. Templer, *Angew. Chem. Int. Ed.*, 1997, **36**, 1315-1317.
32. C. C. Landry, S. H. Tolbert, K. W. Gallis, A. Monnier, G. D. Stucky, P. Norby and J. C. Hanson, *Chem. Mater.*, 2001, **13**, 1600-1608.
33. C. J. Brinker and G. W. Scherer, *Sol-Gel Science: The Physics and Chemistry of Sol-Gel Processing*, Academic Press: New York, 1990.
34. A. C. Voegtlin, F. Ruch, J. L. Guth, J. Patarin and L. Huve, *Micro. Mater.*, 1997, **9**, 95-105.
35. J. M. Kim, Y.-J. Han, B. F. Chmelka and G. D. Stucky, *Chem. Commun.*, 2000, 2437-2438.
36. Q. Huo, D. I. Margolese, U. Ciesla, P. Feng, T. E. Gier, P. Sieger, R. Leon, P. M. Petroff, F. Schuth and G. D. Stucky, *Nature*, 1994, **368**, 317-321.
37. D. Zhao, J. Sun, Q. Li and G. D. Stucky, *Chem. Mater.*, 2000, **12**, 275-279.
38. C. Yu, J. Fan, B. Tian, D. Zhao and G. D. Stucky, *Adv. Mater.*, 2002, **14**, 1742-1745.
39. C. Yu, J. Fan, B. Tian and D. Zhao, *Chem. Mater.*, 2004, **16**, 889-898.
40. Q. Huo, D. I. Margolese and G. D. Stucky, *Chem. Mater.*, 1996, **8**, 1147-1160.
41. J. Patarin, B. Lebeau and R. Zana, *Current Opinion in Colloid & Interface Science*, 2002, **7**, 107-115.
42. B. L. Newalkar and S. Komarneni, *Chem. Mater.*, 2001, **13**, 4573-4579.
43. B. L. Newalkar, S. Komarneni, U. T. Turaga and H. Katsuki, *J. Mater. Chem.*, 2003, **13**, 1710-1716.
44. M. Kruk, M. Jaroniec, C. H. Ko and R. Ryoo, *Chem. Mater.*, 2000, **12**, 1961-1968.

45. F. Zhang, Yan, H. Yang, Y. YanMeng, C. Yu, B. Tu and D. Zhao, *J. Phys. Chem. B.*, 2005, **109**, 8723-8732.
46. R. van Grieken, G. Calleja, G. D. Stucky, J. A. Melero, R. A. GarcÃ-a and J. Iglesias, *Langmuir*, 2003, **19**, 3966-3973.
47. G. S. Attard, J. C. Glyde and C. G. Goltner, *Nature*, 1995, **378**, 366-368.
48. T. Yanagisawa, T. Shimizu, K. Kuroda and C. Kato, *Bull. Chem. Soc. Jpn.*, 1990, **63**, 988-992.
49. Q. Huo, D. I. Margolese, U. Ciesla, D. G. Demuth, P. Feng, T. E. Gier, P. Sieger, A. Firouzi and B. F. Chmelka, *Chem. Mater.*, 1994, **6**, 1176-1191.
50. B. Kesanli and W. Lin, *Chem. Commun.*, 2004, 2284-2285.
51. C. Nozaki, C. G. Lugmair, A. T. Bell and T. D. Tilley, *J. Am. Chem. Soc.*, 2002, **124**, 13194-13203.
52. T. J. Terry, G. Dubois, A. Murphy and T. D. P. Stack, *Angew. Chem. Int. Ed.*, 2007, **46**, 945-947.
53. H. Lakhiari, E. Legendre, D. Muller and J. Jozefonvicz, *J. Chromatogr. B:* 1995, **664**, 163-173.
54. J. E. Schiel, R. Mallik, S. Soman, K. S. Joseph and D. S. Hage, *J. Sep. Sci.*, 2006, **29**, 719-737.
55. J. Li, T. Qi, L. Wang, C. Liu and Y. Zhang, *Materials Letters*, 2007, **61**, 3197-3200.
56. C.-Y. Lai, B. G. Trewyn, D. M. Jeftinija, K. Jeftinija, S. Xu, S. Jeftinija and V. S. Y. Lin, *J. Am. Chem. Soc.*, 2003, **125**, 4451-4459.
57. K. Nozawa, C. Osono and M. Sugawara, *Sensors and Actuators, B: Chemical*, 2007, **126**, 632-640.
58. X. Wang, K. S. K. Lin, J. C. C. Chan and S. Cheng, *Chem. Commun.*, 2004, 2762-2763.
59. X. Wang, K. S. K. Lin, J. C. C. Chan and S. Cheng, *J. Phys. Chem. B.*, 2005, **109**, 1763-1769.
60. Q. Wei, Z. Nie, Y. Hao, Z. Chen, J. Zou and W. Wang, *Materials Letters*, 2005, **59**, 3611-3615.
61. C.-m. Yang, B. Zibrowius and F. Schuth, *Chem. Mater.*, 2003, 1772-1773.
62. R. Marschall, J. Rathousk and M. Wark, *Chem. Mater.*, 2007, **19**, 6401-6407.
63. Q. Wei, H.-Q. Chen, Z.-R. Nie, Y.-L. Hao, Y.-L. Wang, Q.-Y. Li and J.-X. Zou, *Materials Letters*, 2007, **61**, 1469-1473.

64. M. C. J. M. M. F. Frank Hoffmann, *Angew. Chem. Int. Ed.*, 2006, **45**, 3216-3251.
65. D. J. Macquarrie, *Chem. Commun.*, 1996, 1961-1962.
66. S. L. Burkett, S. D. Sims and S. Mann, *Chem. Commun.*, 1996, 1367-1368.
67. E. C. Fowler, S. L. Burkett and S. Mann, *Chem. Commun.*, 1997, 1769-1770.
68. M. H. Lim, C. F. Blanford and A. Stein, *J. Am. Chem. Soc.*, 1997, **119**, 4090-4091.
69. W. V. Rhijn, D. D. Vos, W. Bossaert, J. Bullen, B. Wouters, P. Grobet, P. Jacobs, F. B. C. D. S. G. L. Bonneviot and S. Kaliaguine, *Studies in Surface Science and Catalysis*, Elsevier, 1998, 183-190.
70. A. Corma, M. T. Navarro and F. Rey, *Chem. Commun.*, 1998, 1899-1900.
71. F. Babonneau, L. Leite and S. Fontlupt, *J. Mater. Chem.*, 1999, **9**, 175-178.
72. D. J. Macquarrie, D. B. Jackson, J. E. G. Mdoe and J. H. Clark, *New J. Chem.*, 1999, **23**, 539-544.
73. A. Bhaumik and T. Tatsumi, *Journal of Catalysis*, 2000, **189**, 31-39.
74. N. K. Mal, M. Fujiwara and Y. Tanaka, *Nature*, 2003, **421**, 350-353.
75. N. K. Mal, M. Fujiwara, Y. Tanaka, T. Taguchi and M. Matsukata, *Chem. Mater.*, 2003, **15**, 3385-3394.
76. H. C. Kolb, M. G. Finn and K. B. Sharpless, *Angew. Chem. Int. Ed.*, 2001, **40**, 2004-2021.
77. A. Dondoni, *Angew. Chem. Int. Ed.*, 2008, **47**, 8995-8997.
78. L. M. Campos, I. Meinel, R. G. Guino, M. Schierhorn, N. Gupta, G. D. Stucky and C. J. Hawker, *Adv. Mater.*, 2008, **20**, 3728-3733.
79. R. Huisgen, *Proc. Chem. Soc.*, 1961, 357-369.
80. H. C. Kolb and K. B. Sharpless, *Drug Discovery Today*, 2003, **8**, 1128-1137.
81. J. E. Moses and A. D. Moorhouse, *Chem. Soc. Rev.*, 2007, **36**, 1249-1262.
82. Y. L. Angell and K. Burgess, *Chem. Soc. Rev.*, 2007, **36**, 1674-1689.
83. S. Dedola, S. A. Nepogodiev and R. A. Field, *Org. Biomol. Chem.*, 2007, **5**, 1006-1017.
84. V. O. Rodionov, V. V. Fokin and M. G. Finn, *Angew. Chem. Int. Ed.*, 2005, **44**, 2210-2215.
85. V. O. Rodionov, S. I. Presolski, S. Gardinier, Y.-H. Lim and M. G. Finn, *J. Am. Chem. Soc.*, 2007, **129**, 12696-12704.

86. C. Nolte, P. Mayer and B. F. Straub, *Angew. Chem. Int. Ed.*, 2007, **46**, 2101-2103.
87. M. r. Ahlquist and V. V. Fokin, *Organometallics*, 2007, **26**, 4389-4391.
88. B. F. Straub, *Chem. Commun.*, 2007, 3868-3870.
89. B. R. Buckley, S. E. Dann, D. P. Harris, H. Heaney and E. C. Stubbs, *Chem. Commun.*, 2010, **46**, 2274-2276.
90. B. R. Buckley, S. E. Dann and H. Heaney, *Chem. Eur. J.*, 2010, **16**, 6278-6284.
91. S. S. Y. Chui, M. F. Y. Ng and C.-M. Che, *Chem. Eur. J.*, 2005, **11**, 1739-1749.
92. C. Chu and R. Liu, *Chem. Soc. Rev.*, 2011, **40**, 2177-2188.
93. H. Li, F. Cheng, A. M. Duft and A. Adronov, *J. Am. Chem. Soc.*, 2005, **127**, 14518-14524.
94. J. P. Collman, N. K. Devaraj and C. E. D. Chidsey, *Langmuir*, 2004, **20**, 1051-1053.
95. N. K. Devaraj, G. P. Miller, W. Ebina, B. Kakaradov, J. P. Collman, E. T. Kool and C. E. D. Chidsey, *J. Am. Chem. Soc.*, 2005, **127**, 8600-8601.
96. T. Lummerstorfer and H. Hoffmann, *J. Phys. Chem. B.*, 2004, **108**, 3963-3966.
97. X.-L. Sun, C. L. Stabler, C. S. Cazalis and E. L. Chaikof, *Bioconjugate Chem.*, 2005, **17**, 52-57.
98. Q. Wang, T. R. Chan, R. Hilgraf, V. V. Fokin, K. B. Sharpless and M. G. Finn, *J. Am. Chem. Soc.*, 2003, **125**, 3192-3193.
99. S. S. Gupta, J. Kuzelka, P. Singh, W. G. Lewis, M. Manchester and M. G. Finn, *Bioconjugate Chem.*, 2005, **16**, 1572-1579.
100. A. E. Speers, G. C. Adam and B. F. Cravatt, *J. Am. Chem. Soc.*, 2003, **125**, 4686-4687.
101. A. E. Speers and B. F. Cravatt, *Chem. Bio.*, 2004, **11**, 535-546.
102. N. J. Agard, J. A. Prescher and C. R. Bertozzi, *J. Am. Chem. Soc.*, 2004, **126**, 15046-15047.
103. J. A. Prescher and C. R. Bertozzi, *Nat Chem Biol*, 2005, **1**, 13-21.
104. S. Punna, E. Kaltgrad and M. G. Finn, *Bioconj. Chem.*, 2005, **16**, 1536-1541.
105. M. Slater, M. Snauko, F. Svec and J. M. J. Frechet, *Anal. Chem.*, 2006, **78**, 4969-4975.
106. Z. Guo, A. Lei, X. Liang and Q. Xu, *Chem. Commun.*, 2006, 4512-4514.

107. Z. Guo, A. Lei, Y. Zhang, Q. Xu, X. Xue, F. Zhang and X. Liang, *Chem. Commun.*, 2007, 2491-2493.

108. Z. Guo, Y. Jin, T. Liang, Y. Liu, Q. Xu, X. Liang and A. Lei, *J. Chromatogr. A*, 2009, **1216**, 257-263.

109. Q. Fu, Z. Guo, T. Liang, X. Zhang, Q. Xu and X. Liang, *Analytical Methods*, 2010, **2**, 217-224.

110. L. Yu, X. Li, Z. Guo, X. Zhang and X. Liang, *Chem. Eur. J.*, 2009, **15**, 12618-12626.

111. L. Moni, A. Ciogli, I. D'Acquarica, A. Dondoni, F. Gasparrini and A. Marra, *Chem. Eu. J.*, 2010, **16**, 5712-5722.

112. K. M. Kacprzak, N. M. Maier and W. Lindner, *Tetrahedron Letters*, 2006, **47**, 8721-8726.

113. Y. Wang, Y. Xiao, T. T. Yang Tan and S.-C. Ng, *Tetrahedron Letters*, 2008, **49**, 5190-5191.

114. M. D. Slater, J. M. J. Fréchet and F. Svec, *Journal of Separation Science*, 2009, **32**, 21-28.

115. W. H. Bragg and W. L. Bragg, *The Crystalline State*, Vol. 1, McMillan, New York, 1949.

116. S. Biz and M. L. Occelli, *Catalysis Reviews*, 1998, **40**, 329-407.

117. J. J. Bozzola, in *Electron Microscopy* John Wiley & Sons, Ltd, 2001.

118. J. W. Edington, *Practical electron microscopy in materials science*, Van Nostrand Reinhold Co. (New York), 1976.

119. D. E. Newbury, D. C. Joy, P. Echlin, C. E. Fiori and J. I. Goldstein, *Advanced Scanning Electron Microscopy and X-Ray Microanalysis*, Plenum Press, New York, 1986.

120. J. R. Fryer, *Chemical Applications of Transmission Electron Microscopy*, Academic Press, San Diego, 1979.

121. V. Alfredsson, M. Keung, A. Monnier, G. D. Stucky, K. K. Unger and F. Schuth, *J. Chem. Soc., Chem. Commun.*, 1994, 921-922.

122. J. M. Thomas, O. Terasaki, P. L. Gai, W. Zhou and J. Gonzalez-Calbet, *Acc. Chem. Res.*, 2001, **34**, 583-594.

123. Z. L. Wang, in *Characterization of Nanophase Materials*, Ed: Z. L. Wang, Wiley-VCH, Weinheim, 2000, Chapter 3, pp. 37-80.

124. R. Erni, M. D. Rossell, C. Kisielowski and U. Dahmen, *Physical Review Letters*, 2009, **102**, 096101.

125. M. Jaroniec, M. Kruk and J. P. Olivier, *Langmuir*, 1999, **15**, 5410-5413.

126. J. C. Groen, L. A. A. Peffer and J. Perez-Ramirez, *Micro. Meso. Mater.*, 2003, **60**, 1-17.

127. S. Brunauer, P. H. Emmett and E. Teller, *J. Am. Chem. Soc.*, 1938, **60**, 309-319.

128. M. Kruk, M. Jaroniec, S. Guan and S. Inagaki, *J. Phys. Chem. B.*, 2000, **105**, 681-689.

129. B. C. Smith, *Fundamentals of Fourier Transform Infrared Spectroscopy*, Second Edition, CRC Press, 2011.

130. R. Xu, W. Pang, J. Yu, Q. Huo and J. Chen, in *Chemistry of Zeolites and Related Porous Materials*, John Wiley & Sons, Ltd, pp. 467-601.

131. C. C. Freyhardt, M. Tsapatsis, R. F. Lobo, K. J. Balkus and M. E. Davis, *Nature*, 1996, **381**, 295-298.

132. W. W. Paudler, *Nuclear Magnetic Resonance: General Concepts and Applications*, John Wiley and Sons Inc., New York, 1987.

133. M. Mehring, *High Resolution NMR Spectroscopy in Solids*, Springer-Verlag, Berlin, 1976.

134. G. Engelhardt and D. Michel, *High-Resolution Solid-State NMR of Silicates and Zeolites*, John Wiley and Sons Ltd., Chichester, 1987.

135. G. Engelhardt, *Handbook of Heterogeneous Catalysis, Vol. 2, Eds: G. Ertl, H. Knozinger, J. Weitkamp*, Wiley-VCH, Weinheim, 1997.

136. V. D. Bock, H. Hiemstra and J. H. van Maarseveen, *Eur. J. Org. Chem.*, 2006, **2006**, 51-68.

137. D. A. Fleming, C. J. Thode and M. E. Williams, *Chem. Mater.*, 2006, **18**, 2327-2334.

138. S. Ciampi, T. Bocking, K. A. Kilian, J. B. Harper and J. J. Gooding, *Langmuir*, 2008, **24**, 5888-5892.

139. J. Nakazawa and T. D. P. Stack, *J. Am. Chem. Soc.*, 2008, **130**, 14360-14361.

140. C. Panda, M. Ghosh, T. Panda, R. Banerjee and S. Sen Gupta, *Chem. Commun.*, 2011, **47**, 8016-8018.

CHAPTER 2

"Clickable" Mesoporous Materials

CHAPTER 2

Part A

Synthesis and Characterization of "Clickable"

SBA-15 Mesoporous Materials

2A.1 Introduction

Surface functionalized mesoporous materials have emerged as one of the most important areas of research in the field of advanced functional materials.[1-3] They have found wide spread applications in catalysis,[4-6] separation,[7, 8] decontamination,[9] drug delivery[10] and sensor design.[11] In particular, mesoporous siliceous matrices like SBA-15 are ideal candidates for functionalization due to their high hydrothermal stability, larger pore sizes (~ 90-100Å) and thicker walls that can be easily functionalized using simple silanol chemistry.[12, 13] SBA-15 has been functionalized by various organic functional groups. These include amines,[13, 14] thiols,[15] carboxylic acid,[16] sulfonic acid, [17] vinyl[18] and nitrogen based heterocycles.[9] In general, formulation of a siliceous SBA-15 with covalently linked functional groups can be designed using two different synthetic strategies for surface modification. These are post-synthesis modification (also known as grafting) and direct synthesis or co-condensation.[1, 19] Grafting involves covalent attachment of organic functional groups onto the surface of the mesoporous material by the reaction of a suitable functional group bearing organosilane. In contrast, direct synthesis or co-condensation involves modification of the surface in a single step, typically by co-condensation of organosilane with the silica precursor in presence of a liquid crystalline template. Both methods have their respective advantages and drawbacks. The most significant advantage of the co-condensation method over the grafting method is the uniform distribution of organic groups on the surface of SBA-15, and higher loading of organic functionalities without reducing the pore size of SBA-15. The functional groups installed by such modifications can be used to anchor various synthetic catalysts, biomolecules and polymers to generate novel functional materials.

Development of mesoporous material based biocatalysts[20- 23] and biosensors[11] have attracted a lot of attention currently. Most of these materials have been prepared by immobilization of the enzymes into the pores of the mesoporous channels by physical adsorption.[24, 25] Although simple and efficient, this process is severely limited by the fact that with time, the proteins or enzymes leach out into the solution. To overcome this, enzymes have been covalently immobilized by chemically attaching them to an organo-functionalized mesoporous material bearing aldehyde or amine functional groups. Most of the effort has been directed towards cross linking the amine side-chain of the lysine to the aminopropyl group of modified mesoporous

materials via glutaraldehyde.[26, 27, 28] For example, Wang *et. al.* have covalently immobilized trypsin to a propanal modified SBA-15 via the imine forming reaction.[28] Both these methods have severe limitations, primarily due to limited control of the spatial orientation of the immobilized enzyme within the pores. For example, the orientation of the immobilized enzyme may be such that the active site faces the wall of the mesopore. This would make the enzyme ineffective and indeed be an obstacle in the development of such materials. Hence, there is a need to generate functional mesoporous materials which can provide a platform to perform bio-orthogonal chemoselective ligation.[29] This would provide spatial control over the molecule, such that it may be attached to the silica support at the desired orientation.

The recent discovery of the Cu(I)-catalyzed 1,3-dipolar cycloaddition of organic azides to alkynes has provided the most powerful "click chemistry" tool for conjugation between appropriately functionalized binding partners via an 1,2,3-triazole linkage.[30] The favorable thermodynamics, exceptionally high yields, ease and compatibility with a broad repertoire of functional groups has led to numerous applications of Cu(I)-catalyzed azide-alkyne click chemistry (CuAAC) reaction in various fields of organic, medicinal, polymer, materials and biological chemistry.[31- 33] CuAAC has been successfully used to functionalize metal nanoparticles,[34] single-walled carbon nanotubes,[34] powdered silica,[35, 36] and mesoporous silicon rugate filters.[37] Importantly, one of the most promising applications of this reaction has been in bioconjugation reactions where it has been shown to be much more effective than traditional methods.[38] Therefore, synthesis of azide containing SBA-15 materials would be very useful in the development of functional materials. The presence of an organic azide on SBA-15 gives a handle to anchor various moieties such as enzymes and catalysts via this chemoselective ligation. This study reports the synthesis and characterization of an SBA-15 mesoporous material containing a clickable azide group, and demonstrates its reactions with a number of functional organic molecules bearing alkyne functionality using CuAAC. These materials were characterized by using FT-IR, powder XRD, SEM, TEM, Multinuclear (^{13}C, ^{29}Si) solid state NMR, and BET analysis. Further, this study discusses the binding of fluorescein-labeled protein concanavalin-A to SBA-15 conjugated with mannose.

2A.2 Experimental section

2A.2.1 Materials

Tetraethylorthosilicate (TEOS), 3-chloro-propyltriethoxysilane (Cl-PTES), propargyl alcohol, phenyl acetylene, fluorescein labeled concanavalein A, pent-4-ynoic acid, propargyl amine and ferrocenecarboxylic acid were obtained from Sigma Aldrich. Polyethelene glycol monomethyl ether (PEG, average molecular weight 1000) was obtained from fluka. $CuSO_4$, sodium ascorbate and D-(+)-mannose were obtained from Merck, India. All the chemicals used were of extra pure for biochemistry or of analytical grade and used as received.

2A.2.2 Syntheses

2A.2.2.1 Synthesis of 3-azidopropyltriethoxysilane

3-azidopropyltriethoxysilane was prepared by following the procedure repoted Pichon et al.[39] 3-chloropropyltriethoxysilane (abbreviated as Cl-PTES; 2 g, 8.3 mmol) was added to a solution of sodium azide (1.08 g, 16.6 mmol) and tetrabutylammonium bromide (0.644 g, 2 mmol) in dry acetonitrile (50 mL), under nitrogen atmosphere. The reaction mixture was stirred under reflux for 18 h. After completion of the reaction, the solvent was removed under reduced pressure. The crude mixture was diluted in n-pentane and the suspension was filtered over Celite. Solvent was removed from the resulting filtrate and the crude oil obtained was distilled under reduced pressure of 0.025 mbar at 62°C to give AzPTES (3-azidopropyltriethoxysilane) as a colorless liquid. Yield: 1.52 g, 74%. ^{1}H NMR (500 MHz, $CDCl_3$): δ 0.66 (t, 2H, J= 8.25 Hz), 1.21 (t, 3H, J= 6.88 Hz), 1.66-1.73 (m, 2H), 3.25 (t, 2H, J = 7.16 Hz), 3.80 (q, 2H, J = 6.88 Hz). ^{13}C NMR (50 MHz, $CDCl_3$) δ 7.59, 18.23, 22.64, 53.8, 58.41. FT-IR (NaCl, cm^{-1}): 2098 ($-N=N^+=N^-$, s)

2A.2.2.2 Synthesis of methyl pent-4-ynoate

Methyl pent-4-ynoate was prepared by following procedure reported by Marshall et al.[40] To a solution of 4-pentynoic acid (0.2 g, 2.04 mmol) in dry methanol (3 mL) was added p-toluenesulphonic acid (40 mg, 0.023 mmol) under nitrogen atmosphere. The reaction mixture was stirred under reflux for 6-7 h. Upon cooling of the reaction mixture to RT, 15 mL of water was added and pH of the resulting mixture

was brought to 10 by adding sodium bicarbonate solution. It was then extracted with three portions of 20 mL of ethyl acetate. The ethyl acetate layer was washed with water and brine solution respectively and then dried over anhydrous sodium sulphate. Finally, solvent was removed under reduced pressure to yield a colorless liquid. Yield: 205 mg, 90%. ^{1}H NMR (200 MHz, $CDCl_3$): δ 3.67 (s, 3H), 2.562-2.44 (m, 4H) and 1.97 (t, J=2.5Hz, 1H); ^{13}C NMR (50 MHz, $CDCl_3$): δ 172.1, 82.4, 68.9, 51.7, 33.1, and 14.2.

2A.2.2.3 Synthesis of α-D-propargyl mannopyranoside

α-D-propargyl mannopyranoside was synthesized by a procedure described before.[41] A mixture of D-mannose(1) (1g, 5.56mmol) and propargyl alcohol (1.56ml, 27.80mmol) was taken in a two-necked round bottom flask and kept under nitrogen atmosphere. H_2SO_4-Silica was added from the side and the mixture was continuously stirred for 5 hours while maintaining a temperature of 65°C. α-D-propargyl mannopyranoside was finally purified by column chromatography (silica gel, eluent 95:5 EtOAc:MeOH). Yield: 0.864 g, 71%

The α-D-propargyl mannopyranoside was characterized as its α-D-tetra-O-acetyl-propargyl mannopyranoside derivative. α-D-propargyl mannopyranoside (0.10g, 0.5mmol) and pyridine (0.34ml,4.14mmol) was stirred in a two-neck round bottom flask at 0-5°C. Acetic-anhydride (0.2ml, 2.07mmol) was then slowly added and the reaction mixture was stirred at 0-5 °C for 15-20 min. Finally, catalytic amount of 4-dimethylaminopyridine (5-10mg) was added and the reaction was allowed to proceed for 10-12 hours. The reaction mixture was diluted with 15-20 mL of ethyl acetate and sequentially washed with 1(N) HCl, saturated $NaHCO_3$ solution, water and finally by brine solution. The ethyl acetate layer was dried using anhydrous Na_2SO_4 and the solvent was removed under reduced pressure to yield a white solid which was further purified by column-chromatography (eluent, light petroleum ether and ethyl acetate, 4:1) to yield pure α-D-tetra-O-acetyl-propargyl mannopyranoside. Yield = 0.141 g, 80%. [α]D=+38 (C=1.6,$CHCl_3$); ^{1}H NMR(200 MHz, TMS in $CDCl_3$):δ 5.35-5.25 (m,3H), 5.04(d, *J* =1.4Hz,1H), 4.35-4.26 (m,3H),4.11 (dd, *J* =12.3 Hz, 1H), 4.06-3.99 (m,1H), 2.48 (t, *J* =2.5 Hz, 1H), 2.17 (s, 3H), 2.12 (s, 3H), 2.05 (s, 3H), 2.00 (s, 3H) ppm. ^{13}C NMR (50 MHz, $CDCl_3$):δ 170.6, 170.0, 169.8, 169.7, 96.2, 77.9, 75.6, 69.3, 68.9 (2C), 65.9, 62.3, 54.9, 20.8, 20.7, 20.6(2C) ppm

2A.2.2.4 Synthesis of propargyl ferrocenecarboxamide

Propargylferrocenecarboxamide was prepared by following similar procedure reported in the literature.[42] To a stirred solution of ferrocene carboxylic acid (200 mg, 0.87 mmol) in dry DCM (20 mL) was added 1-hydroxybenzotriazole (HOBt, 149 mg, 0.97 mmol) at 0-5 ˚C under inert atmosphere. After 5 minutes, EDC.HCl (200 mg, 1.04 mmol) was added to the reaction mixture and stirring was continued for another 30 minutes. During this time the solution changed color from orange to red. After 30 minutes, propargyl amine (61 µL, 0.95 mmol) was added and the reaction mixture was allowed to stir for 20 h at room temperature. After completion of reaction, the mixture was sequentially washed with 3M HCl (15 mL), saturated $NaHCO_3$ solution (2 x 15 mL) and brine solution (15 mL). Finally, the organic layer was dried over anhydrous sodium sulphate and evaporated under reduced pressure to obtain orange red colored crude product, which was further purified by column chromatography by eluting with 0-10% methanol in DCM. Yield: 195 mg, 84%. ^{1}H NMR(200 MHz, $CDCl_3$):δ (ppm) 1.71 (s, 1H), 2.27 (t, 1H), 4.14-4.36 (m, 9H), 4.69 (t, 2H).

2A.2.2.5 Synthesis of azide functionalized SBA-15

2A.2.2.5.1 Post synthesis grafting method

SBA-15 material was synthesized by following a procedure reported by Zhao *et al*.[12] with slight modifications. In a typical batch synthesis, 8 g of the nonionic block copolymer Pluronic P123 was taken in a polypropylene beaker and 60 mL distilled deionized water was added to it. The mixture was stirred thoroughly using an overhead stirrer (with teflon blades) for 4 h to dissolve the gel completely. To this solution, 240 mL of HCl (2 N) were added drop wise, and the reaction mixture was allowed to stir for another 1 h at ambient temperature (~301-303 K). The temperature of the mixture was then raised to 313 K and it was allowed to proceed for another hour. To this warm mixture, tetraethylorthosilicate (TEOS, 18 g, 86.4 mmol) were added drop wise with vigorous stirring. Upon the completion of addition, the mixture was allowed to stir for 24 h while maintaining the temperature at 313 K. The synthesis gel thus formed was then loaded in a 500 mL polypropylene bottle, sealed using teflon tape and kept at 373 K for 48 h under static condition. After this, the bottle was removed from the oven, and then allowed to cool to ambient temperature. The contents were then filtered and the residue was washed with copious amount of water

until the pH of the water became neutral. The white solid was allowed to dry in air, and then crushed in a mortar-pestle. Calcination of the as-synthesized solid material was done at 773 K for 6 h in air using a slow heating ramp of 1 degree per minute. The sample was cooled to ambient temperature and preserved under argon atmosphere for further use. (Yield: ~ 4.7 g) This material will be represented as CAL-SBA.

To a suspension of 1 g of CAL-SBA in 50 mL of toluene, 2 mL AzPTES was added and the mixture was stirred for 16 h at 80°C under nitrogen atmosphere. After the completion of reaction, the contents were cooled, filtered and washed with toluene until it became free from AzPTES. The sample was then dried at 80°C for 8h in a vacuum oven and preserved under argon atmosphere for further use. Yield: ~1.2 g. This material will be referred as AZP-SBA-G. Elemental analysis (%): C: 7.56; H: 1.52; N: 8.12.

2A.2.2.5.2 One pot co-condensation method (Direct method)

For the functionalization of SBA-15 using the one-pot co-condensation technique, the typical synthesis of SBA-15 as described previously was modified following the strategies described by Wang *et. al.*[14] The composition of the synthesis gel was 0.9 TEOS: 0.1 AzPTES: 6.1 HCl: 0.017 P123: 165 H_2O. In a typical synthesis batch, 4 g of Pluronic P123 was dissolved in 30 mL H_2O for 4 h, to this 120 mL of 2N HCl was added and stirred for another 1 h at ambient temperature. The temperature was raised to 313 K and the mixture was stirred at 313 K for further 2 h. Then 8.1 g TEOS was added drop wise and the mixture was allowed to prehydrolyze for 3 h before the addition of 1.1 g of AzPTES, after which it was allowed to stir for a total of 24h (including pre hydrolysis) at 313 K. The mixture was transferred to a 250 mL polypropylene vessel and heated at 373 K for 48 h under static conditions. The contents were cooled, filtered, washed with water and dried. The white solid was then refluxed in ethanol for 24 h (200 mL ethanol per 1.5 g of solid), filtered and dried to get the azide-functionalized SBA-15. Yield: ~ 2.9 g. This material will be referred as AZP-SBA-C. Elemental analysis (%): C: 5.45; H: 1.12; N: 5.53.

2A.2.2.6 Modification of azide functionalized SBA-15 by Cu (I) catalyzed azide-alkyne cycloaddition reaction (CuAAC)

For CuAAC, the azide functionalized SBA-15 (AZP-SBA-C or AZP-SBA-G) was incubated with 3 equivalents of the corresponding alkyne (**1-5**, see Scheme 2A.2) in 1:1 water/t-butanol mixture containing $CuSO_4$ (1 equivalent) and sodium ascorbate (4 equivalent). In a typical click reaction, AZP-SBA-C (300 mg, 0.395 mmol of azide) was incubated with propargyl alcohol (70.07 µL, 1.185 mmol) in 10 mL of t-BuOH/water (1:1) containing sodium ascorbate (156.42 mg, 0.790 mmol) and copper sulfate (98.75 mg, 0.395 mmol). The mixture was stirred for 12 h and another 156.42 mg (2 equivalents) of sodium ascorbate was added. The reaction mixture was then incubated for further 12 h. After completion of reaction, the reaction mixture was centrifuged and the residue was first washed with water twice and then sequentially washed with 0.1 M N,N-diethyldithiocarbamate sodium (15 mL), methanol (15 mL) and acetone (15 mL) respectively. The last three washings were repeated thrice. Finally, the faint yellowish white powder obtained was dried at 80°C in vacuum oven for 6-8 h. Yield: ~250 mg.

Note: Click reaction with α-D-propargyl mannopyranoside was carried out in water medium.

2A.2.2.7 Conjugation of mannose functionalized SBA-15 with fluorescein labeled concanavalin A

10 mg of mannose labeled SBA-15 (SBA-C-**5**, see Table 2A.1) or alcohol labeled SBA-15 (SBA-C-**1**, see Table 2A.1) was incubated with fluorescently labeled concanavalin-A (300µL, 1 mg/mL) in 20 mM Tris-HCl buffer (pH 7.4) containing 0.1 mM $MnCl_2$, 0.1 mM $CaCl_2$ and 0.15 M NaCl. After incubation for 30 min both samples were washed extensively (3 times) with the above mentioned buffer. The samples were dispersed in the buffer, and put under a microscope under both bright-field and epi-fluorescence modes (with a 470-490 nm bandpass filter).

2A.2.3. Analytical and characterization methods

Powder X-ray diffraction of all the samples was carried out in a PANalytical X'pert Pro dual goniometer diffractometer. A proportional counter detector was used for low angle experiments and an X'celerator solid state detector was employed in the

low angle experiments. The radiation used was Cu Kα (1.5418Å) with a Ni filter and the data collection was carried out using a flat holder in Bragg–Brentano geometry (0.5 to 5°; 0.2° min^{-1}). Care was taken to avoid sample displacement effects. SEM images were obtained on Leica Stereoscan 440 microscope. HR-TEM images were taken on a FEI Technai F30 operating at 300 kV with FEG. The samples were prepared by dispersing a large number of solid particles in acetone by sonication, and dropping the resulting suspension on a copper grid of 400 mesh and allowed to dry in air. Nitrogen adsorption and desorption studies were carried out at 100°C using Micromeritics instrument. Samples were preheated at 100°C for 12 hours in the vacuum line. Single point BET surface area was obtained from the nitrogen adsorption-desorption data at P/P_0 ~0.249. Pore size distributions were calculated using the BJH method. Semi-quantitative FT-IR spectra were recorded on Perkin Elmer FT-IR spectrum GX instrument by making KBr pellets. Pellets were prepared by mixing 3 mg of sample with 97 mg of KBr. Yields for AACC reactions were calculated from corrected area under the curve characteristic for the azide stretch at ~2100 cm^{-1}. The average of three values was used for all calculations. Qualitative FT-IR spectra were recorded on a Perkin-Elmer spectrometer in the diffuse reflectance mode operating at a resolution of 4 cm^{-1}. Elemental analyses were carried out on Thermo Finnigan FLASH EA 1112 series instrument.

Solid-state NMR: ^{29}Si and ^{13}C Cross Polarization Magic Angle Spinning (CPMAS) NMR experiments were carried out on a Bruker AVANCE 300 wide bore spectrometer equipped with a superconducting magnet with a field of 7.1Tesla. The operating frequencies for ^{13}C and ^{29}Si were 300MHz, 75.4MHz and 59.6MHz respectively. The samples were packed into a 4mm zirconia rotor and loaded into a 4mm BL MAS probe and spun about the magic angle (54.74) at 10KHz using a standard ramp-CP pulse sequence was used for both the experiments. The RF-powers were 50kHz and 60kHz for the ^{29}Si and ^{13}C CPMAS experiments. The contact times were 6ms and 3ms for the ^{29}Si and the ^{13}C CPMAS experiments. All the chemical shifts were referenced to TMS. Typically 10,000 to 25,000 scans with a recycle delay of 3s were collected depending on the sensitivity of the sample.

Epifluorescence Microscopy: Bright-field transmittance and epi-fluorescence microscopy was performed on samples that were drop-cast on glass cover slips. A 150mW Xe Lamp and a 100mW Halogen lamp attached to an inverted microscope

(Nikon 2000U) was used as light source to excite the samples for bright-field and epi-fluorescence modes, respectively, in order to show that the concentrations of the samples near the surface were approximately the same and the same areas were probed in both the imaging methods. For epifluorescence microscopy, proper excitation filters (470-490 nm bandpass filter, Chroma) were chosen to excite fluorescein. A Plan Apo 0.6 NA 40X air-objective was used to collect the fluorescence (500-580 nm emission filter, Chroma), which was subsequently imaged using a color digital camera (Nikon 4500) equipped with a 10X eyepiece and a home-built microscope adapter. For brightfield images, the exposure time was set at 30 ms, while the epi-fluorescence images were captured at lower excitation powers at 250 ms exposure to avoid photobleaching of samples. The images were processed using NIH ImageJ image analyses software and the raw data for both the sample and the control were adjusted to the same brightness and contrast levels to insure that the stark contrast in clearly visible in the electronic format.

2A.3 Results and discussions

2A.3.1 Synthesis strategy of azide functionalized SBA-15

The azide functionalized SBA-15 was synthesized by both one-pot co-condensation and post-synthetic grafting method as presented in the Scheme 2A.1. During the synthesis of AZP-SBA-C via one-pot co-condensation, the ratio of TEOS and AzPTES was kept as 9:1 since the usage of higher amounts of organosilica precursor may lead to functionalized materials with lesser long range order.[14] The organosilica precursor AzPTES was obtained by the displacement of the chloro-group in 3-chloropropyltriethoxysilane with azido group using sodium azide. In the post-synthetic grafting method, the 1 g of calcined SBA-15 (CAL-SBA) was reacted with 8.1 mmol of AzPTES in toluene at 80°C under inert atmosphere to synthesize AZP-SBA-G. The amount of azidopropyl group that was incorporated into the SBA-15 framework was determined by elemental analysis. The concentration of azide was found to be 1.9 mmol/g for AZP-SBA-G while that for AZP-SBA-C was found to be 1.3 mmol/g. Therefore, during co-condensation, approximately 85 % of AzPTES added was incorporated into the silica framework of AZP-SBA-C. The amount of azide incorporated in these materials were estimated to be twice when HPLC grade silica beads[35] were used as the support matrix. The structure and morphology of AZP-

SBA-C and AZP-SBA-G was established unambiguously using XRD, TEM, SEM, NMR and N_2 adsorption-desorption studies.

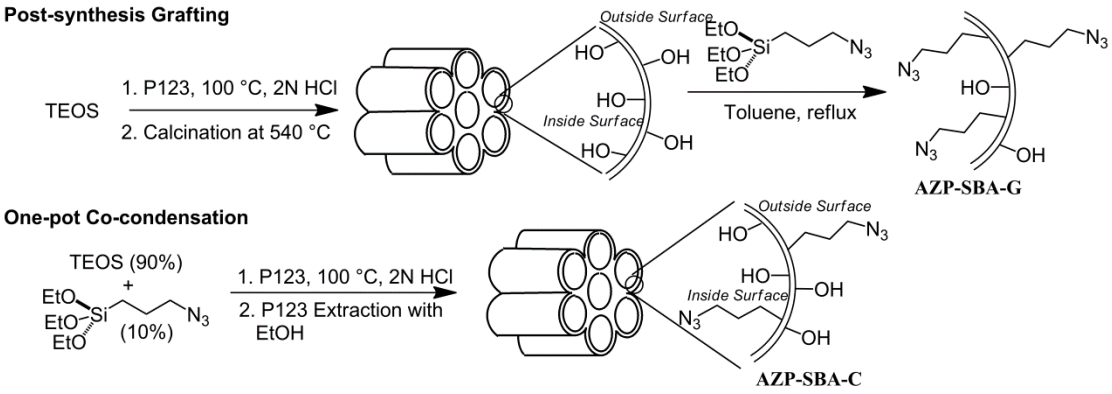

Scheme 2A.1: Synthesis of Azide functionalized SBA-15 materials

2A.3.2 Modification of azide functionalized SBA-15 by Cu (I) catalyzed azide-alkyne cycloaddition (CuAAC) reaction

The azidopropyl labeled silica AZP-SBA-C and AZP-SBA-G were subjected to Cu(I) catalyzed azide alkyne cycloaddition (CuAAC) reaction with various organic substrates (Scheme 2A.2). Propargyl alcohol (**1**) was used as the substrate during the initial experiments to optimize the reaction conditions. The CuAAC was attempted using $CuSO_4$/ascorbate in a mixture of t-BuOH and water. For example, treatment of AZP-SBA-C (25 mg) with **1** (0.1 mmol, 3-fold molar excess with respect to azide groups on azidopropyl grafted silica) using $CuSO_4$/ascorbate in 1:1 H_2O/t-BuOH (1:1) for 24 h converted 85% of the available azide groups into the corresponding triazole product, SBA-C-**1** (Table 2A.1). Control reactions performed without the usage of $CuSO_4$ showed no conversion of the azide. After the reaction, an extensive washing protocol was followed to remove the Cu(I), ascorbate and any unreacted **1**. One of the key steps in the washing was the usage of dithiocarbamate to remove the Cu(I), as reported earlier.[43] Attempt to remove copper by using other chelating reagents like pH 8 Na_2EDTA lead to the loss of a significant amount of the SBA-15 material indicating that a part of the silica had leached out during this process. Use of higher amounts of catalyst and longer reaction times did not improve the yield of the reaction. The extent of the reaction was estimated using FT-IR spectroscopy, by monitoring the decrease in the integrated intensity of the $\nu_{as}(N_3)$ at 2100 cm^{-1} (Figure 2A.6d, Table 2A.1)

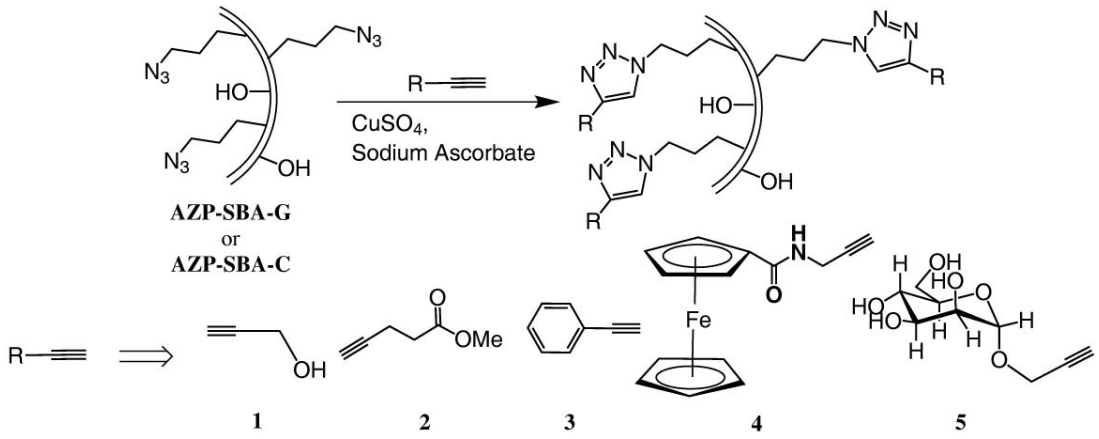

Scheme 2A.2: CuAAC reaction of Azide-functionalized SBA-15 with various substrates

CuAAC was then extended to other substrates to explore the efficiency of this reaction on azidopropyl functionalized SBA-15 (Scheme 2A.2). The reaction was carried out with five fold excess of methyl pent-4-ynoate (**2**), phenylacetylene (**3**), propargyl ferrocenecarboxamide (**4**) and α-D(+)-propargyl mannopyranoside (**5**) as substrates. The extent of the click reaction as observed using FT-IR spectroscopy is shown in Table 2A.1.

Table 2A.1: Yield of CuAAC reaction with different substrates

Mesoporous Material	**Alkyne substrate**	**Product**	**CuAAC reaction yield (%)**
AZP-SBA-C	Propargyl alcohol (**1**)	SBA-C-**1**	85
	Methyl pent-4-ynoate (**2**)	SBA-C-**2**	75
	Phenylacetylene (**3**)	SBA-C-**3**	63
	Propargyl ferrocenecarboxamide (**4**)	SBA-C-**4**	58
	α-D(+)-propargyl mannopyranoside (**5**)	SBA-C-**5**	55
AZP-SBA-G	Propargyl alcohol (**1**)	SBA-G-**1**	90
	Methyl pent-4-ynoate (**2**)	SBA-G-**2**	85
	Phenylacetylene (**3**)	SBA-G-**3**	82
	Propargyl ferrocene carboxamide (**4**)	SBA-G-**4**	78
	α-D(+)-propargyl mannopyranoside (**5**)	SBA-G-**5**	79

All the substrates were successfully incorporated into the azido functionalized SBA-15 by CuAAC. The conversion of available azides was less for propargyl ferrocenecarboxamide, phenylacytelene and α-D(+)-propargyl mannopyranoside than for propargyl alcohol. There may be several factors responsible for this observation. One of them is that propargyl alcohol, a much smaller molecule, is accessible to more azides during the click reacton.

The dependence of the substrate concentration for the conversion of the available azide groups on AZP-SBA-G or AZP-SBA-C by CuAAC is shown in Figure 2A.1. Treatment of AZP-SBA-G (100 mg) with 1.5 equivalents of propargyl alcohol lead to the formation of SBA-C-**1** in which 90% of all available azides were converted to the triazole (Table 2A.1). Similar results were obtained with AZP-SBA-C although 3 equivalents of propargyl alcohol were needed to convert 85% of the available azides (Figure 2A.1). The very high extent of the reaction leads us to conclude that in AZP-SBA-C, most azides are present in the surface of SBA-15. This data is in contrast to amino grafted SBA-15 material that has been synthesized by co-condensation with aminopropyltriethoxysilane.[44] In this material it has been observed that only 25% of the available amino groups are on the surface. Since the azidopropyl group is more hydrophobic than the protonated aminopropyl group, it can act as a co-surfactant and be solubilized by the Pluronic micelles leading to its presence in the micelle-silica interface. The presence of the azides at this interface during synthesis is probably the reason for its high density at the surface of AZP-SBA-C. The presence of the azides mostly on the surface of AZP-SBA-C coupled with the very high efficiency of the CuAAC reaction makes AZP-SBA-C a very attractive material for attachment of alkyne containing functional molecules. It should also be noted that the percentage of available azide for click reaction is more in AZP-SBA-G than in AZP-SBA-C. This can be explained by the fact that during the direct synthesis of AZP-SBA-C by co-condensation, some of the azides may be trapped in the wall and therefore can be unavailable for conjugation.

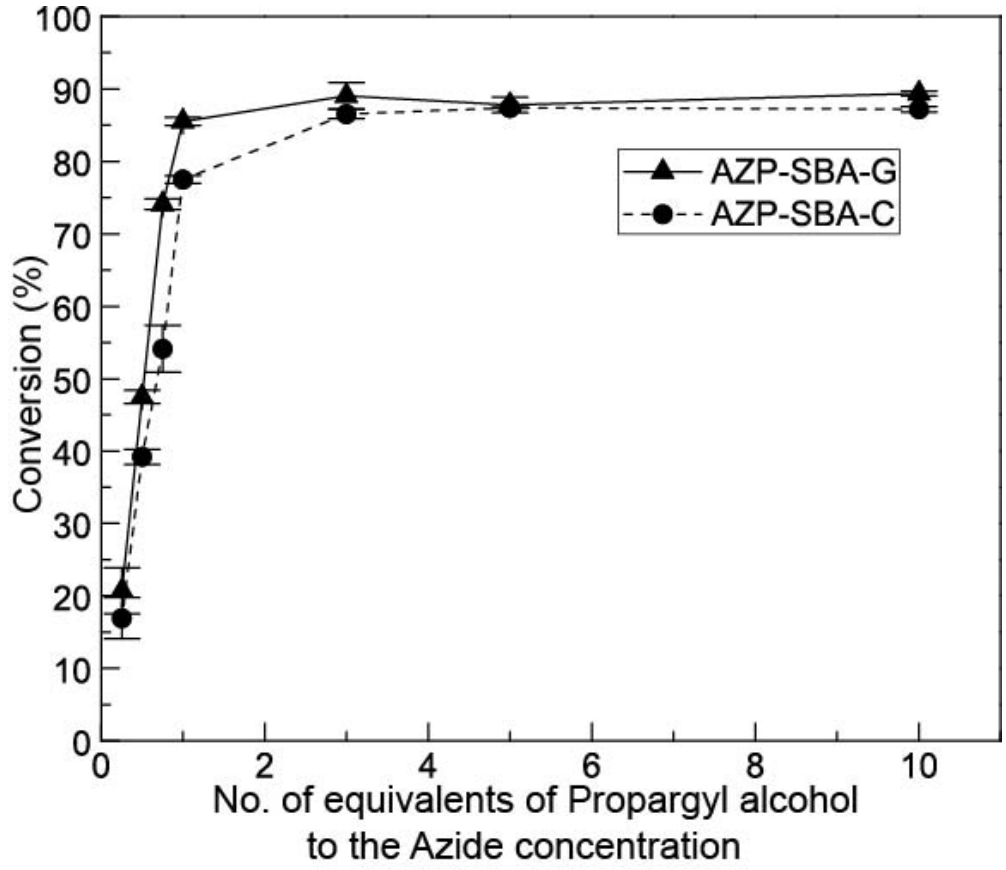

Figure 2A.1: Dependence of the percentage of azide converted in AZP-SBA-C or AZP-SBA-G on propargyl alcohol concentration.

2A.3.3 Characterizations

2A.3.3.1. Powder X-ray diffraction

The powder XRD patterns diiferent SBA-15 mesoporous materials are shown in Figures 2A.2 and 2A.3. All of the materials showed the characteristic high intensity 100 peak near the 2θ value of 1º. The other significant peaks corresponding to (110) and (200) diffractions were also observed indicating that well-ordered one-dimensional hexagonal mesoporous channels of SBA-15 were formed and remained intact under the functionalization environment. However, the higher order (110) and (200) diffractions become significantly less resolved for the azide-functionalized samples AZP-SBA-G (Figure 2A.2b) and AZP-SBA-C (Figure 2A.3a), showing that the long-range order decreases slightly upon incorporation of azidopropyl groups into the SBA-15 matrix. A similar phenomenon has been observed in aminopropyl-functionalized SBA-15 by Wang and co-workers.[14] The powder XRD patterns of click products obtained by clicking propargyl alcohol (**1**) with AZP-SBA-G and

AZP-SBA-C are also presented in figures 1 and 2 respectively. The XRD patterns showed one intense (100) peak diffraction in the proximity of $2\theta = 1°$, indicating well-ordered hexagonal arrays and showing that the mesoporosity of the material does not change after undergoing CuAAC reaction (Figure 2A.2c and 2A.3b).

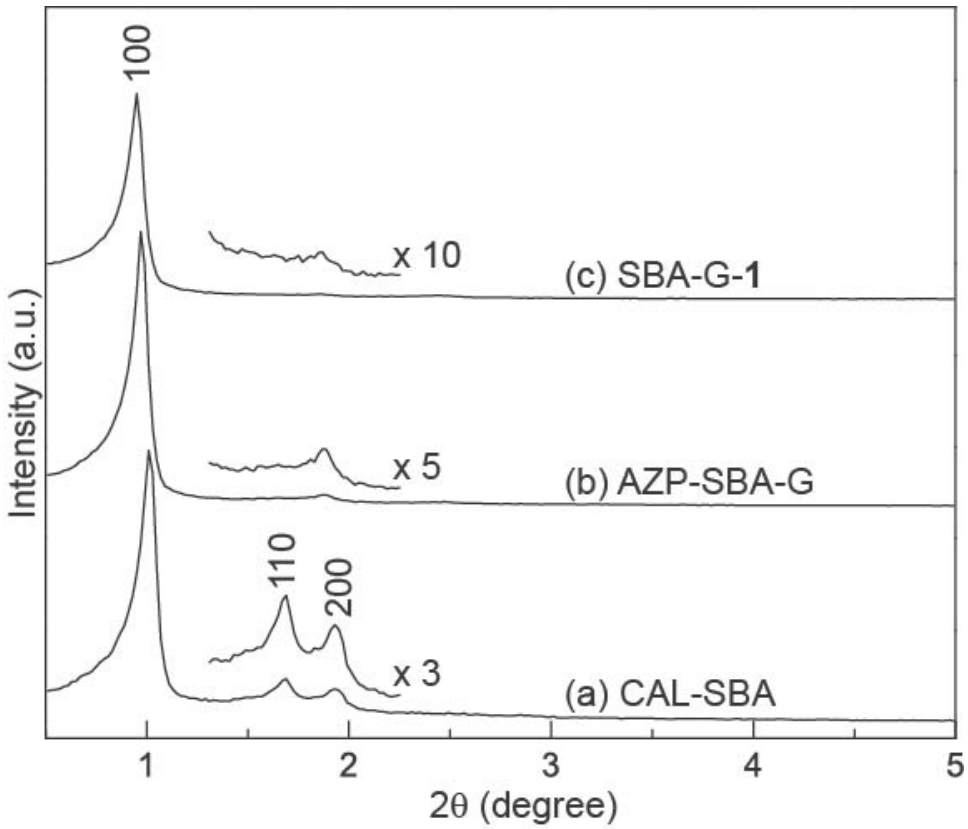

Figure 2A.2: Powder XRD patterns of different SBA-15 samples via post-synthesis grafting (a) CAL-SBA; (b) AZP-SBA-G; (c) SBA-G-1.

The XRD patterns of the products SBA-G-**1** and SBA-C-**1** formed upon reaction of click reaction with propargyl alcohol (**1)** are shown in Figure 2A.2c and 2A.3b respectively. Both the materials displayed intense (100) diffraction peak in the proximity of $2\theta = 1°$ similar to their parent azide functionalized SBA-15, indicating well-ordered hexagonal arrays and showing that the material remained intact and the mesoporosity of the material does not change after undergoing CuAAC reaction and its workup.

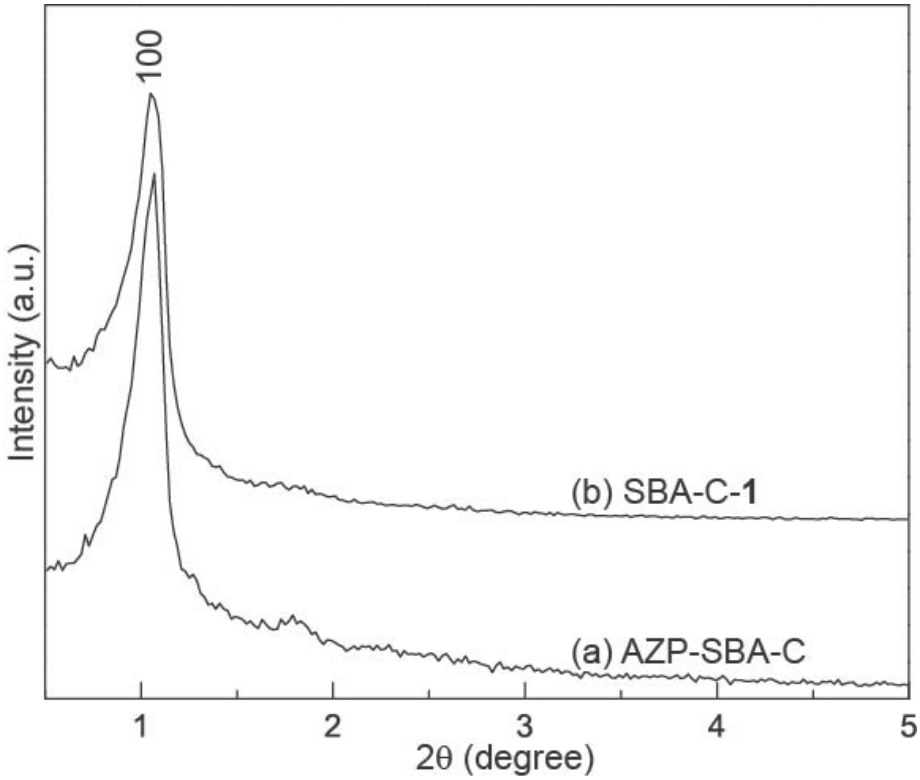

Figure 2A.3: Powder XRD patterns of different SBA-15 samples via co-condensation (a) AZP-SBA-C; (b) SBA-C-1

2A.3.3.2 Scanning and transmission electron microscopy

Scanning electron microscopy (SEM) and transmission electron microscopy (TEM) images of AZP-SBA-G and AZP-SBA-C are displayed in Figure 2A.4. The SEM images of both the AZP-SBA-G and AZP-SBA-C materials indicate formation of highly dispersed wormlike external morphology having a particle size of about 1 μm (Figure 2A.4a and 2A.4c respectively). The TEM micrographs showed the long parallel channel-structure with thick walls of the mesoporous materials AZP-SBA-G and AZP-SBA-C (Figure 2A.4b and 2A.4d respectively). The SEM and TEM pictures indicate that the morphology and the mesoporosity were retained in both the azide grafted SBA-15 materials. Hence both the grafting and co-condensation technique did not interfere with the structural properties of SBA-15.

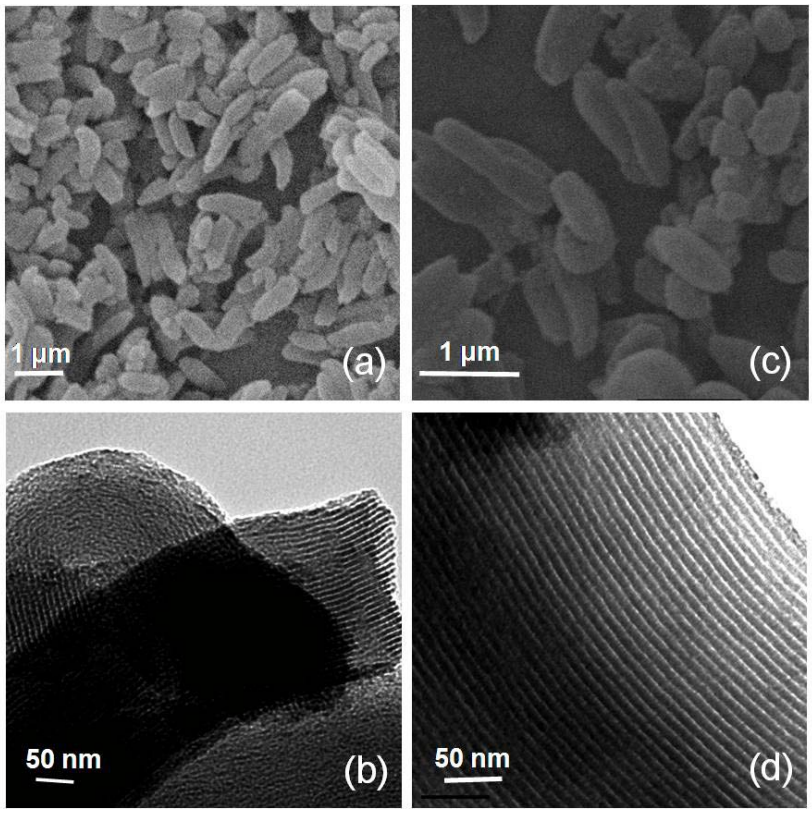

Figure 2A.4: SEM images and TEM micrographs respectively of different azido-functionalized SBA-15 materials.(a) & (b) for AZP-SBA-G; (c) & (d) for AZP-SBA-C

2A.3.3.3 Nitrogen adsorption-desorption studies

Nitrogen adsorption and desorption isotherms of different SBA15 materials are presented in the figure 2A.5. All the isotherms exhibit the characteristic type IV isotherm with steep increase in adsorption at P/P_0 = 0.4-0.7 due to capillary condensation of the nitrogen in the mesopores. The BJH pore-size distribution (PSD) analysis shows very narrow PSD values in the range 4-7 nm. These values are consistent with SBA-15 mesoporous materials reported before. Nitrogen adsorption and desorption isotherms of the clicked product SBA-G-1 exhibit the characteristic type IV isotherm similar to their parent solid. The BJH pore-size distribution (PSD) analysis shows very narrow PSD and decrease in pore size due to incorporation of propargyl alcohol in the pore channels of the material. The pore diameter, multi point BET surface area and pore volume of various samples are listed in Table 2A.1.

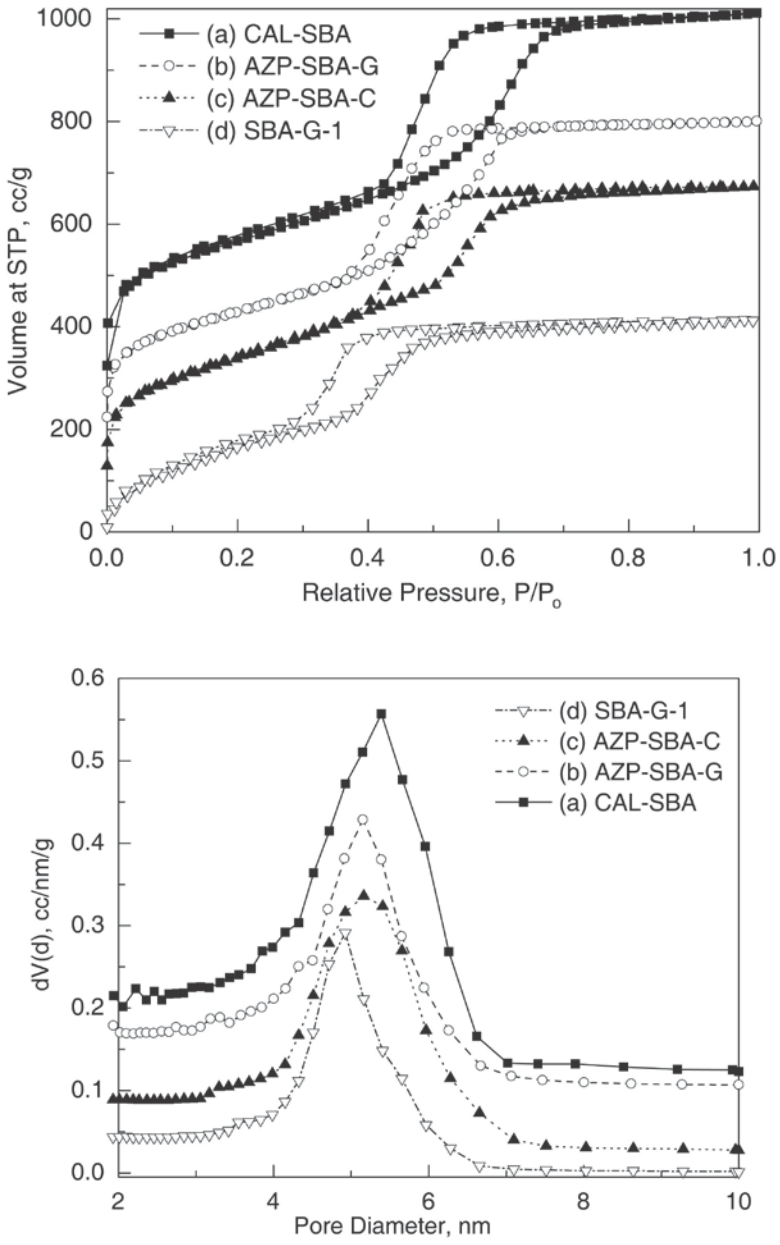

Figure 2A.5 : Nitrogen adsorption-desorption isotherms and pore size distribution of different SBA-15 materials (Y-axis offset by 100 for isotherms).

Table 2A.2: Physical properties of various SBA-15 materials

Sample Name	Azide content (mmol/g)	Pore Diameter (nm)	M_{BET} (m^2/g)	Pore Volume (cm^3/g)
CAL-SBA	-	5.4	965	1.11
AZP-SBA-G	1.9	5.15	680	0.95
AZP-SBA-C	1.3	5.2	555	0.78
SBA-G-1	-	4.92	342	0.57

2A.3.3.4 FT-IR spectroscopy

The FT-IR spectra of the various functionalized SBA-15 materials are presented in the Figure 2A.6. The spectra of both the azido-functionalized SBA-15 materials (AZP-SBA-C and AZP-SBA-G) display an absorbance at ~2100 cm^{-1} which is characteristic stretching vibration of any organic azide (N_3). The absence of this peak in CAL-SBA-15 showed that the azidopropyl group has been successfully incorporated into both AZP-SBA-C and AZP-SBA-G sample. The samples showed absorbance peaks at 1220, 1070, 800 and 466 cm^{-1} respectively. These peaks are typical of Si-O-Si bands that are associated with the formation of the silica networks. Weak peaks associated with Si-OH groups in the 940-960 cm^{-1} range were also observed for the functionalized mesoporous materials. The strong peak around 1630 cm^{-1} might be attributed to the bending vibration of H_2O. Therefore, the FT-IR spectra indicate that the azido group was efficiently incorporated in the matrix of the mesoporous SBA-15 both by post-synthesis grafting and one-pot co-condensation techniques.

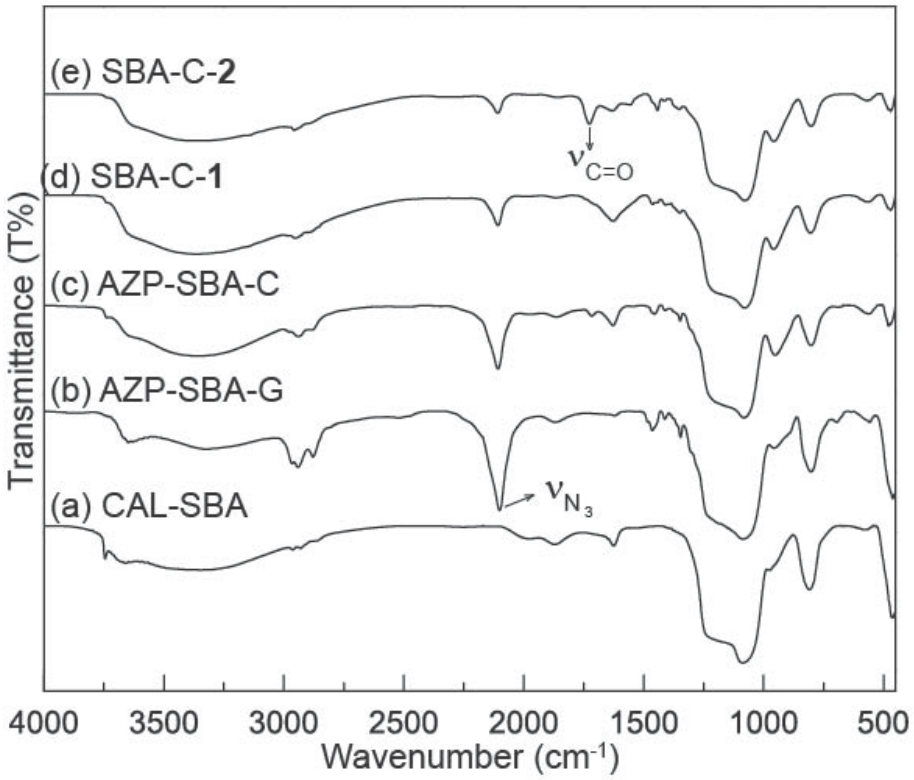

Figure 2A.6: Comparative FT-IR spectra of the different SBA-15 materials

The extent of the click reaction was estimated using FT-IR spectroscopy, by monitoring the decrease in the integrated intensity of the $\nu_{as}(N_3)$ at 2100 cm^{-1} (Figure 2A.6d and 2A.6e). To get a semi-quantitative estimate on the conversion of the azide upon CuAAC, a calibration curve was made using quantitative amounts of AZP-SBA-C in KBr and plotting the integrated intensities of the azide peak at 2100 cm^{-1} to the concentration of the azidopropyl labeled silica in the KBr pellet (see Appendix I, Figure A1). However, it was not possible to observe the appearance of a 1,2,3-triazole stretch since it interfered with a strong peak at 1650 cm^{-1} from the bending vibration of water adsorbed to SBA-15. Since we were unable to observe the appearance of the triazole peak in the IR, we turned our attention to finding substrates that have a characteristic IR peak that does not interfere with the azide functionalized SBA-15 materials. For such substrates, their successful attachment would allow us to follow the reaction both by the appearance of their signature IR peak together with the disappearance of the azide stretch of the starting SBA-15 material. The methyl pent-4-ynoate (**2**) was thus chosen as the substrate for CuAAC since it had a characteristic carbonyl stretch at 1727 cm^{-1}, a region that displayed no peaks for the azide labeled SBA-15 materials. The successful attachment of **2** was confirmed from the IR spectra in which concomitant disappearance of the $\nu_{as}(N_3)$ at 2100 cm^{-1} and the appearance of the ν(C=O) at 1727 cm^{-1} was observed (Figure 2A.6e, SBA-C-**2**).

2A.3.3.5 Solid state CP-MAS NMR spectroscopy

2A.3.3.5.1 ^{13}C CP-MAS NMR spectroscopy

Figure 2A.7 represents the solid state ^{13}C CP-MAS NMR spectra of the functionalized SBA-15 materials. The spectrum of the as-synthesized azido-functionalized SBA-15 material synthesized using co-condensation technique (as-synthesized AZP-SBA-C, Figure 2A.7a) displays signals for both the surfactant $EO_{20}PO_{70}EO_{20}$ and azidopropyl group. The peaks at ~21 and 78 ppm correspond to the peaks for the surfactant while the three peaks C1 (8.68 ppm), C2 (22 ppm), C3 (53 ppm) represent the three C-atoms of the azido-propyl chain in the order as presented. The relative intensity of the C1, C2, C3 appear to be less in comparison to the surfactants because of the higher concentration of the latter in the as-synthesized matrix. After the as-synthesized AZP-SBA-C was extracted with ethanol to remove surfactant, the peaks characteristic of the surfactant disappeared, while the C1, C2,

and C3 peaks of the azido-propyl group remained (Figure 2A.7 b). The ^{13}C CP MAS NMR of the AZP-SBA-G also showed three distinct peaks corresponding to the C1, C2, C3 carbon atoms (Figure 2A.7 c). The ^{13}C CP-MAS NMR spectra of both AZP-SBA-C and AZP-SBA-G displayed similar spectrum which indicated that the same material was produced by co-condensation and grafting methods.

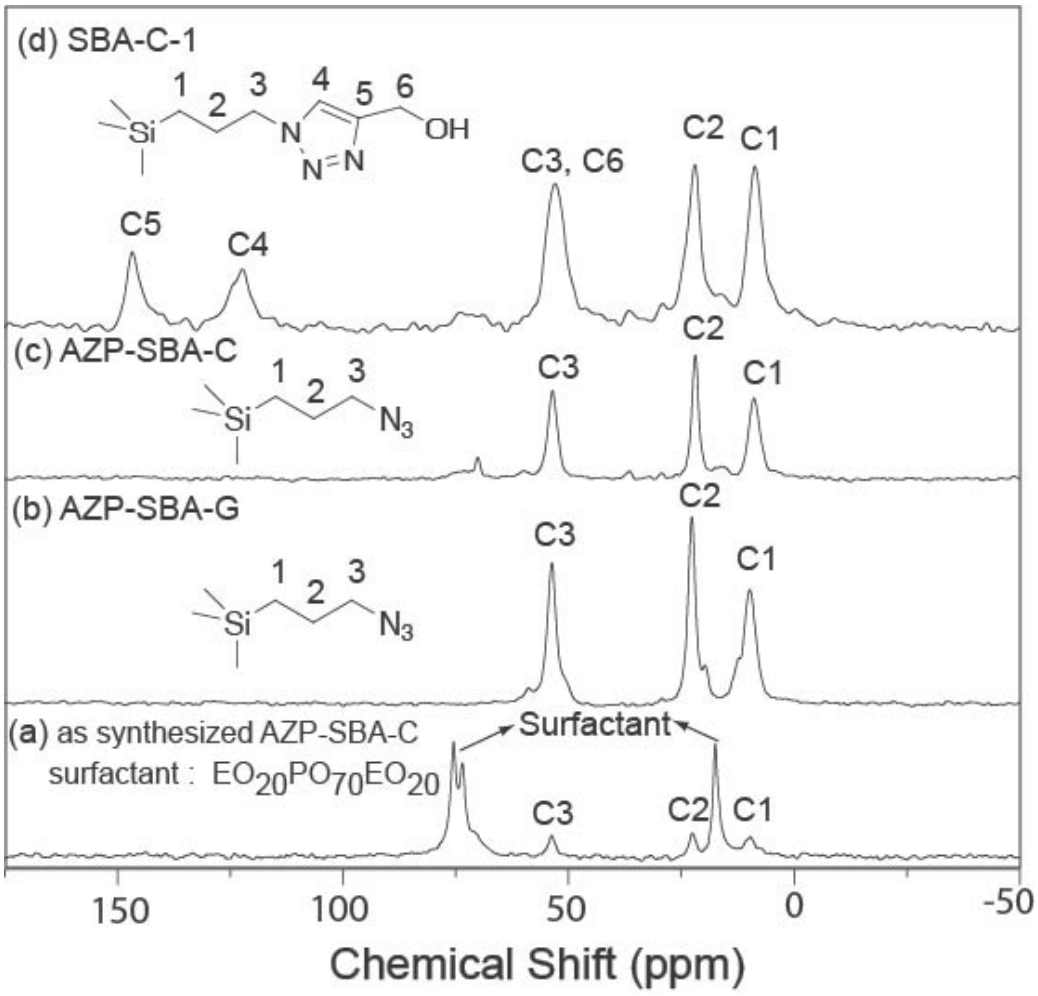

Figure 2A.7: ^{13}C CP MAS NMR spectra of the different functionalized SBA-15 materials

The product SBA-C-**1**, formed upon click reaction of AZP-SBA-C and propargyl alcohol (**1**) was further characterized by ^{13}C CP-MAS NMR spectroscopy. The spectrum shows extra peaks at 122 ppm and 146.7 ppm which corresponds to the C4 and C5 atom of the triazole as shown in Figure 2A.7d. The extra peak due to the C6 carbon is not observed as it is masked by the C3 peak from the linker.

2A.3.3.5.2 ^{29} Si CP-MAS NMR spectroscopy

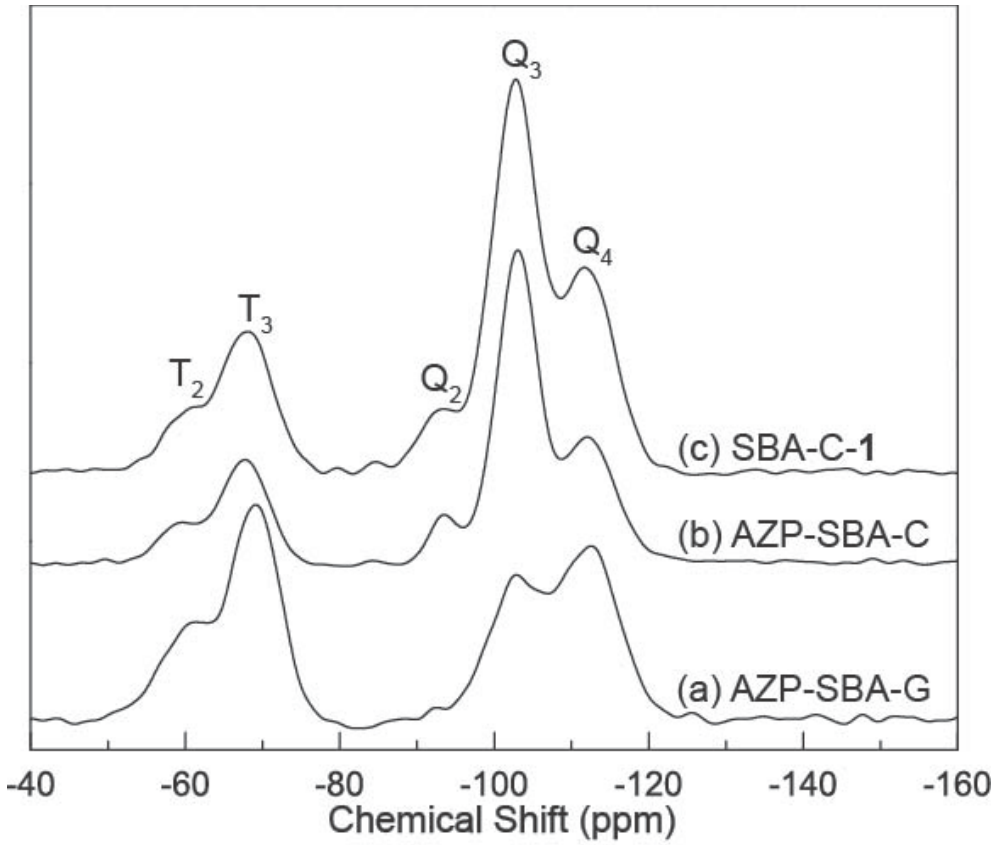

Figure 2A.8: ^{29}Si CP MAS NMR spectra of the different functionalized SBA-15 materials

The ^{29}Si CP MAS NMR spectra of the different azide-functionalized SBA-15 materials are presented in Figure 2A.8. All three spectra display prominent peaks at around -93, -102 and -112 ppm respectively. These may be assigned to the different types of the Si-sites namely Q^2 [$(SiO)_2Si(OH)_2$], Q^3 [$(SiO)_3Si(OH)$] and Q^4 [$(SiO)_4Si$] that are classified based on the total number of silanol groups (Si-OH) at the Si-centre (i.e. 2, 1, 0 respectively). The ^{29}Si MAS spectra were obtained to evaluate the relative intensities of Q^3 and Q^4 for both AZP-SBA-C and AZP-SBA-G (Appendix I, Figure A2). It was observed that in both the samples that intensity of the Q^4 signal was found to be higher than the Q^3 signal. This is expected since SBA-15 is a thick-walled material in which much of the Si exists as $(SiO)_4Si$. Two other distinct peaks that are observed at -59.9 and -68 ppm may be attributed to the functionalized sites of the Si-framework namely T^2 [$R(SiO)_2Si(OH)$] and T^3 [$R(SiO)_3Si$] respectively, where R is the azidopropyl group.

The ^{29}Si CP MAS spectrum of the click product SBA-C-**1** shows little or no change from the starting AZP-SBA-C indicating that the Si-sites does not undergo any chemical change during the reaction and its work-up (Figure 2A.8c). This is expected since the T^1 and T^2 Si-sites are that from the azido-propyl modified silica and should not undergo any change during the course of the click reaction.

2A.3.4 Synthesis of mesoporous silica-protein based hybrid materials

The presence of mannose in the α-D(+)-propargyl mannopyranoside labeled SBA-15, SBA-C-**5**, was confirmed by probing its affinity for the protein concanavalin-A (Con-A). The plant lectin Con-A exists as a tetramer in Tris-HCl buffer (pH 7.4) and binds up to four α-D(+)-mannopyranoside units in the presence of Na^+, Ca^{2+} and Mn^{2+} ions. Commercially available fluorescein labeled Con-A (300 μg) was incubated with both SBA-C-**5** and SBA-C-**1** (10 mg) in Tris-HCl buffer containing Na^+, Ca^{2+} and Mn^{2+} ions. After incubation for 30 min both the samples were extensively washed with Tris-HCl buffer containing Na^+, Ca^{2+} and Mn^{2+} ions. The samples were dispersed in the above mentioned buffer and were then put under a microscope under both bright-field and epi-fluorescence modes (with a 470-490 nm bandpass filter). The fluorescence observed from SBA-C-**5** incubated with Con-A is much more intense than that of the corresponding SBA-C-**1** that was incubated with Con-A (Figure 2A.9). The intense fluorescence is observed since the fluorescently labeled Con-A will bind to the mannose on the exterior surface of SBA-C-**5**. The material SBA-C-**1** was used as a control to eliminate the effect of triazole on the binding on Con-A. The diameter of tetrameric Con-A (each subunit is around 4.2 nm × 3.9 nm × 2 nm)[45] is larger than the pore size of SBA-C-**5** (5 nm) and this would probably attach to the mannose on the external surface of SBA-C-**4**, rather than inside the channels. The observance of intense fluorescence in Fig 2A.9D indicates that mannose successfully conjugates to AZP-SBA-C to form SBA-C-**5** via CuAAC. The weak fluorescence observed in SBA-C-**1** is probably due to the non-specific interaction between fluorescently labeled Con-A with the hydroxyl groups of silica or the 1,2,3-triazole functional group of SBA-C-**1**. This specificity of Con-A for mannose-labeled SBA-15 can be used in the development of sensors. Similar sensors have been developed for sensing ion transport in ion channels using the interaction of biotin-labeled MCM-41 with the protein avidin.[11]

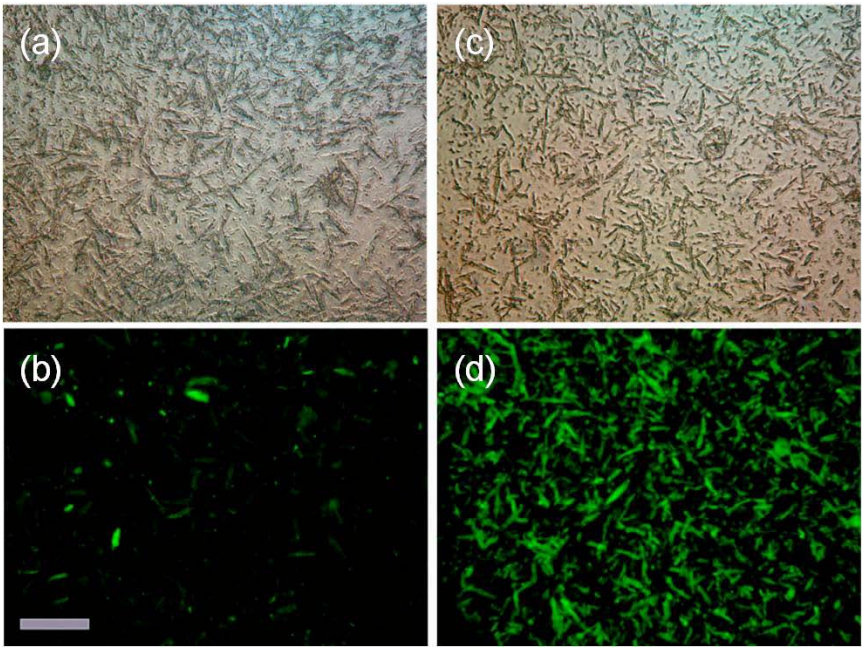

Figure 2A.9: (a) SBA-C-**1** treated with fluorescent labeled Con-A in bright field mode (b) SBA-C-**1** treated with fluorescent labeled Con-A in epi-fluorescence mode (c) SBA-C-**4** treated with fluorescent labeled Con-A in bright field mode (d) SBA-C-**4** treated with fluorescent labeled Con-A in epi-fluorescence mode. The scale bar shown is equivalent to 10 microns.

2A.4 Conclusions

The synthesis of azide labeled SBA-15 has been successfully achieved using both the one-pot co-condensation and post-synthetic grafting method. The azide labeled SBA-15 materials retains their mesoporosity after synthesis and the incorporation of the organic functionality was confirmed by FT-IR and solid state NMR spectroscopy. These materials undergo very efficient CuAAC with a variety of alkynes. When AZP-SBA-G was used, only 1.5 equivalent of alkyne was required to covert 90% of the available azides to triazole. Similar efficiency is much difficult to attain in aqueous solution by using amine and carboxylic labeled SBA-15, which are materials typically used to anchor various functional molecules. All the solid materials have been characterized by various analytical techniques such as powder XRD, SEM, TEM, FT-IR, solid state NMR and nitrogen adsorption-desorption studies etc. The azide labeled SBA-15 was further used as a platform to synthesize a silica-protein hybrid material composing of mannose labeled SBA-15 and Concanavalin-A. Such hybrid materials may be important in the development of

biosensors. The ease of synthesis for the azide labeled SBA-15 material together with its ability to undergo very efficient chemoselective CuAAC in water would make it a very attractive platform for the development of covalently anchored catalysts, enzymes and sensors.

2A.5 References

1. Frank Hoffmann, Maximilian Cornelius, Jürgen Morell and M. Fröba, *Angew. Chem. Int. Ed.*, 2006, **45**, 3216-3251.
2. B. G. Trewyn, I. I. Slowing, S. Giri, H.-T. Chen and V. S. Y. Lin, *Acc. Chem. Res.*, 2007, 846-853.
3. Y. Wan and Zhao, *Chem. Rev.*, 2007, **107**, 2821-2860.
4. B. Kesanli and W. Lin, *Chem. Commun.*, 2004, 2284-2285.
5. C. Nozaki, C. G. Lugmair, A. T. Bell and T. D. Tilley, *J. Am. Chem. Soc.*, 2002, **124**, 13194-13203.
6. T. J. Terry, G. Dubois, A. Murphy and T. D. P. Stack, *Angew. Chem. Int. Ed.*, 2007, **46**, 945-947.
7. H. Lakhiari, E. Legendre, D. Muller and J. Jozefonvicz, *J. Chromatogr. B,*, 1995, **664**, 163-173.
8. J. E. Schiel, R. Mallik, S. Soman, K. S. Joseph and D. S. Hage, *J. Sep. Sci.*, 2006, **29**, 719-737.
9. J. Li, T. Qi, L. Wang, C. Liu and Y. Zhang, *Materials Letters*, 2007, **61**, 3197-3200.
10. C.-Y. Lai, B. G. Trewyn, D. M. Jeftinija, K. Jeftinija, S. Xu, S. Jeftinija and V. S. Y. Lin, *J. Am. Chem. Soc.*, 2003, **125**, 4451-4459.
11. K. Nozawa, C. Osono and M. Sugawara, *Sensors and Actuators, B: Chem.*, 2007, **126**, 632-640.
12. D. Zhao, Q. Huo, J. Feng, B. F. Chmelka and G. D. Stucky, *J. Am. Chem. Soc.*, 1998, **120**, 6024-6036.
13. X. Wang, K. S. K. Lin, J. C. C. Chan and S. Cheng, *Chem. Commun.*, 2004, 2762-2763.
14. X. Wang, K. S. K. Lin, J. C. C. Chan and S. Cheng, *J. Phy. Chem. B*, 2005, **109**, 1763-1769.
15. Q. Wei, Z. Nie, Y. Hao, Z. Chen, J. Zou and W. Wang, *Materials Letters*, 2005, **59**, 3611-3615.

16. C.-m. Yang, B. Zibrowius and F. Schuth, *Chem. Mater.*, 2003, 1772-1773.
17. R. Marschall, J. Rathousk and M. Wark, *Chem. Mater.*, 2007, **19**, 6401-6407.
18. Q. Wei, H.-Q. Chen, Z.-R. Nie, Y.-L. Hao, Y.-L. Wang, Q.-Y. Li and J.-X. Zou, *Materials Letters*, 2007, **61**, 1469-1473.
19. A. Stein, B. J. Melde and R. C. Schroden, *Adv. Mater.*, 2000, **12**, 1403-1419.
20. M. Hartmann, *Chem. Mater.*, 2005, **17**, 4577-4593.
21. H. H. P. Yiu, P. A. Wright and N. P. Botting, *J. Mol. Cat. B: Enzym.*, 2001, **15**, 81-92.
22. Y. Zhu, S. Kaskel, J. Shi, T. Wage and K.-H. van Pee, *Chem. Mater.*, 2007, **19**, 6408-6413.
23. Y. Zhu, W. Shen, X. Dong and J. Shi, *J. Mater. Res.*, 2005, **20**, 2682-2690.
24. J. Kim, J. W. Grate and P. Wang, *Chem. Engg. Sci.*, 2006, **61**, 1017-1026.
25. H. H. P. Yiu, P. A. Wright and N. P. Botting, *Micro. Meso. Mater.*, 2001, **44-45**, 763-768.
26. A. S. M. Chong and X. S. Zhao, *Catalysis Today*, 2004, **93-95**, 293-299.
27. J. He, X. Li, D. G. Evans, X. Duan and C. Li, *J. Mol. Cat. B: Enzymatic*, 2000, **11**, 45-53.
28. P. Wang, S. Dai, S. D. Waezsada, A. Y. Tsao and B. H. Davison, *Biotech. Bioeng.*, 2001, **74**, 249-255.
29. I. S. Carrico, *Chem. Soc. Rev.*, 2008, **37**, 1423-1431.
30. V. V. Rostovtsev, L. G. Green, V. V. Fokin and K. B. Sharpless, *Angew. Chem. Int. Ed.*, 2002, **41**, 2596-2599.
31. V. D. Bock, H. Hiemstra and J. H. van Maarseveen, *Eur. J. Org. Chem.*, 2006, 51-68.
32. A. J. Dirks, J. J. L. M. Cornelissen, F. L. Van Delft, J. C. M. Van Hest, R. J. M. Nolte, A. E. Rowan and F. P. J. T. Rutjes, *QSAR and Combinatorial Science*, 2007, **26**, 1200-1210.
33. L. Jean-François, *Angew. Chem. Int. Ed.*, 2007, **46**, 1018-1025.
34. D. A. Fleming, C. J. Thode and M. E. Williams, *Chem. Mater.*, 2006, **18**, 2327-2334.
35. Z. Guo, A. Lei, X. Liang and Q. Xu, *Chem. Commun.*, 2006, 4512-4514.
36. K. M. Kacprzak, N. M. Maier and W. Lindner, *Tetrahedron Letters*, 2006, **47**, 8721-8726.

37. S. Ciampi, T. Bocking, K. A. Kilian, J. B. Harper and J. J. Gooding, *Langmuir*, 2008, **24**, 5888-5892.
38. Q. Wang, T. R. Chan, R. Hilgraf, V. V. Fokin, K. B. Sharpless and M. G. Finn, *J. Am. Chem. Soc.*, 2003, **125**, 3192-3193.
39. B. P. Pichon, M. Wong Chi Man, C. Bied and J. J. E. Moreau, *J. Organometallic Chemistry*, 2006, **691**, 1126-1130.
40. J. L. Marshall, K. C. Erickson and T. K. Folsom, *Tetrahedron Letters*, 1970, **11**, 4011-4012.
41. B. Roy and B. Mukhopadhyay, *Tetrahedron Letters*, 2007, **48**, 3783-3787.
42. M. Lamač, I. Císařová and P. Štěpnička, *Eur. J. Inorg. Chem.*, 2007, **2007**, 2274-2287.
43. T. J. Terry and T. D. P. Stack, *J. Am. Chem. Soc.*, 2008, **130**, 4945-4953.
44. J. M. Rosenholm and M. LindÃ©n, *Chem. Mater.*, 2007, **19**, 5023-5034.
45. G. M. Edelman, B. A. Cunningham, G. N. Reeke, J. W. Becker, M. J. Waxdal and J. L. Wang, *Proc. Natl. Acad. Sci. U. S. A.*, 1972, **69**, 2580-2584.

CHAPTER 2

Part B

Synthesis and Characterization of "Clickable" MCM-41 Mesoporous Materials for Site Isolation of Prolines

2B.1 Introduction

Since the discovery of mesoporous silica materials, surface functionalization of these materials with organic functional groups has received paramount interest. Functionalization of these materials with organic functional groups provides a handle to tailor the physico-chemical properties of these materials for specific applications.[1] In general, two pathways are available for the synthesis of covalently attached functional groups onto these materials.[1] These are: a) post-synthetic grafting of organosilane onto the surface of purely inorganic mesoporous silica and b) direct synthesis or co-condensation method which involves modification of the surface in a single step by co-condensation of organosilane with the silica precursor in the presence of structure directing agents (SDAs). Both methods have their respective advantages and disadvantages. The most significant advantage of the co-condensation method over the grafting method is the higher loading and uniform distribution of organic functionalities on the surface of mesoporous materials without reducing the pore size.

2B.2 Site-isolation of functional groups on mesoporous silica

In recent years, lot of attention has been focused on the study of loading and distribution of functional groups on the surface of mesoporous materials using both post-synthetic grafting and co-condensation methods.[2] In particular, site isolated functional groups in mesoporous silica has been used for the synthesis of site isolated heterogeneous catalysts.[3] A functional group is said to be site isolated when it is far apart from its neighbouring functional groups and do not interact (physically or chemically) with each other. On the other hand, site dense functional groups are spaced close enough to each other by distances which enable them to interact with each other. For example, SBA-15 functionalized with acetylacetonate (acac) groups were prepared by varying molar% of 3-(3-(triethoxysilyl)propyl)-2,5-pentanedione during co-condensation method and was subsequently chelated with europium salt ($EuCl_3$).[4] For the material containing 14 mol% acac groups, the Eu/acac molar ratio was found to be exactly 0.5 indicating that at this concentration all the acac groups were accessible and used in the complexation reaction since two acac groups chelates one Eu^{III} ion (Scheme 2B.1a). These two acac groups spatially close to each other and chelating with one Eu^{III} ion are called as site dense functionalized. When the

concentration of acac groups was decreased the Eu/acac ratio decreased dramatically. The Eu/acac molar ratio was shown to be 0.035 for the material containing 10% molar in acac and 0 for 5% (Scheme 2B.1b). This drop was believed to result from the increased distance between the acac units. The two acac groups are spacially too far from each other and as a result they cannot take part in complexation with Eu^{III} ion. These are called as site isolated functional groups.

The distance between the two or more functional (catalytic) groups or the degree of their site-isolation is often very crucial for the catalytic processes to yield the desired products with high efficiency.[5] For example, the manganese catalysts reported by Jacobs and co-workers benefit remarkably from the site isolation afforded by immobilization on solid support. While the homogeneous analogues are prone to form Mn dimers that decompose H_2O_2, site isolation through immobilization yields more oxidant-efficient and substrate-efficient epoxidation catalysts.[6, 7] Thus, site-isolation of heterogenized catalysts provides enhanced activity by attenuating deleterious bimolecular catalyst interactions.[8, 9] However, generating site isolated heterogeneous catalysts in mesoporous silica still remain a big challenge.

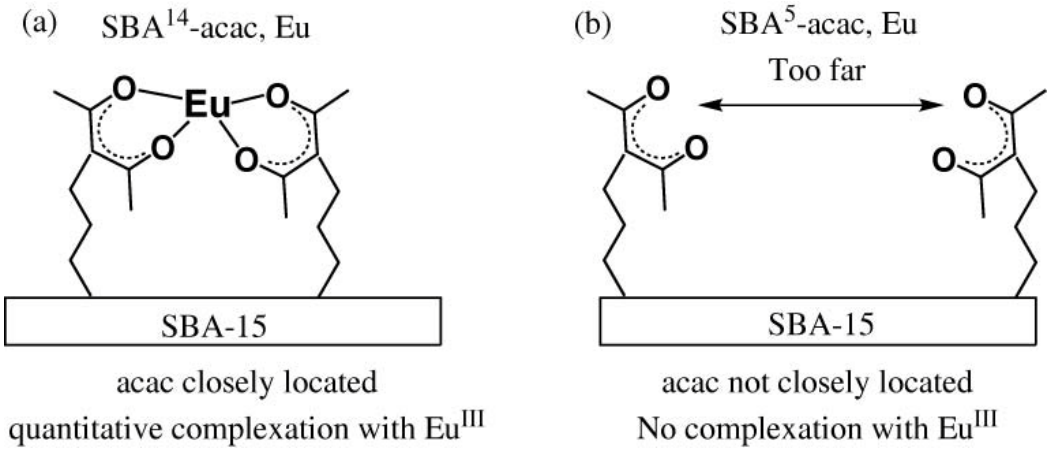

Scheme 2B.1: Distribution of acac groups on to SBA-15 materials[4]

2B.2.1 Site isolation by post synthetic grafting method

In post synthetic grafting method, different strategies have been used in order to achieve site isolation of functional groups.[10-12] For example, change of the solvent used during post-synthetic grafting has been shown to have an effect on the distribution of functional groups.[8, 11] In post synthetic grafting of 3-aminopropyl groups on the surface of MCM-41 using different solvents, it has been shown that

while the reaction in toluene produced aggregates, the reaction where alcohol was used as the solvent resulted in higher degree of site isolation.[8] Jones and co-workers have applied molecular spacer approach to control minimum distance between the surface grafted amino groups by using tritylimine. After grafting, the tritylimine was hydrolysed to yield site isolated primary amine on the surface of mesoporous materials.[13, 14] The site isolated amines were used to generate constrained geometry-inspired catalysts (CGCs) of titanium, which were shown to be 10 times more active than multi-sited catalysts that were prepared using traditional techniques.[14] In another more direct approach, site isolated amines have been obtained by reacting a mixture of 3-aminopropyltrimethoxysilane and methyltrimethoxysilane with mesoporous silica.[15] Stack et al. employed a metal template-metal exchange strategy to synthesize site isolated Fe^{II}-bis(1, 10-phenanthroline) catalyst on the surface of SBA-15 by grafting method.[3] The metal templating method involves the formation of the thermodynamically stabilized Cu^{I}-bis(1, 10-phenanthroline) complex, which is covalently attached to the silica surface via silylation. In the next step copper was removed by treatment with EDTA solution thereby leaving behind 1, 10-phenanthroline immobilized template on the surface. Finally, metalation of immobilized template with $Fe(OTf)_2$ yielded site isolated Fe^{II}-bis(1, 10-phenanthroline) catalyst. This site isolated catalyst has more selective and efficient catalytic activity for olefin epoxidation than the analogous homogeneous catalyst or grafted catalyst under similar conditions.[3]

2B.2.2 Site isolation by co-condensation method

Post synthetic grafting involves multistep syntheses to install site isolated functional groups. On the other hand, co-condensation method allows functional groups to be installed in a single step. At the same time loading of the organic functional group can be controlled systematically by varying the molar ratio of organosilane with respect to silica precursor used during synthesis. Mouawia et al. reported synthesis of various bifunctional SBA-15 mesoporous materials via co-condensation method.[4] The results show that the parameters such as polarity of organic functional groups play an important role in the distribution of the functional groups although the site isolation of functional groups remains a question. Recently, Stack and co-workers have reported a systematic study on investigation of synthesis of site dense to site isolated azide functionalized SBA-15 by co-condensation of 3-

azidopropyltriethoxysilane (AzPTES) with TEOS under acid conditions.[9, 16] The advantage of this approach is that site isolation can be achieved in a single synthetic step and that too using only one functional group precursor in contrast to methods discussed above. Site-isolated and site-dense Cu^{I}-tris(pyridylmethyl)amine and Mn^{II}-tris(pyridylmethyl)amine complexes anchored on the azide functionalized SBA-15 materials via CuAAAC reaction show significant differences in reactivity with molecular oxygen towards epoxidation of alkenes.[9, 16]

2B.2.3 Site-isolated proline as organocatalysts

In recent years proline and its derivatives as organocatalyst have received tremendous attention because of their versatility in catalyzing various important reactions e.g. aldol reaction, Robbinson annulation,[17] Mannich reaction,[18-20] Michael reaction,[21, 22] Diels-Alder reaction[23] and others.[24] In this study, aldol condensation reaction catalysed by proline was chosen as model reaction to study effect of site isolated prolines on the rate of the reaction. Aldol condensation reaction is recognized as one of the most powerful reaction for the construction of C–C bonds in organic synthesis.[25] It can be carried out in an atom-economy[26, 27] manner to yield β-hydroxy ketones which are important building blocks in the synthesis of natural products and several biologically active compounds such as antibiotics and anticancer drugs.[28-30] Generally, proline catalyzed reactions require very high catalyst loading (20-30 mol%) and long reaction times. The high amount of catalyst required is not optimal for scaling up these reactions for the synthesis of bulk chemicals. Therefore, for the successful exploitation of these reactions on a large scale, proline has been heterogenized on various supports such as silica,[31, 32] polymers,[33-36] ionic liquids,[37, 38] magnetite,[39] dendrimers[40] and cyclodextrins[41] for the purpose of easy separation and recycling. In particular, silica mesoporous materials (e.g. MCM-41 and SBA-15) have been the choice of support for the immobilization of proline and its derivatives.[32, 42] However, in all these proline grafted mesoporous silica materials, the proline molecules are randomly grafted and there is no control on the distance between the proline molecules. This might be important since proline molecules grafted close to one another can hydrogen bond with each other. In fact, careful observation of the crystal structure of proline indicates that the amino group of one proline molecule is hydrogen bonded to the carboxylic moiety of another proline molecule. Hence if grafting results in proline molecules being installed close to each other, some of them

will be rendered inactive for reactions such as aldol condensation where the first step is the nucleophilic attack of the 2^o amine of proline onto the carbonyl carbon of the substrate. However if proline molecules are grafted such that they are site-isolated and do not interact with each other, the free 2^o amine and carboxylic group can be used during aldol reaction and would provide enhancement in activity. Hence it would be important to see the effect of site-isolation of proline on mesoporous silica on their activity towards aldol condensation reaction.

Stack and co-workers have demonstrated that site-isolated azide-grafted SBA-15 can be synthesized using the co-condensation method which is performed under acidic conditions using 3-azidopropyltriethoxysilane (AzPTES) and TEOS as precursors.[9, 16] Since synthesis of azide grafted MCM-41 by one pot co-condensation of AzPTES and TEOS mixture is performed under highly basic conditions (unlike SBA-15), it is necessary to systematically study the site isolation of organoazides in MCM-41 materials before they are used for applications involving site-isolated heterogeneous catalysis. Recently, Moitra et al. have reported synthesis of azide functionalized mesoporous silica nanoparticles (MSNs) and have been modified by click chemistry with 1-(propargyloxymethyl)pyrene.[43] Herein we present a systematic study of synthesis of site dense to site isolated azide functionalized MCM-41 mesoporous materials and the efficiency of these materials to undergo Cu(I) catalyzed azide alkyne click chemistry with various organic substrates bearing alkyne functionality. We also report and compare the efficiency of site dense and site isolated proline anchored onto the surface of MCM-41 as a catalyst for the aldol condensation reaction between an aldehyde and a ketone.

2B.3 Experimental

2B.3.1 Materials

Tetraethylorthosilicate (TEOS), Cetyltrimethylammonium bromide (CTAB), 4R-hydroxy-L-proline, 1-Pyrenemethanol, propargyl bromide, propargyl alcohol, phenyl acetylene, bathophenanthroline disulphonic disodium were obtained from Sigma Aldrich. Copper iodide, copper chloride, sodium ascorbate, 4-Nitro Benzaldehyde and acetone were obtained from Merck, India. BOC anhydride, diisopropylcarbodiimide, Sodium hydride, trifluroacetic acid, tetrabutyl ammonium iodide and N,N- Diisopropyl ethyl amine (DIPEA) were obtained from SRL, India.

All the chemicals used were of analytical grade and used as received. All the organic solvents were obtained from Merck, India. Benzyl azide was prepared as reported in the literature.[44]

2B.3.2 Synthesis

2B.3.2.1 Synthesis o*f* 4R-propargyloxy-L-proline (1)

Synthesis of 4R-propargyloxy-L-proline was carried with reported synthetic procedures as described below.[35, 45] 4R-hydroxy-L-proline (2 g, 15.3 mmol) was dissolved in water (20 mL), to this sodium bicarbonate (2.6 g, 30.6 mmol) was added with stirring. The resulting solution was cooled to 5 °C and BOC anhydride (5 g, 23 mmol) was added slowly as a solution in para-dioxane (also cooled to 5 °C). The resulting mixture was stirred at 0° for 1 h and allowed to warm to room temperature overnight. Then water (30 mL) was added and the aqueous layer was extracted three times with EtOAc (50 mL). The organic layer was back extracted twice with saturated sodium bicarbonate solution. The combined aqueous layers were acidified to pH = 1 with 10% HCl, and then extracted three times with EtOAc. The combined organic layers were dried over anhydrous sodium sulfate and EtOAc was evaporated under reduced pressure. The resulting crude was purified by flash chromatography. (EtoAc:Pet Ether, 70:30) to yield pure Boc-L-HyP-OH (2.19 g, 85 % yield).

To *tert*-butanol (2.1 mL, 21.7 mmol) under argon, were added diisopropylcarbodiimide (2.71 mL, 17.32 mmol) and copper chloride (26 mg, 0.26 mmol). The resulting mixture was then left to stir at rt for 3 days, diluted with anhydrous dichloromethane (DCM) (15 mL) and added to a solution of Boc-L-HyP-OH (1 g, 4.33 mmol) in anhydrous DCM (10 mL) under argon and the resulting mixture stirred at rt for 20 h. The urea formed was filtered through a celite pad and solvents were evaporated under reduced pressure. The crude product was purified by flash column chromatography (pet ether/EtOAc: 75/25). (2S, 4R)-*tert*-butyl-N-tert-butyloxycarbonyl-4-hydroxyprolinate was obtained as a colorless oil (1.07 g, 87% yield).

Further (2S, 4R)-*tert*-butyl-N-tert-butyloxycarbonyl-4-hydroxyprolinate (1 g, 3.5 mmol) was dissolved in 10 ml dry dimethyl formamide (DMF) and cooled to

0 ^{o}C in ice bath. Sodium hydride (0.21 g, 8.8 mmol, 2.5 eq) was added in portion-wise to the same. The reaction mixture was stirred for 10 min before the drop wise addition of propargyl bromide (0.39 mL, 4.38 mmol, 1.25 eq). The reaction mixture was stirred additional two hrs at room temperature. Water (10ml) was added to the reaction mixture and extracted with diethyl ether (10 ml x 3). The organic layer was collected and washed with brine solution then dried over sodium sulphate and concentrated under reduced pressure to obtain *tert*-Butyl-(2*S*,4*R*)-*N*-Boc-4-propargyloxyprolinate as a crude product, which was purified through silica gel column chromatography (pet ether/ EtOAc : 10:90). Yield: 1.02 g, 90%. ^{1}H NMR (200.13 MHz, CDCl3) δ ppm 1.32 - 1.48 (m, 18 H), 2.03 (dd, *J*=13.3, 7.0 Hz, 1 H), 2.19 - 2.38 (m, 1 H), 2.42 (t, *J*=2.3 Hz, 1 H), 3.35 - 3.66 (m, 2 H), 4.11 (d, *J*=1.9 Hz, 2 H), 4.15 - 4.37 (m, 2 H). ^{13}C NMR (50.32 MHz, CDCl3) δ ppm 27.89, 27.95(3C), 28.27(3C), 28.32, 35.16, 36.52, 50.97, 51.59, 56.38, 58.43, 74.74, 75.55, 79.23, 79.81, 80.04, 81.12, 81.17, 153.88, 171.99.

tert-Butyl (2*S*,4*R*)-*N*-Boc-4-propargyloxyprolinate (200mg) was dissolved in dichloromethane (5ml) and trifluroacetic acid (5ml) was added to the same at room temperature. The reaction mixture was stirred for overnight. Next day the reaction mixture was concentrated and azeotropically remove the trifluroacetic acid with toluene (20 ml x 3) to obtained title compound **(1)** Yield: 0.103 g, 98%. $[\alpha]_D^{25}$ (H_2O, c 1.1) -26.7 ^{1}H NMR (200 MHz, Solvent) δ ppm 2.10 - 2.33 (ddd, *J*=14.0, 10.0, 4.0 Hz, 1 H), 2.62 (dd, *J*=14.5, 7.9 Hz, 1 H), 2.83 (t, *J*=2.3 Hz, 1 H), 3.47 (dd, *J*=2.0, 1 H), 3.49 - 3.63 (m, 1 H), 4.20 (d, *J*=2.4 Hz, 2 H), 4.47 (dd, *J*=10.4, 8.0 Hz, 1 H), 4.56 (t, *J*=3.9 Hz, 1 H). ^{13}C NMR (50 MHz, Solvent) δ ppm 36.67, 53.18, 58.60, 60.88, 78.61, 79.33, 81.44, 174.22.

2B.3.2.2 Synthesis of propargyloxy-(1-pyrenyl)methane (4)

Propargyloxy-(1-pyrenyl)methane was synthesized by coupling 1-pyrenemethanol with propargyl bromide as described below. In a 10 mL round bottom flasks 1-Pyrenemethanol (0.25 g, 1.08 mmol) was dissolved in 2.5 mL dry DMF and stirred at 0-5 °C under inert atmosphere. To this sodium hydride (0.107 mg, 60% suspension in mineral oil, 2.7 mmol) was added in small fractions at 0-5 °C under inert atmosphere and reaction mixture was stirred for 30 minutes. Then, propargyl bromide (0.15 mL, 80% solution in toluene, 1.35 mmol) and tetrabutyl

ammonium iodide (0.02 g, 0.54 mmol) were added at 0-5 °C and stirred for 2 h. After completion of reaction, 20 ml of water was added to the reaction mixture and extracted thrice with 20 mL of ethyl acetate. Ethyl acetete layer was washed with water, brine solution and dried over anhydrous sodium sulphate. Ethyl acetate was evaporated under reduced pressure to obtain solid product which was further purified by column chromatography by eluting with 0-5% ethyl acetate in pet ether. yield 0.255g (88%). $C_{20}H_{14}O$. ^{1}H NMR (200.13 MHz, $CDCl_3$): δ (ppm) = 2.57 (t, 1H), 4.27 (d, 2H), 5.33 (s, 2H), 7.97 – 8.42 (m, 9H). ^{13}C NMR; (50.32 MHz, $CDCl_3$): δ (ppm) = 57.08, 69.92, 74.91, 79.73, 123.33, 124.43, 124.62, 124.88, 125.25, 125.28, 125.94, 127.34, 127.47, 127.55, 127.85, 129.60, 130.19, 130.75, 131.16, 131.49.

2B.3.2.3 Synthesis of Azide functionalized MCM-41 materials by one pot co-condensation

The azide functionalized MCM-41, *x*-AZP-MCM (where *x* represents the various mole percentage of AzPTES in the initial mixtures during synthesis) mesoporous materials were synthesized by one-pot co-condensation of TEOS and 3-azidopropyltriethoxysilane (AzPTES) by following the procedure reported by Huh et al. with slight modifications.[46] During the synthesis of *x*-AZP-MCM, the molar ratio of AzPTES was varied from 0.2 to 10 mol% with respect to TEOS (Scheme 1). In a typical batch synthesis, CTAB (1 g, 2.75 mmol) was dissolved in 240 mL of de-ionized water and then 2M NaOH (aq) (3.5 mL, 7 mmol) was added. The mixture was stirred vigorously for 30 min at 80 °C to dissolve the surfactant completely. To the clear solution, TEOS [(22.83 - *y*) mmol, (e.g. 4.275 g, 20.55 mmol, 90 mol%)] was added rapidly via injection followed by AzPTES [*y* mmol, (e.g. 0.563 g, 2.283 mmol, 10 mol%)]. The resultant reaction mixture was allowed to stir for another 2 h at 80 °C. The contents were then filtered hot and the white residue was washed with copious amounts of water and methanol and dried at 100°C for 12 h. The template was extracted from the as-synthesized material using methanol (100 mL) and concentrated HCl (1 mL) at 60°C, for 6 hr. The resulting template removed solid product was filtered and washed with methanol and then dried under vacuum at 100 °C for 12 h.

10-AZP-MCM synthesized using AzPTES (*y* = 2.283 mmol). Elemental analysis (%): C: 5.43; H: 0.98; N: 5.54.

5-AZP-MCM synthesized using AzPTES (y = 1.142 mmol). Elemental analysis (%): C: 2.75; H: 0.53; N: 2.91.

1-AZP-MCM synthesized using AzPTES (y = 0.228 mmol). Elemental analysis (%): C: 0.52; H: 0.12; N: 0.49.

0.5-AZP-MCM synthesized using AzPTES (y = 0.114 mmol). Elemental analysis (%): C: 0.29; H: 0.08; N: 0.31.

0.2-AZP-MCM synthesized using AzPTES (y = 0.0457 mmol). Elemental analysis (%): C: 0.12; H: 0.04; N: 0.11.

2B.3.2.4 Modification of *x*-AZP-MCM by Cu(I) catalyzed azide-alkyne cycloaddition reaction (CuAAC)

Azide functionalized MCM-41 materials (*x*-AZP-MCM) where subjected to Cu(I) catalyzed azide-alkyne cycloaddition (CuAAC) reaction by following the procedure reported by our group.[47] For CuAAC, the azide functionalized MCM-41 (*x*-AZP-MCM) was incubated with 2 equivalents of the corresponding alkyne in 1:1 water/DMF mixture containing CuI (1 equivalent), bathophenanthroline disulphonic disodium (1 equivalent) and sodium ascorbate (4 equivalents), with exclusion of dioxygen. In typical click reaction, 5-AZP-MCM (300mg) was incubated with 4-O-propargyl proline (267mg) in 12 mL of 1:1 DMF:water containing sodium ascorbate (312mg), copper iodide (150.36mg) and bathophenathroline disulphonic disodium (211.80 mg) for 24 hour. After completion of the reaction, the reaction mixture was centrifuged. The residue was first washed with water and then sequentially washed with 0.1M N,N-diethyldithiocarbamate sodium in ethanol (15mL) and acetone (15mL) respectively. The last three washings were repeated thrice. Finally, the faint yellowish white powder obtained was dried at 80°C in vacuum oven for 6-8 hour. Yield: 255 mg.

Similarly, other click reactions were carried out with *x*-AZP-MCM using propargyl alcohol, phenyl acetylene and Propargyloxy-(1-pyrenyl)methane.

2B.3.2.5 Click reaction of benzyl azide with 4-O-propargylproline and propargyl alcohol

Benzyl azide (0.812 g, 6.1 mmol) and respective alkyne (6.1 mmol) was dissolved in dry acetonitrile (10 ml). Copper iodide (0.117 g, 0.61 mmol) was added followed by the addition of N,N- Diisopropyl ethyl amine (DIPEA, 3.2 mL,

18.3 mmol). The reaction mixture was allowed to stir for 4hrs. After 4 hrs, 10ml sat. solution of ammonium chloride and 15 ml EtOAc was added to the reaction mixture. The aq layer was extracted with EtOAc (10 ml x 2). The organic layer was collected, washed with brine and concentrated in a rotary evaporator to get crude product **10** (Table 2B.3) which was purified by flash column chromatography (DCM:Methanol-15:85 / EtOAc:pet ether-85:15 resp) Yield (>85%). $[\alpha]_D^{25}$ ($CHCl_3$, c 0.41) -17.3 ^{1}H NMR (200.13 MHz, CDCl3) δ (ppm) = 2.16 (bs., 2 H), 3.43 (bs., 2H), 4.45 (bs, 3 H), 5.48 (s, 2H), 7.07 - 7.38 (m, 5H). ^{13}C NMR (50.32 MHz, CDCl3) δ (ppm) = 36.69, 53.32, 57.05, 79.73, 130.66(2C), 131.38, 131.61(2C), 136.79. LCMS Calcd, 302.33; Found, 303.31 (M^+ + 1).

Similarly, another click reaction was carried out using benzyl azide and propargyl alcohol by following above procedure. The crude product **11** (Table 2B.3) obtained was purified by flash column chromatography (DCM:Methanol-15:85 / EtOAc:pet ether-85:15 resp) Yield (>85%). ^{1}H NMR (200.13 MHz, CDCl3) δ (ppm) = 2.59 (bs., 1 H), 4.78 (bs., 2 H), 5.53 (s, 2 H), 7.06 - 7.61 (m, 5 H)

2B.3.2.6 Aldol reaction catalyzed proline anchored on MCM-41

The aldol condesation reaction between an aldehyde and a ketone was carried out by following the procedure reported in the literature.[32] 4-Nitrobenzaldehyde (0.150 g, 1 mmol) and acetone (0.8 ml, 10 mmol) were dissolved in dry DMF (3 ml). To this x-AZP-MCM-**1** catalyst (0.1 mmol) was added and the reaction mixture was stirred for the specified time. The progress of reaction was monitored through the TLC and LCMS. After completion of reaction the catalyst was separated from the reaction mixture by centrifugation and then water (10 ml) and ether (10 ml) were added to reaction mixture. The aqueous layer was extracted with ether (2 x 10 ml). The organic layer was washed with brine solution, dried over sodium sulphate and concentrated in rotary evaporator to get crude aldol product which was further purified by silica gel column chromatography (pet ether: EtOAc-10:90). **(8)** Yield >90%. $[\alpha]_D^{25}$ ($CHCl_3$, c 0.6) -12.1. ^{1}H NMR (200.13 MHz, CDCl3) δ (ppm) = 2.23 (s, 3 H), 2.86 (d, *J*=6.4 Hz, 3 H), 3.64 (br. s., 1 H), 5.26 (d, *J*=4.4 Hz, 1H), 7.54 (d, *J*=8.3 Hz, 2 H), 8.21 (d, *J*=8.6 Hz, 2 H). ^{13}C NMR (50.32 MHz, CDCl3) δ ppm 30.66, 51.45, 68.79, 123.67 (2C), 126.35 (2C), 147.16, 150.02, 208.49. **(9)** Yield <10%. ^{1}H NMR (200.13 MHz, CDCl3) δ (ppm) = 2.42 (s, 3 H), 6.81 (d, *J*=16.3

Hz, 1 H), 7.53 (d, *J*=16.3 Hz, 1 H), 7.69 (d, *J*=8.6 Hz, 2 H), 8.26 (d, *J*=8.8 Hz, 2H). ^{13}C NMR (50.32 MHz, CDCl3) δ ppm 28.07, 124.21(2C), 128.80(2C), 130.32, 140.09, 196.03.

The recovered catalyst from the reaction mixture was washed once with DMF and twice with ethanol, air dried and then dried at 80°C in vacuum oven for 6 hour. This catalyst was reused for the same reaction for another two times. For third time recylcling, we have provided the LCMS data below.

2B.3.3 Analytical and characterization methods

Powder X-ray diffraction of all the samples was carried out in a PANalytical X'pert Pro dual goniometer diffractometer. A proportional counter detector was used for low angle experiments and an X'celerator solid state detector was employed in the low angle experiments. The radiation used was Cu Kα (1.5418Å) with a Ni filter and the data collection was carried out using a flat holder in Bragg–Brentano geometry (0.5 to 10°; 0.2° min^{-1}). Care was taken to avoid sample displacement effects. SEM images were obtained on Leica Stereoscan 440 microscope. HR-TEM images were taken on a FEI Technai F30 operating at 300 kV with FEG. The samples were prepared by dispersing a large number of solid particles in isopropanol by sonication, and dropping the resulting suspension on a copper grid of 400 mesh and allowed to dry in air. Nitrogen adsorption and desorption studies were carried out using Quantachrome instrument. Samples were preheated at 100°C for 18 hours in the vacuum line. Multi point BET surface area was obtained from adsorption isotherm from P/P_0 0.01-0.1. Pore size distributions were calculated from adsorption isotherm using the BJH method. Elemental analyses were carried out on Thermo Finnigan FLASH EA 1112 series instrument. Semi-quantitative. FT-IR spectra were recorded on Perkin Elmer FT-IR spectrum GX instrument by making KBr pellets. Pellets were prepared by mixing 3 mg of sample with 97 mg of KBr. Yields for CuAAC reactions were calculated from corrected area under the curve characteristic for the azide stretch at ~2100 cm^{-1}. Fluorescence spectra were recorded on Varian Fluorescence Spectrophotometer. All the samples (0.2-0.5 mg) were suspended in 3 ml of CHCl3 with the aid of a sonication bath. Fluorescence steady-state emission spectra (345-700 nm) were measured using 330 nm excitation in 1 cm cell (excitation and detection slit = 1 nm, integration time = 0.2 sec). ^{13}C Cross Polarization Magic Angle

Spinning (CPMAS) NMR experiments were carried out on a Bruker AVANCE 300 wide bore spectrometer equipped with a superconducting magnet with a field of 7.1Tesla operating at 75.4MHz. The samples were packed into a 4mm zirconia rotor and loaded into a 4mm BL MAS probe and spun about the magic angle (54.74) at 10KHz using a standard ramp-CP pulse sequence was used for the experiment. The RF-powers was 60kHz ^{13}C CPMAS experiments. The contact time was 3ms for ^{13}C CPMAS experiments. All the chemical shifts were referenced to TMS. Typically 10,000 to 25,000 scans with a recycle delay of 3s were collected depending on the sensitivity of the sample. ^{1}H and ^{13}C NMR spectra were measured on Bruker (200 MHz) spectrometer & all the chemical shifts were referenced to TMS. For the deuterated solvent proton residuals as internal standard was used. LC-MS was performed on waters acquity instrument using C18 column in water : methanol (65:35) as mobile phase. Chiral HPLC was performed on Shimadzu CLASS-VP V6.12 SP5 using chiralpakAS-H column in IPA : n-Hexane (30:70) as mobile phase.

2B.4 Results and discussion

2B.4.1 Synthesis strategy of azide functionalized MCM-41

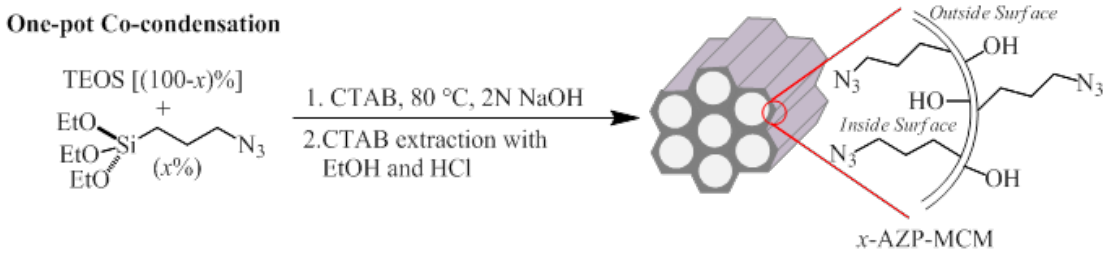

Scheme 2B.2: Synthesis of azide labeled MCM-41 (x = 0.2, 0.5, 1, 5, 10 mol%)

The azide functionalized MCM-41, *x*-AZP-MCM (where *x* represents the various mole percentage of AzPTES in the initial mixtures during synthesis) mesoporous materials were synthesized by one-pot co-condensation of TEOS and AzPTES using CTAB as structure directing agent under basic conditions as presented in the Scheme 2B.1.[46, 43] During the synthesis of *x*-AZP-MCM, the molar ratio of AzPTES was varied from 0.2 to 10 mol% with respect to TEOS. After synthesis, template was removed by stirring the as-synthesized material in methanol and hydrochloric acid. The amount of azidopropyl groups incorporated into the MCM-41 framework was determined by elemental analysis (Table 2B.2). The structure and

morphology of *x*-AZP-MCM materials were established unambiguously using XRD, TEM, SEM, NMR and N_2 adsorption-desorption studies.

2B.4.2 CuAAC of *x*-AZP-MCM with various alkyne containing substrates

The azidopropyl labeled silica *x*-AZP-MCM materials were subjected to Cu(I) catalyzed azide alkyne cycloaddition reaction (CuAAC) with various organic substrates (Scheme 2B.2).[47] The CuAAC was attempted using Copper iodide as the metal source (1 equivalent), sulfonated bathophenanthroline as the ligand (1 equivalent) and sodium ascorbate as the reducing agent (4 equivalents) in a mixture of DMF and water. The solution was degassed with argon prior to the addition of copper iodide. For example, treatment of 5-AZP-MCM (300 mg) with 4R-propargyloxy-L-proline **(1)** (2-fold molar excess with respect to azide groups on azidopropyl grafted silica), using CuI/ascorbate in H_2O/DMF (1:1) for 24 h, converted 90% of the available azide groups into the corresponding triazole product. Control reactions performed without the usage of CuI showed no conversion of the azide. After the reaction, an extensive washing protocol was followed to remove Cu(I), ascorbate, ligand and any unreacted alkyne as reported earlier.[9, 47] Absence of copper in ICP analysis shows the efficient removal of copper from the clicked product. The extent of the click reaction was estimated using IR spectroscopy by monitoring the decrease in the integrated intensity of the $\nu_{as}(N_3)$ at 2100 cm^{-1} (Fig. 2B.6, Table 2B.1). The CuAAC was then extended to other substrates to explore the efficiency of this reaction on azidopropyl functionalized MCM-41. The reaction was carried out with 2 fold excess of propargyl alcohol (**2**), phenylacetylene (**3**), propargyloxy-(1-pyrenyl)methane (**4**). The extent of the click reactions for the different substrates is tabulated in Table 2. All the substrates were successfully incorporated into the azido functionalized MCM-41 with high yields. The clicked products formed by the reaction of *x*-AZP-MCM with 4R-propargyloxy-L-proline (**1**) were further characterized by powder XRD, nitrogen adsorption-desorption studies and solid state CP-MAS NMR spectroscopy.

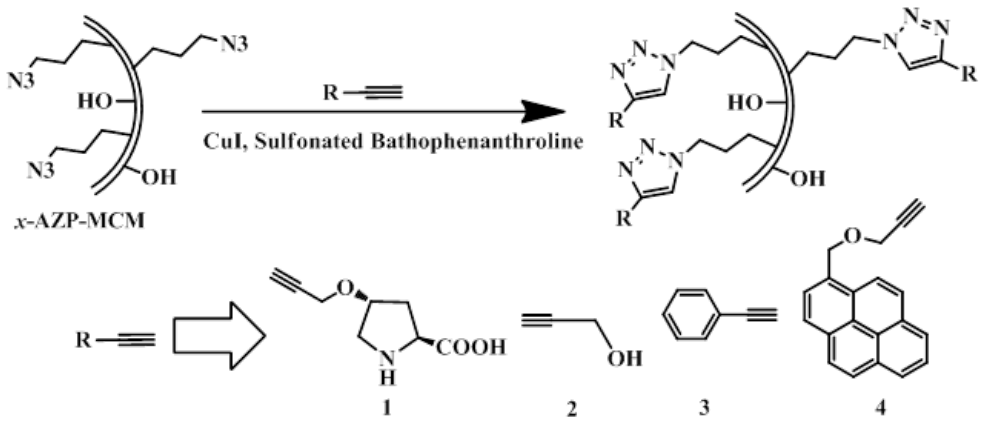

Scheme 2B.3: CuAAC reaction of Azide-functionalized MCM-41 with various substrates

Table 2B.1: Yield of CuAAC reaction with different substrates

Mesoporous Material	**Alkyne substrate**	**Product**	**CuAAC yield (%)**
1-AZP-MCM	4R-propargyloxy-L-proline (**1**)	1-AZP-MCM-**1**	93
	Propargyl alcohol (**2**)	1-AZP-MCM-**2**	>99
	Phenylacetylene (**3**)	1-AZP-MCM-**3**	96
	Propargyloxy-(1-pyrenyl)methane (**4**)	1-AZP-MCM-**4**	90
5-AZP-MCM	4R-propargyloxy-L-proline (**1**)	5-AZP-MCM-**1**	90
	Propargyl alcohol (**2**)	5-AZP-MCM-**2**	>99
	Phenylacetylene (**3**)	5-AZP-MCM-**3**	94
	Propargyloxy-(1-pyrenyl)methane (**4**)	5-AZP-MCM-**4**	85
10-AZP-MCM	4R-propargyloxy-L-proline (**1**)	10-AZP-MCM-**1**	86
	Propargyl alcohol (**2**)	10-AZP-MCM-**2**	98
	Phenylacetylene (**3**)	10-AZP-MCM-**3**	89
	Propargyloxy-(1-pyrenyl)methane (**4**)	10-AZP-MCM-**4**	78

2B.4.3 Characterizations

2B.4.3.1 Powder X-ray diffraction

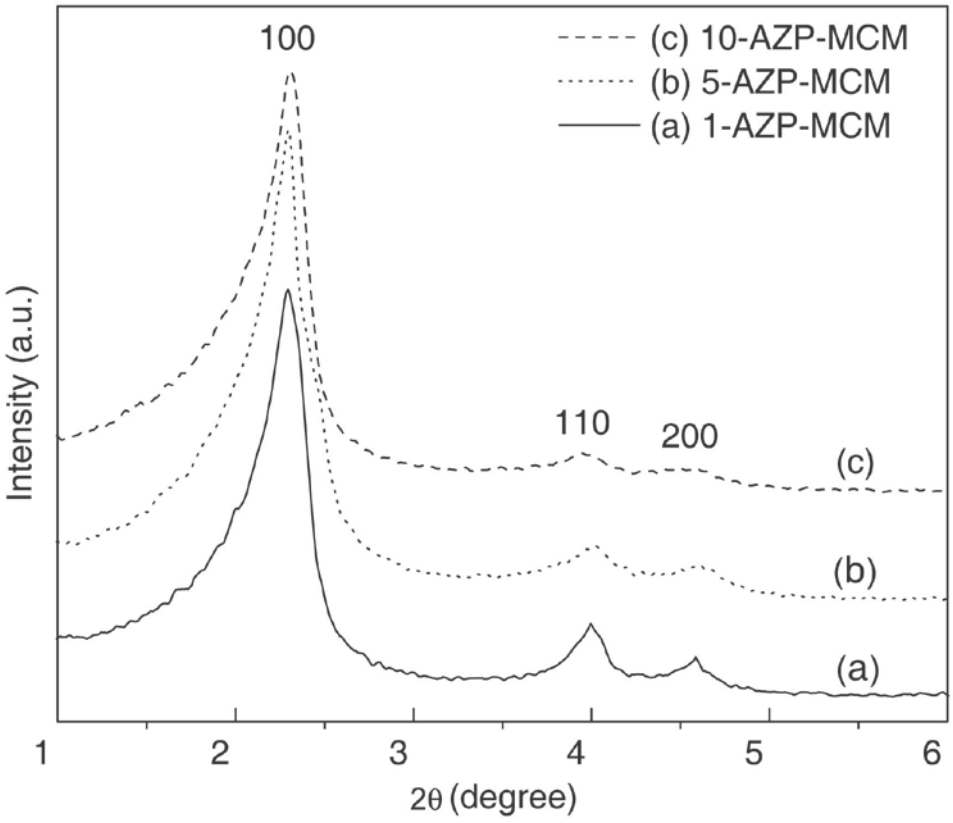

Figure 2B.1: Powder XRD patterns of different MCM-41 samples (a) 1-AZP-MCM; (b) 5-AZP-MCM and (c) 10-AZP-MCM

The powder XRD patterns of selected *x*-AZP-MCM materials (*x* = 0.2%-10%) are shown in Figure 2B.1. All materials showed the characteristic high intensity (100) diffraction peak at 2θ ~2.3°. The other significant peaks corresponding to (110) and (200) diffractions were also observed indicating that well-ordered one-dimensional hexagonal mesoporous channels of MCM-41 were formed and remained intact under the functionalization environment. However, the higher order (110) and (200) diffractions became less resolved as the amount of azide incorporation increased in the samples (Figure 2B.1C). This shows that the long-range order decreases slightly upon incorporation of higher amounts of azidopropyl groups into the MCM-41 matrix.

The powder XRD patterns of click products obtained by clicking 4R-propargyloxy-L-proline (**1**) with *x*-AZP-MCM are presented in figure 2B.2. The powder XRD patterns showed an intense (100) diffraction peak near $2\theta \sim 2.3$ indicating well-ordered hexagonal arrays and showing that the mesoporosity of the material does not change after undergoing CuAAC reaction.

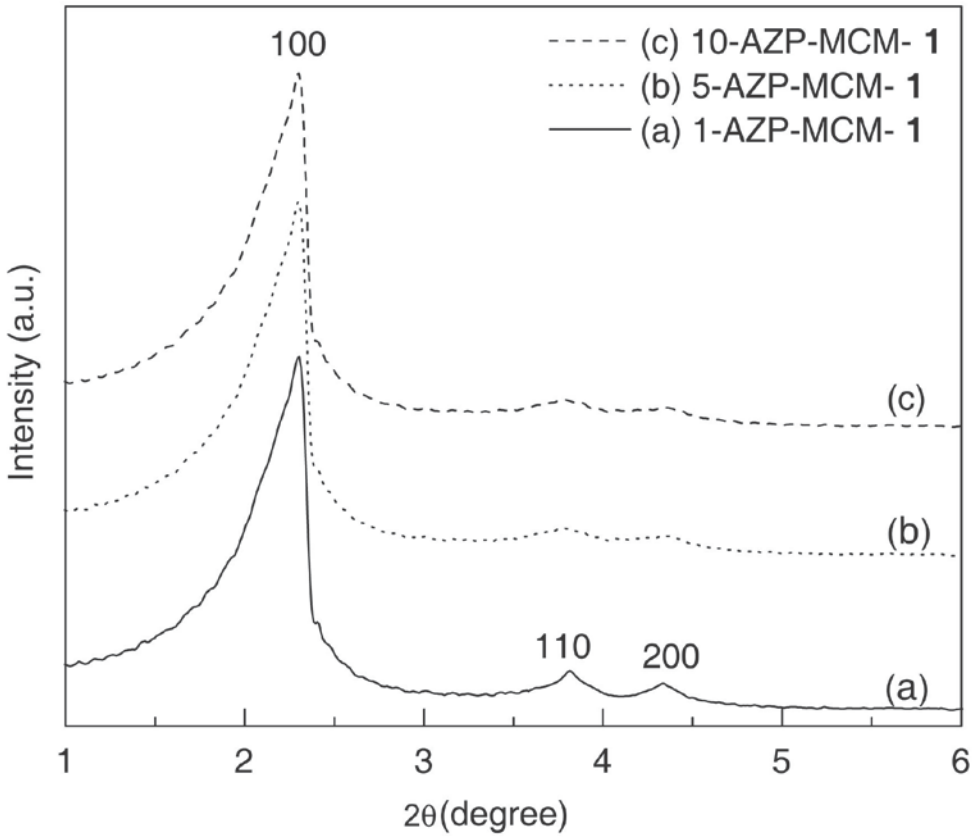

Figure 2B.2: Powder XRD patterns of different MCM-41 samples (a) 1-AZP-MCM-**1**; (b) 5-AZP-MCM-**1** and (c) 10-AZP-MCM-**1**

2B.4.3.2 Scanning and transmission electron microscopy

SEM and TEM images displayed formation of well-ordered two-dimensional hexagonal mesoporous particles with an elongated sphere-like morphology having particle size of 400±50 nm (Fig. 2B.3). The TEM and SEM pictures indicate that the mesoporosity and morphology of the particles was retained in the azide functionalized MCM-41 materials. Hence, incorporation of the azidopropyl group did not interfere with the structural properties of MCM-41.

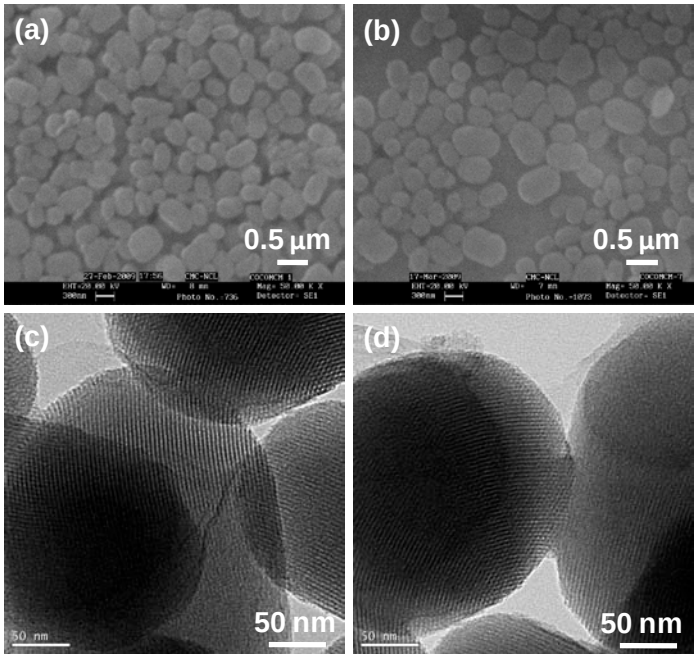

Figure 2B.3: SEM and TEM images of different azide functionalized MCM-41 materials: (a) and (c) of 1-AZP-MCM; (b) and (d) of 10-AZP-MCM

2B.4.3.3 Nitrogen adsorption-desorption studies

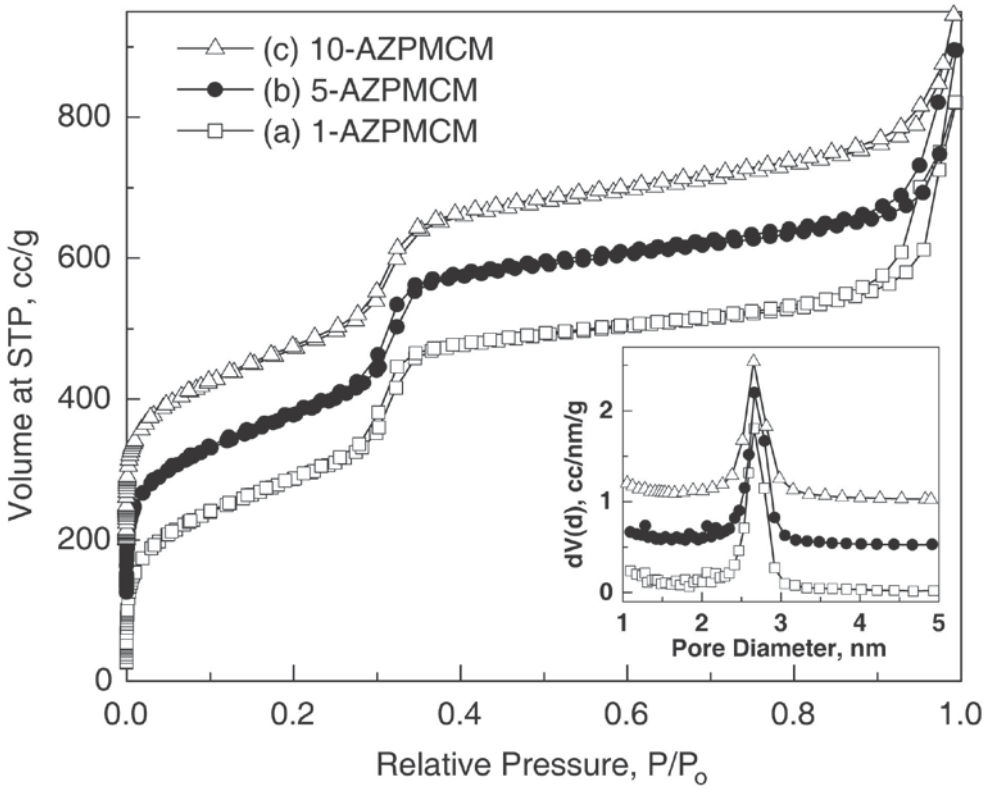

Figure 2B.4: Nitrogen adsorption isotherms of various MCM-41 materials (a) 1-AZP-MCM; (b) 5-AZP-MCM and (c) 10-AZP-MCM (Y axis, Offset by 100)

Nitrogen adsorption and desorption isotherms of selected *x*-AZP-MCM materials are presented in the figure 2B.4. All the isotherms exhibit the characteristic type IV isotherm with steep increase in adsorption at $P/P_0 \sim 0.3$ due to slight capillary condensation of the nitrogen in the mesopores. The BJH pore-size distribution (PSD) analysis shows very narrow PSD values in the range 2-3 nm. The pore diameter, multi point BET surface area and pore volume of various samples are listed in Table 2B.2. These values are consistent with other organo-functionalized MCM-41 materials reported before.[43, 46] Nitrogen adsorption and desorption isotherms of various clicked products are presented in the figure 2B.5. All the isotherms exhibit the characteristic type IV isotherm similar to their parent solids. The pore diameter, multi point BET surface area and pore volume of various samples are listed in Table 2B.2. The BJH pore-size distribution (PSD) analysis shows very narrow PSD and decrease in pore size due to incorporation of proline in the pore channels of the materials.

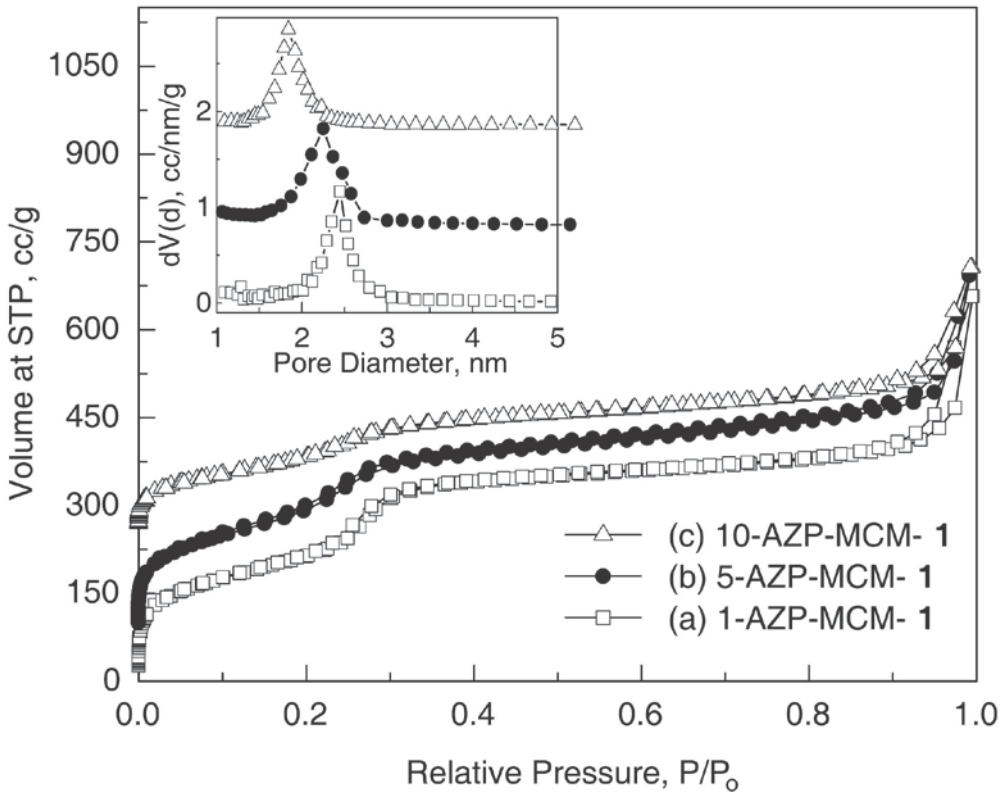

Figure 2B.5: Nitrogen adsorption isotherms of various MCM-41 materials (a) 1-AZP-MCM-**1**; (b) 5-AZP-MCM-**1** and (c) 10-AZP-MCM-**1**

Table 2B.2: Physical properties of various MCM-41 materials

Sample Name	Azide content (mmol/g)	Pore Diameter (nm)	M_{BET} (m^2/g)	Pore Volume (cm^3/g)
1-AZP-MCM	0.12	2.66	1000	1.12
5-AZP-MCM	0.69	2.66	961	1.05
10-AZP-MCM	1.32	2.65	932	1.00
1-AZP-MCM-**1**	-	2.48	724	0.72
5-AZP-MCM-**1**	-	2.25	632	0.64
10-AZP-MCM-**1**	-	1.84	436	0.5

2B.4.3.4 FT-IR spectroscopy

The FT-IR spectra of various materials are presented in the Figure 2B.6. The spectra of the azido-functionalized MCM-41 materials (*x*-AZP-MCM, *x* = 1, 5 and 10 mol% of azido-propyl groups) display an absorbance at ~2100 cm^{-1}, which is the characteristic stretching vibration of an organic azide (N_3). The presence of this peak in the materials shows that the azidopropyl group were successfully incorporated into the *x*-AZP-MCM samples. The samples also showed absorbance peaks at 1230, 1080, 805 and 465 cm^{-1} respectively. These peaks are typical of Si-O-Si bands that are associated with the formation of the silica networks. Weak peaks associated with Si-OH groups in the 940-960 cm^{-1} range were also observed for the functionalized mesoporous materials. The strong peak around 1658 cm^{-1} might be attributed to the bending vibration of H_2O. Thus, the FT-IR spectra indicate that the azido groups were efficiently incorporated in the matrix of the mesoporous MCM-41 by the one-pot co-condensation technique. The extent of the click reaction was estimated using FT-IR spectroscopy, by monitoring the decrease in the integrated intensity of the $\nu_{as}(N_3)$ at 2100 cm^{-1} (Figure 2B.6d and 2B.6e; Table 2B.1).

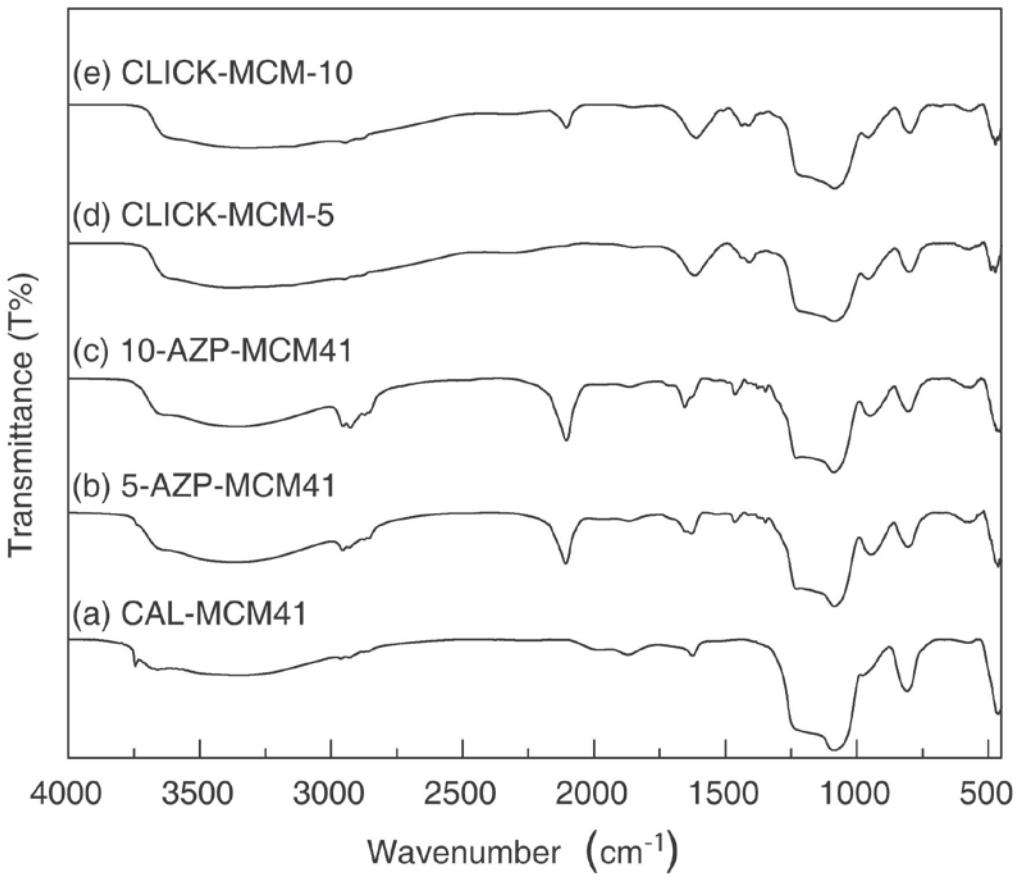

Figure 2B.6: FT-IR spectra of (a) 1-AZP-MCM; (b) 5-AZP-MCM; (c) 10-AZP-MCM; (d) 1-AZP-MCM-**1** and (e) 10-AZP-MCM-**1**

2B.4.3.5 Solid State CP-MAS NMR spectroscopy

2B.4.3.5.1 ^{13}C CP-MAS NMR spectroscopy

Figure 2B.7 represents the solid state ^{13}C CP-MAS NMR spectra of azide functionalized MCM-41 material, 10-AZP-MCM. The spectrum displays three peaks that correspond to the C1 (9.7 ppm), C2 (23 ppm) and C3 (55 ppm) C-atoms of the azido-propyl chain. The ^{13}C CP-MAS NMR spectra clearly show that the azidopropyl group has been incorporated into the MCM-41 material.

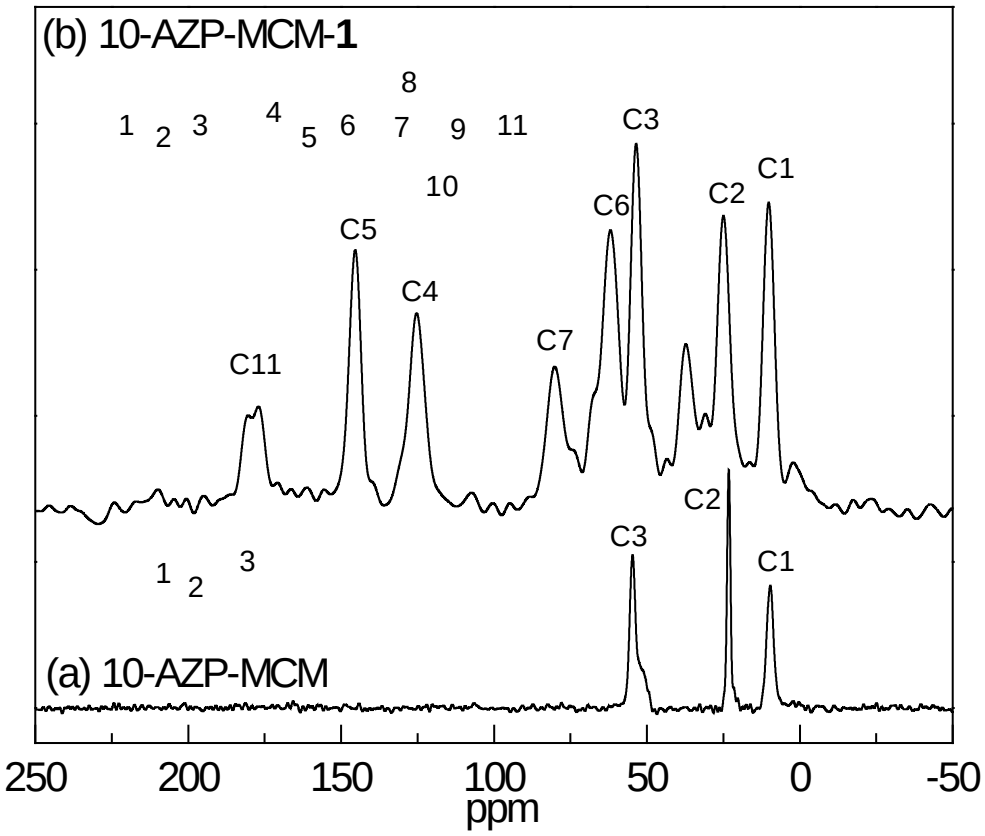

Figure 2B.7: ^{13}C CP MAS NMR spectra of (a) 10-AZP-MCM; (b) 10-AZP-MCM after click with 4R-propargyloxy-L-proline

The ^{13}C CP-MAS NMR spectrum of 10-AZP-MCM-**1** shows characteristic peaks of compound **1** with the addition of two extra peaks at 125 ppm and 146 ppm which corresponds to the C4 and C5 atom of the triazole, as shown in Figure 2B.7b. The peak at 177 ppm is very characteristic and arises due to the carboxylic acid moiety of proline. This data clearly indicates successful incorporation of proline on the surface of MCM-41 via CuAAC reaction.

2B.4.3.5.2 ^{29}Si CP-MAS NMR spectroscopy

The ^{29}Si CP MAS NMR spectra of the different azide-functionalized MCM41 materials are presented in Figure 2B.8. The ^{29}Si CP MAS NMR spectrum of 10-AZP-MCM displays prominent peaks at around -92, -101 and -110 ppm these may be assigned to the Si-sites Q^2 $[(SiO)_2Si(OH)_2]$, Q^3 $[(SiO)_3Si(OH)]$ and Q^4 $[(SiO)_4Si]$ respectively that are classified based on the total number of silanol groups (Si-OH) at the Si-centre (i.e. 2, 1, 0 respectively). Two other distinct peaks that are observed at -59 and -66 ppm may be attributed to the functionalized sites of the Si-framework

namely T^2 $[R(SiO)_2Si(OH)]$ and T^3 $[R(SiO)_3Si]$ respectively, where R is the azidopropyl group.

The ^{29}Si CP MAS spectrum of the 10-AZP-MCM-**1** material shows no change from the starting material 10-AZP-MCM, indicating that the Si-sites does not undergo any chemical change during the reaction and its work-up (Figure 2B.8b).

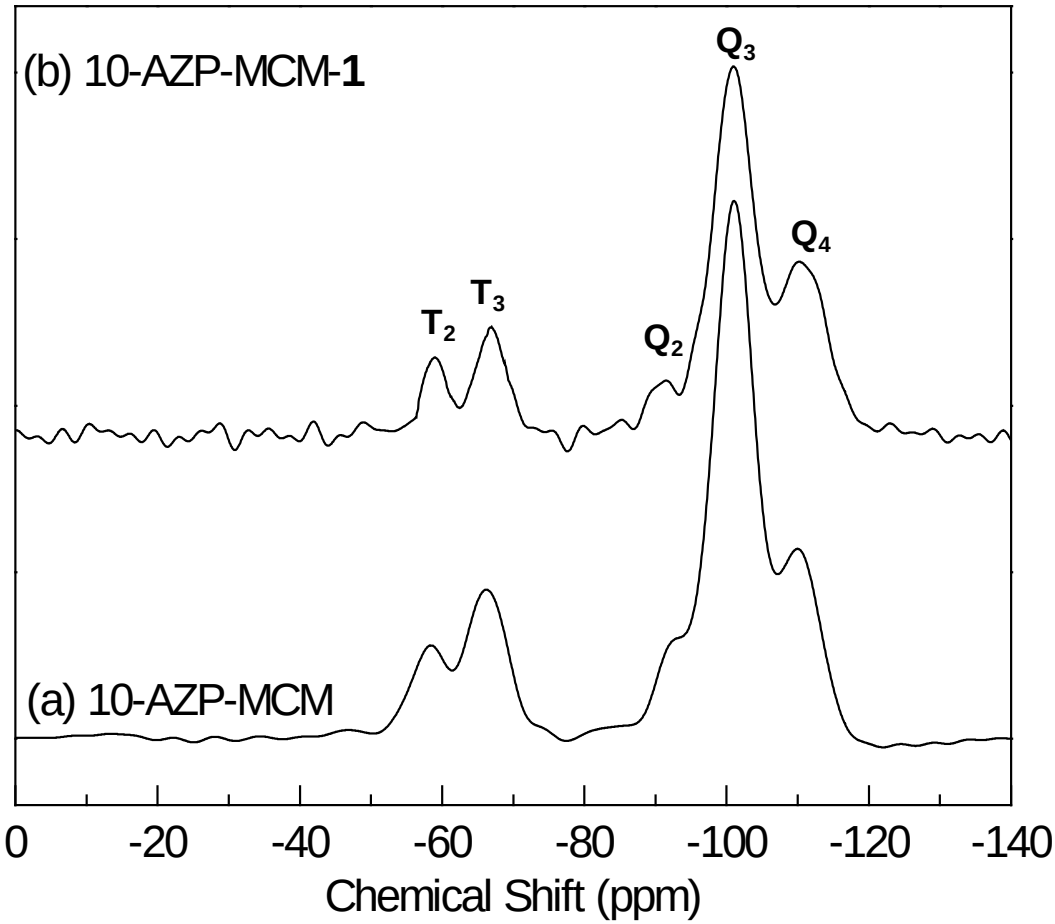

Figure 2B.8: ^{29}Si CP MAS NMR spectra (a) 10-AZP-MCM; (b) 10-AZP-MCM after clicked with 4R-propargyloxy-L-proline.

2B.4.3.6 Fluorescence spectroscopy: study of site isolation azides using pyrenes

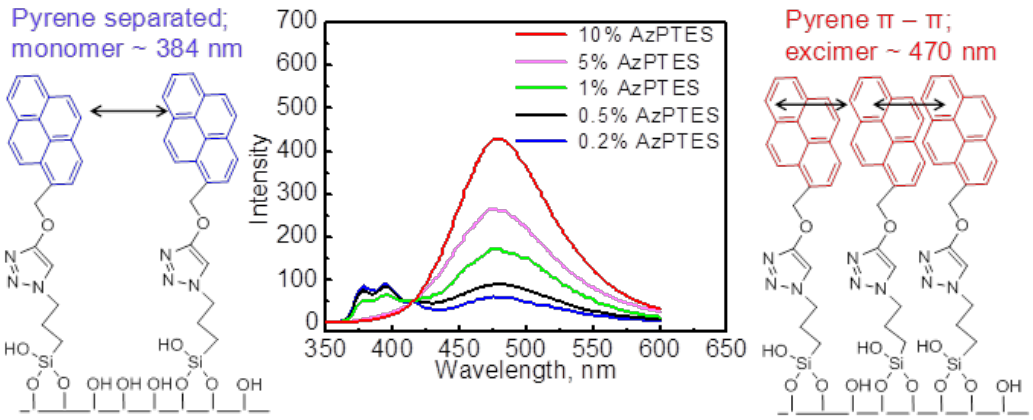

Figure 2B.9: Fluorescence spectra of propargyloxy-(1-pyrenyl)methane (**4**) clicked to *x*-AZP-MCM (*x* = 0.2, 0.5, 1, 5 and 10 mol%) suspended in chloroform, λ_{ex} = 330 nm. For comparison the spectra were normalized at 415 nm.

The distribution of azido-propyl groups on the surface was determine by measuring the fluorescence spectra of propargyloxy-(1-pyrenyl)methane (**4**) that was clicked onto various azide functionalized MCM-41 materials synthesized by co-condensation of AzPTES and TEOS at different molar ratios (*x*-AZP-MCM; *x* = 0.2, 0.5, 1, 5, 10 mol%) (Fig 2B.9).[9, 43] Closely spaced (site dense) pyrene molecules form excimers when they interact with each other via π-π stacking to give a broad excimer emission band centered at 480 nm.[48, 49] On the other hand pyrene molecules apart from each other by a distance of 1 nm or more (site isolation) give monomeric emission band at 384 nm.[48] Hence the nature of the fluorescence spectra would give information about the relative position of the azide groups in the MCM-41 material. The fluorescence of the 0.2-AZP-MCM clicked with propargyloxy-(1-pyrenyl)methane (**4**) showed appreciable monomeric pyrene fluorescence at 384 nm (Fig 2B.9). As the amount of azidopropyl groups was increased, the fluorescence of pyrene clicked to them showed decrease in the monomeric pyrene fluorescnce peak at 384 nm with concomitant increase in excimer fluorescence peak at 480 nm due to π-π interaction of closely positioned pyrenes. 10-AZP-MCM clicked with propargyloxy-(1-pyrenyl)methane (**4**) showed only excimer fluorescence indicating all the azido-propyl groups are very close to each other allowing pyrenes to interact with each other. Thus, the fluorescence spectra of propargyloxy-(1-pyrenyl)methane (**4**) clicked to azide functionalized MCM-41

materials show that complete site isolated azido-propyl functionalized MCM-41 materials can be synthesized under basic conditions using 0.2 mole% of AzPTES. With 1 mol% AzPTES, approximately 33% site-isolation was observed. These site isolated azide functionalized MCM-41 materials would be very useful for the synthesis of site isolated organo or organo-metallic catalysts.

2B.4.3.7 Aldol reaction catalyzed by proline anchored on MCM-41

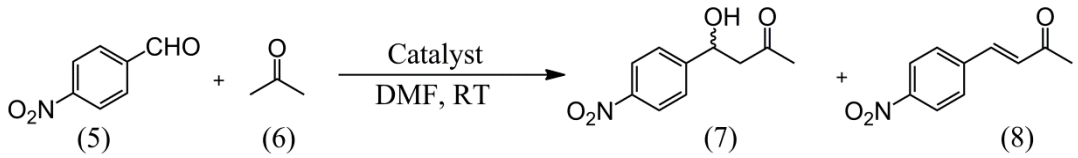

Scheme 2B.4: Aldol reaction catalyzed by Proline immobilized on MCM-41

Proline functionalized MCM-41 materials were used as catalyst for the aldol reaction between p-nitrobenzaldehyde and acetone to yield aldol product **(7)** (scheme 2B.3; Table 2B.3).[32] Initially to find out optimum concentration of proline catalyst required for the reaction, the reactions were carried out using 1, 5, and 10 mole% proline in 1-AZP-MCM-**1** catalyst in DMF (Table 2B.3, entries 1, 2 and 3). Conversion of the starting *p*-nitrobenzaldehyde and yield of the aldol products were determined by using LC-MS technique. These results show that 10 mole% of proline in 1-AZP-MCM-**1** catalyst was sufficient enough to yield 93 % conversion to aldol product **7** in 10 h (Table 2B.3). Hence for all subsequent experiments, 10 mole% proline was chosen as optimum amount of catalyst for the reaction. To confirm that the reaction was catalyzed only by proline, control experiments were carried out to evaluate the effect of surface silanol groups and triazole moiety on the aldol condensation reaction. The absence of the aldol condensation product **7** when 1-AZP-MCM and 1-AZP-MCM-**2** was used as catalyst clearly shows that the surface silanol groups (Table 2B.3, entries 7) and triazole moiety (Table 2B.3, entries 6, and 10) were unable to catalyze the aldol condensation reaction. Next we went on to explore the effect of proline loading onto MCM-41 on the rate of aldol condensation reaction. Three materials 1-AZP-MCM-**1,** 5-AZP-MCM-**1** and 10-AZP-MCM-**1** having proline loadings of 0.112 mmol/g, 0.621 mmol/g and 1.135 mmol/g respectively were used as catalysts for the aldol reaction. (Table 2B.3, entries 3, 4 and 5) The results show that the catalyst 1-AZP-MCM-**1**, obtained by click reaction

Table 2B.3: Aldol reaction catalyzed by Proline-functionalized MCM-41

Sr. No.	Catalyst	Proline incorporated (mmol/g)	Conc. of catalyst (mol%)	Time (h)	Conversion (%) (7)	(8)
1.	1-AZP-MCM-**1**	0.112	1	10	10	1
2.	1-AZP-MCM-**1**	0.112	5	10	76	7
3.	1-AZP-MCM-**1**	0.112	10	10	93	4
4.	5-AZP-MCM-**1**	0.621	10	24	3	0
5.	10-AZP-MCM-**1**	1.135	10	24	2	0
6.	1-AZP-MCM-**2**	0	10	24	0	0
7.	1-AZP-MCM	0	10	24	0	0
8.		-	10	24	64	0
9.		-	10	24	18	0
10.		-	10	24	0	0
11.	1-AZP-MCM-**1**$^{\#}$	0.112	10	10	91	4

two times recycled catalyst

between 1% azide functionalized MCM-41 (1-AZP-MCM; proline loading (0.112 mmol/g)) and 4R-propargyloxy-L-proline (**1**) yielded the aldol product **7** in very high yield where as for the other two materials the yield of the aldol product **7** was <5%. The high efficiency of the 1-AZP-MCM-**1** catalyst may be attributed to the presence of immobilized site isolated proline molecules inside the pores of MCM-41. Using pyrene fluorescence studies we have already observed that 1-AZP-MCM has appreciable amount of site isolated azido-propyl groups; whereas for both 10-AZP-MCM and 5-AZP-MCM the azido-propyl groups are located very close to each other. As a result, prolines that were clicked to 1-AZP-MCM remain mostly far apart from each other and are therefore site isolated. In contrast, the prolines clicked to 10-AZP-MCM and 5-AZP-MCM are located close to each other and probably undergo intermolecular hydrogen bonding with each other through the amine and

carboxylic groups (Scheme 2B.4). The site isolated prolines in 1-AZP-MCM-**1** have free 2° amine and carboxylic acid groups that are easily accessible for aldol condensation reaction. This probably results in dramatic increase in the rate of the reaction. In 5-AZP-MCM-**1** and 10-AZP-MCM-**1**, the proline molecules are anchored rigidly onto the surface of the MCM-41and this can lead to very high intermolecular H-bonding between the adjacent proline molecules. As a result, the free 2° amine and carboxylic acid groups necessary for the aldol condensation reaction remains unavailable. This results in extremely slow aldol condensation reaction between the aldehyde and the ketone. To rule out the possibility that the observed rate differences are due to mass transfer effects (since by weight different amounts of porous materials are used in the reaction), the reactions were carried out using equal weights of 1-AZP-MCM-**1** and 10-AZP-MCM-**1** (Table 2B.3, entries 1 and 5). It is observed that the reaction rates were higher for 1-AZP-MCM-**1** although the amount of catalyst used was 10 times less in 1-AZP-MCM-**1** in comparison to 10-AZP-MCM-**1** (Table 2B.3. Entry 1)**.** It is also interesting to note that the rate of aldol condensation catalyzed by 1-AZP-MCM-**1** is faster than that of pure L- proline under homogeneous condition (Table 2B.3, entries 3, 8 and 9). This is expected, since even under homogeneous conditions the zwitter ionic proline is under dynamic equilibrium between H-bonded prolines and non H-bonded prolines which leads to reduced reaction rates in comparison to 1-AZP-MCM-**1** where most of the prolines are free. We were also able to recycle the catalyst up to three cycles without significant loss of activity (Table 2B.3, entry 11). Even though enantiomerically 4R-propargyloxy-L-proline was used to form covalently anchored proline catalyst, formation of less than 10% enantiomerically pure aldol product **7** was observed. Similar decrease in enantioselectivity by covalent anchoring of proline on silica gel and mesoporous materials has been reported before.[32, 50, 51]

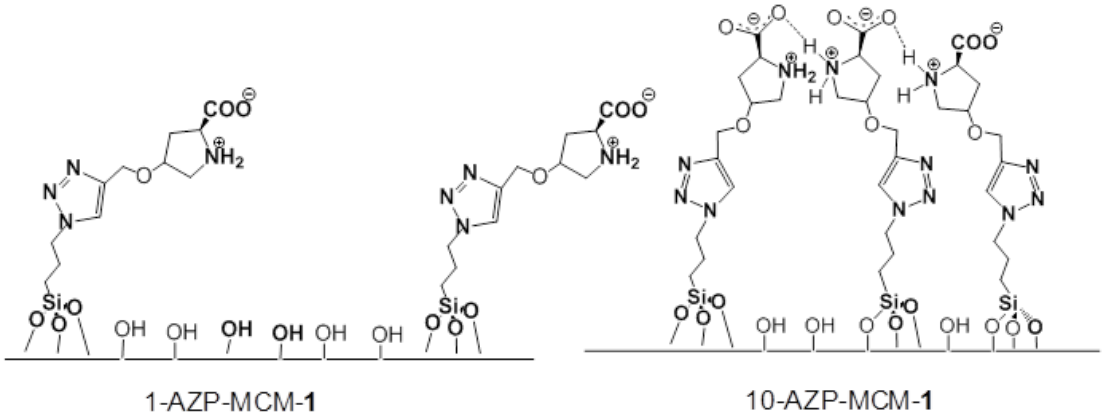

Scheme 2B.5: Schematic illustration of site isolated and site dense proline on 1-AZP-MCM-**1** and 10-AZP-MCM-**1** respectively

2B.5 conclusions

In conclusion, we have reported the synthesis of site dense to site isolated proline anchored on MCM-41 via Cu(I) catalyzed azide alkyne click chemistry between azide functionalized MCM-41 mesoporous materials and 4R-propargyloxy-L-proline. The density of azidopropyl groups on the surface of MCM-41 was varied by varying the molar ratio of AzPTES with respect to TEOS during one pot co-condensation synthesis. The efficiency of these azide functionalized MCM-41 materials to undergo CuAAC reaction has been demonstrated by using variety of organic substrates bearing alkyne functionality. These materials have been well characterized by using various analytical techniques. The heterogeneous site isolated proline catalyst shows dramatic increase in the catalytic rates for the aldol condensation reaction. This strategy can be used to synthesize other organo-catalysts or organo-metallic complexes for the development of catalysts with improved reactivity.

2B.6 References

1. Frank Hoffmann, Maximilian Cornelius, Jürgen Morell and M. Fröba, *Angew. Chem. Int. Ed.*, 2006, **45**, 3216-3251.
2. D. Bruhwiler, *Nanoscale*, 2010, **2**, 887-892.
3. T. J. Terry, G. Dubois, A. Murphy and T. D. P. Stack, *Angew. Chem. Int. Ed.*, 2007, **46**, 945-947.

4. R. Mouawia, A. Mehdi, C. Reye and R. J. P. Corriu, *J. Mater. Chem.*, 2008, **18**, 4193-4203.
5. T. Okino, Y. Hoashi, T. Furukawa, X. Xu and Y. Takemoto, *J. Am. Chem. Soc.*, 2005, **127**, 119-125.
6. D. E. De Vos, B. F. Sels and P. A. Jacobs, *Adv. Syn. Catal.*, 2003, **345**, 457-473.
7. D. E. De Vos, S. de Wildeman, B. F. Sels, P. J. Grobet and P. A. Jacobs, *Angew. Chem. Int. Ed.*, 1999, **38**, 980-983.
8. K. K. Sharma and T. Asefa, *Angew. Chem. Int. Ed.*, 2007, **46**, 2879-2882.
9. J. Nakazawa and T. D. P. Stack, *J. Am. Chem. Soc.*, 2008, **130**, 14360-14361.
10. H. Salmio and D. Bruhwiler, *J. Phy. Chem. C*, 2007, **111**, 923-929.
11. K. K. Sharma, A. Anan, R. P. Buckley, W. Ouellette and T. Asefa, *J. Am. Chem. Soc.*, 2008, **130**, 218-228.
12. K. K. Sharma, R. P. Buckley and T. Asefa, *Langmuir*, 2008, **24**, 14306-14320.
13. M. W. McKittrick and C. W. Jones, *Chem. Mater.*, 2003, **15**, 1132-1139.
14. M. W. McKittrick and C. W. Jones, *J. Am. Chem. Soc.*, 2004, **126**, 3052-3053.
15. M. Luechinger, R. Prins and G. D. Pirngruber, *Micro. Meso. Mater.*, 2005, **85**, 111-118.
16. J. Nakazawa, B. J. Smith and T. D. P. Stack, *J. Am. Chem. Soc.*, 2012, **134**, 2750-2759.
17. T. Bui and C. F. Barbas III, *Tetrahedron Letters*, 2000, **41**, 6951-6954.
18. B. List, *J. Am. Chem. Soc.*, 2000, **122**, 9336-9337.
19. A. CÃ³rdova, W. Notz, G. Zhong, J. M. Betancort and C. F. Barbas, *J. Am. Chem. Soc.*, 2002, **124**, 1842-1843.
20. Y. Hayashi, W. Tsuboi, I. Ashimine, T. Urushima, M. Shoji and K. Sakai, *Angew. Chem. Int. Ed.*, 2003, **42**, 3677-3680.
21. B. List, P. Pojarliev and H. J. Martin, *Org. Lett.*, 2001, **3**, 2423-2425.
22. I. K. Mangion and D. W. C. MacMillan, *J. Am. Chem. Soc.*, 2005, **127**, 3696-3697.
23. R. Thayumanavan, B. Dhevalapally, K. Sakthivel, F. Tanaka and C. F. Barbas III, *Tetrahedron Letters*, 2002, **43**, 3817-3820.
24. M. Gruttadauria, F. Giacalone and R. Noto, *Chem. Soc. Rev.*, 2008, **37**, 1666-1688.
25. C.-J. Li, *Chem. Rev.*, 2005, **105**, 3095-3166.

26. B. M. Trost, *Angew. Chem. Int. Ed. in English*, 1995, **34**, 259-281.
27. R. A. Sheldon, *Pure and Applied Chemistry*, 2000, **72**, 1233-1246.
28. K. A. Scheidt, T. D. Bannister, A. Tasaka, M. D. Wendt, B. M. Savall, G. J. Fegley and W. R. Roush, *J. Am. Chem. Soc.*, 2002, **124**, 6981-6990.
29. Y. Guan, J. Wu, L. Sun and W.-M. Dai, *J. Org. Chem.*, 2007, **72**, 4953-4960.
30. D. Menche, J. Hassfeld, J. Li, K. Mayer and S. Rudolph, *J. Org. Chem.*, 2009, **74**, 7220-7229.
31. K. Sakthivel, W. Notz, T. Bui and C. F. Barbas, *J. Am. Chem. Soc.*, 2001, **123**, 5260-5267.
32. D. Dhar, I. Beadham and S. Chandrasekaran, *Proc. Indian Acad. Sci-Chem. Sci.*, 2003, **115**, 365-372.
33. M. Benaglia, G. Celentano and F. Cozzi, *Adv. Syn. Catal.*, 2001, **343**, 171-173.
34. M. Benaglia, M. Cinquini, F. Cozzi, A. Puglisi and G. Celentano, *Adv. Syn. Catal.*, 2002, **344**, 533-542.
35. D. Font, C. Jimeno and M. A. Pericas, *Org. Lett.*, 2006, **8**, 4653-4655.
36. M. Gruttadauria, F. Giacalone, A. Mossuto Marculescu, P. Lo Meo, S. Riela and R. Noto, *Eur. J. Org. Chem.*, 2007, 4688-4698.
37. P. Kotrusz, I. Kmentova, B. Gotov, S. Toma and E. Solcaniova, *Chem. Commun.*, 2002, 2510-2511.
38. T.-P. Loh, L.-C. Feng, H.-Y. Yang and J.-Y. Yang, *Tetrahedron Letters*, 2002, **43**, 8741-8743.
39. G. Chouhan, D. Wang and H. Alper, *Chem. Commun.*, 2007, 4809-4811.
40. E. Bellis and G. Kokotos, *J. Mol. Catal. A: Chemical*, 2005, **241**, 166-174.
41. J. Huang, X. Zhang and D. W. Armstrong, *Angew. Chem. Int. Ed.*, 2007, **46**, 9073-9077.
42. E. G. Doyaguez, F. Calderon, R. Fernández, F. Sanchez and A. Fernandez-Mayoralas, *J. Org. Chem.*, 2007, **72**, 9353-9356.
43. N. Moitra, P. Trens, L. Raehm, J.-O. Durand, X. Cattoen and M. W. Chi Man, *J. Mater. Chem.*, 2011, **21**, 13476-13482.
44. S. G. Alvarez and M. T. Alvarez, *Synthesis*, 1997, 413-414.
45. P. Chabaud, G. r. Pape, J. r. m. Courcambeck and M. Camplo, *Tetrahedron*, 2005, **61**, 3725-3731.
46. S. Huh, J. W. Wiench, J.-C. Yoo, M. Pruski and V. S. Y. Lin, *Chem. Mater.*, 2003, **15**, 4247-4256.

47. M. Kar, B. Malvi, A. Das, S. Panneri and S. S. Gupta, *J. Mater. Chem.*, 2011, **21**, 6690-6697.

48. F. M. Winnik, *Chem. Rev.*, 1993, **93**, 587-614.

49. A. Katz and M. E. Davis, *Nature*, 2000, **403**, 286-289.

50. A. Sakthivel, A. K. Hijazi, A. I. Al Hmaideen and F. E. Kuhn, *Micro. Meso. Mater.*, 2006, **96**, 293-300.

51. W. He, F. Zhang, X. Shi and H. Li, *Eur. J. Org. Chem.*, 2012, 3753-3758.

CHAPTER 3

Development of Hydrogen Peroxide and Glucose Sensor using [Fe^{III}-(biuret-amide)] Anchored on MCM-41 (MSNs)

3.1 Introduction

Development of biosensors has received enormous attention because of their applications in various fields including health-care, environmental monitoring, food and agriculture industry.[1] A biosensor is an analytical device which converts a biological response into a signal. Now a days, the term 'biosensor' is used in a much broader sense to cover sensor devices used in order to determine the concentration of substances and other parameters of biological interest even where they do not utilize a biological system directly. One of the important component of a biosensor is bioreceptor, which is an immobilized sensitive biological element (e.g. enzyme, DNA probe, antibody etc) recognizing the analyte (e.g. enzyme substrate, complementary DNA, antigen).[2, 3] Enzymes are the most commonly used biosensing elements in biosensors because of their excellent properties such as high substrate specificity and high efficiency under mild conditions.[3]

Among different classes of enzymes, peroxidase enzymes are ubiquitous in nature and are known to activate hydrogen peroxide to perform a variety of chemical reactions such as oxidations.[4] They have been extensively studied for many industrial applications such as bleaching inducer, for example, in the detergent and pulp industries.[5] Although, peroxidases have potential commercial applications in many different areas, the most developed field for their commercial application is in analytical diagnostics.[4, 6] For example, horseradish peroxidase (HRP), a heme-containing peroxidase, is widely used for detection of glucose and in immunoassays where the key step is the peroxidase catalyzed conversion of a non-luminescent substrate into a luminescent one, thus amplifying the signal many fold.[7, 8] However, HRP being a natural enzyme can be easily denatured by environmental changes (such as heating or pH change) because the minor change in their protein conformation could result in significant loss of their catalytic activity.[9] The preparation, purification and storage of natural enzymes are usually time-consuming and expensive. These features of HRP hinder the commercial applications. Hence, for several decades a significant amount of research has been carried out to make systems that mimic HRP. Small molecule analogs that have been reported as peroxidase mimics include synthetic porphyrins, sulfonated phthalocyanins and Fe-TAML's.[10-13] For example porphyrin complexes have been used for the analysis of various analytes.[14-16] However, one of the main shortcomings of porphyrins suffers is that their optimum

reaction occurs in strongly alkaline solution at pH ~ 11, which is higher than that of HRP (pH ~ 6).[17-19] This greatly limits its applications in biological systems where a near neutral pH is required. Another serious disadvantage imposed by these systems is that rather their very acute stability in the aqueous medium due to auto-oxidation and destruction of the porphyrin catalyst itself.[20] The main reason for this is that the environments of the catalytic active sites of porphyrins and HRP are very different. In a natural enzyme, the active site is surrounded by a protein matrix, which protects the active site from such harmful effects.

Recently, various nanomaterials including Fe_3O_4 magnetic NPs,[21, 22] positvely charged gold NPs,[23] and cupric oxide NPs,[24] ceria NPs,[25] graphene oxide,[26] CNTs,[27] carbon nanodots[28] and folate-polyoxometalate hybrid spheres[29] reported to possess peroxidase like activity and have been used for the visual detection of H_2O_2 and glucose. But these NPs display peroxidase activity only in acidic pH, which makes their application as biosensor unwieldy. For example, quantitative detection of glucose by these NPs involves a two step process: first incubation of glucose with glucose oxidase (GOX) at pH 7.4 to generate H_2O_2 and then subsequent incubation of this glucose reaction mixture with NPs at low pH (~4) to oxidize a peroxidase substrate like 3, 3′,5,5′-Tetramethylbenzidine (TMB) to generate a visual signal.[22-24] Thus there is a need for the development of robust materials that can be used in biosensors[30] and immunoassays at physiological pH.

We hereby report the synthesis of mesoporous silica (MSN) based hybrid material (Fe-MSN) that mimics the enzyme HRP and functions as a biosensor at physiological pH. This hybrid material contains a robust small molecule peroxidase mimic [Fe^{III}(biuret-amide)] developed in our group [31] that is covalently attached to azide containing MSN particles by Cu(I) catalyzed azide alkyne cycloaddition reaction (CuAAC).[32, 33] Fe-MSN has several attributes that make them very attractive (i) the small molecule peroxidase mimic [Fe^{III}(biuret-amide)] in Fe-MSN exhibit excellent reactivity and very high stability, especially at low pH and high ionic strength[31] (ii) the co-condensation method used to synthesize the azide grafted material allows the attachment of [Fe^{III}(biuret-amide)] catalysts mostly inside the MSN pore which limits its interaction with enzymes like GOX during one-pot glucose detection[34, 35] (iii) usage of MSN particles having 1% azide groups also allows reasonable site-isolation of the catalyst and this is expected to reduce intermolecular

degradation of the catalyst as has been shown before[33] (iv) Site isolation of [Fe^{III}-(biurate-amide)] catalyst inside the pore channels in Fe-MSN is analogous to the prosthetic group of the enzyme embedded in the cavity surrounded by protein matrix. Analogous in the sense of site isolation which, enhances the stability and activity of the complex by overcoming intermolecular degradation and attenuating formation of μ-oxo dimer complex and (v) the silanol groups on the outer surface of MSN can be further functionalized to incorporate targeting ligands such as antigens/antibodies for usage in immunoassays like ELISA. The synthesized Fe-MSN nanoparticles were characterized by several techniques such as FT-IR, EPR, ICP and nitrogen adsorption-desorption experiments. We also show that these hybrid MSN particles can be used as a biosensor for the quantitative detection of H_2O_2 and glucose in a one-pot method.

3.2 Experimental

3.2.1 Materials

Tetraethylorthosilicate (TEOS), Cetyltrimethylammonium bromide (CTAB), Amino guanidine hydrochloride (AG.HCl), glucose oxidase (GOX) and 3 ,3′, 5, 5′-Tetramethylbenzidine (TMB) were obtained from Sigma Aldrich. $CuSO_4$, Sodium ascorbate, hydrogen peroxide, glucose and fructose were obtained from Merck, India. Maltose and lactose were obtained from SRL. All the chemicals used were of extrapure for biochemistry grade or of analytical grade and used as received. Tris(3-hydroxypropyltriazolylmethyl)amine (THPTA)[36] was prepared by following procedure reported in the literature.[36] For all the experiments de-ionized water was used.

3.2.2 Syntheses

3.2.2.1 Synthesis of Azide grafted MSN by one pot co-condensation

The azide functionalized MSN was synthesized by co-condensation of TEOS with AzPTES (3-azidopropyltriethoxysilane) by following procedure reported in literature[37, 38] with slight modifications. In a typical batch synthesis, CTAB (1 g, 2.744 mmol) was dissolved in 480 mL of water and 2M aqueous NaOH (3.5 mL, 7 mmol). The mixture was stirred thoroughly at 600 rpm for 30 min at 80 °C to dissolve the surfactant completely. To this clear solution, TEOS (4.702g, 22.56 mmol) was injected rapidly followed by AzPTES (0.0563 g, 0.228 mmol). A white

precipitate was observed within 1-2 min after the addition was completed. The resultant reaction mixture was allowed to stir at 600 rpm for 2 h at 80 °C. The hot contents were then filtered and the white residue was washed with copious amounts of water and methanol and dried under vacuum at 100 °C over night (yield ~1.7 g). The template was extracted by stirring the as-synthesized sample (0.8 g) in 150 mL methanol and 1 ml concentrated hydrochloric acid at 60 °C for 6 hr. The resulting template removed solid product, was filtered and washed with copious amount of methanol and then dried under vacuum at 100 °C over night (yield ~0.48 g). This azide grafted MSN will be simply denoted as N_3-MSN. Elemental analysis : C, 0.53; H, 0.1; N, 0.51% .

3.2.2.2 Modification of N_3-MSN by Cu(I) catalyzed azide-alkyne aycloaddition reaction (CuAAC)

For CuAAC, the azide functionalized MSN (N_3-MSN) was incubated with 3 equivalents of the alkyne tailed [Fe^{III}(biuret-amide)] complex in 100 mM phosphate buffer containing THPTA (2.5 equivalent), AG.HCl (4 equivalent), $CuSO_4$ (0.5 equivalent) and sodium ascorbate (4 equivalent). In a typical click reaction, N_3-MSN (10 mg, 1.2 µmol of azide) was incubated with alkyne tailed [Fe^{III}(biuret-amide)] complex (3 mg, 3.6 µmol) in 1mL, 100 mM phosphate buffer containing THPTA (1.3 mg, 3 µmol), AG.HCl (0.54 mg, 4.8 µmol), $CuSO_4$ (0.16 mg, 0.6 µmol). The reaction mixture was freeze pump thawed thrice and sodium ascorbate (0.96 mg, 4.8 µmol) was added and the mixture was stirred for 24 h. After completion of reaction, the reaction mixture was centrifuged and the residue was first washed with phosphate buffer twice and then sequentially washed with 10 mM N,N-diethyldithiocarbamate sodium solution in 100 mM phosphate buffer and acetone respectively. The last two washings were repeated thrice. Finally, the yellowish white powder obtained was dried at 80°C in vacuum oven for 8 h. Yield: ~9 mg. This [Fe^{III}(biuret-amide)] functionalized MSN will be simply denoted as Fe-MSN.

Similarly, one more click reaction was carried out with N_3-MSN using propargyl alcohol. This product was denoted as PrOH-MSN.

3.2.2.3 Detection of hydrogen peroxide

Preparation of phosphate buffers: Stocks of 0.5 M phosphate buffers of required pH were prepared using phosphate salts and then diluted with de-ionized water to the required strength. The pH was adjusted again if required, autoclaved and preserved at 4 ˚C for further use.

Stock solutions: 50 mM solution of TMB was prepared in 0.1N aqueous hydrochloric acid. Hydrogen peroxide solutions of various concentrations were prepared in de-ionized water. 1 mg/mL of Fe-MSN catalyst solution was prepared in phosphate buffer (150 mM, pH 7) and particles were dispersed by sonication.

Procedure: In 1.5 mL eppendorf tubes, 10 μL of TMB solution, 747 μL of de-ionized water, 133 μL of phosphate buffer (150 mM, pH 7), 200 μL hydrogen peroxide solutions of various concentrations and 10 μL of catalyst solution were mixed and allowed to stand at room temperature with occasional shaking for 15 min. At the 15^{th} min, the mixture was centrifuged and absorbance was noted at 650 nm.

3.2.2.4 Kinetics of TMB Oxidation

The kinetics was monitored in kinetic mode of the spectrophotometer (Perkin-Elmer –λ35) using 1 ml quartz cuvette of 1.00 cm path length at 650 nm (one of the absorption peaks of oxidized product of TMB) in thermostatic (40.0 ± 0.5 °C) cell housing. Initial rates of TMB oxidation were calculated from the linear absorbance versus time plots using the extinction coefficients of 39000 $M^{-1}cm^{-1}$ which stands for oxidation product of TMB at 650 nm when the conversion of the TMB did not exceed 10 – 20%. 1 mg of Catalyst was dissolved in 1mL double distilled water and was treated as stock solution. Concentration of H_2O_2 was calculated from the UV absorbance at 240 nm using the characteristic molar extinction coefficient of H_2O_2 at 240 nm (ε = 43.6 dm^3 $M^{-1}cm^{-1}$). For mechanistic studies, H_2O_2 was varied from 4.7×10^{-3} to 3.5×10^{-1} M while keeping the TMB concentration fixed at 4.7×10^{-4} M. For TMB variation, the reverse procedure was followed ($[H_2O_2] = 4.0 \times 10^{-3}$ M; [TMB] = $2.8 \times 10^{-5} – 2.8 \times 10^{-4}$ M). In all kinetic runs, the catalyst concentration was kept constant. In each set of H_2O_2 variation, 10 μL stock catalyst solution was added while in case of TMB variation 15 μL stock catalyst solution was added. Phosphate buffer having the appropriate pH of 4, 5, 6, 7 was used

for different runs. For each set, after completion of reaction pH of the solution was measured with a pH meter (LABINDIA, PICO+) using calibrated electrode. The kinetic parameters were calculated according to the equation,

$$v = V_{max} \times \frac{[S]}{K_m + [S]}$$

where v stands for initial rate or initial velocity, V_{max} is the maximal velocity, [S] is the concentration of the substrate and K_m is the Michaelis constant.

3.2.2.5 Detection of glucose

Stock solutions: 5 mg/mL solution of glucose oxidase was prepared in phosphate buffer (10 mM, pH 7.4). 50 mM solution of TMB was prepared in 0.1N aqueous hydrochloric acid. Glucose and mannose solutions of various concentrations were prepared in phosphate buffer (10 mM, pH 7.4). 1 mg/mL Fe-MSN catalyst solution was prepared in phosphate buffer (10 mM, pH 7.4) and the nanoparticles were dispersed by sonication.

Procedure: In 1.5 mL eppendorf tubes, 750 µL glucose solution with varying concentration, 60 µL of glucose oxidase solution, 10 µL of TMB solution and 15 µL of catalyst solution were incubated at 37 °C with occasional shaking for 50 min. At the 50^{th} min, reaction mixture was centrifuged and absorbance was noted at 650 nm. Absorbance versus concentration of glucose were plotted and fitted according to the linear equation y = a + b*x where a = 0.0247 ± 0.002, b = 444 ± 16 and R^2 = 0.9910.

3.2.2.5.1 Detection of glucose in blood plasma

Blood plasma obtained from a healthy mice was diluted 30, 40, 60 and 120 times respectively with 10 mM phosphate buffer of pH 7.4 and detection of glucose was carried out as mentioned above.

3.3 Analytical and characterization methods

Powder X-ray diffraction of all the samples was carried out in a PANalytical X'pert Pro dual goniometer diffractometer. A proportional counter detector was used for low angle experiments and an X'celerator solid state detector was employed in the low angle experiments. The radiation used was Cu Kα (1.5418Å) with a Ni filter and

the data collection was carried out using a flat holder in Bragg–Brentano geometry (0.5 to 5°; 0.2° min^{-1}). Care was taken to avoid sample displacement effects. SEM images were obtained on Leica Stereoscan 440 microscope. HR-TEM images were taken on a FEI Technai F30 operating at 300 kV with FEG. The samples were prepared by dispersing a large number of solid particles in isopropanol by sonication, and dropping the resulting suspension on a copper grid of 400 mesh and allowed to dry in air. Nitrogen adsorption and desorption studies were carried out at 100°C using Quantachrome instrument. Samples were preheated at 100°C for 18 hours in the vacuum line. Single point BET surface area was obtained from the nitrogen adsorption-desorption data at P/P_0 ~0.249. Pore size distributions were calculated using the BJH method. Semi-quantitative FT-IR spectra were recorded on Perkin Elmer FT-IR spectrum GX instrument by making KBr pellets. Pellets were prepared by mixing 3 mg of sample with 97 mg of KBr. Yields for CuAAC reactions were calculated from corrected area under the curve characteristic for the azide stretch at ~2100 cm^{-1}. ICP experiments were performed on a Thermo IRIS Intrepid spectrum apparatus. In a typical procedure, sample was prepared by heating a known amount of solid sample in 20 mL aqua-regia to demetalate the Fe^{+3} ions from the ligand environment and then mixture was concentrated to about 3 mL by heating. This was subsequently diluted with de-ionized water and then filtered to make and the volume up to 10 mL using de-ionized water for the quantitative analysis of Fe and Cu using the ICP instrument. UV-Vis experiments were carried out on Perkin Elmer PL Lambda 950 spectrophotometer using 1 mL cuvettes with 10 mm path length. Thermogravimetric analysis (TGA) of the silica nanoparticles were carried out using a TA Instrument SDT Q600 analyzer between 100 and 800°C in air (flow 25 ml min^{-1}) at a heating rate of 5° min^{-1}. All samples were stirred in water overnight, centrifuged and dried under vacuum at 80°C overnight prior to TGA runs. The graft density of the grafted organic moiety on the silica surface was determined by TGA using the following equation:

$$\text{graft density (mmol/g)} = \frac{\left(\frac{W_{\text{grafted MSN(150-750)}}}{100 - W_{\text{grafted MSN(150-750)}}} \times 100\right) - \left(\frac{W_{\text{MSN(150-750)}}}{100 - W_{\text{MSN(150-750)}}} \times 100\right)}{M \times 100} \times 10^3 \quad \text{..... (Eq. 3.1)}$$

where $W_{grafted\ MSN(150\text{-}750)}$ is the weight loss between 150^0C and 750^0C corresponding to the decomposition of the organic moiety from silica surface corrected from the thermal degradation**,** and M is the molecular weight of the decomposed organic moiety, while $W_{MSN(150\text{-}750)}$ represents the weight loss of calcined silica without organic functional groups (CAL-MSN). EPR spectrum was recorded on a Bruker EMX X-band spectrometer operating at a field modulation of 100 kHz, modulation amplitude of 4 G and microwave radiation power of 4 mW. The solid Fe(III) complex was taken in a quartz: tube and the spectrum was recorded at 94 K.

3.4 Results and discussion

3.4.1 Synthesis of azide functionalized mesoporous silica nanoparticles

The azide functionalized mesoporous nanoparticles (N_3-MSN) were prepared by one pot co-condensation of TEOS and AzPTES using CTAB as structure directing agent under basic conditions, as shown in the scheme 3.1.[37, 38] For the synthesis of N_3-MSN via one pot co-condensation method the molar ratio of TEOS to AzPTES used was 9.9:1. After synthesis, template was removed by stirring the as-synthesized sample in methanol/HCl at 60 °C. The elemental analysis of the AZP-MSN shows incorporation of 0.12 mmol of azide functional goups per gram of MSN particles. After template removal, N_3-MSN was characterized by a variety of analytical techniques such as powder XRD, SEM, TEM, TGA, nitrogen adsorption-desorption experiments etc.

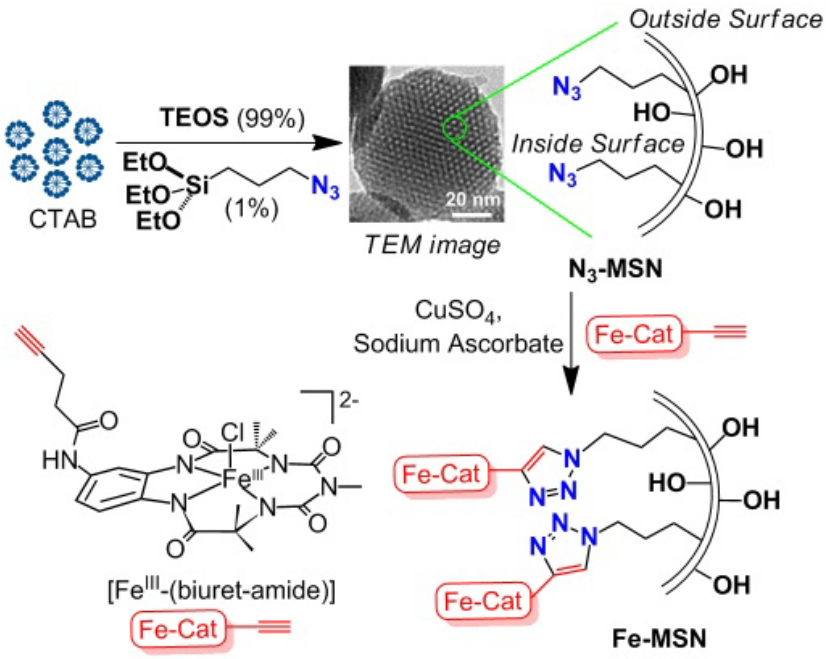

Scheme 3.1: Synthesis of [Fe^{III}(biuret-amide)] functionalized MSN

3.4.2 Modification of N_3-MSN by Cu(I) catalyzed azide-alkyne cycloaddition reaction (CuAAC)

The azido propyl labelled MSN's (N_3-MSN) were subjected to Cu(I) catalyzed azide-alkyne cycloaddition reaction(CuAAC) with Fe^{III}-(biuret-amide)]-alkyne complex using $CuSO_4$ and sodium ascorbate (Scheme 3.1). For the efficient CuAAC various reagents were employed during the click reaction as described in the literature.[36] After the click reaction, an extensive washing protocol was used to remove Cu (I) and other reagents used. One of the key steps in washing protocol was the use of dithiocarbamate to remove Cu(I), as reported earlier.[33] Efficient removal of copper during the washing protocol has been observed from the absence of copper in ICP analysis. This material is labelled as Fe-MSN and it has been characterized by variety of analytical techniques.

3.4.3 Characterizations

3.4.3.1 Powder X-ray diffraction

Powder XRD patterns of the obtained mesoporous materials were shown in the Fig. 3.1. Powder XRD pattern of N_3-MSN shows characteristic high intensity 100 peak at 2θ = ~2.3º. The other significant peaks corresponding to 110 and 200

diffractions were also observed indicating that well-ordered two-dimensional hexagonal mesoporous channels were formed and remained intact under one pot co-condensation functionalization environment. To characterize the click product by powder XRD, propargyl alcohol clicked MSNs (PrOH-MSN) were used to obtain p-XRD patterns. The p-XRD showed one intense (100) diffraction peak near 2θ~2.3° showing that the mesoporosity of the material does not change after undergoing click reaction.

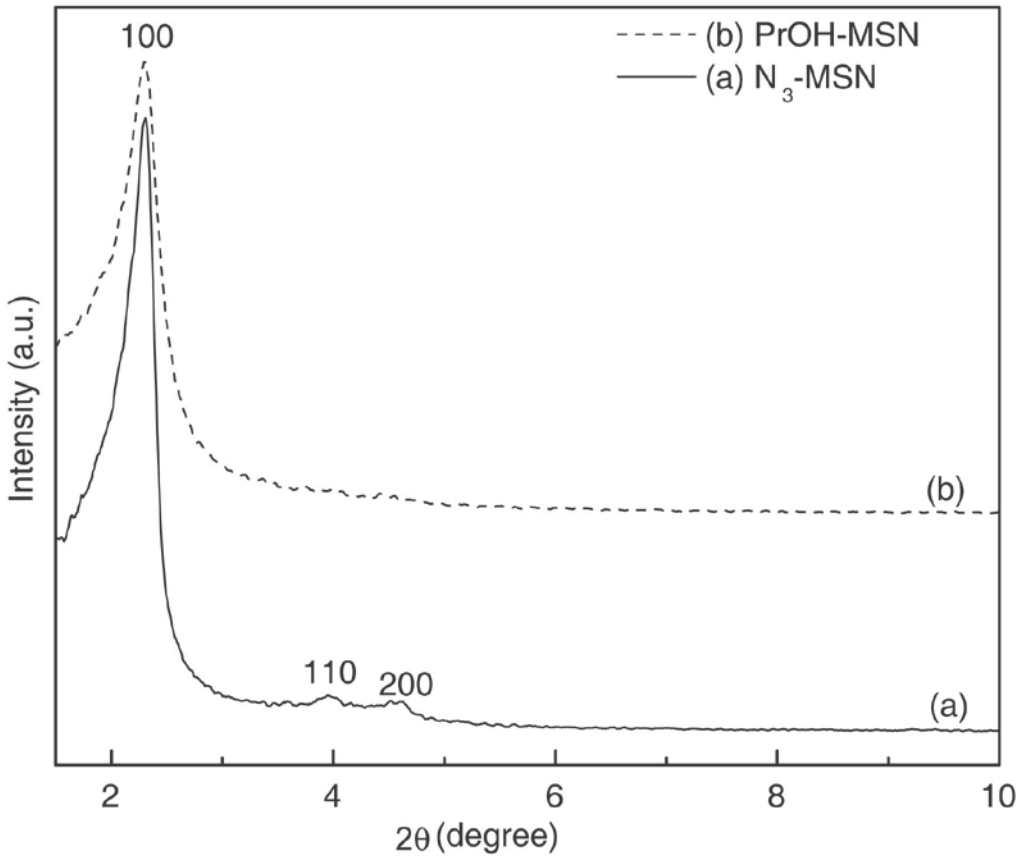

Figure 3.1: Powder XRD patterns of (a) azide functionalized MSNs (N3-MSN and (b) N3-MSN clicked with propargyl alcohol (Pr-OH MSN).

3.4.3.2 Scanning and transmission electron microscopy

Scanning electron microscopy (SEM) and transmission electron microscopy (TEM) images of N_3-MSN are displayed in Fig. 3.2. SEM and TEM showed formation of well-ordered two-dimensional hexagonal mesoporous particles with a spherical morphology having particle size of 100±10 nm

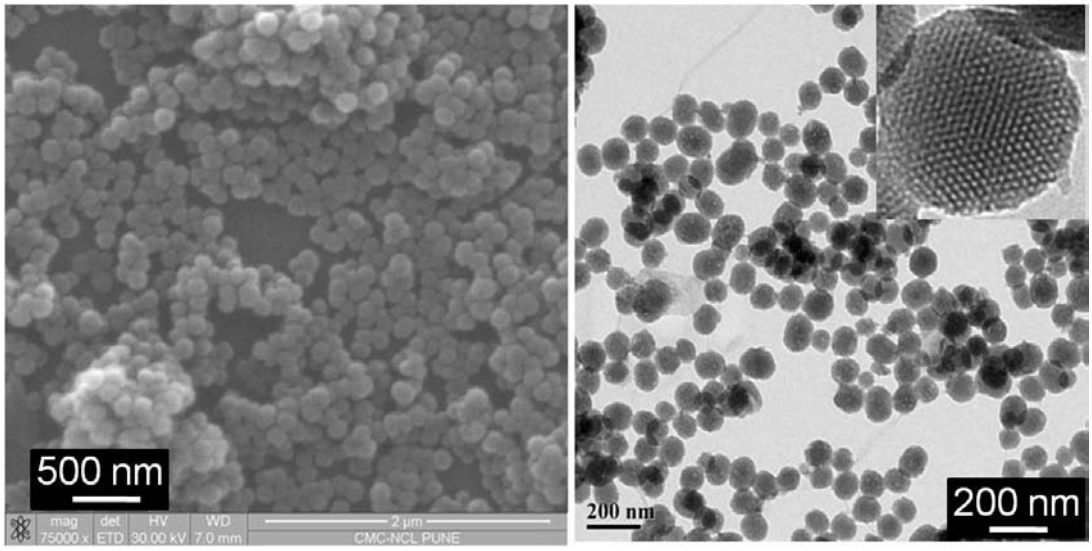

Figure 3.2: (a) SEM and (b) TEM images of N_3-MSN respectively

3.4.3.3 Nitrogen adsorption-desorption studies

The nitrogen adsorption-desorption isotherms of various functionalized mesoporous material are presented in Fig. 3.3. Nitrogen adsorption-desorption isotherm of N_3-MSN exhibit the characteristic type IV isotherm with slight increase in adsorption at P/P_0 0.2-0.4 due to slight capillary condensation of the nitrogen in the mesopores. The BJH pore-size distribution (PSD) analysis shows very narrow PSD values in the range 2-3 nm. The pore diameter, BET surface area and pore volume are listed in Table 3.1. These values are consistent with other organo-functionalized MSNs reported before.[37, 38] The N_2 adsorption-desorption isotherm of Fe-MSN displayed similar profile to its parent N_3-MSN, which indicates that the material did not undergo any physical change during the course of the click reaction and its subsequent workup.

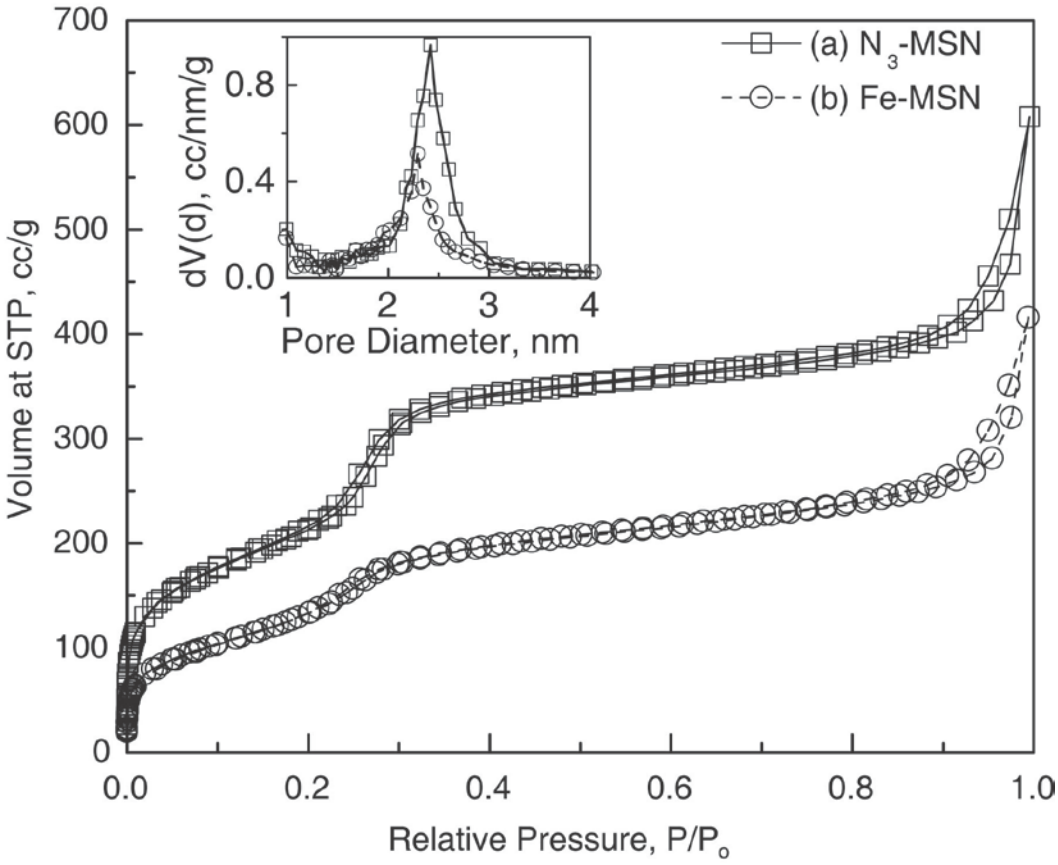

Figure 3.3: Nitrogen adsorption-desorption isotherms of (a) N_3-MSN and (b) Fe-MSN

Table 3.1: Physical properties of N_3-MSN and Fe-MSN materials

Sample Name	M_{BET} (m^2/g)	Pore Diameter (nm)	Pore Volume (cm^3/g)
N_3-MSN	724	2.4	0.93
Fe-MSN	517	2.3	0.64

3.4.3.4 FT-IR spectroscopy

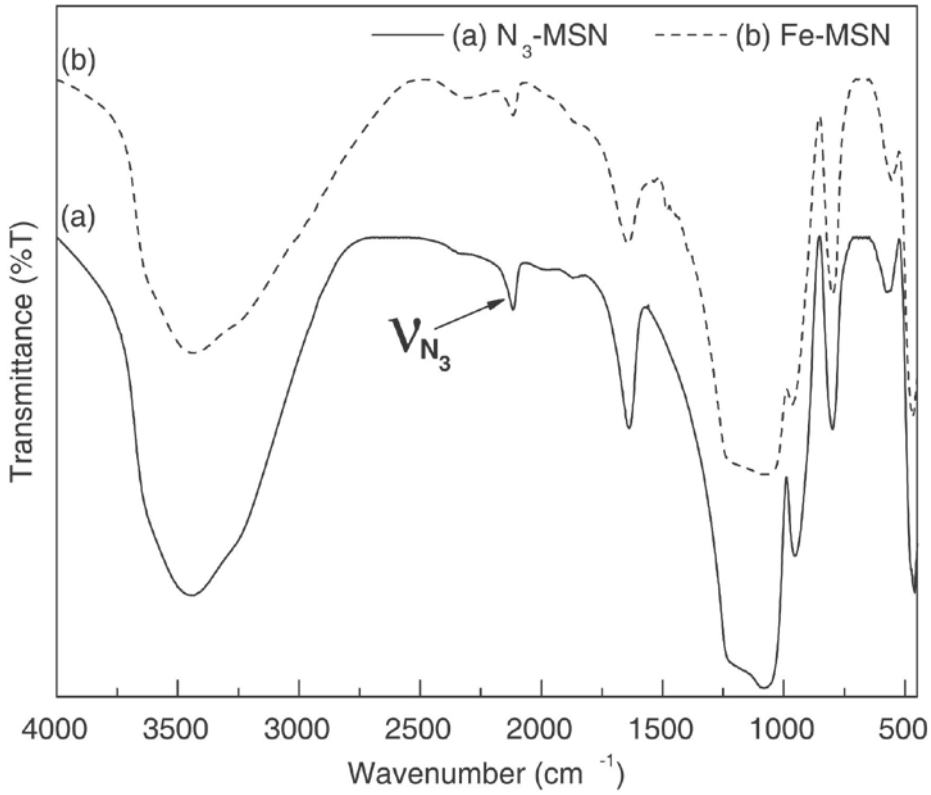

Figure 3.4: FT-IR spectra of (a) N_3-MSN and (b) Fe-MSN

The FT-IR spectra of various materials are presented in the Fig. 3.4. The spectra of the N_3-MSN display an absorbance at ~2100 cm^{-1}, which is the characteristic stretching vibration of an organic azide (Fig. 3.4a). The presence of this peak in the materials shows that the azidopropyl groups were successfully incorporated into N_3-MSN samples. The samples also showed absorbance peaks at 1230, 1080, 805 and 465 cm^{-1} respectively. These peaks are typical of Si-O-Si bands that are associated with the formation of the silica networks. Weak peaks associated with Si-OH groups in the 940-960 cm^{-1} range were also observed for the functionalized mesoporous materials. The strong peak around 1658 cm^{-1} might be attributed to the bending vibration of H_2O. Thus, the FT-IR spectra indicate that the azido groups were efficiently incorporated in the matrix of the mesoporous silica nanoparticles by the one-pot co-condensation technique. IR spectrum of Fe-MSN shows about 50% decrease in the integrated intensity of $\nu_{as}(N_3)$ at 2100 cm^{-1} (Fig. 3.4b).

3.4.3.5 Thermogravimetric analysis

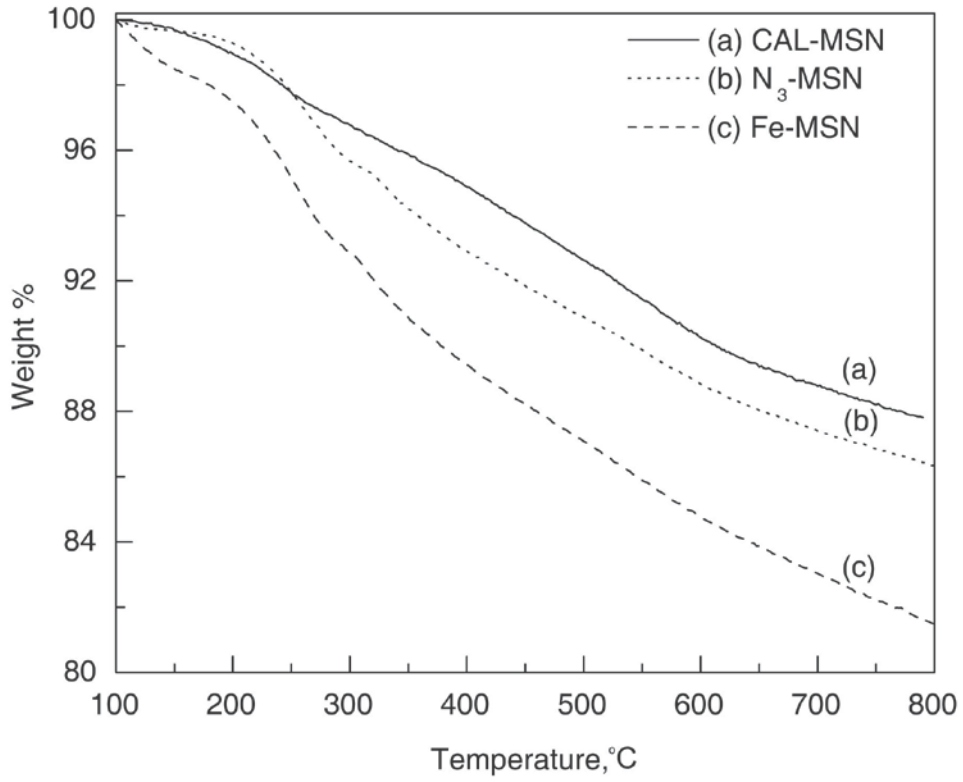

Figure 3.5: TGA graphs for various MSN materials (a) Calcined MSN (b) N_3-MSN and (c) Fe-MSN

The TGA graphs of various MSNs materials are presented in the Fig. 3.5. The amount of azido-propyl groups present in the N_3-MSN were determined by the weight loss obtained in the thermogravimetric analysis (TGA). The samples were heated in air at 5 °C/ minute to 800 °C so that the azidopropyl groups were completely decomposed and removed from the samples. Fig. 3.5b shows the TGA thermographs of the N_3-MSN sample, the weight loss between 150 – 750 °C corresponds to 0.2 mmol of azide groups/g of N_3-MSN (Fig. 3.5, Eq. 3.1). Also from the elemental analysis the amount of azide groups present on the surface of N_3-MSN was determined to be 0.12 mmol/g. The calcined MSNs (CAL-MSN) show a weight loss of about 11.48 %, which can be attributed to the loss water molecules strongly adsorbed of the silica surface as well as loss of water molecules due to condensation of silanol groups at high temperature. Similar weight losses have been also reported by Wei et al.[39, 40] The TGA analysis of Fe-MSN indicated a weight loss of 16.24% between 150 – 750 °C which corresponds to a loading of 0.056 mmol of

[Fe^{III}(biuret-amide)] complex per gram of Fe-MSN (Fig. 3.5, Eq. 3.1). Also from the ICP analysis the amount of catalyst incorporated was determined to be 0.048 mmol/g.

3.4.3.6 Electron paramagnetic resonance spectroscopy

The EPR spectrum of Fe-MSN is shown in Fig. 3.6. The solid Fe-MSN sample was taken in a quartz tube and the spectrum was recorded at 94 K. The resonance peak at around 3390 G corresponds to 'g' value of 1.96 and the other resonance peak at around 1570 G corresponds to 'g' value of 4.2. Both these peaks refer to an oxidation state of Fe(III) characteristic of [Fe^{III}-(biuret-amide)] complex.[31]

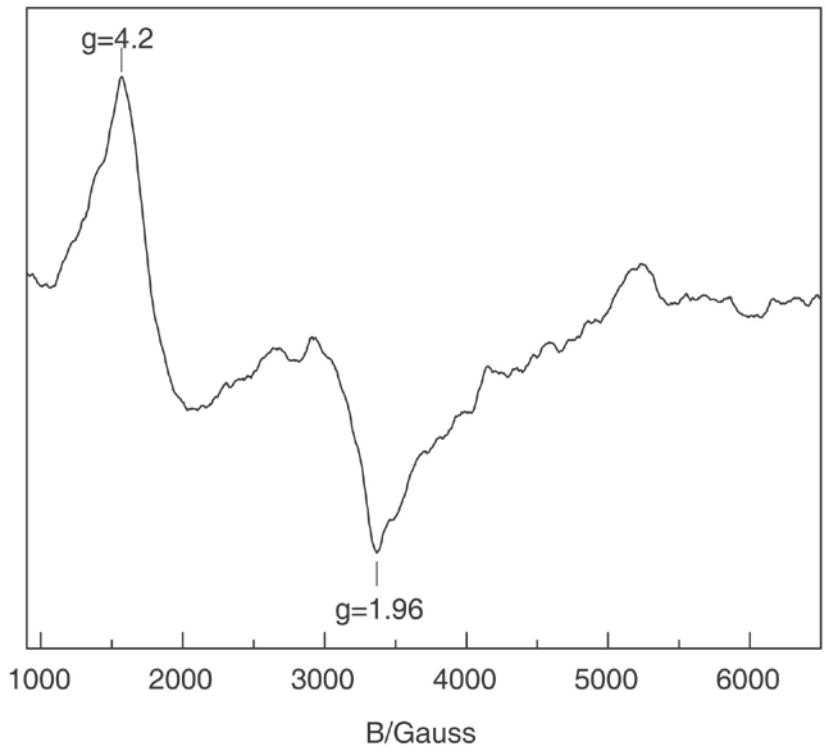

Figure 3.6: X-band EPR spectrum of Fe-MSN solid at 94K

3.4.4 Detection of hydrogen peroxide

To investigate the peroxidase like activity of the Fe-MSN particles, the catalytic oxidation of peroxidase substrate 3, 3′,5,5′-Tetramethylbenzidine (TMB) in the presence of hydogen peroxide was tested (Fig. 3.7). Catalytic oxidation of TMB by Fe-MSN in presence of H_2O_2 yields a blue colored solution. The blue color of the solution results from the product formed by the oxidation of TMB, which gives a maximum absorbance at 650 nm in UV-Vis spectrum. To confirm the blue color is formed because of the catalytic activity of the [Fe^{III}(biuret-amide)] complex anchored

on the surface of MSN's, a series of control experiments were carried out using azide functionalized MSN particles (N_3-MSN) and propargyl alcohol clicked MSN particles (PrOH-MSN). Both the materials did not produce blue color to the solution even after 3 h of incubation time. Thus the blue color to the solution originates from the catalytic activity of the [Fe^{III}(biuret-amide)] complex anchored on the MSN particles. Since the catalytic activity of the Fe-MSN is dependent on the concentration of the hydrogen peroxide in the solution, this method can be used for the quantitative estimation of hydrogen peroxide. Fig. 3.8 shows, the change in absorbance at 650 nm with increase in the concentration of the hydrogen peroxide in solution. The calibration graph of the absorbance at 650 nm to concentration of hydrogen peroxide is linear in the range 1.0×10^{-4} to 5.0×10^{-3} M with a detection limit at 1.0×10^{-5} M.

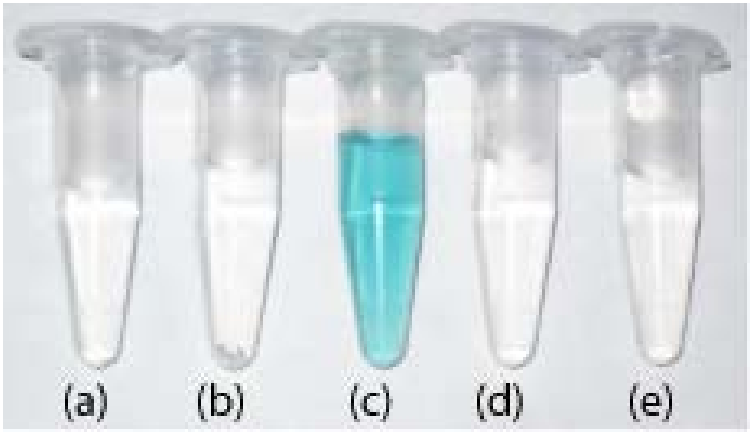

Figure 3.7: Typical images of: (a) TMB and H_2O_2 in the absence of Fe-MSN, (b) TMB and Fe-MSN in the absence of H_2O_2, (c) TMB and H_2O_2 in the presence of Fe-MSN, (d) TMB and H_2O_2 in the presence of N_3-MSN and (e) TMB and H_2O_2 in the presence of propargyl alcohol clicked MSN particles (PrOH-MSN).

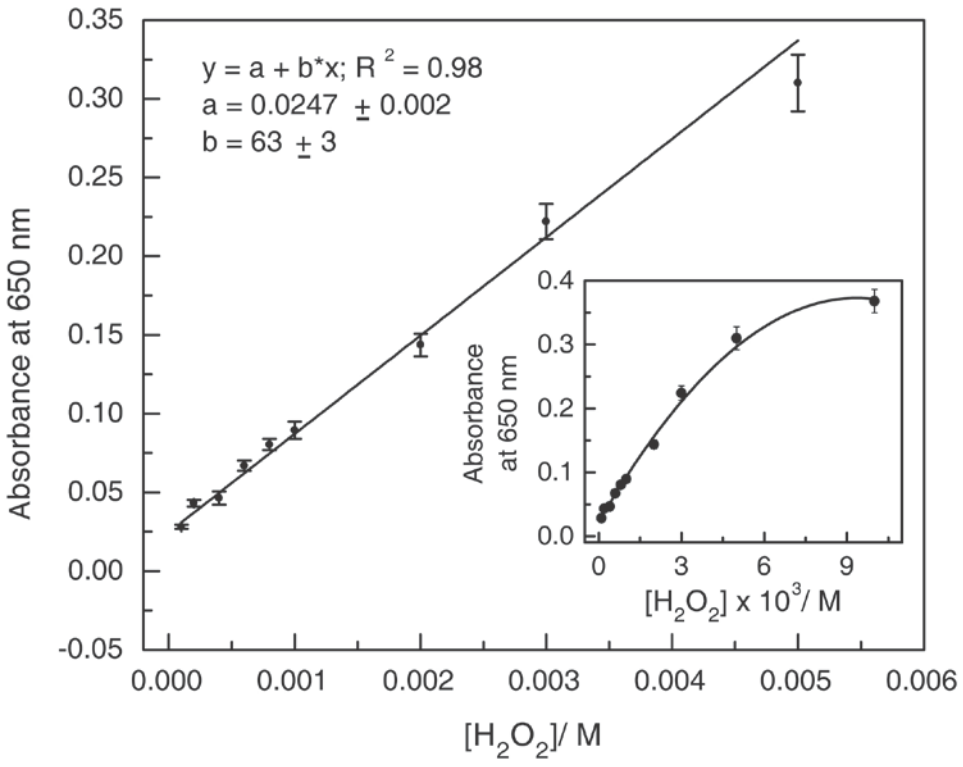

Figure 3.8: Linear calibration plot between the absorbance at 650 nm and concentration of H_2O_2 at pH 7. The insert shows the dependence of the absorbance at 650 nm on the concentration of H_2O_2 in the range 0.1 mM to 10 mM.

3.4.4.1 Kinetic studies of TMB oxidation by Fe-MSN

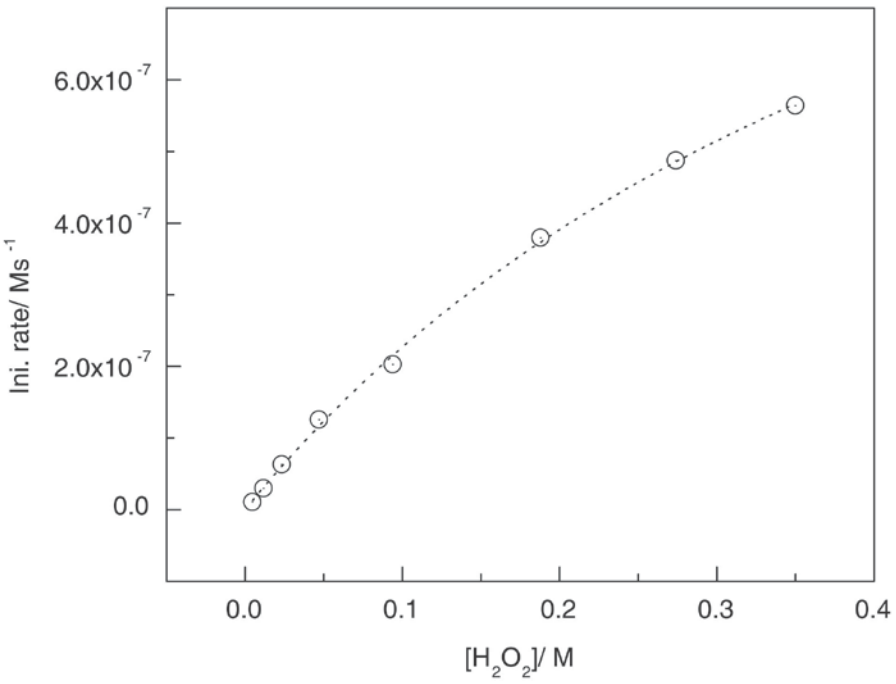

Figure 3.9: Plot of initial rate (v) *vs.* $[H_2O_2]$

Black dots were experimental points. The dotted line was drawn according to the equation $v = V_{max} \times [S]/(K_m + [S])$ where V_{max} is the maximal reaction velocity and K_m stand for Michaelis constant. In all the kinetic runs, [TMB] = 4.7×10^{-4} M; 1 ml reaction solution contained 10 µL of 1mg/ ml catalyst solution. *I* = 10 mM; pH 7.4 (phosphate buffer); T = 40 °C

To investigate the peroxidase like activity of Fe-MSN, we studied the apparent steady-state kinetic parameters for the TMB oxidation reaction by Fe-MSN. The kinetic data were fitted perfectly to a typical Michaelis-Menten curve (Fig. 3.9 and 3.10). The K_m (Michaeilis constant) and V_{max} (maximal reaction velocity) values determined from the Michaelis-Menten curve are given below (Table 3.2). The K_m value of the Fe-MSN with H_2O_2 as the substrate was significantly higher than that of HRP [21] (Table 3.2) consistent with the observation that a higher concentration of H_2O_2 was required to observe maximal activity for the MSN where as K_m value of the Fe-MSN with TMB as the substrate was about 10 times lower than HRP, suggesting that the Fe-MSN have a higher affinity for TMB than HRP.[21]

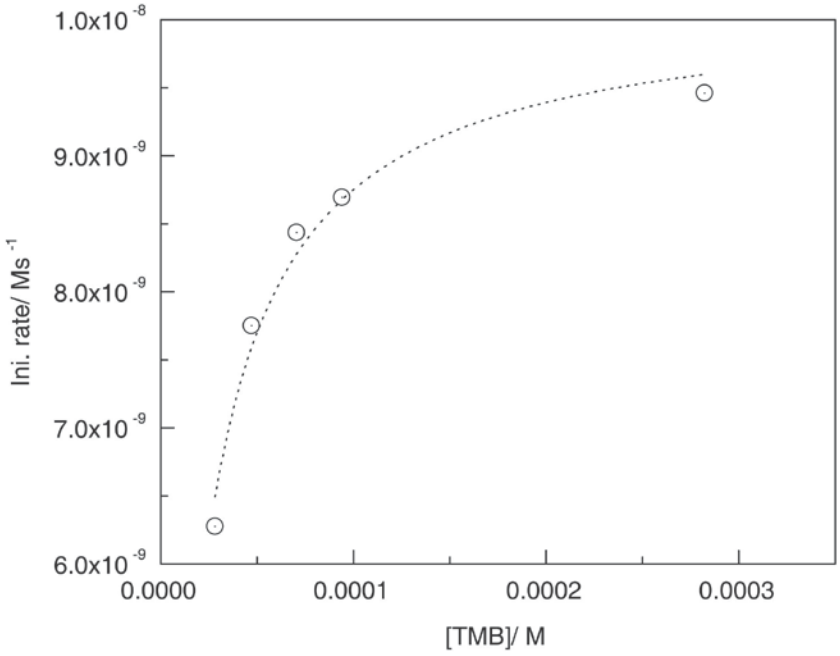

Figure 3.10: Plot of initial rate(v) *vs.* [TMB].

Black dots were experimental points. The dotted line was drawn according to the equation $v = V_{max} \times [S]/(K_m + [S])$. In all the kinetic runs, $[H_2O_2] = 4.0 \times 10^{-3}$ M;

1 ml reaction solution contained 15 µL of 1mg/ ml catalyst solution. *I* = 10 mM; pH 7.4 (phosphate buffer); T = 40 °C (See Table 3.2)

Table 3.2: Comparison of kinetic parameters of TMB oxidation by Fe-MSN and HRP

Catalyst	Substrate	V_{max}/ Ms^{-1}	K_m/ M
MSN	TMB	1.01×10^{-8}	1.58×10^{-5}
	H_2O_2	1.41×10^{-6}	5.2×10^{-1}
HRP [21]	TMB	10.0×10^{-8}	4.34×10^{-4}
	H_2O_2	8.71×10^{-8}	3.70×10^{-3}

3.4.5 Detection of glucose

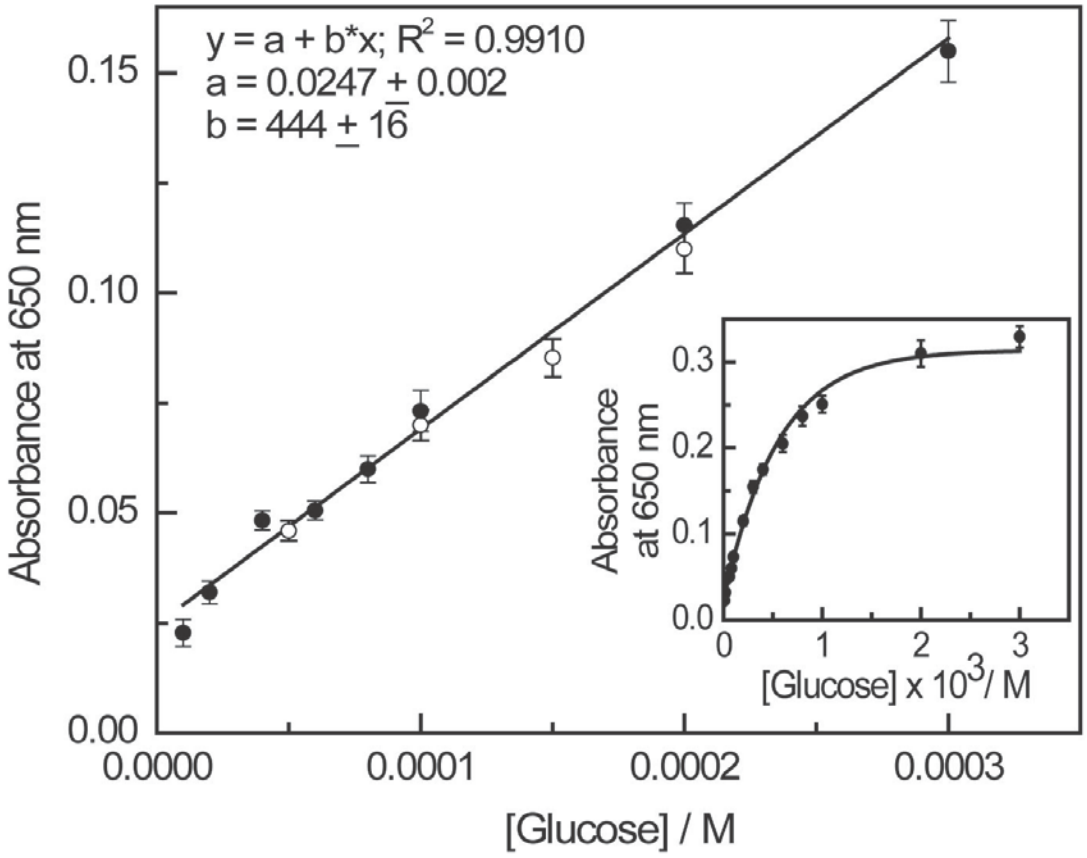

Figure 3.11: (●)Linear calibration plot between the absorbance at 650 nm and concentration of glucose at pH 7.4. The insert shows the dependence of the absorbance at 650 nm on the concentration of glucose in the range 0.01 mM to 3 mM. (○) Glucose in mice blood plasma analysis.

Further, we extended the peroxidase like activity of the Fe-MSN particles for the detection of glucose by coupling the above catalytic reaction with glucose oxidation reaction by glucose oxidase (GOX). The GOX oxidizes glucose to form gluconic acid and H_2O_2 quantitatively; the H_2O_2 thus produced is then utilized by Fe-MSN to oxidize TMB to produce a blue colored solution. Using this methodology, the calibration graph of the absorbance at 650 nm to concentration of glucose was found to be linear in the range 2.0×10^{-5} to 3.0×10^{-4} M with a detection limit of 1.0×10^{-5} M under the experimental conditions (Fig. 3.11). The limit of detection (LOD) of Fe-MSN is slight lower than that of gold nanoparticles[23] (LOD 1.8×10^{-5} M) and Fe_3O_4 nanoparticles[22] (LOD 5×10^{-5} M). Our methodology allows detection of glucose in one pot reaction at physiological pH in which the GOX, glucose and Fe-MSN are all added together. This is in contrast to most other literature methods using nanoparticles which use a two-step process as described before.[22-24] In Fe-MSN nanoparticles, most of the [Fe^{III}(biuret-amide)] catalysts are anchored inside the 2.3 nm pore channels which allows access to small molecules such as H_2O_2 and TMB while large molecules like glucose oxidase are excluded since they cannot enter the pore channels because of their large size. As a result, multistep reactions occur at two different parts of the material, i.e. generation of H_2O_2 from glucose using GOX occurs outside the pore channels while the oxidation of TMB by [Fe^{III}(biuret-amide)] complex takes place inside the pore channels. This allows two different catalytic reactions to proceed simultaneously at two parts of the material without interfering with each other. Further, control experiments using 5 mM of fructose, maltose and lactose showed the specificity of the developed method towards glucose as no detectable color was observed in control reactions (Fig. 3.12).

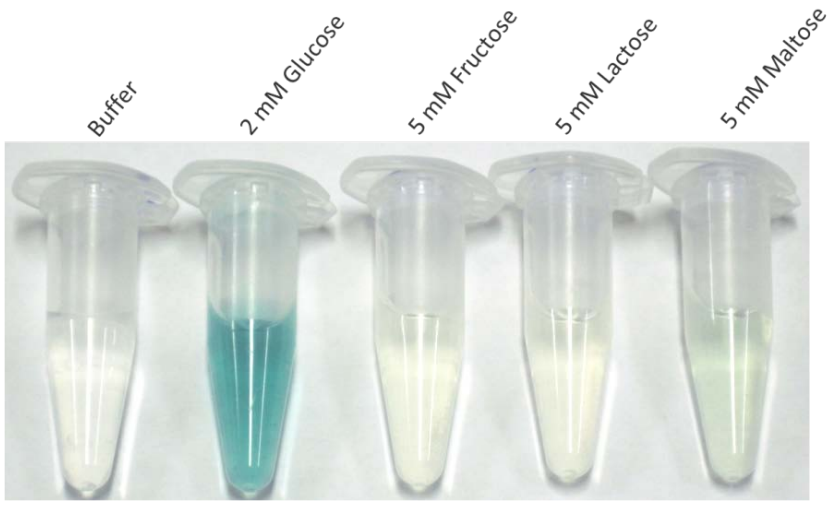

Figure 3.12: Typical photographs of glucose detection by the colorimetric method developed using GOX and Fe-MSN

3.4.5.1 Detection of glucose in blood plasma

In order to test our methodology works in real sample analysis, experiments were carried out with mice blood plasma containing glucose. Blood plasma obtained from a healthy mice containing glucose (concentration 5.88 mM) was serially diluted with phosphate buffer (10 mM, pH 7.4) as shown in the table and detection of glucose was carried out as described below. Glucose content is calculated according to the equation $y = a + b*x$ where $a = 0.0247 \pm 0.002$, $b = 444 \pm 16$ and $R^2 = 0.9910$ which was already used in Fig. 3.11 for glucose detection. One sample calculation is shown below for the 30-fold dilution.

$$[\text{Glucose}]_{30 \text{ times dilution}} = (0.110 - 0.0247)/ 444 = 1.92 \times 10^{-4}.$$

Table 3.3: Detection of glucose in blood plasma

Dilution factor	Absorbance at 650 nm	Concentration according to dilution (M)	Concentration found (M)
30	0.110	1.96×10^{-4}	1.92×10^{-4}
40	0.0853	1.47×10^{-4}	1.36×10^{-4}
60	0.07	9.8×10^{-5}	1.02×10^{-5}
120	0.046	4.9×10^{-5}	4.8×10^{-5}

The average concentration of glucose in plasma was determined to be 5.77 mM (Fig. 3.11 and Table 3.3). Thus, this study demonstrates that the Fe-MSN can be used for the analysis of real samples.

3.4.6 Mechanism of TMB oxidation by [Fe^{III}(biuret-amide)]

Scheme 3.2 shows the proposed mechanism of oxidation of TMB by [Fe^{III}(biuret-amide)]. The active intermediate has been proposed to be a high valent iron-oxo species but the identity of the species has not been confirmed. It is proposed the high valent iron-oxo species to be either an iron(V)-oxo or an μ-oxo Fe(IV) dimer. [41]

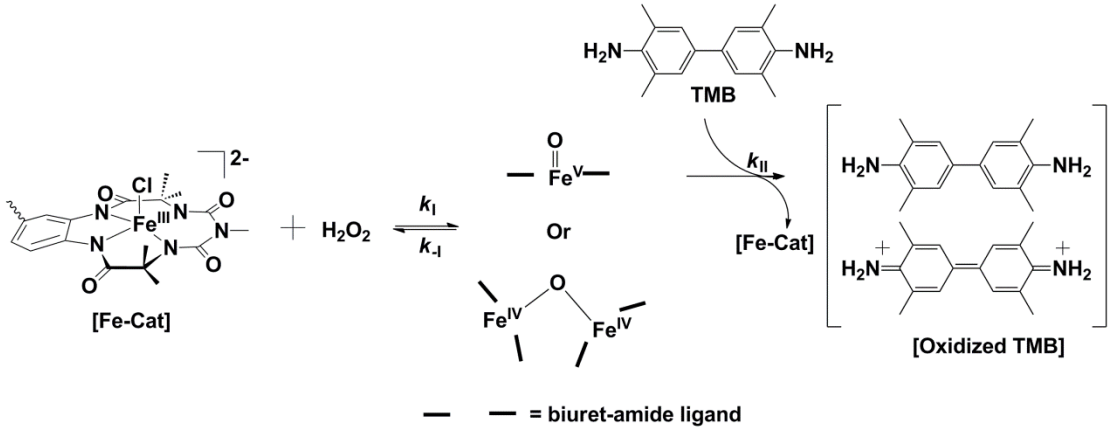

Scheme 3.2: Proposed mechanism of TMB oxidation by [Fe^{III}(biuret-amide)]

3.5 Conclusions

In conclusion, we have reported immobilization of [Fe^{III}(biuret-amide)] complex on mesoporous silica nanoparticles using Cu(I) catalyzed azide alkyne click chemistry. This organic-inorganic hybrid material functions as an efficient peroxidase mimic and has been used successfully for the colorimetric assay of H_2O_2 and glucose in one-pot. Further, the presence of silanol groups on the outer surface of Fe-MSN allows easy functionalization to install targeting ligands so that these materials can be used for immunoassays.

3.6 References

1. S. Kroger, A. P. F. Turner, K. Mosbach and K. Haupt, *Anal. Chem.*, 1999, **71**, 3698-3702.
2. Z. Cheng, E. Wang and X. Yang, *Biosensors & Bioelectronics*, 2001, **16**, 179-185.
3. A. Sassolas, L. c. J. Blum and B. a. D. Leca-Bouvier, *Biotechnology Advances*, 2012, **30**, 489-511.
4. H. B. Dunford, *Heme Peroxidases; Wiley-VCH: New York*, 1999.
5. P. Peralta-Zamora, E. Esposito, R. Pelegrini, R. Groto, J. Reyes and N. Duran, *Environmental Technology*, 1998, **19**, 55-63.
6. Y. P. Chau and K. S. Lu, *Cells Tissues Organs*, 1995, **153**, 135-144.
7. T. P. Whitehead, G. H. G. Thorpe, T. J. N. Carter, C. Groucutt and L. J. Kricka, *Nature*, 1983, **305**, 158-159.
8. V. Sanz, S. de Marcos, J. R. Castillo and J. Galban, *J. Am. Chem. Soc.*, 2005, **127**, 1038-1048.
9. W. Chen, B. Li, C. Xu and L. Wang, *Biosensors & Bioelectronics*, 2009, **24**, 2534-2540.
10. A. Brausam, S. Eigler, N. Jux and R. van Eldik, *Inorg. Chem.*, 2009, **48**, 7667-7678.
11. M. Nango, T. Iwasaki, Y. Takeuchi, Y. Kurono, J. Tokuda and R. Oura, *Langmuir*, 1998, **14**, 3272-3278.
12. R. A. W. Johnstone, P. A. Stocks and A. J. Simpson, *Chem. Commun.*, 1997, 2277-2278.
13. T. J. Collins, *Acc. Chem. Res.*, 2002, **35**, 782-790.
14. M. Motsenbocker, Y. Ichimori and K. Kondo, *Anal. Chem.*, 1993, **65**, 397-402.
15. Y. Saito, S. Nakashima, M. Mifune, J. Odo, Y. Tanaka, M. Chikuma and H. Tanaka, *Anal. Chim. Acta*, 1985, **172**, 285-287.
16. Y. Saito, M. Mifune, T. Kawaguchi, J. Odo, Y. Tanaka, M. Chikuma and H. Tanaka, *Chem. Pharm. Bull.*, 1986, **34**, 2885-2889.
17. G. Zhang and P. K. Dasgupta, *Anal. Chem.*, 1992, **64**, 517-522.
18. Y.-Z. Li and A. Townshend, *Anal. Chim. Acta*, 1997, **340**, 159-168.
19. Y.-z. Li, N. He and Y.-x. Ci, *Analyst*, 1998, **123**.

20. A. Gonsalves, R. A. W. Johnstone, M. M. Pereira, A. M. P. deSantAna, A. C. Serra, A. Sobral and P. A. Stocks, *Heterocycles*, 1996, **43**, 829-838.
21. L. Z. Gao, J. Zhuang, L. Nie, J. B. Zhang, Y. Zhang, N. Gu, T. H. Wang, J. Feng, D. L. Yang, S. Perrett and X. Yan, *Nature Nanotech.*, 2007, **2**, 577-583.
22. H. Wei and E. Wang, *Anal. Chem.*, 2008, **80**, 2250-2254.
23. Y. Jv, B. X. Li and R. Cao, *Chem. Commun.*, 2010, **46**, 8017-8019.
24. W. Chen, J. Chen, A. L. Liu, L. M. Wang, G. W. Li and X. H. Lin, *ChemCatChem*, 2011, **3**, 1151-1154.
25. M. Ornatska, E. Sharpe, D. Andreescu and S. Andreescu, *Anal. Chem.*, 2011, **83**, 4273-4280.
26. Y. J. Song, K. G. Qu, C. Zhao, J. S. Ren and X. G. Qu, *Adv. Mater.*, 2010, **22**, 2206-2013.
27. Y. Song, X. Wang, C. Zhao, K. Qu, J. Ren and X. Qu, *Chem. Eur. J.*, 2010, **16**, 3617-3621.
28. W. Shi, Q. Wang, Y. Long, Z. Cheng, S. Chen, H. Zheng and Y. Huang, *Chem. Commun.*, 2011, **47**, 6695-6697.
29. J. Wang, X. Mi, H. Guan, X. Wang and Y. Wu, *Chem. Commun.*, 2011, **47**, 2940.
30. M. Zhou and S. Dong, *Acc. Chem. Res.*, 2011, **44**, 1232-1243.
31. C. Panda, M. Ghosh, T. Panda, R. Banerjee and S. Sen Gupta, *Chem. Commun.*, 2011, **47**, 8016-8018.
32. A. Schlossbauer, D. Schaffert, J. Kecht, E. Wagner and T. Bein, *J. Am. Chem. Soc.*, 2008, **130**, 12558-12559.
33. J. Nakazawa and T. D. P. Stack, *J. Am. Chem. Soc.*, 2008, **130**, 14360-14361.
34. S. Huh, J. W. Wiench, J.-C. Yoo, M. Pruski and V. S. Y. Lin, *Chem. Mater.*, 2003, **15**, 4247-4256.
35. Y. Huang, S. Xu and V. S. Y. Lin, *Angew. Chem. Int. Ed*, 2011, **50**, 661-664.
36. V. Hong, S. I. Presolski, C. Ma and M. G. Finn, *Angew. Chem. Int. Ed.*, 2009, **48**, 9879-9883.
37. C.-Y. Lai, B. G. Trewyn, D. M. Jeftinija, K. Jeftinija, S. Xu, S. Jeftinija and V. S. Y. Lin, *J. Am. Chem. Soc.*, 2003, **125**, 4451-4459.
38. R. Mortera, J. Vivero-Escoto, I. I. Slowing, E. Garrone, B. Onida and V. S. Y. Lin, *Chem. Commun.*, 2009, 3219-3221.
39. Y. Wei, J. Xu, H. Dong, J. H. Dong, K. Qiu and S. A. Jansen-Varnum, *Chem.*

Mater., 1999, **11**, 2023-2029.

40. Y. Wei, J. Xu, Q. Feng, H. Dong and M. Lin, *Mater. Lett.*, 2000, **44**, 6-11.

41. S. Kundu, J. V. K. Thompson, A. D. Ryabov and T. J. Collins, *J. Am. Chem. Soc.*, 2011, **133**, 18546-18549.

CHAPTER 4

Encapsulation of Enzymes into the Pores of Spherical SBA-15 Mesoporous Materials: “Ship-in-a-Bottle” Approach

4.1 Introduction

Enzymes are versatile biocatalysts that perform chemical reactions at ambient temperature and pressure.[1, 2] Advantages of using enzymes as catalysts are: 1) they are highly efficient biocatalysts with very high turnover numbers; 2) they perform strictly chemo-, regio- and stereo-specific reactions; 3) they are non-toxic and reactions can be performed in aqueous medium under mild conditions; 4) they carry out atom-economical reactions without need of protection-deprotection chemistry. Because of these characteristics and specificities of enzymes, their use in various processes at industrial scale has been considered as a green technology process.[1-4] But the short lifetime of enzymes presently limit their usefulness. Therefore, an improvement in enzyme stability and reusability are required to increase their lifetime so as to further enable practical applications.[1-4] One of the approaches to improve enzyme reusability is via enzyme immobilization which represents the attachment or incorporation of enzyme molecules into large structures that render them insoluble in water. This allows efficient recovery of the enzyme after the reaction and hence can be reused several times.

4.2 Immobilization of enzymes

Generally, immobilization of enzymes follows empirical guidelines. Knowledge of structural characteristics of support and enzyme are helpful in achieving high performance immobilized enzymes. Size of enzyme, isoelectric points of enzyme and support, pore diameter of support (in case of porous material), stability of the support and pH of the buffer solution used for immobilization are some of the important factors to be considered while immobilization of enzymes. Generally, there are three methods used for the immobilization of enzymes: carrier binding, encapsulation and cross-linking.[3-6]

4.2.1 Carrier binding

Carrier binding involves attachment of enzymes to the solid support through physical adsorption, ionic interactions or covalent bond between enzyme and support [7]. In physical adsorption, an enzyme is bound to support through hydrogen bonding and/or van der Waal's interactions. This causes little or no conformational changes in the enzyme adsorbed and as a result yields highly active immobilized

enzyme. The method suffers from a serious disadvantage that the enzyme leaches out from the support during the catalytic reaction due to weak binding force between enzyme and solid support. The ionic binding method involves binding of the enzyme to the support through ion-exchange residues.[7] Usually polysaccharides or synthetic polymers having ion-exchange centers are used as supports. The binding of an enzyme to the support is easily carried out under mild conditions. Hence, this method causes little changes in the conformation and the active sites of the enzymes. Therefore, in most cases, this method yields immobilized enzymes with high activity. However, enzymes may leach out from the support in substrate solutions of high ionic strength or upon variation of pH. In covalent binding, an enzyme is attached by covalent bond to the solid support. Generally, amino, carboxyl, hydroxyl or thiol groups on the surface of enzyme are used to make a covalent bond with the support. Conditions used for covalent binding are harsh, which may cause changes in the conformation or in the active site of the enzyme. This may lead to significant loss of enzyme activity. But, the advantage of this method is that no leaching of enzyme occurs.

4.2.2 Cross linking

Immobilization of enzymes has been carried out by intermolecular cross-linking of the enzymes, either to other enzyme molecules or to the functional groups on an insoluble solid support matrix.[6] Cross-linking an enzyme to it-self is both expensive and inefficient since it may lead to blocking of some of the active sites during crosslinking. Generally, cross-linking is best used in conjunction with one of the other methods. It is mostly used as a means of stabilizing adsorbed enzymes and also for preventing leaching of enzyme from the support matrix. Glutaraldehyde, hexamethelenediisocynate, or toluenediisocynate are used as cross-linking reagents. Cross-linking reactions are carried out under relatively harsh conditions, which can alter conformational structure and active sites of the enzyme. Therefore this method can lead to significant loss of activity of the enzyme. Recently, cross-linked enzyme crystal (CLECs) and cross-linked enzyme aggregates (CLEAs) based on multipoint attachment between enzyme molecules have been developed to improve the stability of enzymes by reducing protein unfolding.[8-10]

4.2.3 Encapsulation

The encapsulation of enzymes involves localization of an enzyme within the lattice of a polymer matrix or membrane or inside pore spaces of porous materials. It is done in such a way as to retain enzymes inside while allowing easy diffusion of the substrate and products. Various organic polymers such as polacrylamide, polyvinyl alcohol, polysaccharides, polystyrenes etc. have been used for the encapsulation of enzymes.[1, 11] Membrane devices such as a hollow fiber or a microcapsule have also been employed for encapsulating enzymes.[11] Encapsulation of enzymes using silica sol-gel process involving either silanation or coating with microporous silica to reduce the mesopore opening has been employed.[5, 12, 13] In most of the cases, conditions used for chemical polymerization reactions are harsh and loss of activity has been reported.

4.3 Mesoporous materials as support for immobilization of enzymes

A range of supports have been used for the immobilization of enzymes. This includes sol-gels,[14] hydrogels,[15] organic microparticles ,[16] nonporous[17, 18] and porous[19] inorganic supports. Various inorganic solid supports used includes alumina,[20] silica,[18] zeolites[21, 22] and mesoporous silica materials.[3, 5, 23] In particular mesoporous silica materials are very good candidates for the immobilization of enzymes since their ease of synthesis, high surface area (up to 1000 m^2/g) and tuneable pore size (2-50 nm) enables researchers to tailor these materials suitably so that the immobilization of a variety of proteins and enzymes is feasible.[19] Thus, the development of mesoporous materials based biocatalysts has attracted a lot of attention. A range of enzymes with different sizes and isoelectric point have been immobilized on the mesoporous materials. Table 4.1 lists some of the important enzymes with their characteristics and mesoporous structures that have been used to generate biocatalysts. Most of these materials have been prepared by immobilization of the enzymes into the pores of the mesoporous channels by physical adsorption.[2, 24] Although simple and efficient, this process is severely limited by the fact that with time these adsorbed enzymes leach out into the solution. To overcome this, enzymes have been covalently immobilized by chemically attaching them to an organo-functionalized mesoporous material via amino acid side-chains like lysine.[25, 26] Recently, Bein et al. have attached alkyne labeled trypsin covalently on the surface of azide functionalized SBA-15 by Cu(I)

catalyzed azide alkyne click chemistry (CuAAC) approach.[27] However, after covalent immobilization there is limited control of the spatial orientation of the immobilized enzyme within the pores which in turn affects the reactivity. Another approach to prevent enzyme leaching is via a "ship-in-a-bottle" approach where the pores of the mesopore are partially closed after adsorption of the enzyme; thereby preventing the enzyme from leaching out while the diffusion of the substrate and product remains unaffected.[12, 13] For example, Wang and Caruso have encapsulated enzymes in bimodal mesoporous silica (BMS) by enzyme adsorption followed by assembly of a multilayer shell on the particle surface by layer–by-layer electrostatic assembly of oppositely charged species to prevent the enzyme from leaching.[28] However with changes in pH or salt concentration, these multilayer shell may disassemble or cause changes in their permeability properties thereby limiting possible applications in catalysis.[29] Hence, there is a need to generate new porous materials that can efficiently immobilize native enzymes that have activity similar to the native enzyme and can also be recycled several times without loss of activity.

Table 4.1:List of enzymes used for immobilization on to mesoporous materials [23]

Enzyme, reference no.	**pI**	**Size (nm)**	**Mesoporous material**	**Pore Size (nm)**
cytochrome c[12, 30-32]	10.7	2.6 x 3.2 x 3.3	MCM-41, PMO, Al-MCM-48	2.5-13
lysozyme[33-37]	11.3	1.5 x 2.5 x 4.3	MCM-41, SBA-15, MCM-48, PMO	3.2-9.1
horseradish peroxidase[38-40]	7.2	4.0 x 4.4 x 6.8	MCM-41, SBA-15, FSM-16	2.7-13
hemoglobin[41, 42]	6.8-7	5.3 x 5.4 x 6.5	SBA-15, FSM	3-10
penicillin acylase[43, 44]	7.0	7.0 x 5.0 x 5.5	MCM-41, SBA-15	6-9
bovine serum albumin[33-35]	4.9	5.0 x 7.0 x 7.0	MCM-41, SBA-15, Al-MCM-41	2.5-24
porcine pancreatic lipase[13, 45, 46]	-	4.6 x 2.6 x 1.1	MCM-41, SBA-15	4.5-6.6
papain [12, 47]	8.75	3.7 x 3.7 x 5.0	MCM-41, MCM-48	4-6.2
trypsin [12, 27, 48- 50]	8–10	3.8 x 3.8 x 3.8	MCM-41, SBA-15	2.8-18
α-amylase [51]	-	7-10	SBA-15, MCM-41, MCF	2.6-34

4.4 Experimental

4.4.1 Materials

Tetraethylorthosilicate (TEOS), Poly(ethylene glycol)-*block*-poly(propylene glycol)-*block*-poly(ethylene glycol) (Pluronic P-123, average molecular weight 5800), Cetyltrimethylammonium bromide (CTAB), 3-aminopropyltriethoxy-silane (APTES), 1, 3, 5-triisopropyl benzene (TIPB), Amino guanidine hydrochloride (AG.HCl), 4-Pentynoic acid, N-Hydroxy succinimide, Rhodamine B isothiocyanate (RBITC, mixed isomers), Trypsin and dialysis tubing cellulose membrane (cut off molecular weight 12kD) were obtained from Sigma Aldrich. Polyethelene glycol monomethyl ether (PEG, average molecular weight 1000) and 5 (6)-carboxy fluorescein-N-hydroxy succinimidyl ester were obtained from fluka. $CuSO_4$, Sodium ascorbate,

triethyl amine, were obtained from Merck, India. All the chemicals used were of extra pure for biochemistry or of analytical grade and used as received. Tris(3-hydroxypropyltriazolylmethyl)amine (THPTA)[52] was prepared as reported earlier. For all the experiments de-ionized water was used.

4.4.2 Synthesis

4.4.2.1 Synthesis of *N*-(4-Pentynoyloxy)succinimide

N-(4-Pentynoyloxy)succinimide was synthesized by following the procedure reported by Galibert et al.[53] To a stirred solution of pent-4-ynoic acid (0.5 g, 5.1 mmol) and *N*-hydroxysuccinimide (0.6 g, 5.1 mmol) in ethyl acetate/dioxane (60 mL, 1:1) at 0 °C was added DCC (1.05 g, 5.1 mmol). The resulting mixture was stirred at room temperature for 6 h. The solid of DCU formed was filtered off and the filtrate concentrated under reduced pressure. The obtained residue was dissolved in ethyl acetate (200 mL), and the solution was washed with 5% aqueous NaHCO3 (2 x 50 mL), water (50 mL), and brine (50 mL). The organic layer was separated, dried over anhydrous Na_2SO_4, filtered and concentrated. Recrystallization from dichloromethane/n-pentane to give *N*-(4-Pentynoyloxy)succinimide as white solid which was used without further purification (yield 0.83 g). ^{1}H NMR (200.13 MHz, $CDCl_3$): δ = 2.04 (1H, t), 2.59 (2H, td), 2.83 (4H, s), 2.86 (2H, t); ^{13}C NMR (50.32 MHz, $CDCl_3$): δ = 14.04, 25.53, 30.27, 69.99, 80.82, 166.98, 168.87.

4.4.2.2 Synthesis of fluorescein labeled trypsin

10 mg of trypsin was added to 10 mL of phosphate buffer (50 mM, pH 7.4) containing 0.4 mg of 5 (6)-carboxy fluorescein-N-hydroxy succinimidyle ester and stirred at 4 °C for 12 h. After 12 h the solution was dialyzed using cellulose membrane (cut off molecular weight 12kD) in 10 mM ammonium bicarbonate buffer (4 x 500 mL). Finally the solution was lypholized to obtain fluorescein labeled trypsin in solid form.

4.4.2.3 Synthesis of mesoporous materials

4.4.2.3.1 Synthesis of Azide functionalized spherical SBA-15

Spherical SBA-15 mesoporous material was prepared by following the procedure reported by Katiyar et al. with slight modification using 1, 3, 5-triisopropyl

benzene (TIPB) as swelling agent.[54] In a typical batch process triblock copolymer P123 (3 g) was dissolved in 1.5 M HCl (60 ml) using a mechanical stirrer. To this solution a mixture of CTAB (0.6 g) and TIPB (0.517g) in 25 mL of de-ionized water and 20 mL absolute ethanol were added. The resulting surfactant solution was stirred vigorously at 35 °C for 15 minutes and then TEOS (10 mL) was added drop by drop and stirred vigorously at 35 °C for 45 minutes. The resulting mixture was transferred into an air tight metallic reactor lined with teflon and subjected to hydrothermal synthesis at 75 °C for 10 h and then aging at 125 °C for 48 h. After 48 h cooled to room temperature, the white precipitate was recovered by filtration and washed with copious amount of water until neutral to pH paper. The white solid was air dried and template was removed by calcination at 550 °C for 6 h at a slow heating rate of 1 °C per minute (Yield 2.45 g). This calcined SBA-15 was denoted as CAL-SBA.

To a suspension of 1 g of CAL-SBA in 100 mL of dry toluene, AzPTES (0.247 g, 1 mmol) and triethyl amine (0.02 g, 0.1 mmol) were added, and the mixture was stirred for 18 h at 80°C under nitrogen atmosphere. After the completion of reaction, the contents were cooled, filtered and washed with toluene until it became free from AzPTES. The sample was then dried at 80°C for 8h in a vacuum oven and preserved under argon atmosphere for further use. Yield: ~1.05 g. This material was referred as AZP-SBA. Elemental analysis : C, 2.23; H, 0.45; N, 2.3%

4.4.2.3.2 Synthesis of outer surface alkyne functionalized and inner surface rhodamine B functionalized MSN

Selectively outer surface alkyne functionalized MSN was synthesized in three steps by following procedures reported in literature with slight modifications (scheme S1).[55, 56] In a typical batch synthesis, CTAB (1 g, 2.744 mmol) was dissolved in 480 mL of water and 2M aqueous NaOH (3.5 mL, 7 mmol). The mixture was stirred thoroughly at 600 rpm for 30 min at 80 °C to dissolve the surfactant completely. To this clear solution, TEOS (4.75g, 22.83 mmol) was injected rapidly. A white precipitate was observed within 1-2 min after the addition was completed. The resultant reaction mixture was allowed to stir at 600 rpm for 2 h at 80 °C. The hot contents were then filtered and the white residue was washed with copious amounts of water and methanol and dried under vacuum at 100 °C over night (yield ~1.7 g). This as-synthesized MSNs was denoted as AS-MSN.

1 g of AS-MSN was suspended in 200 mL of dry toluene by sonication for 10 minutes. To this APTES (0.179 g, 1 mmol) was added, and the mixture was stirred for 18 h at 80°C under nitrogen atmosphere. After the completion of reaction, the contents were cooled, filtered and washed with toluene until it became free from APTES. The sample was then dried at 100°C for 8h in a vacuum oven The template was extracted by stirring the as-synthesized sample (1 g) in 200 mL methanol and 2 ml concentrated hydrochloric acid at 60 °C for 6 hr. The resulting template removed solid product, was filtered and washed with methanol (100 mL) and 1% triethyl amine in methanol (50 mL). Finally, again washed with methanol (50) then dried under vacuum at 100 °C over night (yield ~0.64 g). This material will be referred as NH_2-MSN. Elemental analysis : C, 3.1; H, 0.88; N, 1.1%

0.5 g of NH_2-MSN was suspended in 100 mL of dry DCM by sonication for 10 minutes. To this *N*-(4-Pentynoyloxy)succinimide (0.225 g, 2.3 mmol) was added, and the mixture was stirred for 12 h at room temperature. After completion of reaction, the contents were filtered and washed with DCM. The sample was then dried at 80°C for 3 h in a vacuum oven (yield ~0.51 g). This material was referred as ALK-MSN. Formation of alkyne fuctionalized MSN (ALK-MSN) was confirmed by simple ninhydrin and $KMnO_4$ tests and ^{13}C CPMAS NMR spectroscopy (Fig.4.10). In ninhydrin test, ALK-MSN gave no blue color to the solution, while NH_2-MSN gave intense blue color, which shows absence of primary amines in ALK-MSN, due to formation of amide linkage. While in $KMnO_4$ test, ALK-MSN showed quick de-colorization of dilute alkaline $KMnO_4$ solution in comparison to slow de-colorization by NH_2-MSN. Quick de-colorization by ALK-MSN was due to presence of easily oxidisable C-C triple bond.

0.1 g of ALK-MSN was suspended in 20 mL of dry toluene by sonication for 10 minutes. To this APTES (0.018 g, 0.1 mmol) was added, and the mixture was stirred for 18 h at 80°C under nitrogen atmosphere. After the completion of reaction, the contents were cooled, filtered and washed with toluene until it became free from APTES. The sample was then dried at 100°C for 8h in a vacuum oven (yield ~0.1 g). This material was referred as ALK-NH_2-MSN.

0.02 g of ALK-NH_2-MSN was suspended in 5 mL of dry DCM by sonication for 10 minutes. To this rhodamine B isothiocyanate (RBITC, 2 mg, 3.7 μmol) was

added, and the mixture was stirred for 12 h at room temperature. After completion of reaction, the contents were filtered and washed vigorously with DCM, methanol and phosphate buffer (100 mM, pH 7) to remove unreacted RBITC. The sample was then dried at 80°C for 3 h in a vacuum oven. This material was referred as ALK-RH-MSN.

4.4.2.4 Encapsulation of trypsin in spherical SBA-15 using MSN

For the encapsulation of trypsin in spherical SBA-15 using MSN as via Cu(I) catalyzed azide-alkyne cycloaddition reaction (CuAAC), first trypsin was adsorbed on the azide functionalized SBA-15 (AZP-SBA) in phosphate buffer (100 mM, pH 7) at 4 °C, and then incubated with the alkyne functionalized MSN, THPTA (2.5 equivalent), $CuSO_4$ (0.5 equivalent), AG.HCl (4 equivalent) and sodium ascorbate (4 equivalent). In a typical trypsin encapsulation click reaction, AZP-SBA (12 mg, 7.2 µmol of azide) in 1.1 mL, 100 mM phosphate buffer was freeze pump thawed thrice and then to this 0.6 mg of trypsin was added under inert atmosphere and stirred at 4 °C for 12 h to adsorb trypsin in the pores of AZP-SBA. After 12 h, centrifuged and washed once with 1mL, 100 mM freeze pump thawed phosphate buffer. Centrifugate and washing were collected together and absorbance at 280 nm noted to determine amount of trypsin present in solution. Residue was redispersed in the 1 mL phosphate buffer. To this a mixture of ALK-MSN (6 mg) in 1mL, 100 mM phosphate buffer containing THPTA (7.8 mg, 18 µmol), $CuSO_4$ (0.9 mg, 3.6 µmol), AG.HCl (3.2 mg, 28.8 µmol) freeze pump thawed thrice was added. Then sodium ascorbate (5.7 mg, 28.8 µmol) was added under inert atmosphere and the mixture was stirred for 24 h. After completion of reaction, the reaction mixture was centrifuged and the residue was washed with 10% PEG solution in 50 mM, pH 8 tris buffer in order to leach out physically adsorbed trypsin on the outer surface and then twice with 50 mM, pH 8 tris buffer [57]. This material will be referred as Trypsin-SBA-MSN. The amount of trypsin encapsulated in Trypsin-SBA-MSN was determined by TGA. The residue was preserved at 4 °C and further used for activity determination of trypsin using BAPNA in 50 mM, pH 8 tris buffer.

For the comparison of activity of trypsin, two control experiments were carried out by following the above procedure. In one of the control experiment, after adsorption of trypsin on AZP-SBA only ALK-Ms

SN was added and all other click reaction reagents were excluded, as a result, trypsin was only physically adsorbed on surface. Finally this material was centrifuged and quickly once washed with 1 mL phosphate buffer. Centrifugate and washing were collected together and absorbance at 280 nm noted to determine of amount of trypsin remained unadsorbed. This material was referred as PHY-SBA-MSN. In second control experiment, PHY-SBA-MSN was treated with 1.5 mL of 10% PEG solution in tris buffer (50 mM, pH 8) for 1 h on rotaspin in order to study the leaching of the adsorbed trypsin. Finally this material was centrifuged and the amount of trypsin leached out with PEG solution was estimated by reading the absorbance at 280 nm in UV-Vis spectrophotometer. This material was referred as PEG-SBA-MSN.

Similarly other click reactions were carried out as described above for the purpose of characterization of hierarchical porous material, one click reaction was carried out with AZP-SBA and ALK-MSN without adsorption of trypsin. After completion of reaction, the reaction mixture was centrifuged and the residue was first washed twice with phosphate buffer and then sequentially washed with 10 mM N,N-diethyldithiocarbamate sodium solution in 100 mM phospate buffer and acetone respectively.[58, 59] The last two washings were repeated thrice. Finally, the residue obtained was dried at 80°C in vacuum oven for 8 h. This material will be referred as CLICK-SBA-MSN. Another click reaction was carried out using AZP-SBA and rhodamine B labeled MSNs (ALK-RH-MSN) by following the procedure mentioned above.

4.4.3 Determination of activity of trypsin

Preparation of 2 mM BAPNA solution: 22 mg of BAPNA dissolved in 0.4 mL of DMSO and diluted to 25 mL.

Activity Determination: 1.5 mL of BAPNA solution (2 mM) was added to the residue containing encapsulated enzyme in a 2 mL eppendorf tube and spinned on a rotaspin at 30 rpm for 20 minutes. At 20th minute solution was centrifuged and quickly washed with tris buffer (50 mM, pH 8) three times (1 x 1.5 mL and then 2 x 1 mL). Centrifugate and washings were collected together (total volume ~5 mL) and absorbance was noted at 405 nm. Trypsin encapsulated solid was used for the next cycle. The activity of the trypsin was calculated as micromoles of *p*-nitroaniline (PNA) formed per gram of trypsin per minute.

4.4.4 Characterization

Powder X-ray diffraction of all the samples was carried out in a PANalytical X'pert Pro dual goniometer diffractometer. A proportional counter detector was used for low angle experiments and an X'celerator solid state detector was employed in the low angle experiments. The radiation used was Cu Kα (1.5418 Å) with a Ni filter and the data collection was carried out using a flat holder in Bragg–Brentano geometry (0.5 to 10°; 0.2° min^{-1}). Care was taken to avoid sample displacement effects. SEM images were obtained on Leica Stereoscan 440 microscope. HR-TEM images were taken on a FEI Technai F30 operating at 300 kV with FEG. The samples were prepared by dispersing a large number of solid particles in isopropanol by sonication, and dropping the resulting suspension on a copper grid of 400 mesh and allowed to dry in air. Nitrogen adsorption and desorption studies were carried out using Quantachrome instrument. Samples were preheated at 100°C for 18 hours in the vacuum line. Multi point BET surface area was obtained from adsorption isotherm from P/P_0 0.1-0.3. Pore size distributions were calculated from adsorption isotherm using the BJH method. Semi-quantitative FT-IR spectra were recorded on Perkin Elmer FT-IR spectrum GX instrument by making KBr pellets. Pellets were prepared by mixing 3 mg of sample with 97 mg of KBr. Yields for CuAAC reactions were calculated from corrected area under the curve characteristic for the azide stretch at ~2100 cm^{-1}. UV-Vis experiments were carried out on Perkin Elmer PL Lambda 950 spectrophotometer using 1 mL cuvettes with 10 mm path length. ^{13}C Cross Polarization Magic Angle Spinning (CPMAS) NMR experiments were carried out on a Bruker AVANCE 300 wide bore spectrometer equipped with a superconducting magnet with a field of 7.1Tesla operating at 75.4MHz. The samples were packed into a 4mm zirconia rotor and loaded into a 4mm BL MAS probe and spun about the magic angle (54.74) at 10 KHz using a standard ramp-CP pulse sequence was used for the experiment. The RF-powers was 60kHz ^{13}C CPMAS experiments. The contact times was 3ms for ^{13}C CPMAS experiments. All the chemical shifts were referenced to TMS. Typically 10,000 to 25,000 scans with a recycle delay of 3s were collected depending on the sensitivity of the sample. Confocal laser scanning microscopy (CLSM) images were taken with Carl Zeiss confocal system equipped with a 20x objective. Optical slices in the center of the particle were selected. Thermogravimetric analysis (TGA) of the silica mesoporous materials were carried out using a TA

Instrument SDT Q600 analyzer between 100 and 800°C in air (flow 25 ml min^{-1}) at a heating rate of 5° min^{-1}. All samples were stirred in water overnight, centrifuged and dried under vacuum at 80°C overnight prior to TGA runs. The amount of trypsin encapsulated on the silica surface was determined by TGA using the following equation:[59]

……. (Equation 4.1)

where $W_{Trypsin\text{-}SBA\text{-}MSN(150\text{-}750)}$ is the weight loss between 150^0C and 750^0C corresponding to the decomposition of the organic substance from Trypsin-SBA-MSN corrected from the thermal degradation**,** while $W_{CLICK\text{-}SBA\text{-}MSN(150\text{-}750)}$ represents the weight loss between 150^0C and 750^0C from CLICK-SBA-MSN. M is the molecular weight of the decomposed organic matter (trypsin).

4.5 Results and Discussion

4.5.1 Synthesis of azide functionalized spherical SBA-15

The azide functionalized spherical SBA-15 (AZP-SBA) was prepared by post synthetic grafting method. Spherical SBA-15 mesoporous material was prepared under highly acidic conditions by following the procedure reported by Katiyar et al. with slight modification using TEOS as silica precusor, Pluoronic 123 surfactant as template, CTAB as cosurfactant and 1, 3, 5-triisopropyl benzene (TIPB) as swelling agent.[54] Calcined spherical SBA-15 (CAL-SBA) was obtained by template removal from as-synthesized material by calcination at 540 ˚C. Then, 1 g of calcined SBA-15 (CAL-SBA) was reacted with 2 mmol of AzPTES in the presence of catalytic amount of triethyl amine (0.1 mmol) in dry toluene at 80 ˚C under an inert atmosphere to synthesize azide functionalized spherical SBA-15 (AZP-SBA). The amount of azide groups grafted on the surface of AZP-SBA was determined to be 0.6 mmol/g by elemental analysis. AZP-SBA was further characterized by a variety of analytical techniques such as powder XRD, SEM, TEM, nitrogen adsorption-desorption studies and ^{13}C CP-MAS NMR spectroscopy.

4.5.2 Synthesis of outer surface alkyne functionalized and inner surface rhodamine B functionalized MSNs

Mesoporous silica nanoparticles (MSNs) having alkyne groups present on the outer surface (ALK-MSN) were synthesized in a three-step procedure (Scheme. 1).[57, 60] First, as-synthesized mesoporous nanoparticles (MSNs) were prepared by using TEOS as silica precursor and CTAB as structure directing agent under basic conditions, as shown in the scheme 1. In the second step, as-synthesized MSNs were subjected to outer surface amine grafting using 3-amino-propyltriethoxysilane (APTES) followed by removal of template to yield NH_2-MSN. The amount of amine groups grafted on the surface of NH_2-MSN was determined to be 0.78 mmol/g by elemental analysis. Finally, amines on NH_2-MSN were coupled with *N*-(4-Pentynoyloxy)succinimide to yield alkyne grafted MSNs (ALK-MSN). ALK-MSN was characterized by a variety of analytical techniques such as powder XRD, TEM and ^{13}C CP-MAS NMR spectroscopy.

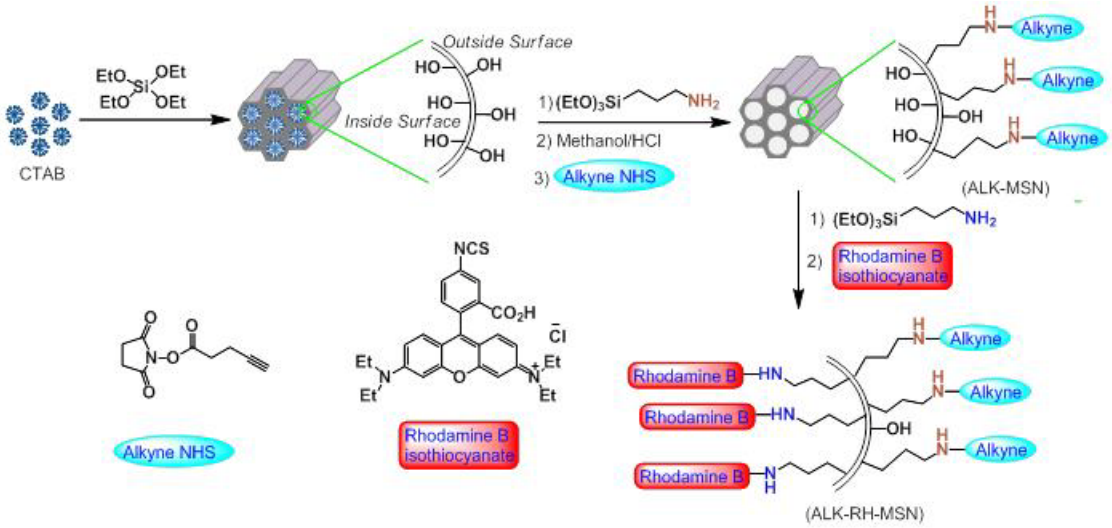

Scheme 4.1: Synthesis of outer surface alkyne functionalized and inner surface rhodamine B functionalized MSNs

Further for the synthesis of inner surface rhodamine B functionalized MSNs, ALK-MSNs were first subjected to inner surface amine grafting using 3-amino-propyltriethoxysilane (APTES) followed by coupling of amines with rhodamine B isothiocyanate to yield outer surface alkyne functionalized and inner surface rhodamine B functionalized MSNs (ALK-RH-MSN).

4.5.3 Encapsulation of trypsin using CuAAC

For the encapsulation of trypsin, the azidopropyl labeled SBA-15, AZP-SBA was first subjected to trypsin adsorption in phosphate buffer (100 mM, pH 7) at 4 °C (Scheme 2) and then subjected to CuAAC with ALK-MSN using $CuSO_4$ and sodium ascorbate at 4 °C as described in the literature.[27], [52] The reaction mixtures were subjected to freeze–pump–thaw cycles at various stages of click reaction as mentioned in the synthesis protocols for rigorous exclusion of dioxygen. An improved click reaction protocol was employed by using a new copper chelating ligand, tris(3-hydroxypropyltriazolylmethyl)amine (THPTA) developed by Finn and coworkers.[52] After the click reaction the enzyme encapsulated material (Trypsin-SBA-MSN) was washed with 10% PEG solution in 50 mM pH 8 tris buffer to leach out any weakly adsorbed trypsin on the surface of the material.[57] The amount of trypsin encapsulated in Trypsin-SBA-MSN was determined by TGA. For complete characterization of the hierarchical mesoporous hybrid material formed using CuAAC, another material CLICK-SBA-MSN was synthesized by clicking AZP-SBA (without trypsin adsorbed) with ALK-MSN and was extensively characterized by FT-IR, nitrogen adsorption-desorption and ^{13}C CP-MAS NMR spectroscopy experiments. For further characterization and comparison of activity of trypsin other control experiments were carried out by following the above procedure as described in experimental section.

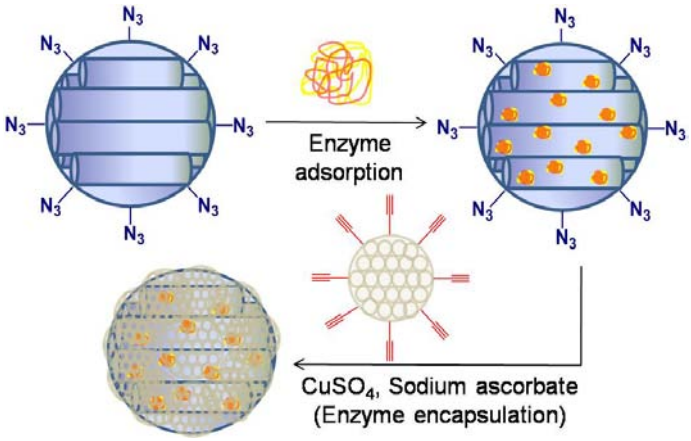

Scheme 4.2: Encapsulation of trypsin in hierarchical mesoporous material. The particle in blue represents azide functionalized spherical SBA-15 (diameter 5-8 μm) and the particle in grey represents alkyne functionalized MSN nanoparticles (diameter ~100 nm)

4.5.4 Characterizations

4.5.4.1 Powder X-ray diffraction

Powder XRD patterns of the mesoporous materials were shown in the Fig. 4.1. Powder XRD pattern of AZP-SBA shows characteristic high intensity 100 peak at 2θ ~0.91º indicating formation of mesoporous structure. Absence of higher order 110 and 200 peaks indicates lack of long range order in mesopores.[60] Powder XRD pattern of ALK-MSN shows characteristic high intensity 100 peak at 2θ ~2.3º indicating that well-ordered two-dimensional hexagonal mesoporous channels were formed.

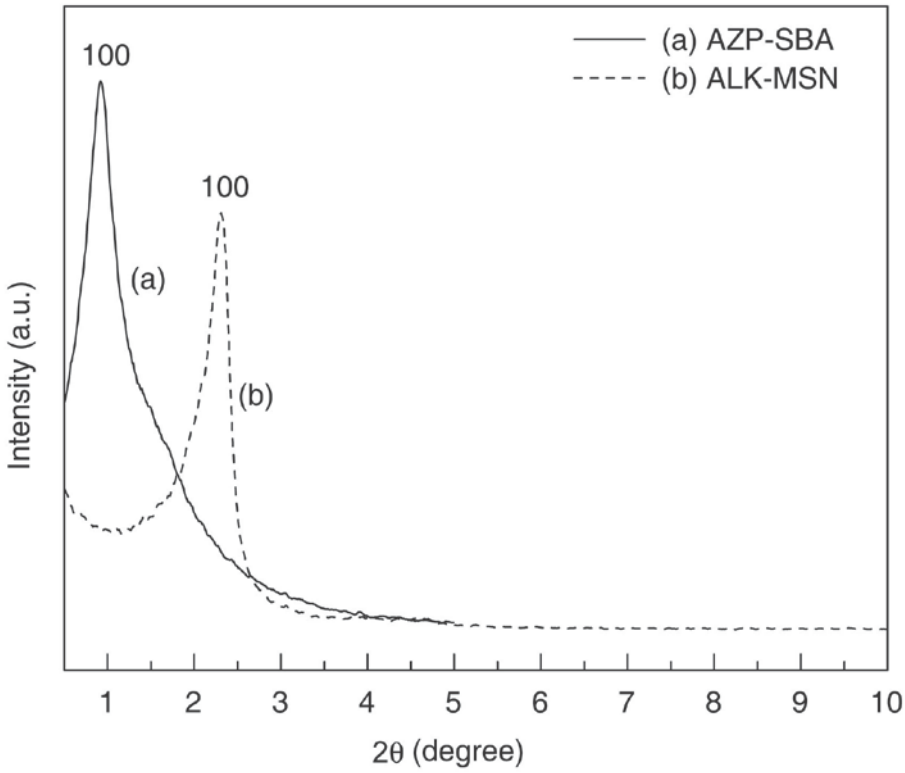

Figure 4.1: Powder XRD patterns of various silica materials: (a) AZP-SBA, (b) ALK-MSN

4.5.4.2 Scanning and transmission electron microscopy

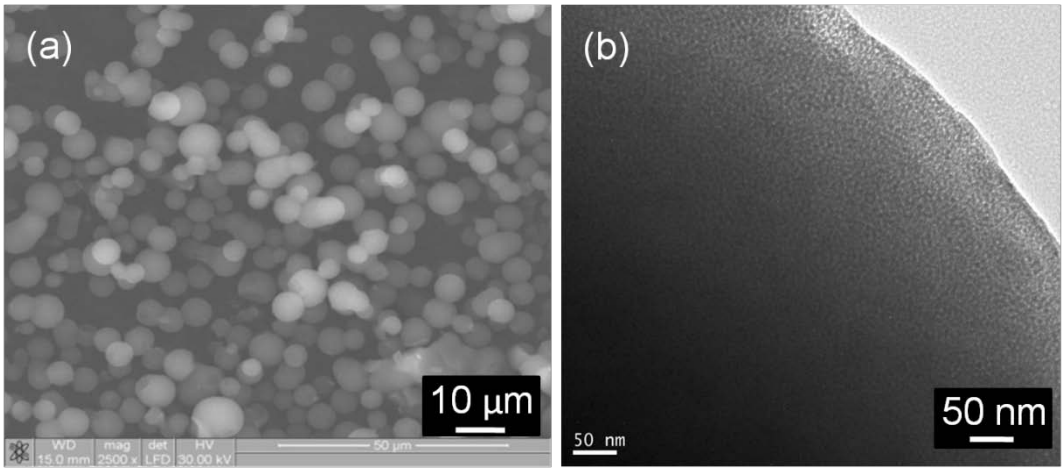

Figure 4.2: (a) SEM and (b) TEM images of AZP-SBA

Scanning electron microscopy (SEM) and transmission electron microscopy (TEM) images of AZP-SBA are displayed in Fig. 4.2. SEM image shows formation of of monodisperse and perfectly spherical morphology of the particles with particle diameters ranging from 5 to 8 µm (Fig. 4.2a). TEM image of AZP-SBA shows formation of disordered mesopores with relatively uniform pore sizes (Fig. 4.2a and 4.4a). This result is in good agreement with the XRD patterns shown in Fig. 4.1a. It has been well known that mesoporous silica with a hexagonal structure can be prepared via the co-assembly of either P123 or CTAB with cationic silica species in acidic conditions.[61, 62] Ma et al. have shown that the mesoporous silica products obtained in the presence of either P123 or CTAB under acid synthesis conditions have not produced the spherical morphology, suggesting that the presence of both P123 and CTAB are necessary for the formation of the spherical morphology of mesoporous silica.[60] In the present synthesis, the molar ratio between P123 and CTAB is about 0.3 but the weight ratio between them is actually very high (~ 5). Therefore, the polymer P123 contributes largely to the final mesopores whereas CTAB mainly plays the role of a cosurfactant. The fact that the mesoporous silica obtained by using the mixed P123–CTAB templates shows a monodisperse rather than bimodal pore size distribution (sees Fig. 4.7a, insert) indicates that the mesopores could be formed by the co-assembly of the mixed P123–CTAB micelles with cationic silica species. Since the mixed P123–CTAB micelles are not that uniform as that of individual P123 or CTAB micelles, the final mesopore structure tends to lack a long-range hexagonal

order resulting in the formation of disordered mesoporous material.[60] Large pore SBA-15 can be synthesized by using 1, 3, 5-triisopropyl benzene (TIPB) as swelling agent. TIPB gets solubilized in the hydrophobic region of P123 leading to the increased size of cylindrical micelles which results in the mesoporous materials with a large pore size.[39, 63]

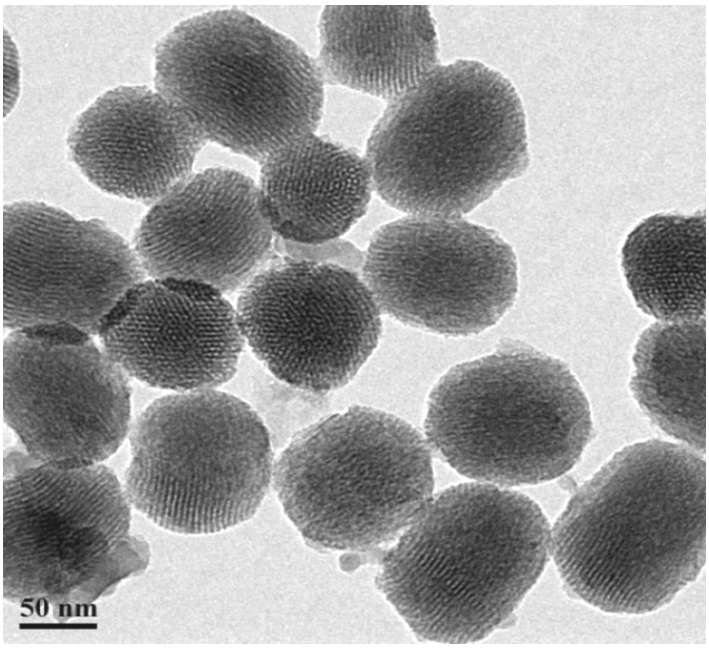

Figure 4.3: TEM of ALK-MSN

TEM image of ALK-MSN showed formation of well-ordered two-dimensional hexagonal mesoporous particles with a spherical morphology having particle size of ~ 100 nm (Fig. 4.3). TEM of Trypsin encapsulated hierarchical mesoporous material (Trypsin-SBA-MSN) is displayed in the Fig. 4.4b. The TEM image shows trypsin adsorbed spherical SBA-15 particles were very well covered by MSNs also demonstrating the formation of the hierarchical mesoporous structure (Fig. 4.4a and 4.4b).

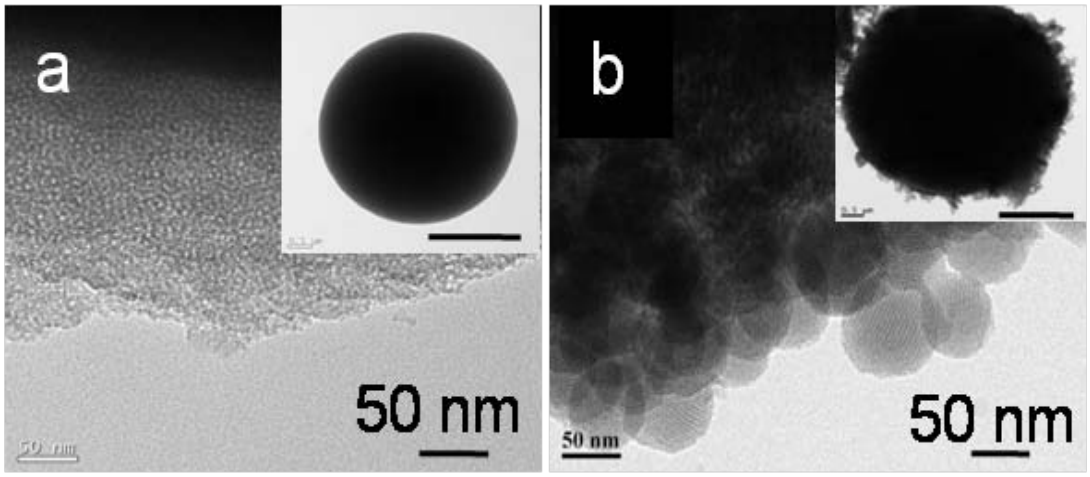

Figure 4.4: (a) TEM of the outer surface of spherical SBA-15(AZP-SBA) (*Inset*) TEM of an individual AZP-SBA, scale bar represents 2 μm; (b) TEM of Trypsin encapsulated hierarchical mesoporous material (Trypsin-SBA-MSN) (*Inset*) TEM of an individual Trypsin-SBA-MSN, scale bar represents 2 μm.

4.5.4.3 Fourier transform infra red spectroscopy

In order to find out optimum ratio of ALK-MSN to AZP-SBA required for the complete coverage of AZP-SBA by ALK-MSN to form hierarchical mesoporous material; CuAAC reaction between AZP-SBA and ALK-MSN were carried out with various weight ratios as presented in the Fig. 4.5. The percentage of click reaction was estimated by FT-IR spectroscopy by comparing the decrease in the integrated intensity of $\nu_{as}(N_3)$ at 2100 cm^{-1} with respect to corresponding reference samples without click reaction between AZP-SBA and ALK-MSN (physical mixtures of AZP-SBA and ALK-MSN with same weight ratio as used for click reaction). The loading curve shows that saturation occurs for a ratio between ALK-MSN and AZP-SBA at 0.3. That means the ratio between ALK-MSN and AZP-SBA should be 0.3 or above for the complete coverage of trypsin adsorbed AZP-SBA to form an efficient encapsulated biocatalyst. Hence all the click reactions were carried out by using little excess of ALK-MSN with a ratio of 0.5. FT-IR spectrum of CLICK-SBA-MSN shows about 25% decrease in the integrated intensity of $\nu_{as}(N_3)$ at 2100 cm^{-1} in comparison to the sample SBA-MSN (Fig. 4.6).

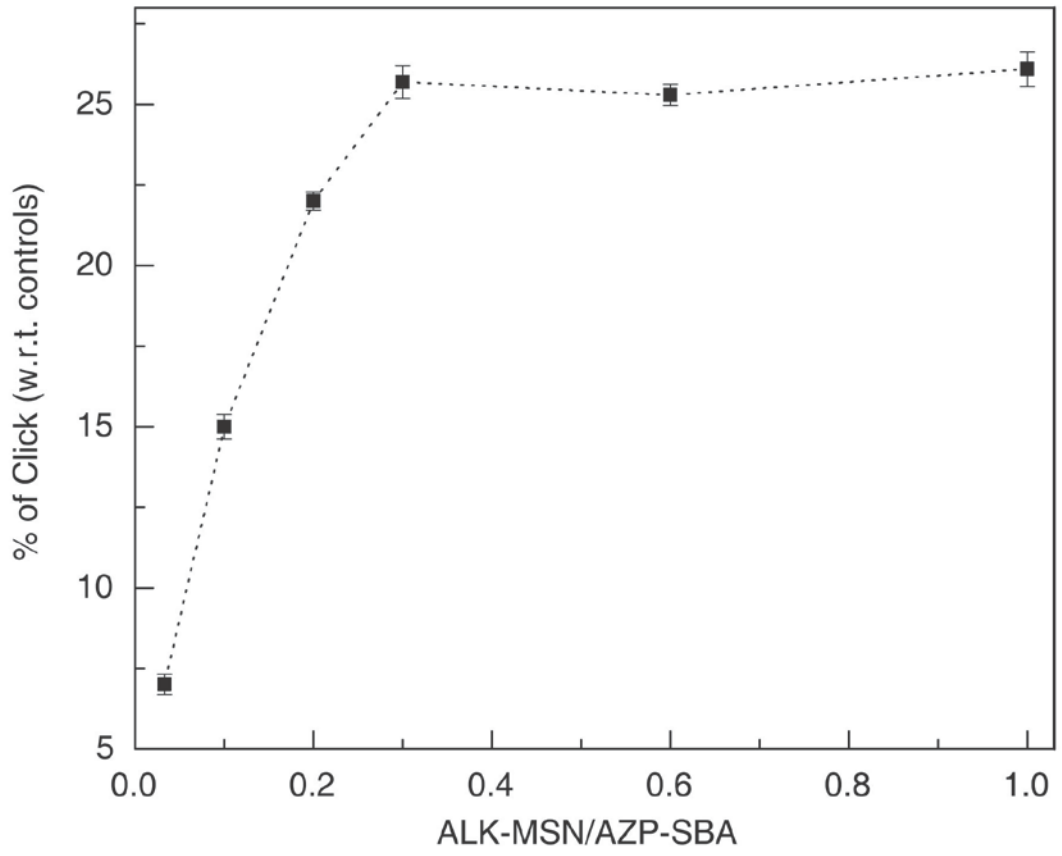

Figure 4.5: Loading curve for CuAAC reaction between AZP-SBA and ALK-MSN

4.5.4.4 Nitrogen adsorption-desorption studies

The nitrogen adsorption-desorption isotherms of various functionalized mesoporous material are presented in Fig. 4.7. The isotherm of AZP-SBA exhibit the characteristic type IV isotherm with steep increase in adsorption at P/P_0 = 0.6-0.8 due to capillary condensation of the nitrogen in the mesopores (Fig. 4.7a). The BJH pore-size distribution (PSD) analysis shows very narrow PSD values in the range 6-10 nm (Fig. 4.7a, insert). The pore diameter, BET surface and pore volume are given in the Table 4.2. These values are consistent with other organo-functionalized SBA-15 materials that have been reported before.[54]

Nitrogen adsorption-desorption isotherm of outer surface alkyne functionalized MSNs (ALK-MSN) is presented in the Fig. 4.7b. The isotherm exhibit the characteristic type IV isotherm with slight increase in adsorption at $P/P_0 \sim 0.2$ due to slight capillary condensation of the nitrogen in the mesopores. The BJH pore-size distribution (PSD) analysis shows very narrow PSD values in the range 2-3 nm. The

pore diameter, BET surface area and pore volume are listed in Table 4.2. These values are consistent with other organo-functionalized MSNs reported before.[55, 56]

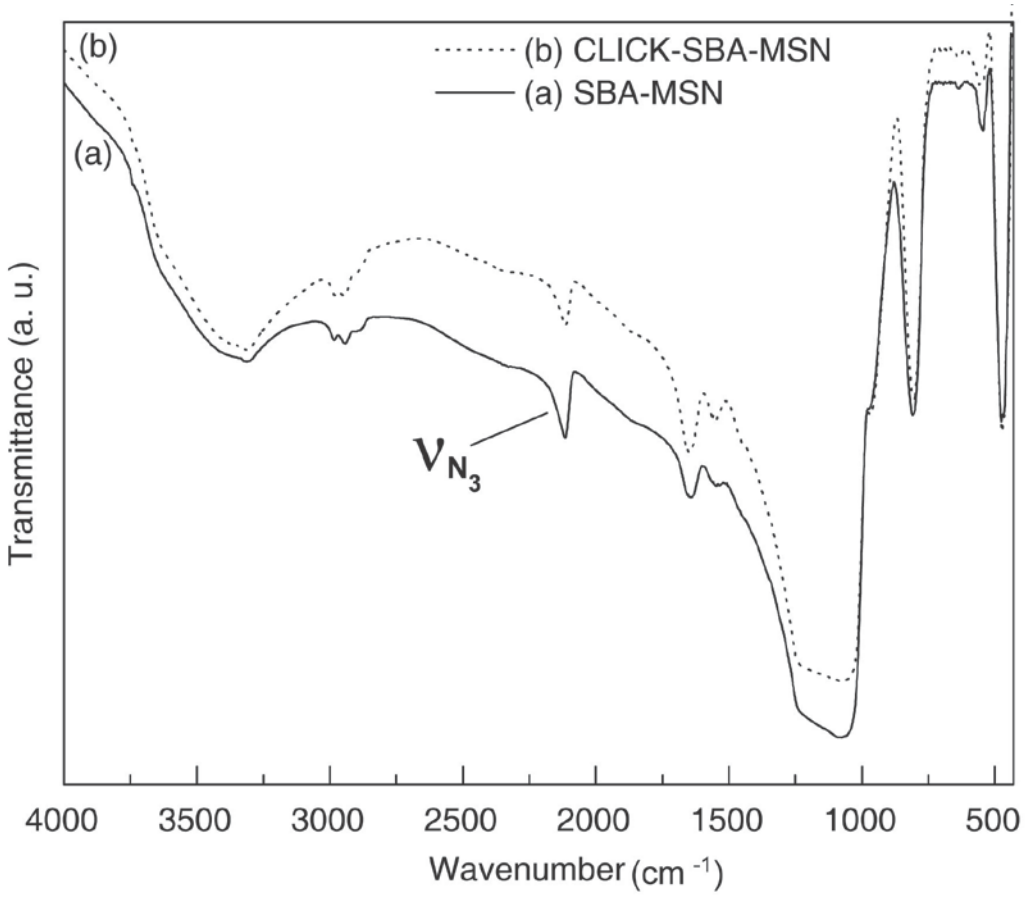

Figure 4.6: FT-IR spectra of (a) SBA-MSN, (b) CLICK-SBA-MSN

Nitrogen adsorption and desorption isotherms of the hierarchical mesoporous hybrid material obtained by clicking AZP-SBA (without trypsin adsorbed) with ALK-MSN to yield CLICK-SBA-MSN is presented in the Fig. 4.7c. The isotherm exhibit the characteristic type IV isotherm similar to parent mesoprous material AZP-SBA with slight decrease in BET surface area and pore volume. BJH pore size distribution of CLICK-SBA-MSN shows presence of hierarchical pore structure having pore sizes 8.18 nm and 2.2 nm consistent with pore sizes of parent mesoporous materials used for the synthesis of hierarchical mesoporous material (Fig. 4.7c, insert).

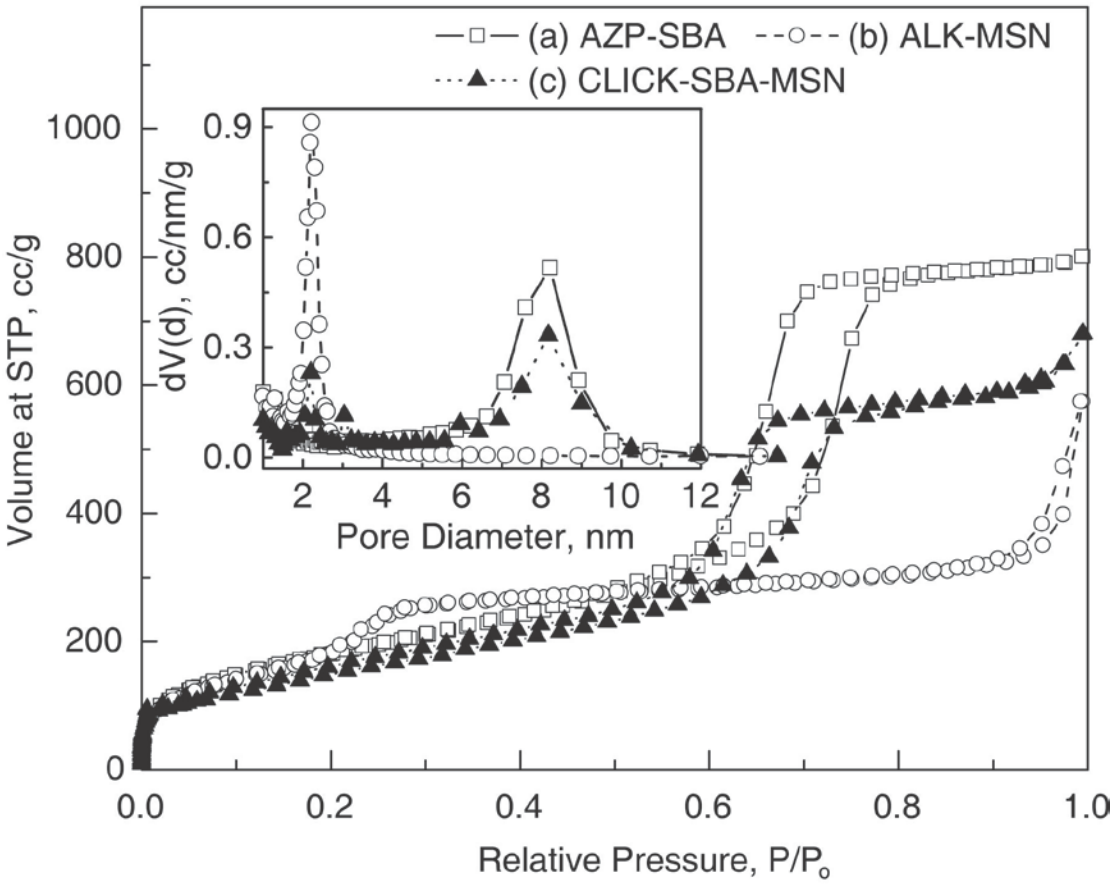

Figure 4.7: Nitrogen adsorption-desorption isotherms of (a) AZP-SBA, (b) ALK-MSN and (c) CLICK-SBA-MSN

Table 4.2: Physical properties of various mesoporous silica materials

Sample Name	Multi point BET (m^2/g)	Pore Diameter (nm)	Pore Volume (cm^3/g)
AZP-SBA	666	8.2	1.24
ALK-MSN	587	2.2	0.84
CLICK-SBA-MSN	542	8.18 and 2.2	0.96

4.5.4.5 Thermogravimetric analysis

Amount of trypsin encapsulated was determined by TGA and UV-Vis spectrophotometer. The TGA graphs of silica materials are presented in the Fig. 4.8. Samples were heated in air at 5 °C/ minute to 800 °C so that the organic contents were

completely decomposed and removed from the samples. Fig. 4.5a represents the TGA curve for the sample CLICK-SBA-MSN which was obtained by clicking AZP-SBA with ALK-MSN without encapsulation of trypsin, which shows a weight loss of 8.28% between 150 – 750 °C. TGA curve for encapsulated enzyme sample, Trypsin-SBA-MSN was presented in Fig. 4.5b, which gives a weight loss of 10.7% between 150 – 750 °C. By using these values in equation 4.1, amount of trypsin encapsulated was estimated to be 31±1 mg (~ 1.3 μmol) of trypsin per gram of Trypsin-SBA-MSN, which corresponds to 85% of enzyme encapsulation efficiency. The amount of trypsin adsorbed was also estimated from UV-Vis analysis of the residual trypsin that remained unadsorbed. UV-Vis analysis shows 88% of trypsin adsorbed in PHY-SBA-MSN (see Appendix III, Fig. C1).

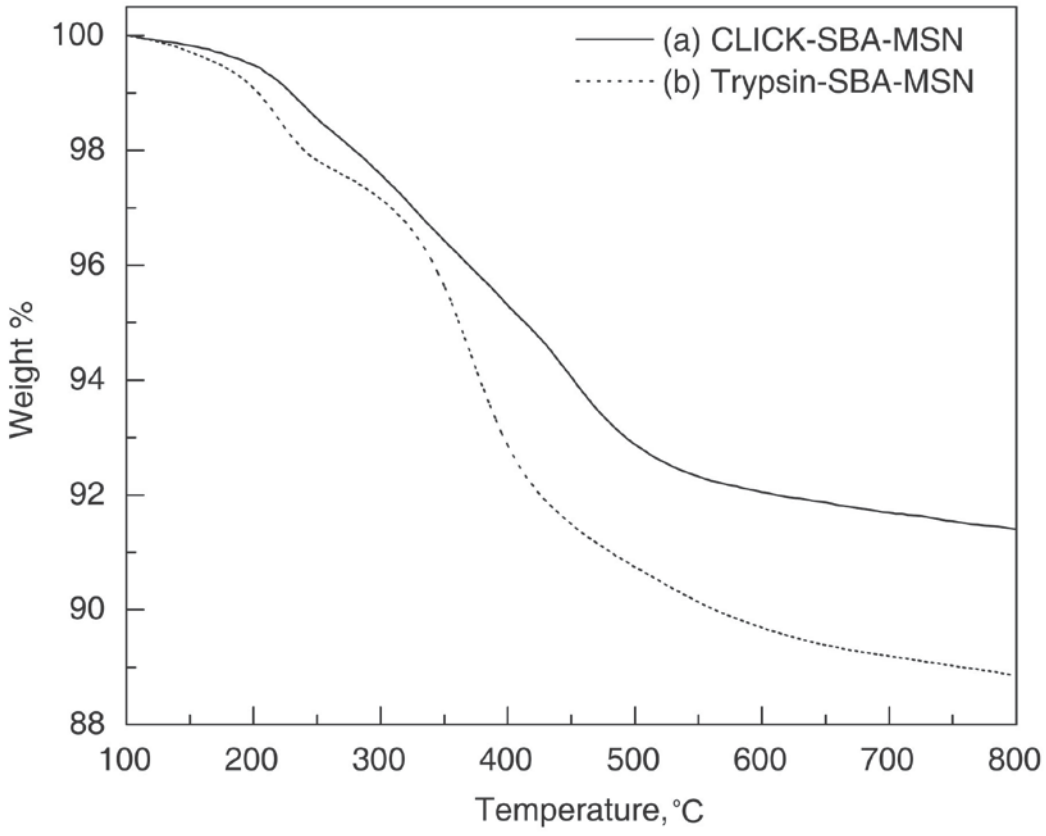

Figure 4.8: TGA graphs of (a) CLICK-SBA-MSN (b) Trypsin-SBA-MSN

4.5.4.6 Confocal laser scanning microscopy

To investigate the distribution of trypsin in the pores of AZP-SBA, fluorescein labeled trypsin was immobilized on AZP-SBA (Trypsin-AZP-SBA) and observed under confocal laser scanning microscope (CLSM). Confocal image of

Trypsin-AZP-SBA shows uniform distribution of trypsin inside AZP-SBA pores (Fig. 4.9a). In another experiment AZP-SBA was clicked with rhodamine B functionalized MSN (ALK-RH-MSN) and the resultant material was imaged by CLSM. This hierarchical material shows, a uniform coverage of rhodamine B functionalized MSNs (red) on the outer surface of AZP-SBA (Fig. 4.9b) [64].

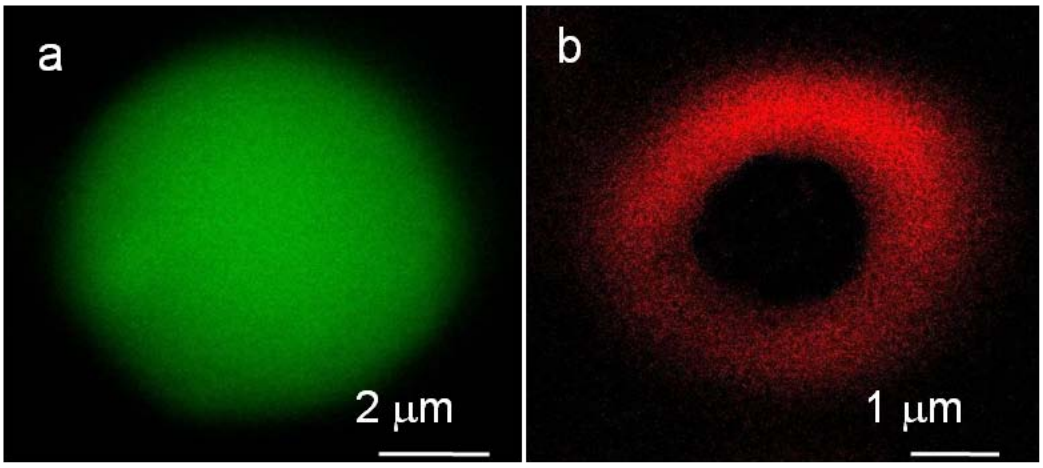

Figure 4. 9: (a) Fluorescein labelled trysin absorbed onto AZP-SBA; (b) AZP-SBA clicked with rhodamine B labelled MSNs showing that the MSN particles are present on the outer surface of SBA-15

4.5.4.7 Solid state ^{13}C CP MAS NMR spectroscopy

The solid state ^{13}C CP-MAS NMR spectra of various functionalized mesoporous materials are presented in Fig. 4.10. The spectrum of the azide-functionalized SBA-15 material (AZP-SBA) displays three peaks at ~9 ppm, 23 ppm and 54 ppm corresponding to the three C-atoms of the azido-propyl chain of AZP-SBA. The spectrum of the alkyne functionalized MSNs (ALK-MSN) shows presence of all the peaks corresponding to carbon chain. The important peaks at 67 ppm and 83 ppm due to acetylene C-atoms and another peak at ~ 175 ppm is due to presence of amide carbonyl carbon atom can be easily observed. ^{13}C CP-MAS NMR spectrum of CLICK-SBA-MSN in the Fig. 4.10c confirms the formation of hierarchical mesopore structure. The peaks at 124 and 147 ppm observed are due to formation of triazole by the click reaction between AZP-SBA and ALK-MSN.[57, 58]

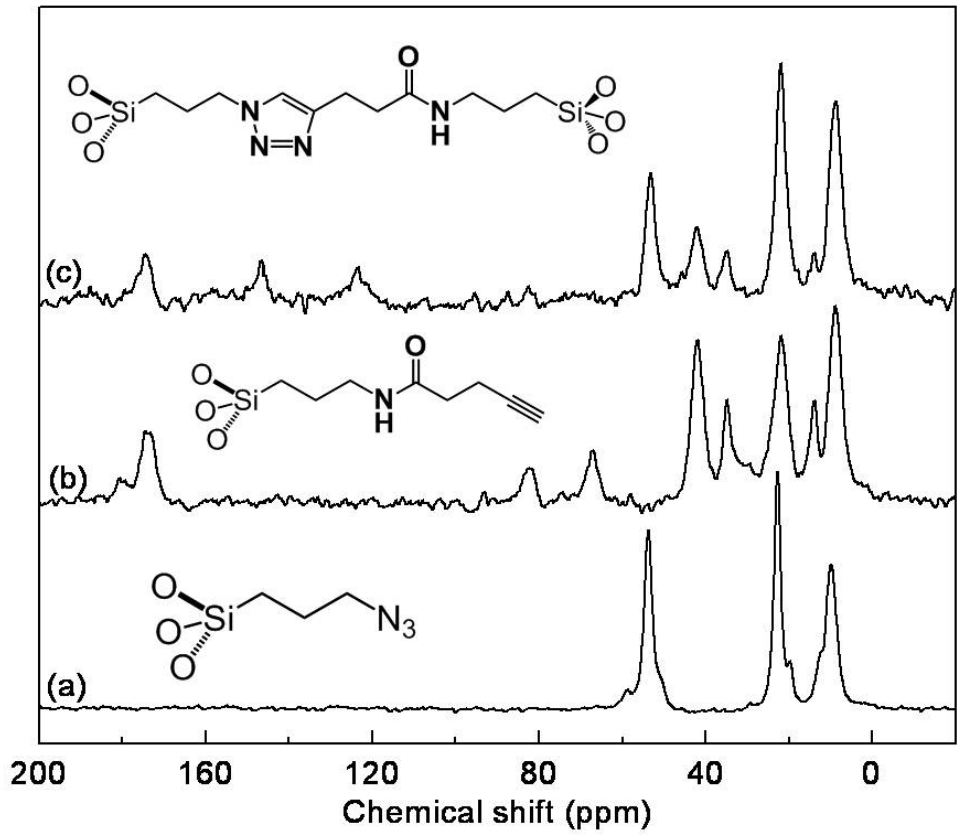

Figure 4.10: ^{13}C CP-MAS spectra of various silica materials: (a) AZP-SBA, (b) ALK-MSN, (c) CLICK-SBA-MSN

4.5.5 Mechanism of substrate specificity in trypsin

The catalytic residues (His57 and Ser195) and an aspartic acid residue present at the bottom of the substrate binding pocket are responsible for the observed substrate specificity in trypsin. The substrate having positively charged either arginine or lysine side chain is attracted by the negatively charged aspartate (Asp 189) located at the bottom of substrate binding pocket. This interaction helps to position the scissile peptide bond for the nucleophilic attack by the polarized hydroxyl group of Ser 195. Thus, an aspartic acid residue (Asp189) located at the bottom of the substrate binding pocket is responsible for the selectivity of trypsin towards substrates with positively charged side-chains.[12, 65]

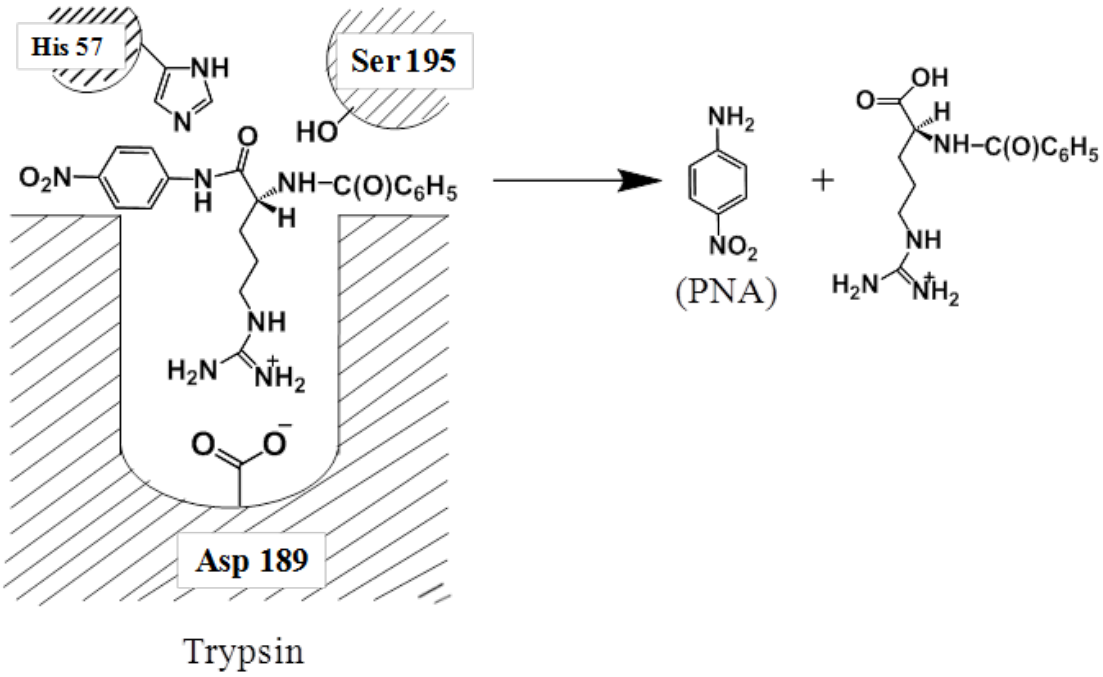

Scheme 4.3: Schematic presentation mechanism of substrate specificity in trypsin

4.5.6 Determination of activity of trypsin

Catalytic activity of trypsin for amide hydrolysis can be readily assessed colorimetrically using BAPNA as substrate, since *p*-nitroaniline (PNA) formed by the hydrolysis of BAPNA strongly absorbs at 405 nm in UV-Visible spectrum (Scheme 4.3).[49] To investigate the activity of the encapsulated trypsin, Trypsin-SBA-MSN was treated with 2 mM BAPNA in tris buffer (50 mM, pH 8).[49] The activity of the encapsulated trypsin was found to be 44 $\mu molg^{-1}min^{-1}$ and remained almost constant even after 10 cycles. (Fig. 4.11) This shows that the enzyme is active and remains encapsulated efficiently. This encapsulated enzyme has comparable activity with the activity of the physically adsorbed trypsin on post synthetic functionalized SBA-15 with thiols, amines and carboxylic acids.[49] For further comparison of the activity, two control experiments were carried out. In one case, trypsin was physically adsorbed on AZP-SBA and then ALK-MSN was added in the same ratio as was used for encapsulation of trypsin. This material was referred as PHY-SBA-MSN. In another control, the PHY-SBA-MSN hybrid material described above was subjected to the same workup protocol that was carried out during the encapsulation reaction (washing with 10% PEG solution in 50 mM, pH 8 tris buffer). This is referred as PEG-SBA-MSN. Both the materials were subjected to activity study with BAPNA

solution. The results (Fig. 4.11) show that even though the activity of PHY-SBA-MSN is about twofold higher than that of the activity of the encapsulated enzyme (Trypsin-SBA-MSN), the activity of the PHY-SBA-MSN decreases significantly with each cycle due to leaching of the adsorbed enzyme in the solution.[49] After 10 cycles activity of the adsorbed enzyme was decreased by ~75% where as encapsulated enzyme shows almost no loss in activity. Two fold decrease in activity of the trypsin upon encapsulation in comparison to activity of adsorbed enzyme observed may be due to increased mass transport limitations; as BAPNA molecules have to diffuse through the pore channels of MSNs and SBA-15 to reach to the encapsulated trypsin. It is likely that the BAPNA molecules being positively charged were strongly adsorbed inside pore channels of MSNs which resulted in slow diffusion of BAPNA molecules onto the immobilized trypsin inside the pores of SBA-15. [24] On the other hand, PEG-SBA-MSN showed 87% less activity as compared to activity by PHY-SBA-MSN. UV-Vis studies on estimation of amount of trypsin leached out shows that 89% of trypsin leached out during PEG solution treatment (Appendix III, Fig. C2).[57] These results conclusively show that encapsulated trypsin in the hierarchically porous silica material functions as an efficient bio-catalyst and can be reused several times without loss of activity.

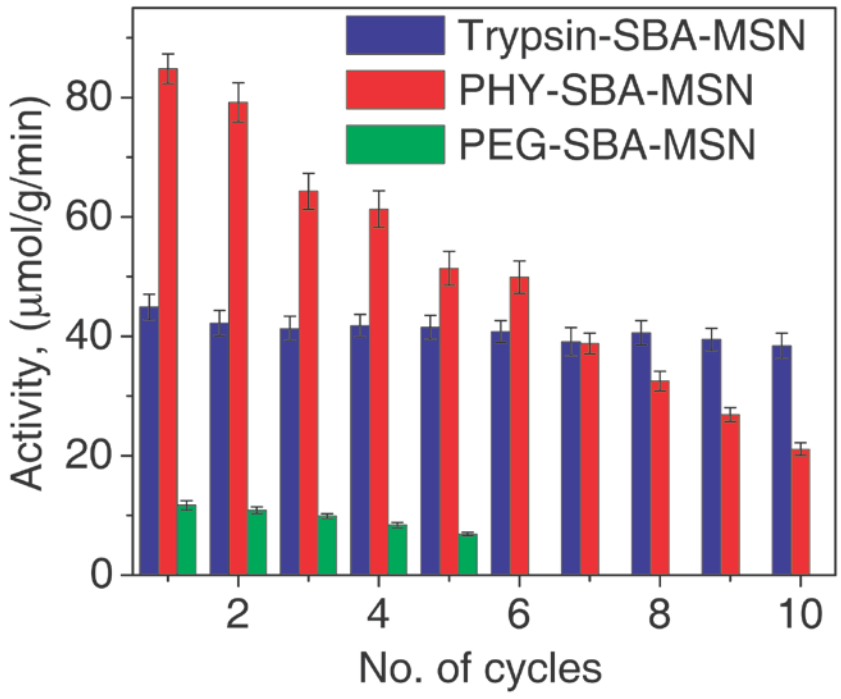

Figure 4.11: Activity of trypsin encapsulated or immobilized on different silica materials using 2 mM BAPNA in 50 mM, pH 8 tris buffer

4.6 Conclusions

In conclusion, a facile and efficient route for the development of hierarchical mesoporous materials and its application in the encapsulation of enzymes is described. Transmission electron microscopy, Nitrogen adsorption, FT-IR spectroscopy, TGA and confocal microscopy analysis unambiguously establish the formation of hierarchical mesoporous material. The encapsulated enzyme functions as an efficient biocatalyst over 10 cycles without loss of activity. In general, the method can be used for the encapsulation of other enzymes of interest. Such encapsulated enzymes can be used in the development of continuous flow bio-reactors. Further, chemoselective reactions can be achieved by the modification of inner pores surface of MSNs which can act as a gate-keeper for the substrates. Also diffusion of the substrate from MSNs pores into the pores of SBA-15 can be restricted by pore size of the MSNs, as a result size selective reaction of the substrates can be carried out.

4.7 References

1. R. A. Sheldon, *Adv. Syn. Catal.*, 2007, **349**, 1289-1307.
2. J. Kim, J. W. Grate and P. Wang, *Chemical. Engineering Science*, 2006, **61**, 1017-1026.
3. M. Hartmann and D. Jung, *J. Mater. Chem.*, 2010, **20**, 844-857.
4. A. Schmid, J. S. Dordick, B. Hauer, A. Kiener, M. Wubbolts and B. Witholt, *Nature*, 2001, **409**, 258-268.
5. H. H. P. Yiu and P. A. Wright, *J. Mater. Chem.*, 2005, **15**, 3690-3700.
6. C.-H. Lee, T.-S. Lin and C.-Y. Mou, *Nano Today*, 2009, **4**, 165-179.
7. J. Kim, H. F. Jia and P. Wang, *Biotechn. Adv.*, 2006, **24**, 296-308.
8. D. Haring and P. Schreier, *Curr. Opin. Chem. Bio.*, 1999, **3**, 35-38.
9. L. Cao, F. van Rantwijk and R. A. Sheldon, *Org. Lett.*, 2000, **2**, 1361-1364.
10. P. López-Serrano, L. Cao, F. van Rantwijk and R. A. Sheldon, *Biotechn. Lett.*, 2002, **24**, 1379-1383.
11. Y. Dror, J. Kuhn, R. Avrahami and E. Zussman, *Macromolecules*, 2008, **41**, 4187-4192.
12. J. F. Díaz and K. J. Balkus, *J. Mol. Catal. B: Enzym.*, 1996, **2**, 115-126.
13. H. Ma, J. He, D. G. Evans and X. Duan, *J. Mol. Catal. B: Enzym.*, 2004, **30**, 209-217.

14. I. Gill and A. Ballesteros, *J. Am. Chem. Soc.*, 1998, **120**, 8587-8598.
15. K. Y. Lee and S. H. Yuk, *Prog. Poly. Sci.*, 2007, **32**, 669-697.
16. E. S. Lee, M. J. Kwon, H. Lee and J. J. Kim, *International Journal of Pharmaceutics*, 2007, **331**, 27-37.
17. I. Chibata, *Immobilised Enzymes*, Hastel, New York, 1978.
18. A. Petri, P. Marconcini and P. Salvadori, *J. Mol. Catal. B: Enzym.*, 2005, **32**, 219-224.
19. M. Hartmann, *Chem. Mater.*, 2005, **17**, 4577-4593.
20. R. Reshmi, G. Sanjay and S. Sugunan, *Catal. Commun.*, 2006, **7**, 460-465.
21. A. P. V. Goncalves, J. M. Lopes, F. Lemos, F. Ramoa Ribeiro, D. M. F. Prazeres, J. M. S. Cabral and M. R. Aires-Barros, *J. Mol. Catal. B: Enzym.*, 1996, **1**, 53-60.
22. F. N. Serralha, J. M. Lopes, F. Lemos, D. M. F. Prazeres, M. R. Aires-Barros, J. M. S. Cabral and F. Ramoa Ribeiro, *J. Mol. Catal. B: Enzym.*, 1998, **4**, 303-311.
23. S. Hudson, J. Cooney and E. Magner, *Angew. Chem. Int. Ed*, 2008, **47**, 8582-8594.
24. H. H. P. Yiu, P. A. Wright and N. P. Botting, *Micro. .Meso. Mater.*, 2001, **44-45**, 763-768.
25. A. S. M. Chong and X. S. Zhao, *Catalysis Today*, 2004, **93-95**, 293-299.
26. P. Wang, S. Dai, S. D. Waezsada, A. Y. Tsao and B. H. Davison, *Biotechnology and Bioengineering*, 2001, **74**, 249-255.
27. A. Schlossbauer, D. Schaffert, J. Kecht, E. Wagner and T. Bein, *J. Am. Chem. Soc.*, 2008, **130**, 12558-12559.
28. Y. Wang and F. Caruso, *Chem. Commun.*, 2004, 1528-1529.
29. A. Yu, Y. Wang, E. Barlow and F. Caruso, *Adv. Mater.*, 2005, **17**, 1737-1741.
30. I. I. Slowing, B. G. Trewyn and V. S. Y. Lin, *J. Am. Chem. Soc.*, 2007, **129**, 8845-8849.
31. C.-H. Lee, J. Lang, C.-W. Yen, P.-C. Shih, T.-S. Lin and C.-Y. Mou, *J. Phy. Chem. B*, 2005, **109**, 12277-12286.
32. S. Z. Qiao, C. Z. Yu, W. Xing, Q. H. Hu, H. Djojoputro and G. Q. Lu, *Chem. Mater.*, 2005, **17**, 6172-6176.
33. A. Katiyar, L. Ji, P. G. Smirniotis and N. G. Pinto, *Micro. Meso. Mater.*, 2005, **80**, 311-320.

34. A. Katiyar, L. Ji, P. Smirniotis and N. G. Pinto, *J. Chromatog. A*, 2005, **1069**, 119-126.

35. A. Vinu, V. Murugesan and M. Hartmann, *J. Phy. Chem. B*, 2004, **108**, 7323-7330.

36. S. Z. Qiao, H. Djojoputro, Q. Hu and G. Q. Lu, *Prog. Solid State Chem.*, 2006, **34**, 249-256.

37. C. Li, J. Liu, X. Shi, J. Yang and Q. Yang, *J. Phy. Chem. C*, 2007, **111**, 10948-10954.

38. H. Takahashi, B. Li, T. Sasaki, C. Miyazaki, T. Kajino and S. Inagaki, *Chem. Mater.*, 2000, **12**, 3301-3305.

39. H. Takahashi, B. Li, T. Sasaki, C. Miyazaki, T. Kajino and S. Inagaki, *Micro. Meso. Mater.*, 2001, **44-45**, 755-762.

40. J. Deere, E. Magner, J. G. Wall and B. K. Hodnett, *J. Phy. Chem. B*, 2002, **106**, 7340-7347.

41. Y. Liu, Q. Xu, X. Feng, J.-J. Zhu and W. Hou, *Anal. Bioanal. Chem.*, 2007, **387**, 1553-1559.

42. Y. Urabe, T. Shiomi, T. Itoh, A. Kawai, T. Tsunoda, F. Mizukami and K. Sakaguchi, *ChemBioChem*, 2007, **8**, 668-674.

43. P. Xue, G. Lu, Y. Guo, Y. Wang and Y. Guo, *J. Mol. Catal. B: Enzym.*, 2004, **30**, 75-81.

44. A. S. M. Chong and X. S. Zhao, *Appl. Surf. Sci.*, 2004, **237**, 398-404.

45. J. He, Z. Song, H. Ma, L. Yang and C. Guo, *J. Mater. Chem.*, 2006, **16**, 4307-4315.

46. J. He, Y. Xu, H. Ma, Q. Zhang, D. G. Evans and X. Duan, *Journal of Colloid and Interface Science*, 2006, **298**, 780-786.

47. B. Zhao, B. Shi and R. Ma, *Eng. Life Sci.*, 2005, **5**, 436-441.

48. L. Qiao, Y. Liu, S. P. Hudson, P. Yang, E. Magner and B. Liu, *Chem. Eur. J.*, 2008, **14**, 151-157.

49. H. H. P. Yiu, P. A. Wright and N. P. Botting, *J. Mol. Catal. B: Enzym.*, 2001, **15**, 81-92.

50. J. M. Kisler, A. Dahler, G. W. Stevens and A. J. O'Connor, *Micro. Meso. Mater.*, 2001, **44-45**, 769-774.

51. P. H. Pandya, R. V. Jasra, B. L. Newalkar and P. N. Bhatt, *Micro. Meso. Mater.*, 2005, **77**, 67-77.

52. V. Hong, S. I. Presolski, C. Ma and M. G. Finn, *Angew. Chem. Int. Ed.*, 2009, **48**, 9879-9883.

53. M. Galibert, P. Dumy and D. Boturyn, *Angew. Chem. Int. Ed*, 2009, **48**, 2576-2579.

54. A. Katiyar, S. Yadav, P. G. Smirniotis and N. G. Pinto, *J. Chromatogr. A*, 2006, **1122**, 13-20.

55. C.-Y. Lai, B. G. Trewyn, D. M. Jeftinija, K. Jeftinija, S. Xu, S. Jeftinija and V. S. Y. Lin, *J. Am. Chem. Soc.*, 2003, **125**, 4451-4459.

56. R. Mortera, J. Vivero-Escoto, I. I. Slowing, E. Garrone, B. Onida and V. S. Y. Lin, *Chem. Commun.*, 2009, 3219-3221.

57. D. Goradia, J. Cooney, B. K. Hodnett and E. Magner, *J. Mol. Catal. B: Enzym.*, 2005, **32**, 231-239.

58. J. Nakazawa and T. D. P. Stack, *J. Am. Chem. Soc.*, 2008, **130**, 14360-14361.

59. M. Kar, B. Malvi, A. Das, S. Panneri and S. S. Gupta, *J. Mater. Chem.*, 2011, **21**, 6690-6697.

60. Y. Ma, L. Qi, J. Ma, Y. Wu, O. Liu and H. Cheng, *Colloids and Surfaces A: Physicochem. Eng. Aspects*, 2003, **229**, 1-8.

61. J. Y. Ying, C. P. Mehnert and M. S. Wong, *Angew. Chem. Int. Ed*, 1999, **38**, 56-77.

62. D. Zhao, Q. Huo, J. Feng, B. F. Chmelka and G. D. Stucky, *J. Mol. Catal. B: Enzym.*, 1998, **120**, 6024-6036.

63. L. Cao, T. Man and M. Kruk, *Chem. Mater.*, 2009, **21**, 1144-1153.

64. N. Gartmann and D. Brühwiler, *Angew. Chem. Int. Ed*, 2009, **48**, 6354-6356.

65. J. J. Perona and C. S. Craik, *J. Biol. Chem.*, 1997, **272**, 29987-29990.

CHAPTER 5

Conclusions and Future Work

5.1 Summary and conclusions

This thesis describes the synthesis and characterization of azide functionalized SBA-15 and MCM-41 mesoporous materials by both grafting and co-condensation methods followed by the evaluation of the ability of these azide functionalized mesoporous materials to undergo Cu(I)-catalyzed azide alkyne cycloaddition (CuAAC) reaction with various organic molecules bearing alkyne functionality. Using this methodology, several hybrid MCM-41 and SBA-15 type materials were synthesized. The application of these materials as catalysts and biosensors has also been evaluated in this thesis. This chapter presents summary and conclusions of the work described in previous chapters and scope of future work based on this thesis.

Chapter 1 provides mainly a review on the literature of mesoporous materials including synthetic strategies for mesoporous materials, mechanism of formation of mesoporous materials and different approaches for the synthesis of hybrid organic-inorganic mesoporous materials by incorporation of functional organic groups onto mesoporous materials. Physical principles for the various analytical techniques used for the characterization of mesoporous materials are also described. A brief introduction to click chemistry is also provided.

Chapter 2 describes synthesis and characterization of “clickable” SBA-15 and MCM-41 mesoporous materials. This chapter is divided into two parts.

Part A describes synthesis of azide labeled SBA-15 using both one-pot co-condensation and post-synthetic grafting method. SBA-15 was synthesized by sol-gel hydrothermal synthesis using pluronic P123 as structure directing agent and TEOS as silica precursor. The azide functionalized SBA-15 was obtained by grafting of 3-azidopropyltriethoxysilane (AzPTES) on calcined SBA-15. In the case of synthesis of azide labeled SBA-15 via one-pot co-condensation method, the ratio of TEOS and AzPTES was kept as 9:1 since the usage of higher amounts of organosilica precursor may lead to functionalized materials with lesser long range order. These materials underwent very efficient Cu(I) catalyzed azide alkyne cycloaddition (CuAAC) reaction with a variety of alkynes. When AZP-SBA-G was used, only 1.5 equivalent of alkyne was required to covert 90% of the available azides to triazole. Similar efficiency is much difficult to attain in aqueous solution by using amine and carboxylic labeled SBA-15, which are materials typically used to anchor various

functional molecules. The azide labeled SBA-15 materials and organically modified materials retained their mesoporosity as revealed by powder XRD, SEM, TEM, nitrogen adsorption-desorption studies and solid state ^{29}Si CP-MAS NMR spectroscopy. The incorporation of the organic functionality was confirmed by FT-IR and solid state ^{13}C CP-MAS NMR spectroscopy. One of the silent feature presented in this chapter is semi-quantitative estimation of yields of CuAAC reaction by FT-IR spectroscopy by monitoring decrease in the integrated intensity of the $\nu_{as}(N_3)$ at 2100 cm^{-1}. The azide labeled SBA-15 was further used as a platform to synthesize a silica-protein hybrid material composed of mannose labeled SBA-15 and concanavalin-A. Such hybrid materials may be important in the development of biosensors. The ease of synthesis for the azide labeled SBA-15 material together with its ability to undergo very efficient chemoselective CuAAC in water would make it a very attractive platform for the development of covalently anchored catalysts, enzymes and sensors.

Part B describes synthesis of azide functionalized MCM-41materials by one-pot co-condensation method using CTAB as structure directing agent under basic conditions. The density of azidopropyl groups on the surface of MCM-41 was varied by varying the molar ratio of AzPTES (0.2 to 10 mol%) with respect to TEOS during one pot co-condensation synthesis. The efficiency of these azide functionalized MCM-41 materials to undergo CuAAC reaction has been demonstrated by using variety of organic substrates bearing alkyne functionality. In case of MCM-41 materials, amount of azide groups available for CuAAC reaction is more in comparison to SBA-15 materials prepared by one-pot co-condensation reaction. This is because MCM-41 has thinner walls than SBA-15 and as a result most of the azide groups are exposed outside pore walls and are available for further modification. The azide functionalized MCM-41(*x*-AZP-MCM) and the subsequent organically modified hybrid materials retain their structure and mesoporosity as revealed by powder XRD, SEM, TEM, nitrogen adsorption-desorption studies and solid state ^{29}Si CP-MAS NMR spectroscopy. The incorporation of the organic functionality was confirmed by FT-IR and solid state ^{13}C CP-MAS NMR spectroscopy. The synthesis of site-isolated and site-dense azide labeled MCM-41 was confirmed my measuring the pyrene fluorescence emission spectra at 330 nm of *x*-AZP-MCM (x = 0.2, 0.5, 1, 5, 10 mol%) materials that were clicked with propargyloxy(1-pyrenyl)methane.

Further, the heterogeneous site isolated proline catalyst shows increase in rate when it was used as a catalyst for aldol condensation reaction. This strategy can be used to synthesize other organo-catalysts or organo-metallic catalysts for the development of improved catalyst activity.

Chapter 3 describes the synthesis of mesoporous silica nanoparticles (MCM-41 type) based hybrid material (Fe-MSN) that mimics the enzyme HRP and functions as a biosensor at physiological pH. This hybrid material contains a robust small molecule peroxidase mimic [Fe^{III}(biuret-amide)] developed in our group[1] that is covalently attached to azide containing MSN particles by Cu(I) catalyzed azide alkyne cycloaddition(CuAAC) reaction. The azide functionalized mesoporous nanoparticles (N_3-MSN) were synthesized by one pot co-condensation of TEOS and AzPTES using CTAB as structure directing agent under basic conditions. For the synthesis of N_3-MSN via one pot co-condensation method the molar ratio of TEOS to AzPTES used was 99:1 which allows reasonable site-isolation of the azidopropyl groups and the catalyst as established in the previous chapter. This is expected to reduce intermolecular degradation of the catalyst and therefore increase its turnover number. The co-condensation method used to synthesize the azide grafted material allows the attachment of [Fe^{III}(biuret-amide)] catalysts mostly inside the MSN pore which limits its interaction with enzymes like glucose oxidase during one-pot glucose detection. Formation of well-ordered two-dimensional hexagonal mesoporous particles with a spherical morphology has been established by powder XRD, TEM and nitrogen adsorption-desorption studies. Formation of Fe-MSN by attachment of [Fe^{III}(biuret-amide)] by CuAAC reaction has been confirmed by FT-IR, EPR, ICP and nitrogen adsorption-desorption experiments. These hybrid MSN particles were then used as a biosensor for the quantitative detection of H_2O_2 and glucose in a one-pot method. It was observed that the detection of hydrogen peroxide was linear in the range 1.0×10^{-4} to 5.0×10^{-3} M with a detection limit at 1.0×10^{-5} M, while detection of glucose was linear in the range 2.0×10^{-5} to 3.0×10^{-4} M with a detection limit of 1.0×10^{-5} M. Finally our methodology was used to determine glucose in mice blood plasma. Blood plasma obtained from a healthy mice containing glucose concentration 5.88 mM was serially diluted with phosphate buffer and detection of glucose was carried out. The average concentration of glucose in plasma was determined to be 5.77 mM. Thus, this study demonstrates that the Fe-MSN can be used for analysis of

real life samples. The hybrid material being truly biocompatible peroxidase mimic and because of its robustness, stability and ease of preparation opens up a range of new potential applications in the fields of biotechnology and environmental chemistry.

Chapter 4 describes synthesis of hierarchical mesoporous silica based hybrid material and its application as a support for the immobilization of trypsin in a "ship-in-a-bottle" approach. Enzyme adsorbed onto an azide functionalized mesoporous spherical SBA-15 with pores larger than the diameter of the enzyme were capped with alkyne functionalized mesoporous silica nanoparticles (MSNs) by covalent linkage using efficient CuAAC reaction. The mesoporous silica nanoparticles (MSNs) have pores that are large enough to allow small molecules such as reactants and products to diffuse in and out of SBA-15 but do not allow enzyme to leach out of SBA-15. Hence, in this hierarchical silica mesoporous hybrid material, the pores of MSNs on the surface of spherical SBA-15 act as windows for enzyme and effectively stops the enzyme from leaching. The bio-orthogonal nature of CuAAC ensures that the efficient capping of organoazide groups on spherical SBA-15 particles and can be carried out with alkyne functionalized MSN without loss of activity of the enzyme. Transmission electron microscopy, Nitrogen adsorption, FT-IR spectroscopy, TGA and confocal laser scanning microscopy (CLSM) analysis unambiguously establish the formation of enzyme encapsulated hierarchical mesoporous material. The encapsulated trypsin functions as an efficient biocatalyst over 10 cycles without loss of activity. In general, the method can be used for the encapsulation of other enzymes of interest. Further, chemoselective reactions can be achieved by the modification of inner pore surface of MSNs which can act as a gate-keeper for the substrates. Also diffusion of the substrate from MSNs pores into the pores of SBA-15 can be restricted by pore size of the MSNs which can then allow size selective reactions to be carried out.

5.2 Scope of future work

The work described in this thesis opens up several new opportunities that can be subsequently carried out. Some of them are listed below.

1) Site isolated catalysis

In chapter 2 part B we have shown the site isolation of azido-propyl groups on

the surface of MCM-41 mesoporous materials. These site isolated azides can be used to develop site-isolated heterogeneous catalysts such as [Fe^{III}-(biurate-amide)] peroxidase mimics that has been developed in our laboratory.[1] Site isolation of catalysts such as [Fe^{III}-(biurate-amide)] inside the pore channels of SBA-15 or MCM-41 mesoporous materials would be analogous to the active site of the enzyme embedded in the cavity surrounded by protein matrix. This would enhance the stability and activity of the complex by overcoming intermolecular degradation of the catalyst and attenuating formation of μ-oxodimer complex, which is known to be catalytically inactive.[2, 3] The efficacy of these site isolated catalysts can be evaluated for the oxidation of various organic substrates in presence of oxidants like H_2O_2.

2) Development of new bio-sensors

In the chapter 3 we have developed mesoporous silica (MSN) based hybrid material (Fe-MSN) that mimics the enzyme HRP and functions as a biosensor at physiological pH. This hybrid material contains a robust small molecule peroxidase mimic [Fe^{III}(biuret-amide)] developed in our group[1] that is covalently attached to azide containing MSN particles by Cu(I) catalyzed azide alkyne cycloaddition (CuAAC) reaction. These hybrid MSN particles were used as a biosensor for the quantitative detection of H_2O_2 and glucose. For the detection of glucose, peroxidase like activity of Fe-MSN was coupled with glucose oxidation reaction by glucose oxidase (GOX). The GOX oxidizes glucose to form gluconic acid and H_2O_2 quantitatively; the H_2O_2 thus produced is then utilized by Fe-MSN to oxidize chromogenic substrate to an oxidized colored product that can be easily detected colorimetrically. In a similar fashion, colorimetric biosensors can be developed for the detection of other biological samples. For example, (a) Uric acid sensor can be developed by coupling uric acid oxidation reaction by uricase also known to quantitatively produce hydrogen peroxide[4, 5] with the peroxidase like catalytic activity of Fe-MSN. (b) Cholesterol sensor can be developed by coupling cholesterol oxidation reaction by cholesterol oxidase to produce hydrogen peroxide quantitatively[6] with the peroxidase like catalytic activity of Fe-MSN.

Further, the silanol groups on the outer surface of Fe-MSN can be functionalized to incorporate targeting ligands such as antigens/antibodies for usage in immunoassays like ELISA.

3) Encapsulation of enzymes

In the chapter 4 we have developed a new method of synthesis of hierarchical mesoporous silica based hybrid material and its application as a support for the immobilization of trypsin in a "ship-in-a-bottle" approach. The pores of the azide functionalized mesoporous spherical SBA-15 containing adsorbed enzyme were capped with alkyne functionalized mesoporous silica nanoparticles (MSNs) by covalent linkage using efficient CuAAC reaction. Thus, the pores of MSNs on the surface of spherical SBA-15 act as windows for enzyme and effectively stops the enzyme from leaching. The methodology developed by us is general and can be further expanded for other applications. Some of the ideas are listed below:

a) Hierarchical mesoporous silica based immobilization enzyme technique developed by us can be further improved by using SBA-15 particles embedded with magnetic iron oxide nanoparticles for easy separation of nanoreactors simply by using external magnetic field after completion of reaction. Incorporation of magnetic iron oxide nanoparticles inside pore walls or pore channels can be achieved either by co-condensation method or by post synthetic functionalization method using procedures reported in the literature.[7-9]

b) The inner pore surface of MSNs can be further functionalized to tune the hydrophobic/hydrophilic property of the surface for selective diffusion of either hydrophobic or hydrophilic substrates for carrying out chemoselective reaction.

c) Diffusion of the substrate from MSNs pores into the pores of SBA-15 can be restricted by pore size of the MSNs. As a result size selective reaction of substrates can be carried out. This will find applications in peptidomics and proteomics for the analysis of low molecular weight proteins from complex biological samples.[10-12]

d) Storage stability, stability to heat, pH and organic solvents can be evaluated for different substrates and enzymes to expand the scope of the developed methodology.

5.3 References

1. C. Panda, M. Ghosh, T. Panda, R. Banerjee and S. Sen Gupta, *Chem. Commun.*, 2011, **47**, 8016-8018.
2. A. Ghosh, F. Tiago de Oliveira, T. Yano, T. Nishioka, E. S. Beach, I. Kinoshita, E. Munck, A. D. Ryabov, C. P. Horwitz and T. J. Collins, *J. Am. Chem. Soc.*, 2005, **127**, 2505-2513.
3. J. Nakazawa and T. D. P. Stack, *J. Am. Chem. Soc.*, 2008, **130**, 14360-14361.
4. D. Martinez-Perez, M. L. Ferrer and C. R. Mateo, *Anal. Biochem.*, 2003, **322**, 238-242.
5. G. Minas, J. S. Martins, J. C. Ribeiro, R. F. Wolffenbuttel and J. H. Correia, *Sensors and Actuators A* 2004, **110**, 33-38.
6. J. Li, T. Peng and Y. Peng, *Electroanalysis*, 2003, **15**, 1031-1037.
7. C. Y. Liu, C. F. Chen, J. P. Leu and Y. C. Lin, *J. Sol-Gel Sci. Technol.*, 2007, **43**, 47-51.
8. S. M. Zhu, Z. Y. Zhou, D. Zhang, C. Jin and Z. Q. Li, *Micro. Meso. Mater.*, 2007, **106**, 56-61.
9. Y. Zhu, S. Kaskel, J. Shi, T. Wage and K.-H. van Pee, *Chem. Mater.*, 2007, **19**, 6408-6413.
10. F. Li, B. Dever, H. Zhang, X.-F. Li and X. C. Le, *Angew. Chem. Int. Ed*, 2012, **51**, 3518-3519.
11. Q. Min, R. a. Wu, L. Zhao, H. Qin, M. Ye, J.-J. Zhu and H. Zou, *Chem. Commun.*, 2010, **46**, 6144-6146.
12. Q. Min, X. Zhang, R. a. Wu, H. Zou and J.-J. Zhu, *Chem. Commun.*, 2011, **47**, 10725-10727.

Appendix I

Calibration Curve for semi-quantitative estimation of Azide groups in SBA-15

To obtain a semi-quantitative estimation of the percentage of azide functionalized, a calibration curve was prepared using various quantities of AZP-SBA-**C**. Typically, various quantities of AZP-SBA-**C** and KBr were mixed such that the total weight was 100 mg. Pellets were prepared from this mixture and the IR spectrum was taken. Finally, the area under the 2100 cm^{-1} peak (that is characteristic of the azide) was plotted against the concentration of AZP-SBA-**C** used. For all data points, an average of three values was used.

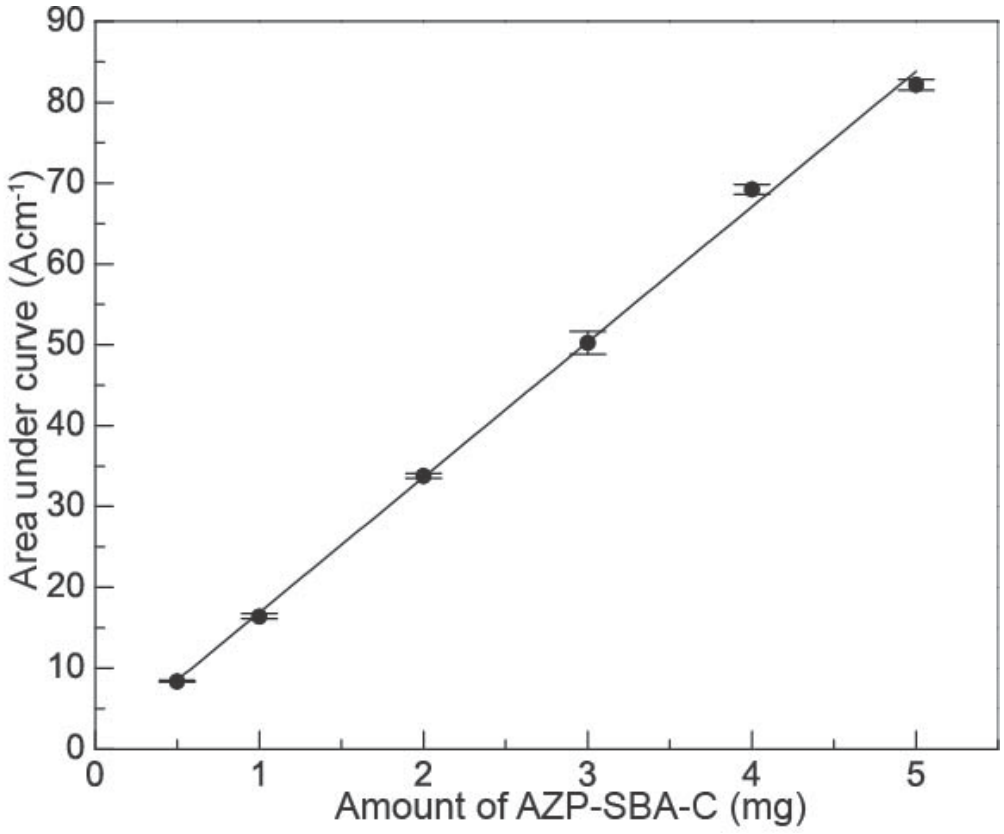

Figure A1: *Calibration curve for estimation of azide in* ***AZP-SBA-C***

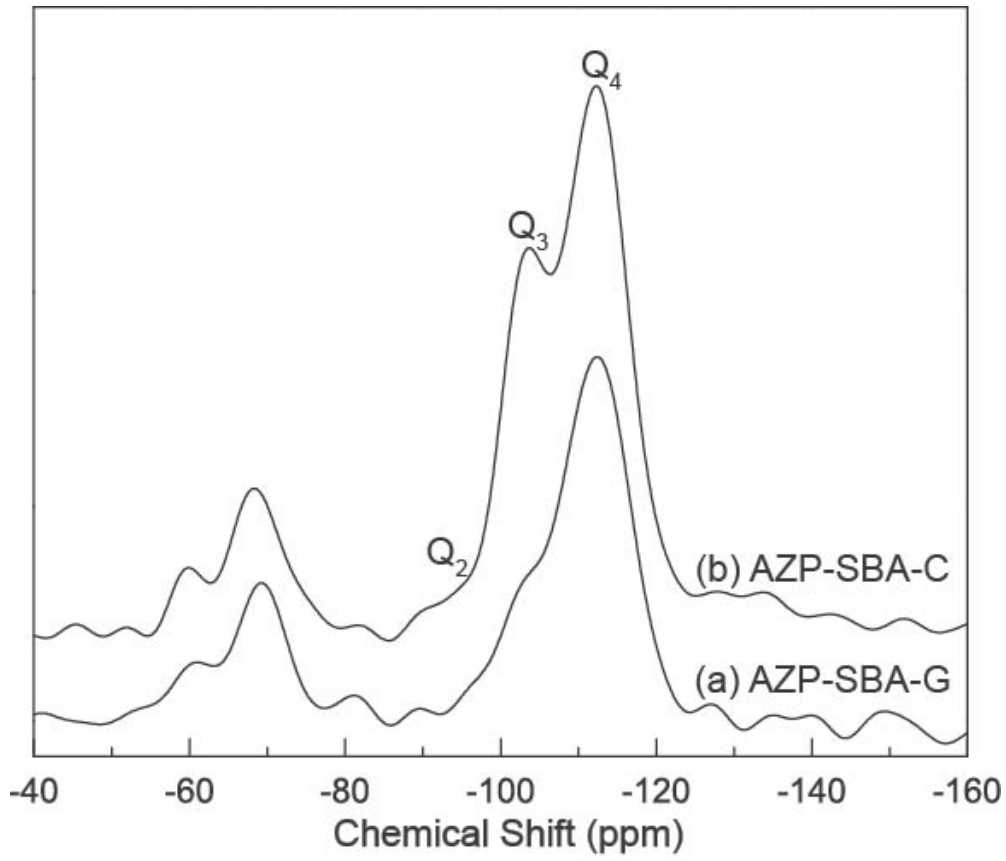

***Figure A2**: [29]Si MAS spectra of the different functionalized SBA-15 materials*

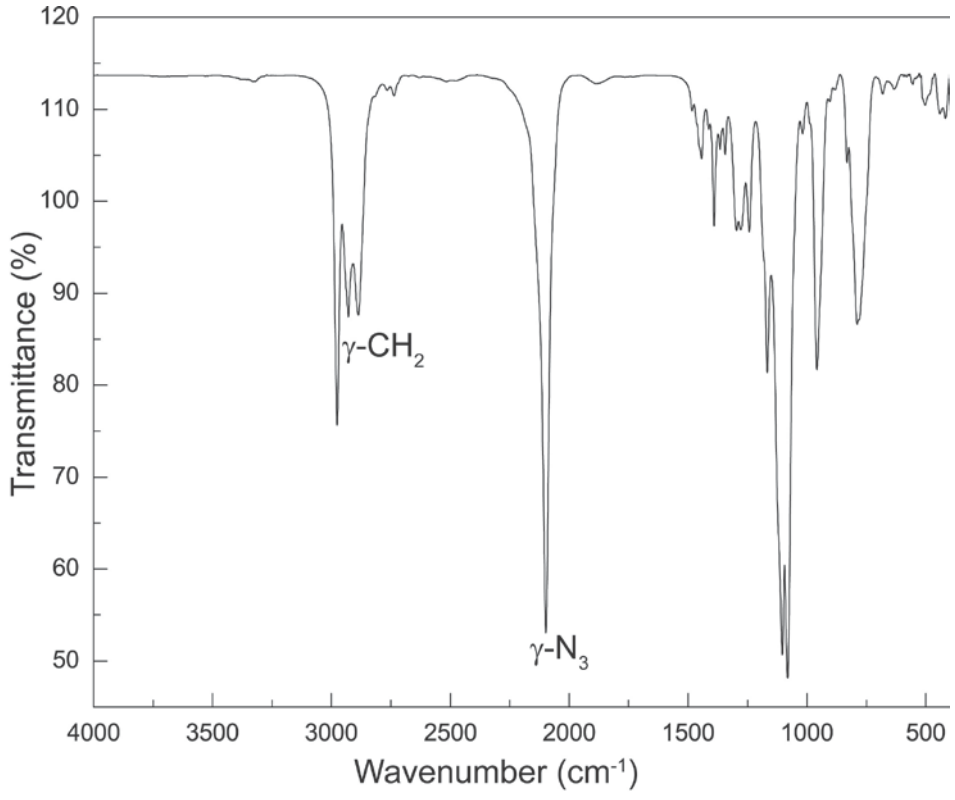

***Figure A3**:FT-IR spectrum of 3-azidopropyltriethoxysilane*

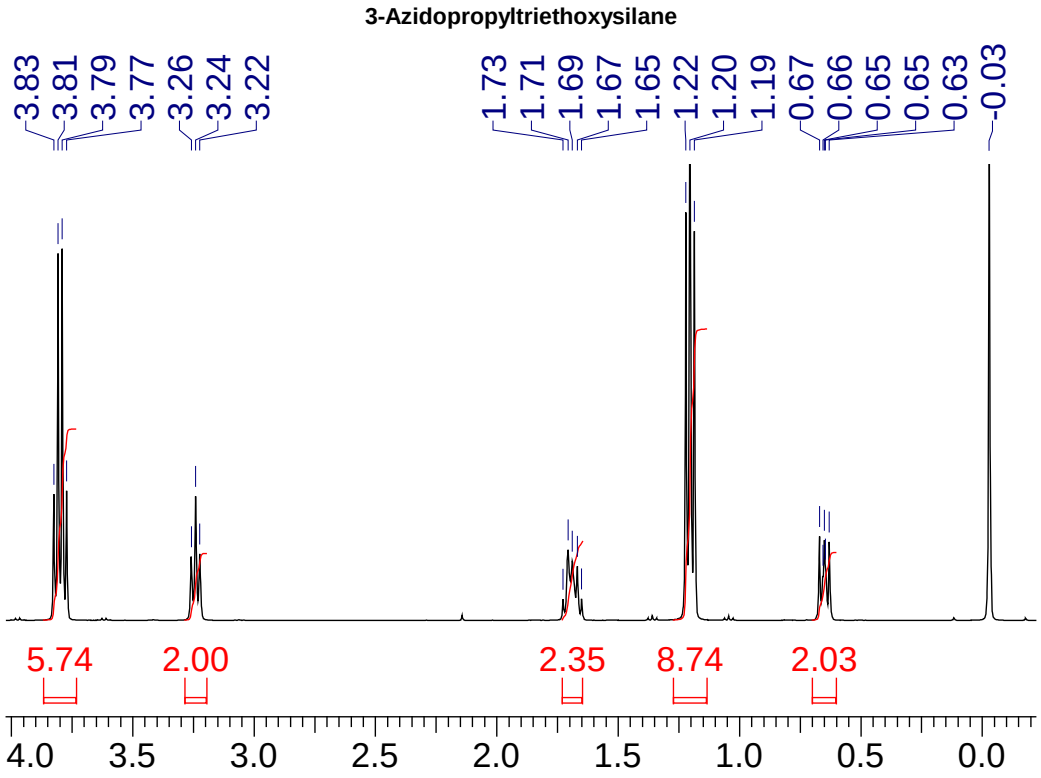

***Figure A4**:[1]H NMR spectrum of 3-azidopropyltriethoxysilane*

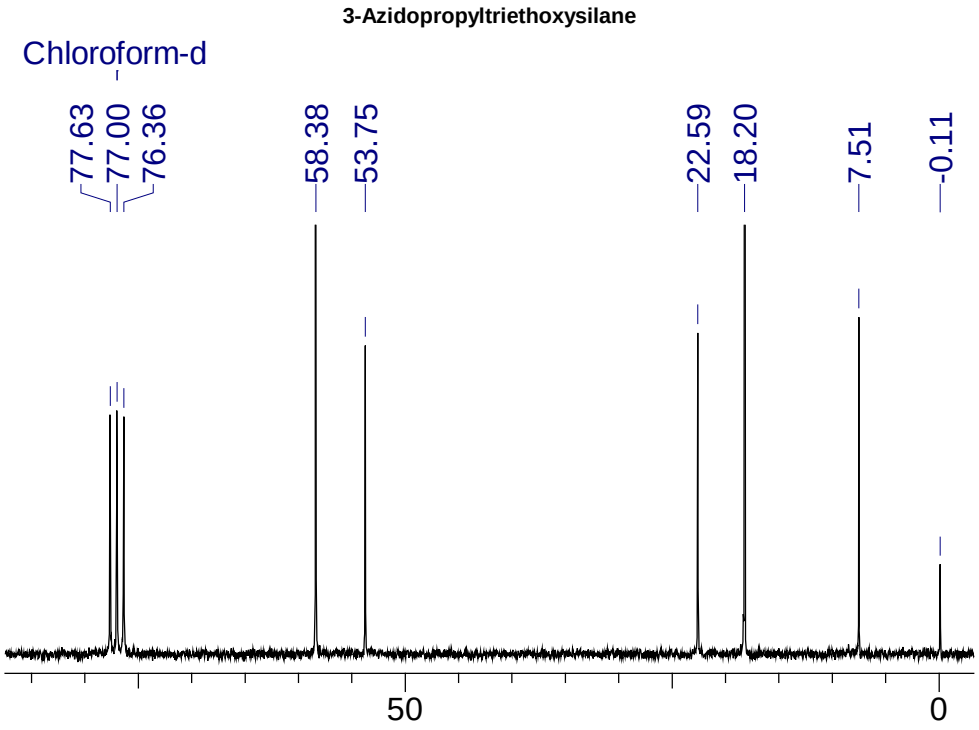

***Figure A5**:[13]C NMR spectrum of 3-azidopropyltriethoxysilane*

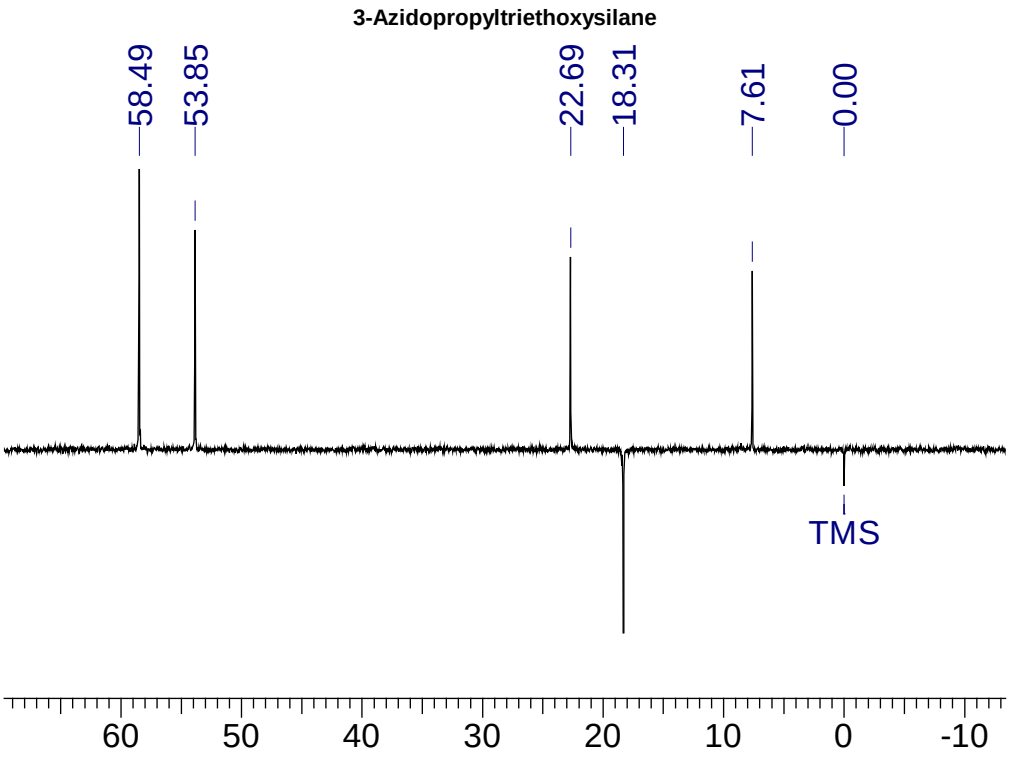

***Figure A6**:[13]C DEPT-NMR spectrum of 3-azidopropyltriethoxysilane*

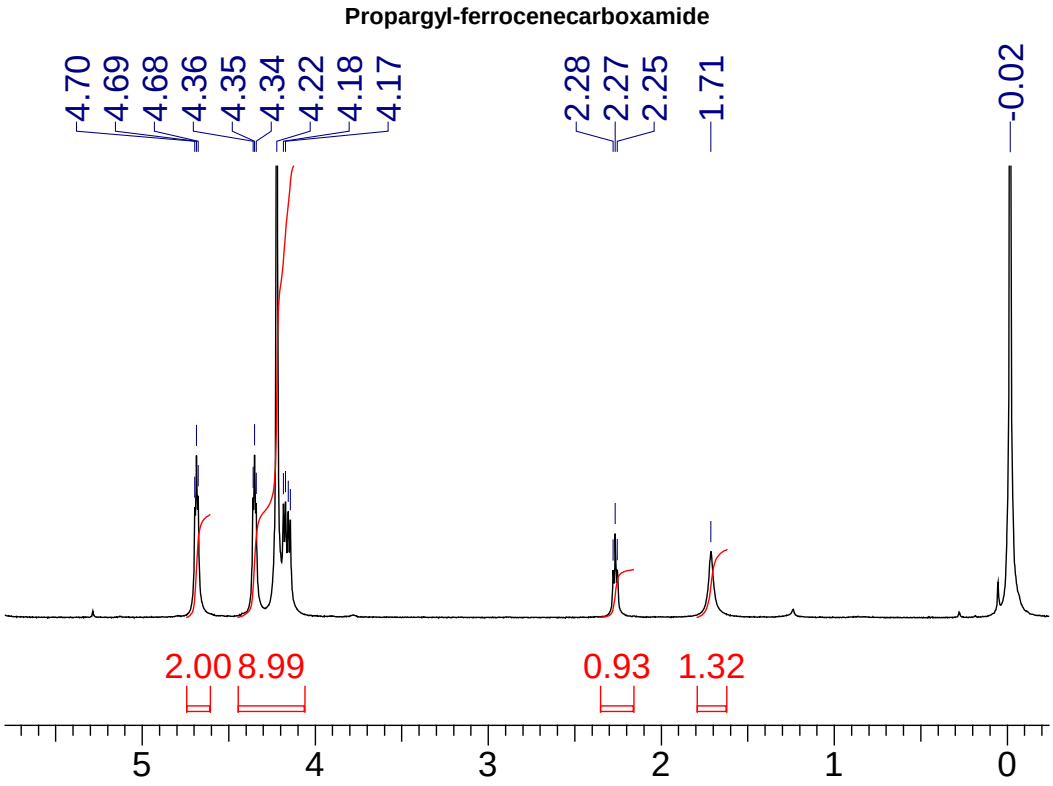

***Figure A7**:[1]H NMR spectrum of* propargyl ferrocenecarboxamide

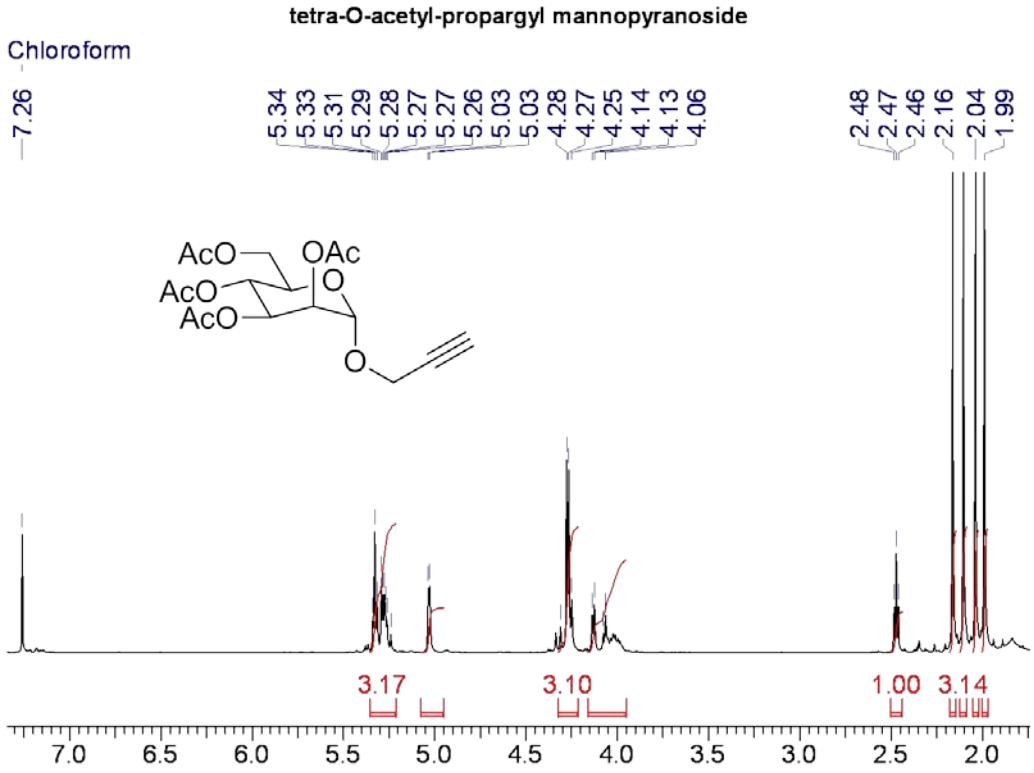

***Figure A8**:[1]H NMR spectrum of α-D(+)-propargyl mannopyranoside*

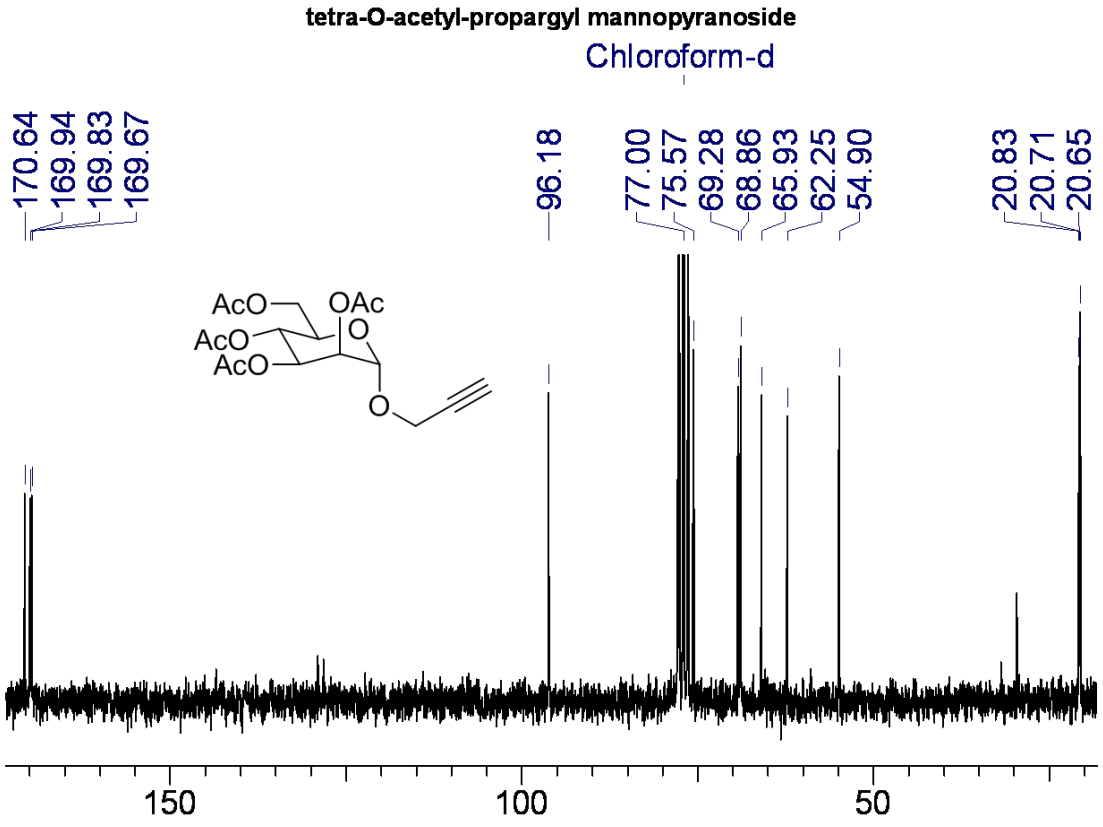

***Figure A9**:[13]C NMR spectrum of α-D(+)-propargyl mannopyranoside*

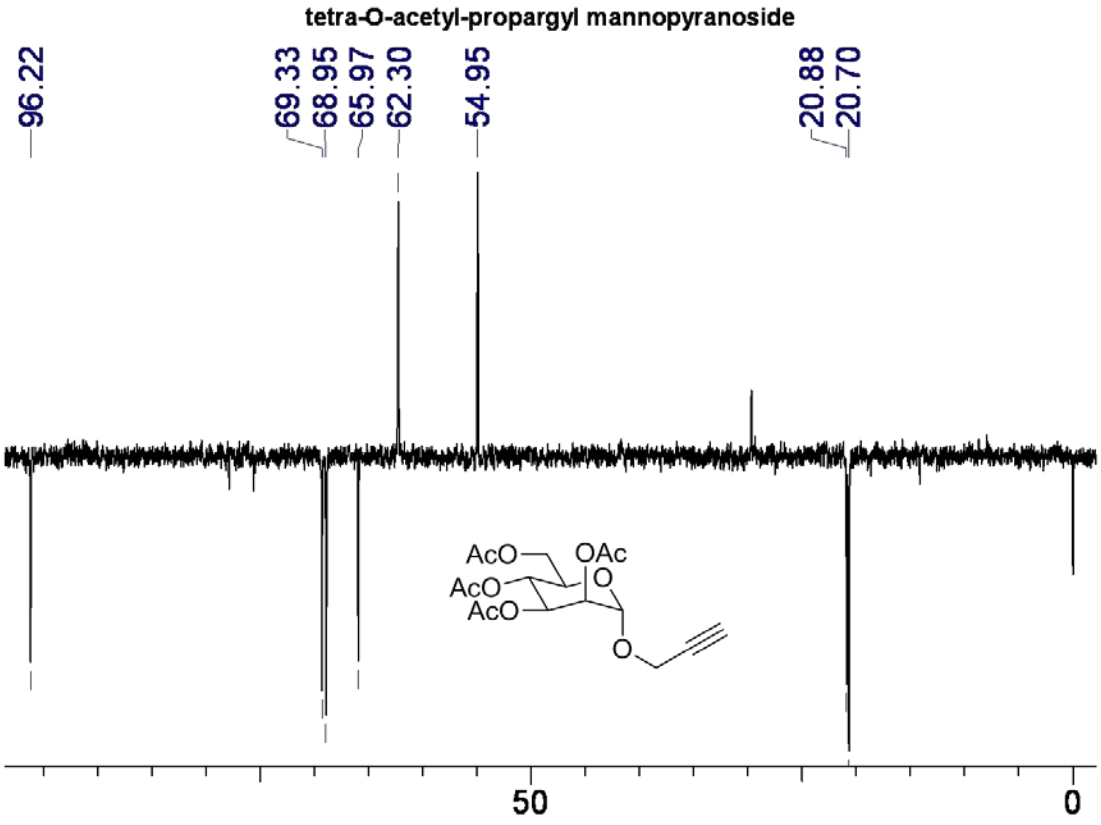

***Figure A10**:[13]C DEPT- NMR spectrum of α-D(+)-propargyl mannopyranoside*

Appendix II

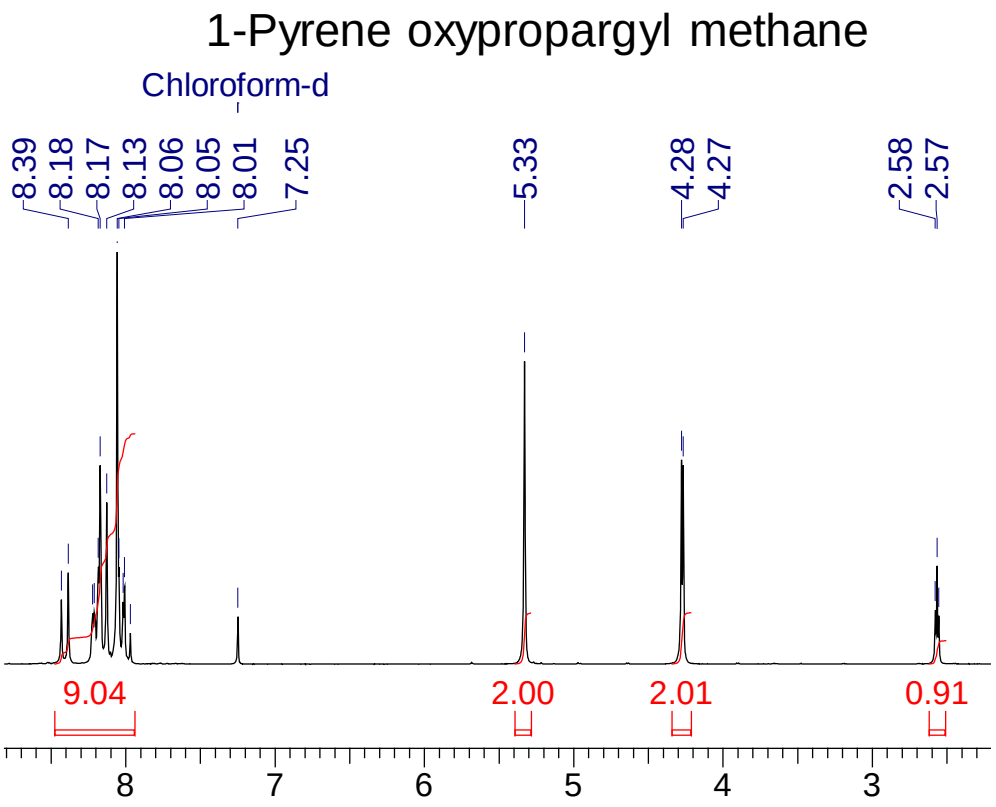
1-Pyrene oxypropargyl methane
Chloroform-d
8.39
8.18
8.17
8.13
8.06
8.05
8.01
7.25
5.33
4.28
4.27
2.58
2.57
9.04
2.00
2.01
0.91
8
7
6
5
4
3

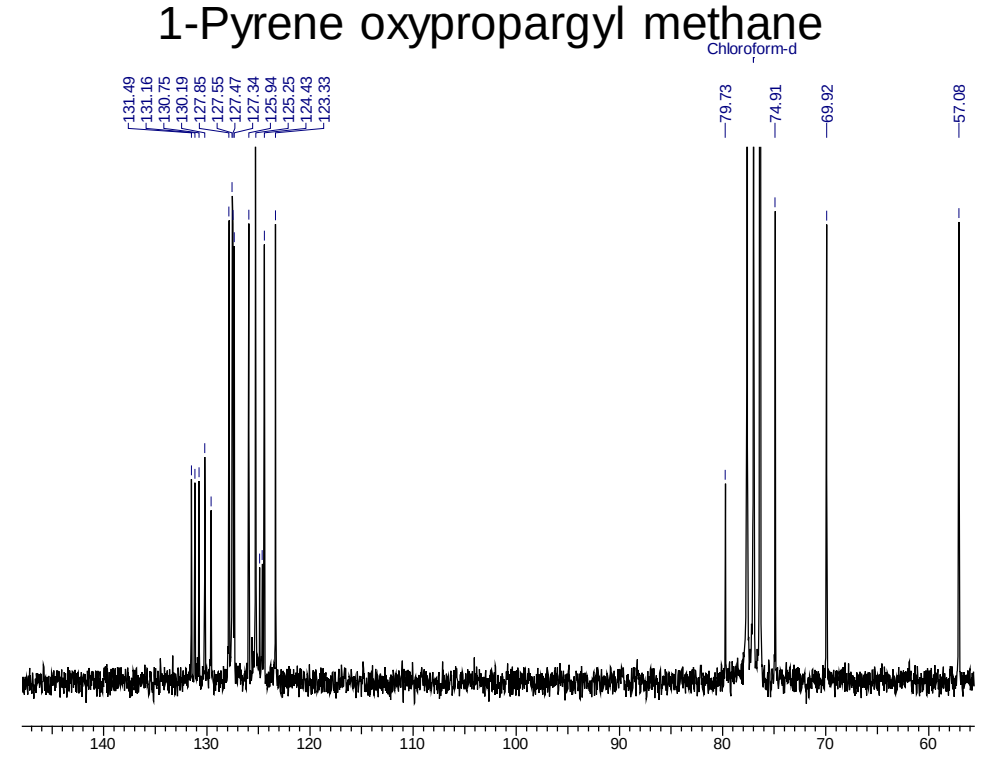
1-Pyrene oxypropargyl methane
Chloroform-d
131.49
131.16
130.75
130.19
127.85
127.55
127.47
127.34
125.94
125.25
124.43
123.33
79.73
74.91
69.92
57.08
140
130
120
110
100
90
80
70
60

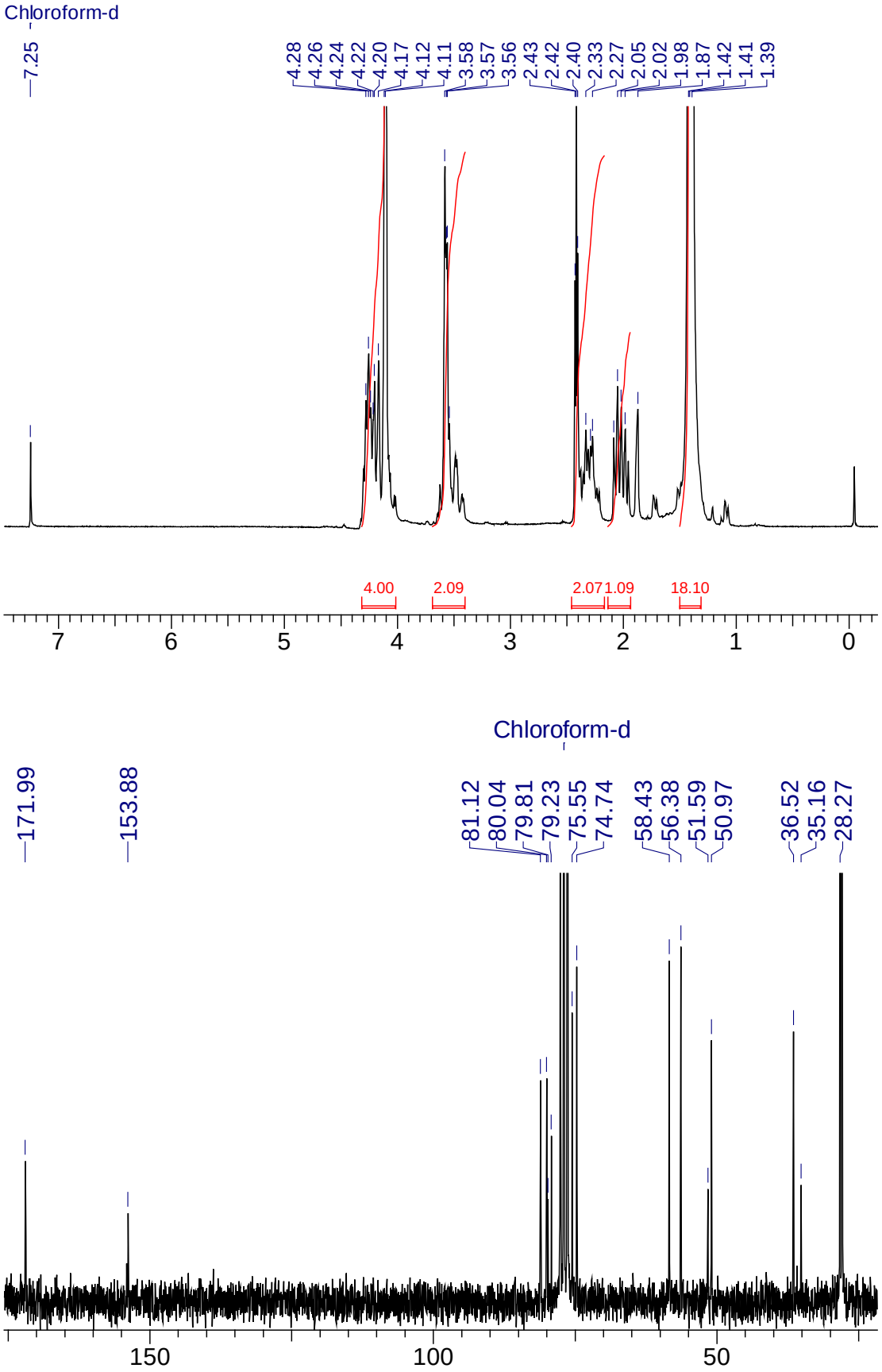
Chloroform-d
7.25
4.28
4.26
4.24
4.22
4.20
4.17
4.12
4.11
3.58
3.57
3.56
2.43
2.42
2.40
2.33
2.27
2.05
2.02
1.98
1.87
1.42
1.41
1.39
4.00
2.09
2.07
1.09
18.10
7
6
5
4
3
2
1
0
Chloroform-d
171.99
153.88
81.12
80.04
79.81
79.23
75.55
74.74
58.43
56.38
51.59
50.97
36.52
35.16
28.27
150
100
50

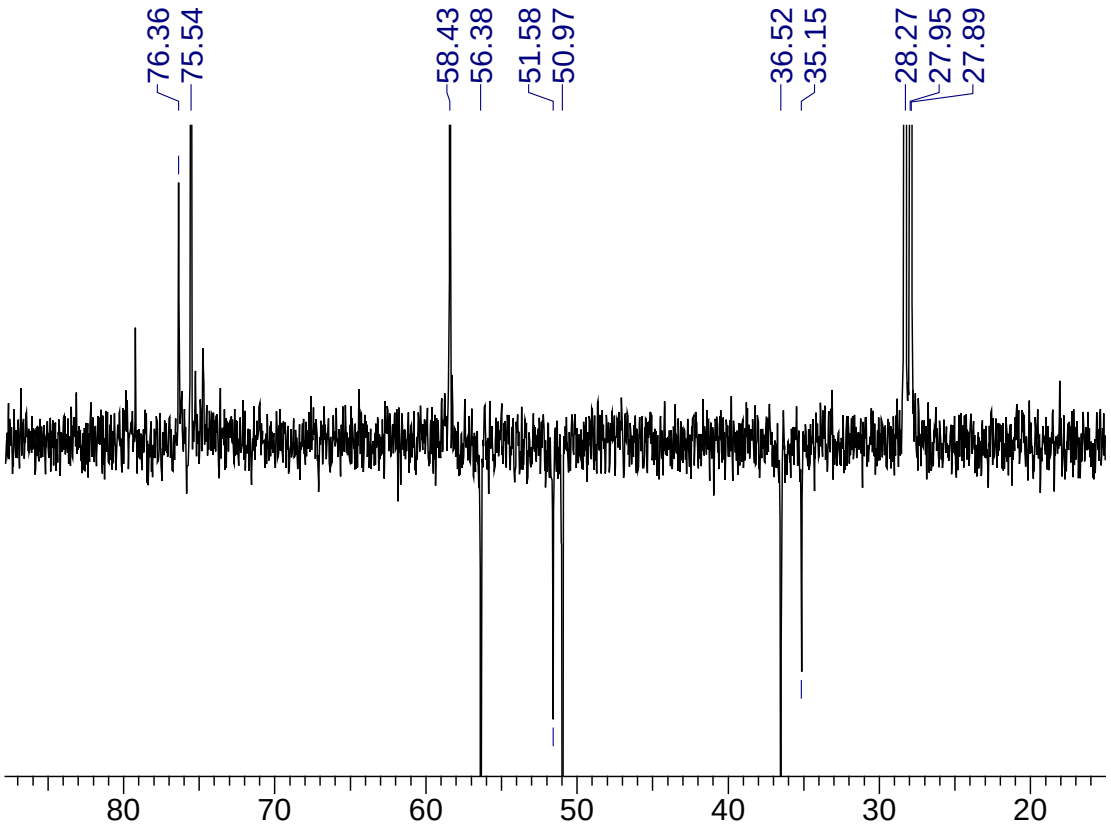
76.36
75.54
58.43
56.38
51.58
50.97
36.52
35.15
28.27
27.95
27.89
80
70
60
50
40
30
20

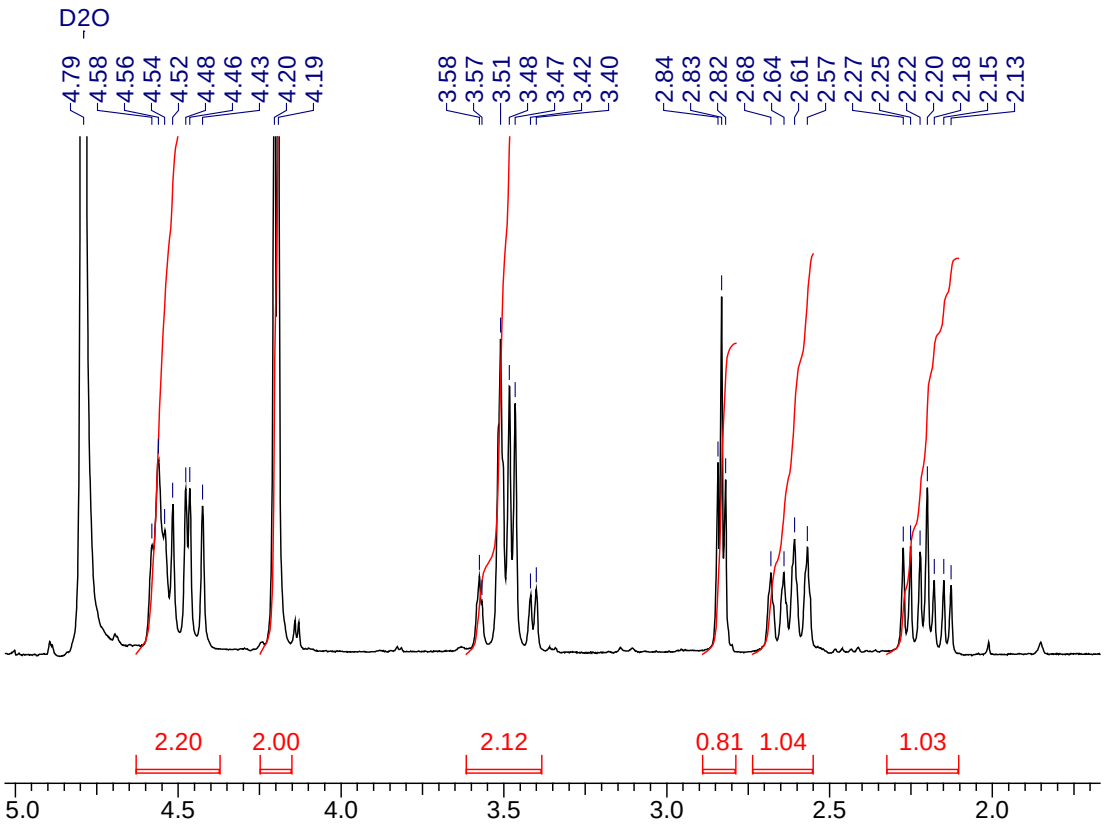
D2O
4.79
4.58
4.56
4.54
4.52
4.48
4.46
4.43
4.20
4.19
3.58
3.57
3.51
3.48
3.47
3.42
3.40
2.84
2.83
2.82
2.68
2.64
2.61
2.57
2.27
2.25
2.22
2.20
2.18
2.15
2.13
2.20
2.00
2.12
0.81
1.04
1.03
5.0
4.5
4.0
3.5
3.0
2.5
2.0

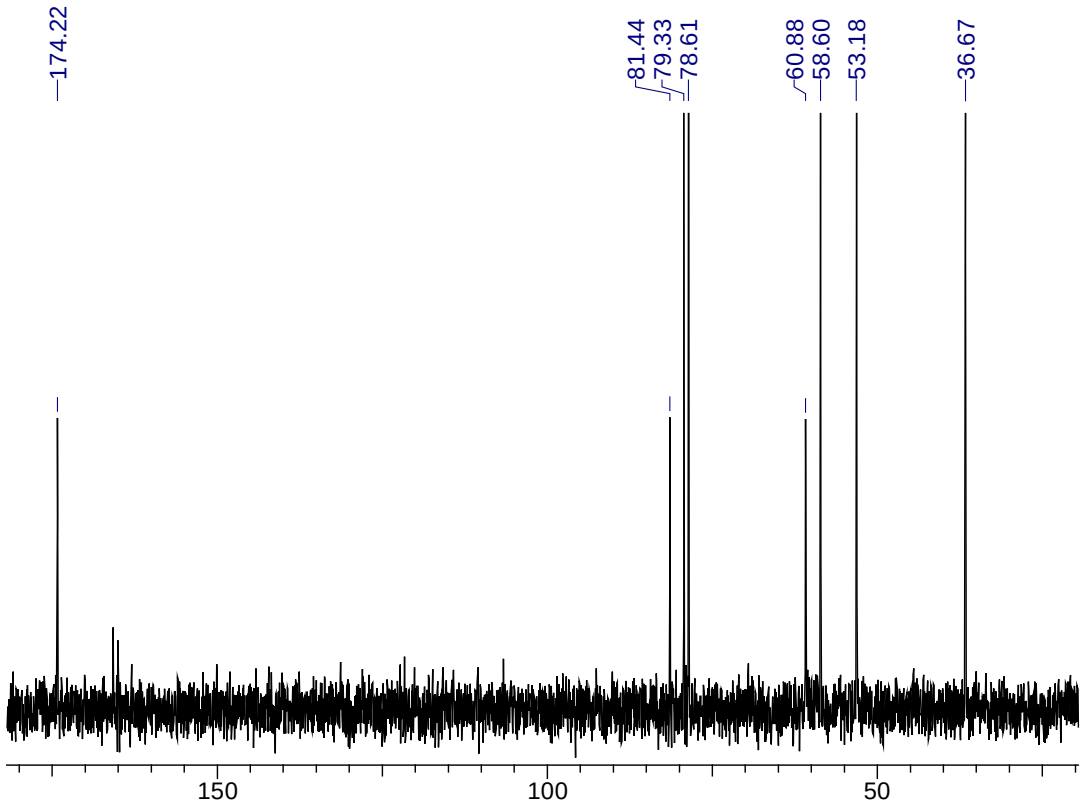
174.22
81.44
79.33
78.61
60.88
58.60
53.18
36.67
150
100
50

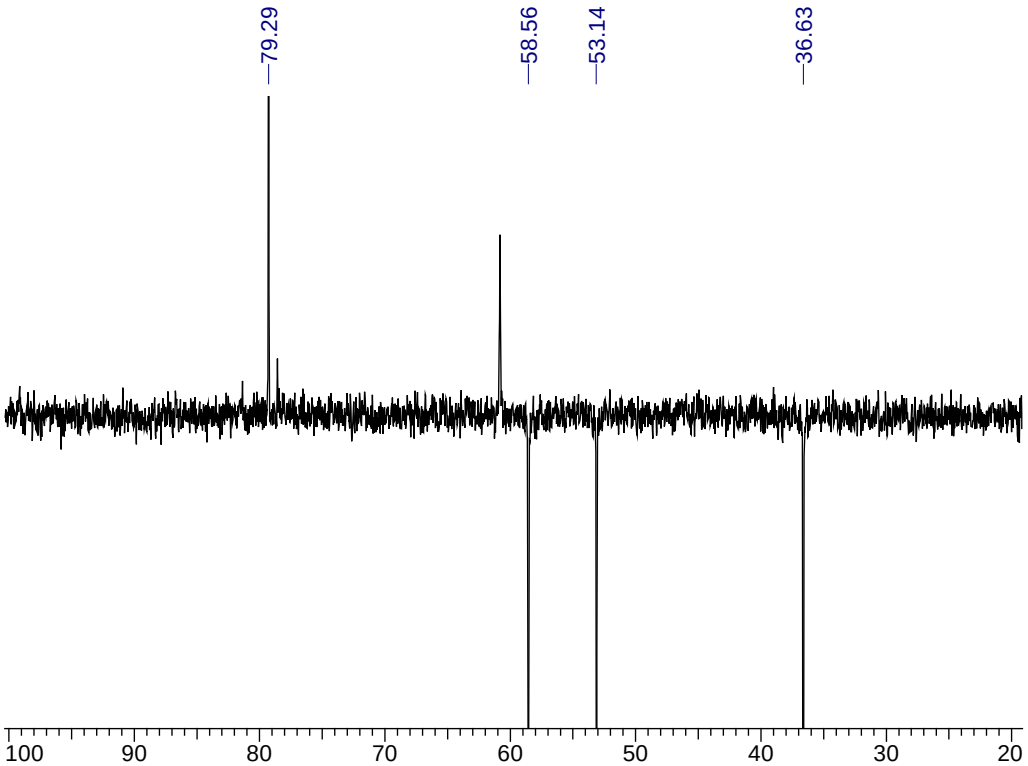
79.29
58.56
53.14
36.63
100
90
80
70
60
50
40
30
20

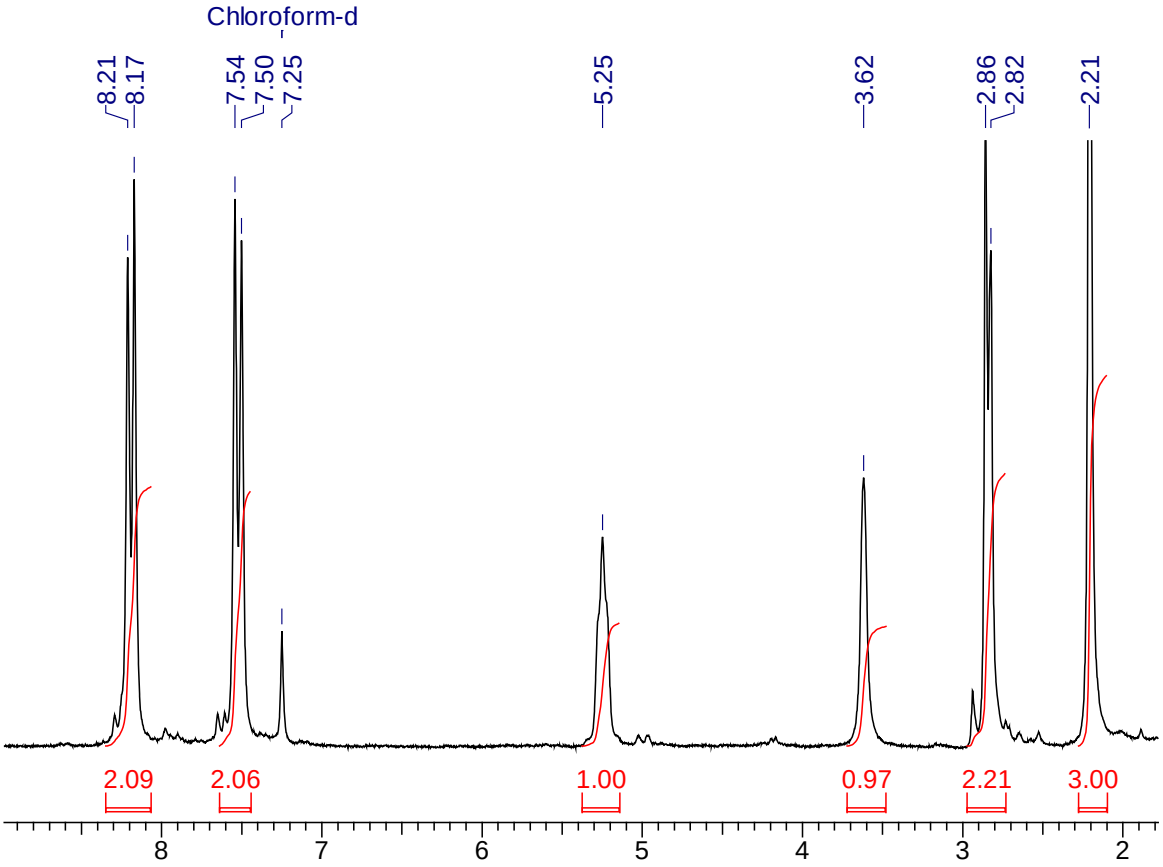
Chloroform-d
8.21
8.17
7.54
7.50
7.25
5.25
3.62
2.86
2.82
2.21
2.09
2.06
1.00
0.97
2.21
3.00
8
7
6
5
4
3
2

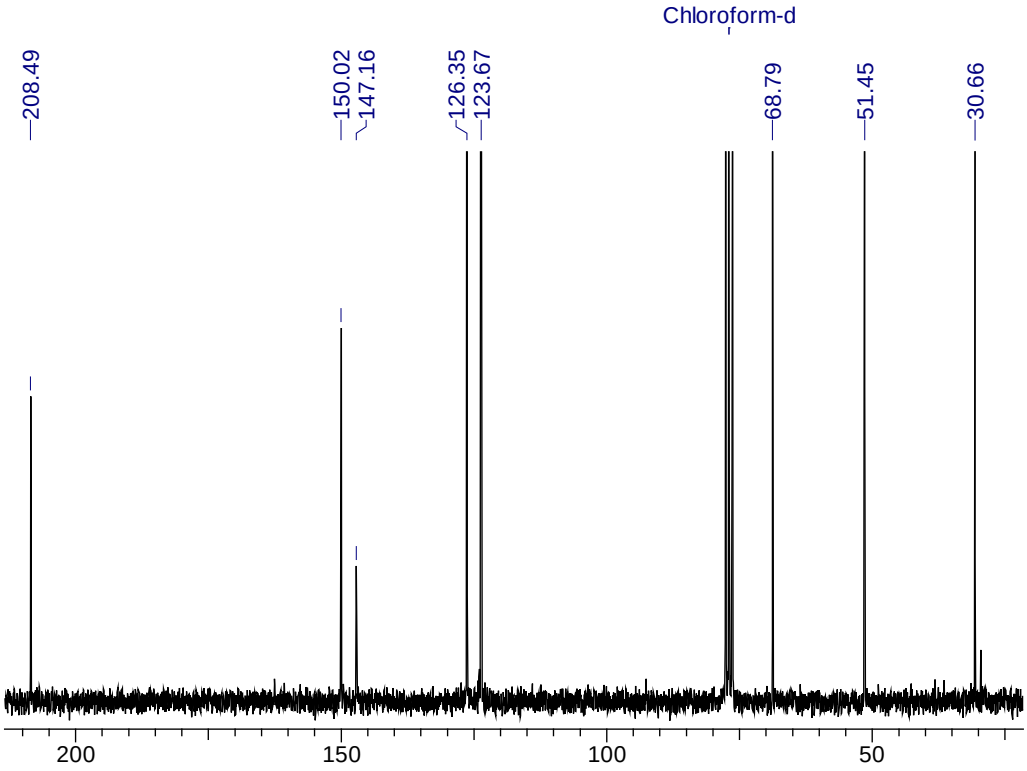
Chloroform-d
208.49
150.02
147.16
126.35
123.67
68.79
51.45
30.66
200
150
100
50

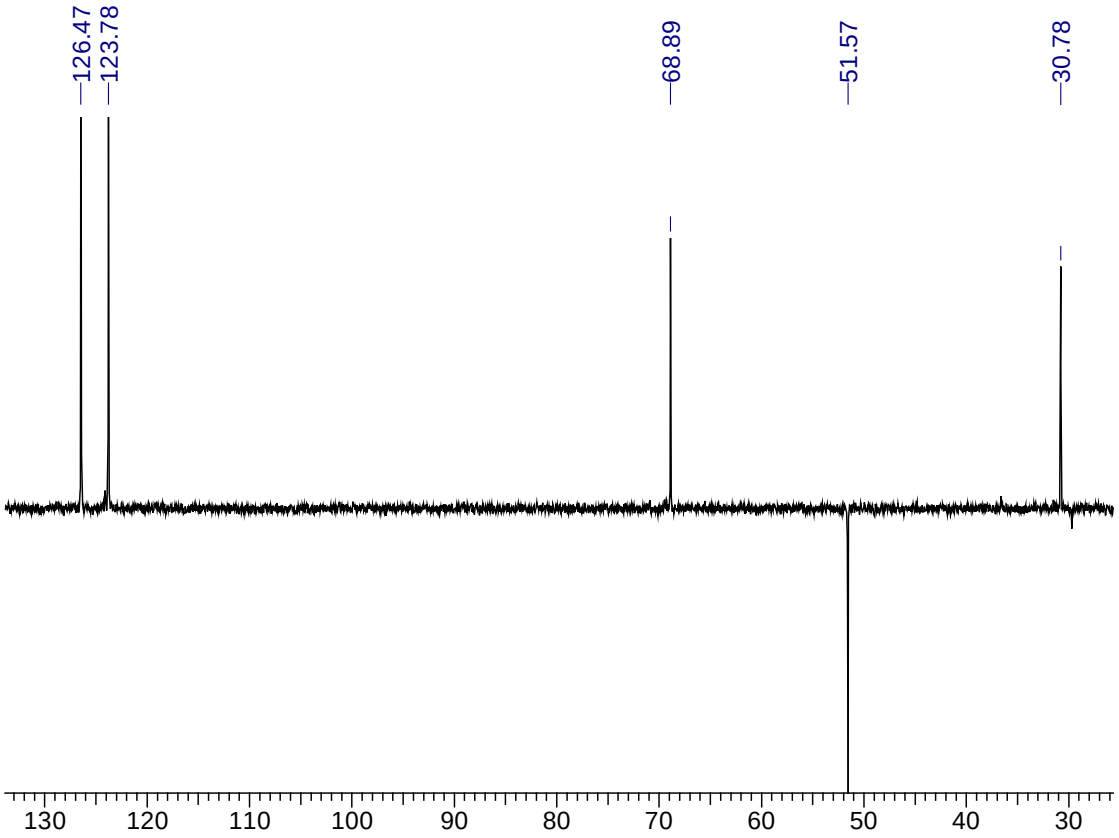
126.47
123.78
68.89
51.57
30.78
130
120
110
100
90
80
70
60
50
40
30

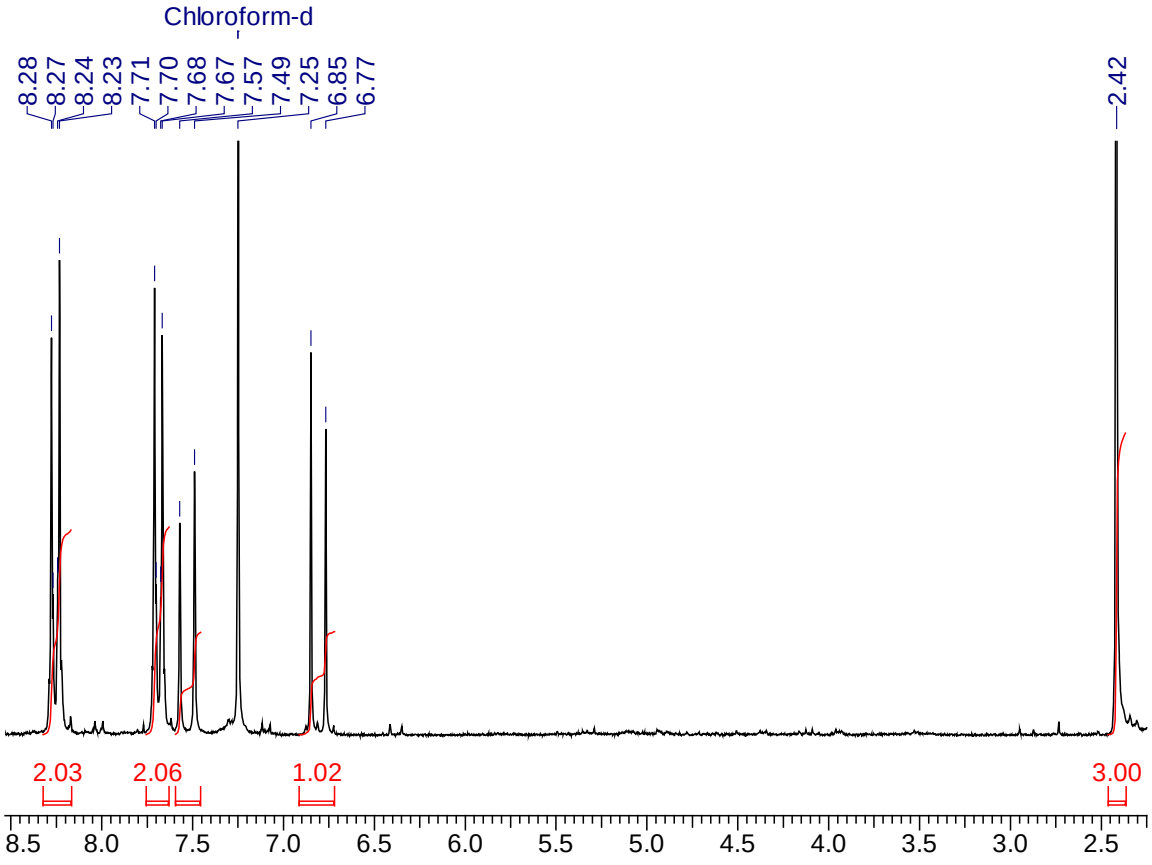
Chloroform-d
8.28
8.27
8.24
8.23
7.71
7.70
7.68
7.67
7.57
7.49
7.25
6.85
6.77
2.42
2.03
2.06
1.02
3.00
8.5
8.0
7.5
7.0
6.5
6.0
5.5
5.0
4.5
4.0
3.5
3.0
2.5

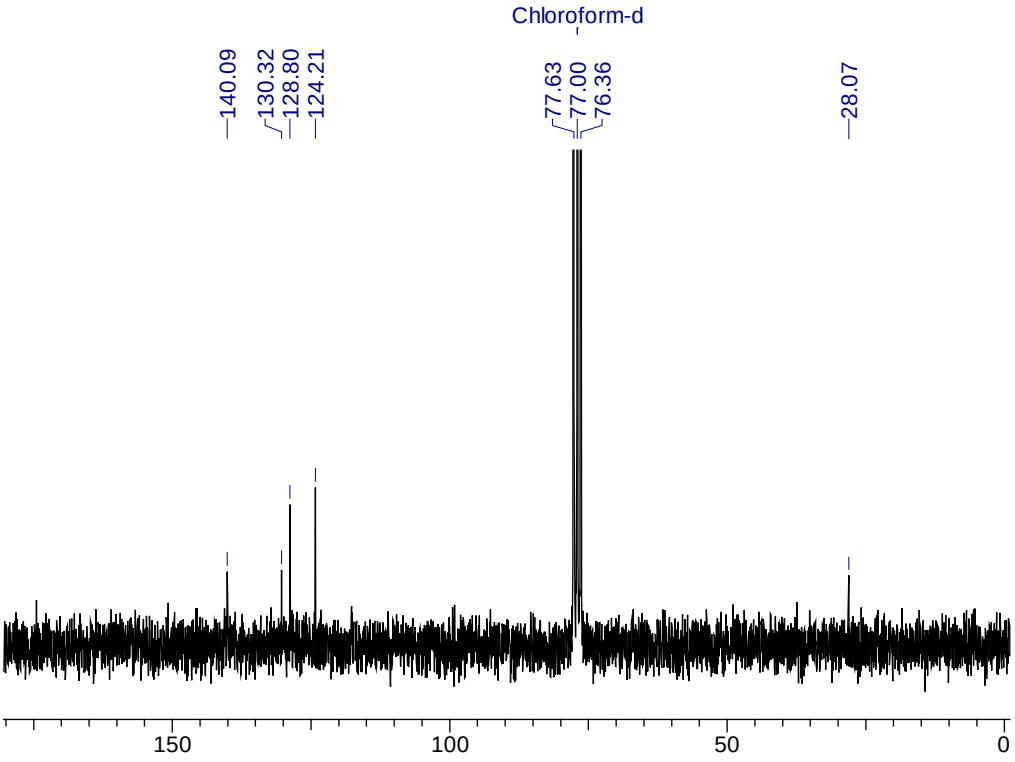
Chloroform-d
140.09
130.32
128.80
124.21
77.63
77.00
76.36
28.07
150
100
50
0

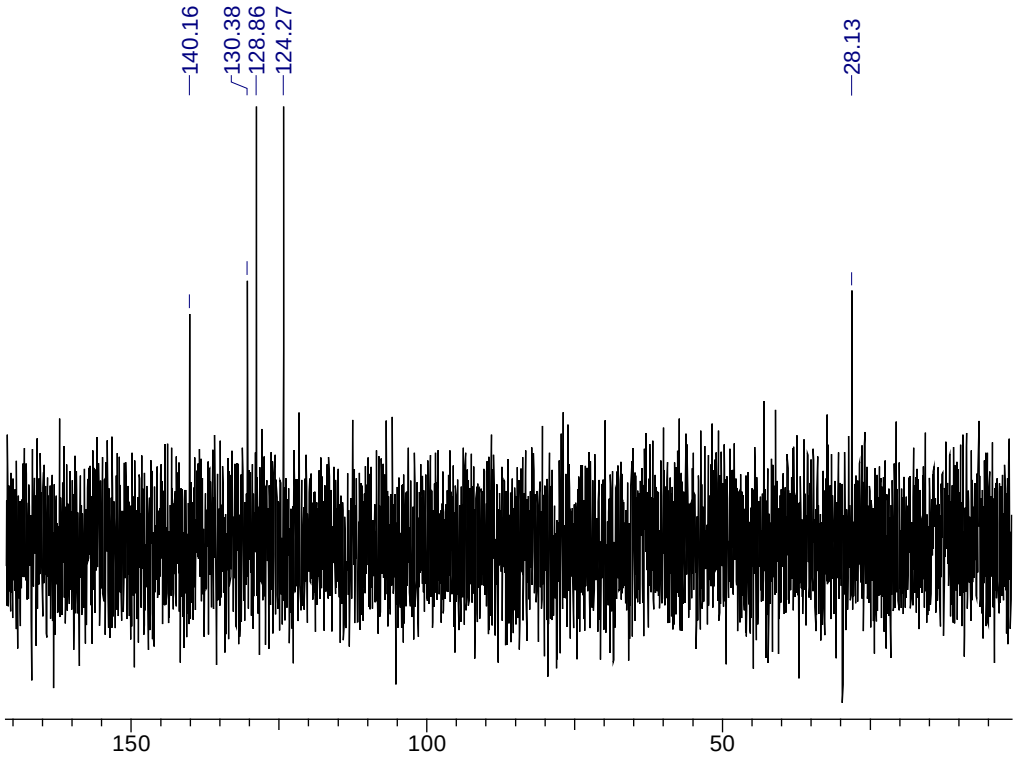
140.16
130.38
128.86
124.27
28.13
150
100
50

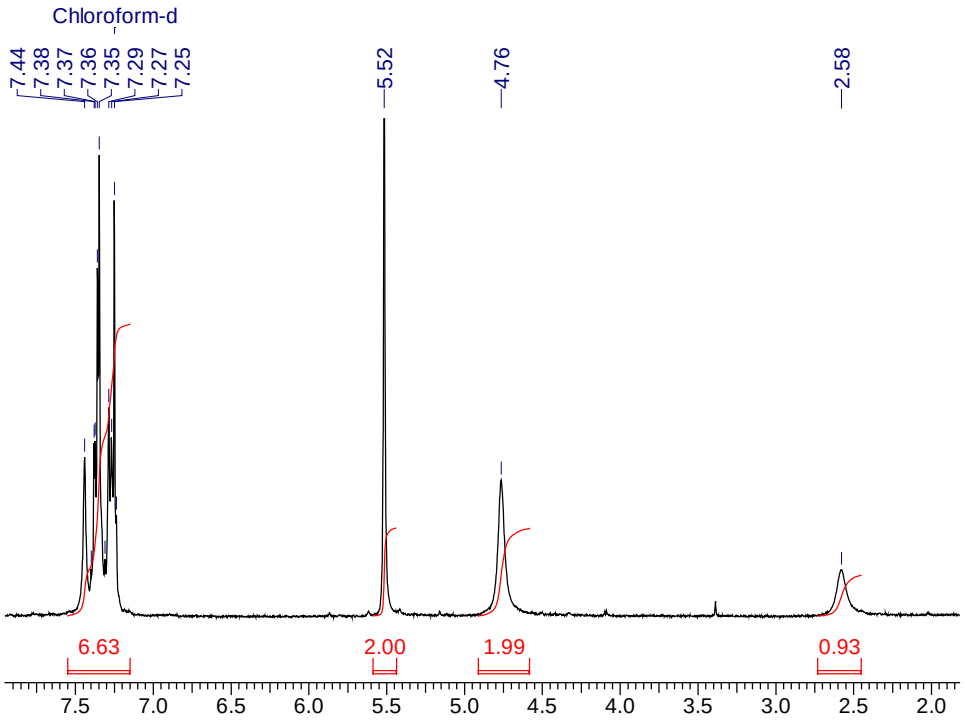
Chloroform-d
7.44
7.38
7.37
7.36
7.35
7.29
7.27
7.25
5.52
4.76
2.58
6.63
2.00
1.99
0.93
7.5
7.0
6.5
6.0
5.5
5.0
4.5
4.0
3.5
3.0
2.5
2.0

LC-MS, Profile (A): Standard runs

Standard runs of p-nitrobenzaldehyde (**5**) and aldol product (**7**)

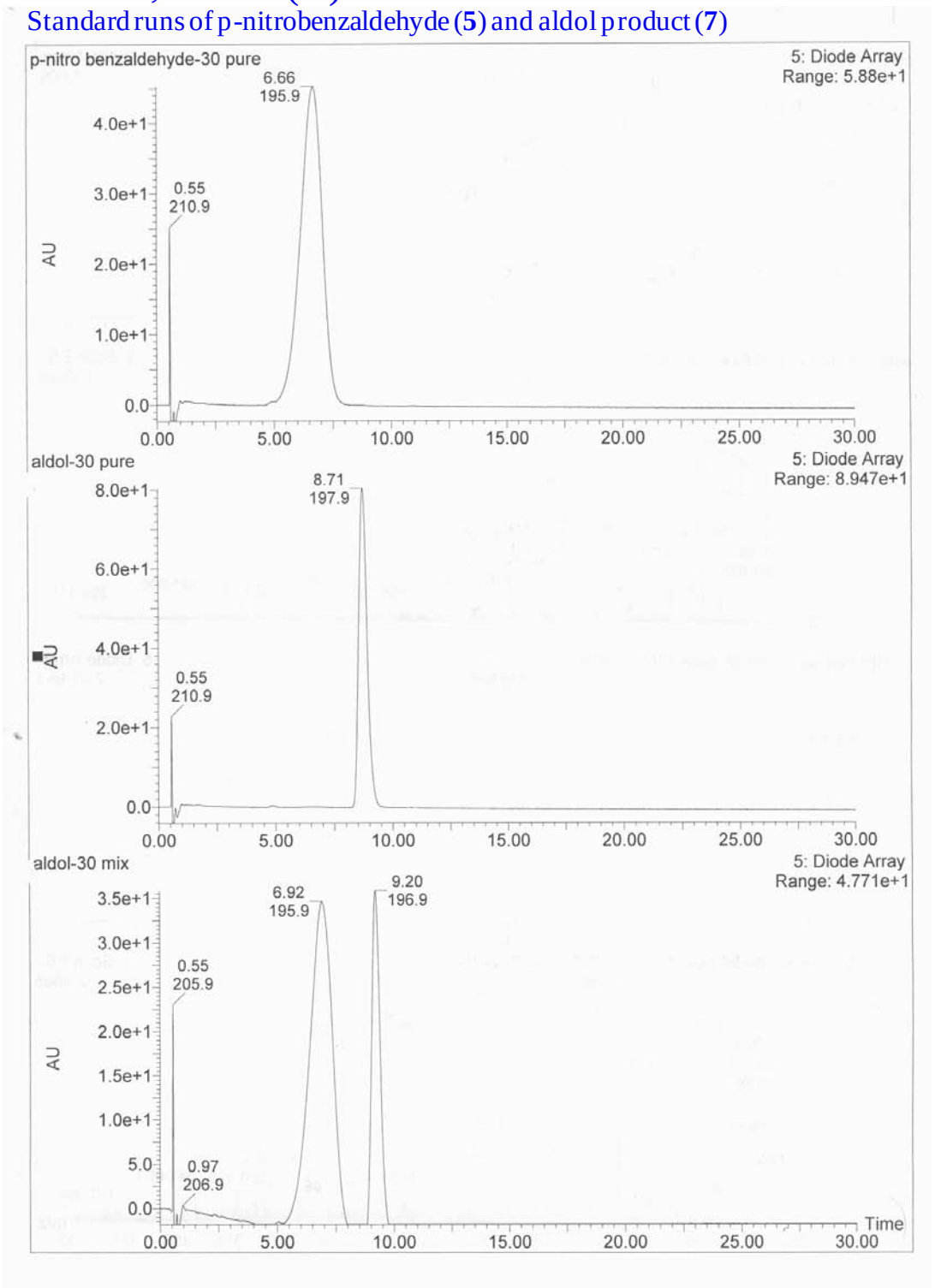

LC-MS Profile (B): Aldol reactions

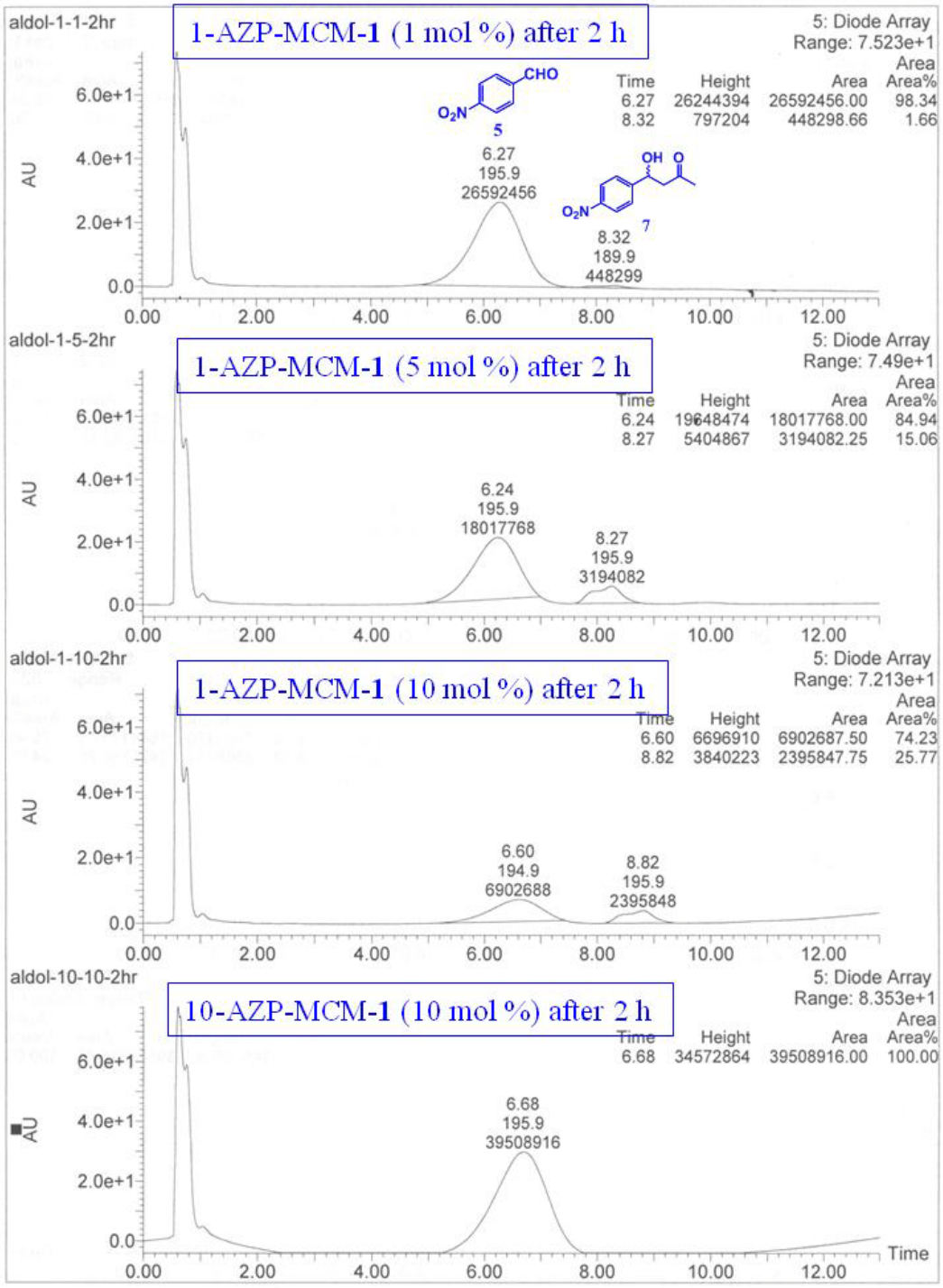

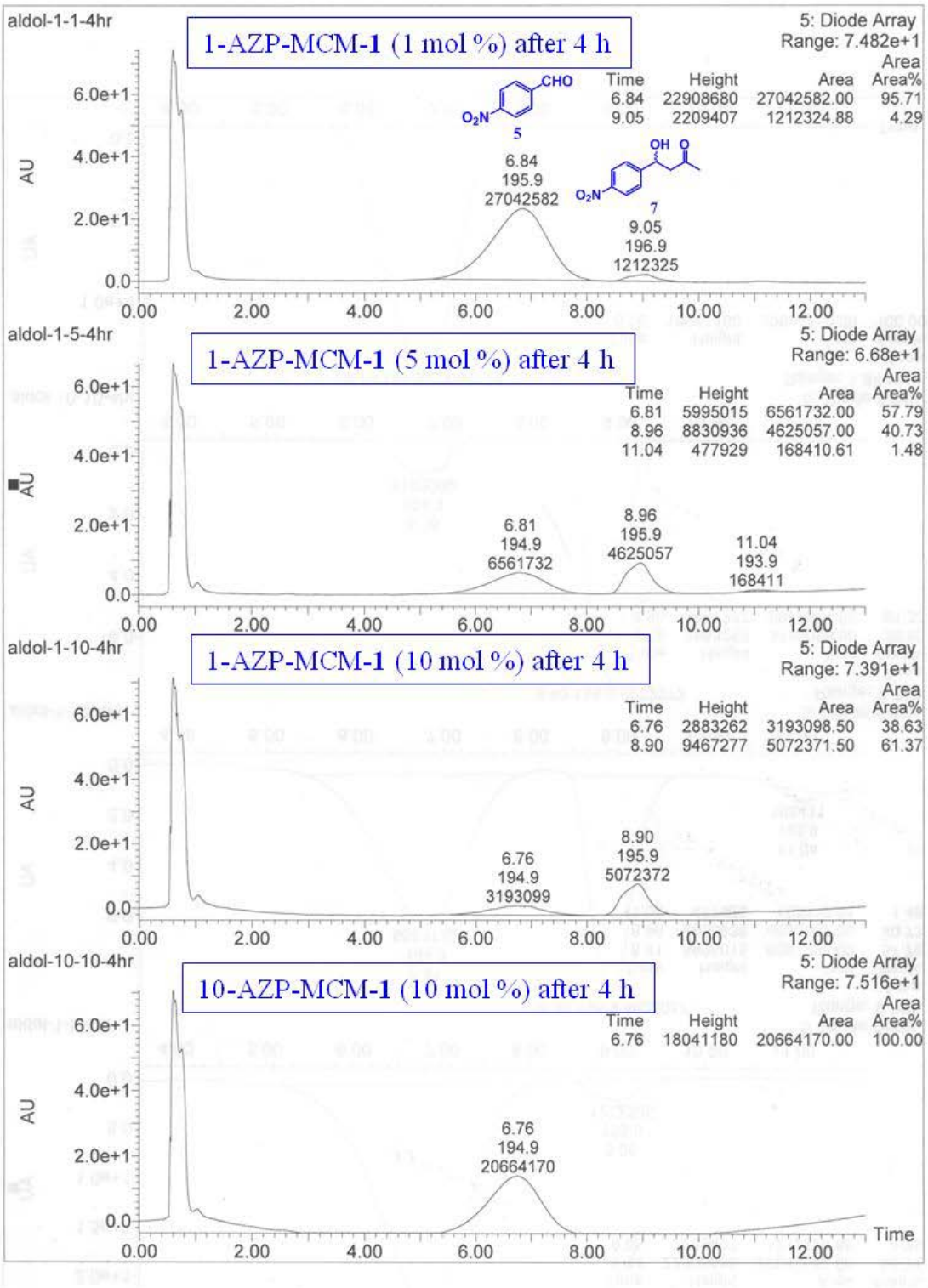
aldol-1-1-4hr
1-AZP-MCM-1 (1 mol %) after 4 h
5: Diode Array
Range: 7.482e+1
Time Height Area Area%
6.84 22908680 27042582.00 95.71
9.05 2209407 1212324.88 4.29
CHO
O2N
5
OH O
O2N
7
6.84
195.9
27042582
9.05
196.9
1212325
aldol-1-5-4hr
1-AZP-MCM-1 (5 mol %) after 4 h
5: Diode Array
Range: 6.68e+1
Time Height Area Area%
6.81 5995015 6561732.00 57.79
8.96 8830936 4625057.00 40.73
11.04 477929 168410.61 1.48
6.81
194.9
6561732
8.96
195.9
4625057
11.04
193.9
168411
aldol-1-10-4hr
1-AZP-MCM-1 (10 mol %) after 4 h
5: Diode Array
Range: 7.391e+1
Time Height Area Area%
6.76 2883262 3193098.50 38.63
8.90 9467277 5072371.50 61.37
6.76
194.9
3193099
8.90
195.9
5072372
aldol-10-10-4hr
10-AZP-MCM-1 (10 mol %) after 4 h
5: Diode Array
Range: 7.516e+1
Time Height Area Area%
6.76 18041180 20664170.00 100.00
6.76
194.9
20664170
AU
Time
6.0e+1
4.0e+1
2.0e+1
0.0
0.00
2.00
4.00
6.00
8.00
10.00
12.00

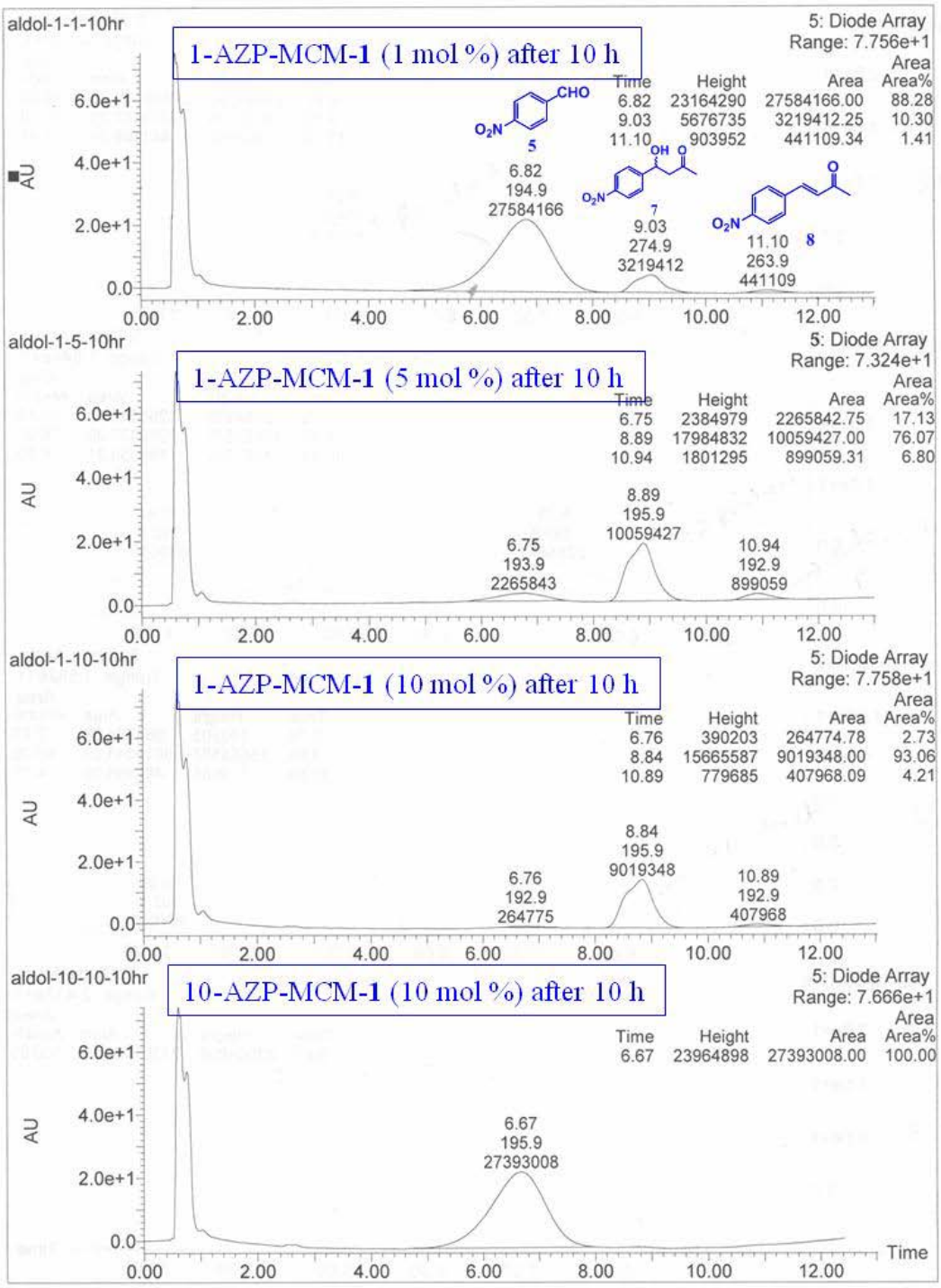
aldol-1-1-10hr
1-AZP-MCM-1 (1 mol %) after 10 h
5: Diode Array
Range: 7.756e+1
Time Height Area Area%
6.82 23164290 27584166.00 88.28
9.03 5676735 3219412.25 10.30
11.10 903952 441109.34 1.41
6.82
194.9
27584166
9.03
274.9
3219412
11.10
263.9
441109
aldol-1-5-10hr
1-AZP-MCM-1 (5 mol %) after 10 h
5: Diode Array
Range: 7.324e+1
Time Height Area Area%
6.75 2384979 2265842.75 17.13
8.89 17984832 10059427.00 76.07
10.94 1801295 899059.31 6.80
8.89
195.9
10059427
6.75
193.9
2265843
10.94
192.9
899059
aldol-1-10-10hr
1-AZP-MCM-1 (10 mol %) after 10 h
5: Diode Array
Range: 7.758e+1
Time Height Area Area%
6.76 390203 264774.78 2.73
8.84 15665587 9019348.00 93.06
10.89 779685 407968.09 4.21
8.84
195.9
9019348
6.76
192.9
264775
10.89
192.9
407968
aldol-10-10-10hr
10-AZP-MCM-1 (10 mol %) after 10 h
5: Diode Array
Range: 7.666e+1
Time Height Area Area%
6.67 23964898 27393008.00 100.00
6.67
195.9
27393008
AU
Time
0.0
2.0e+1
4.0e+1
6.0e+1
0.00
2.00
4.00
6.00
8.00
10.00
12.00

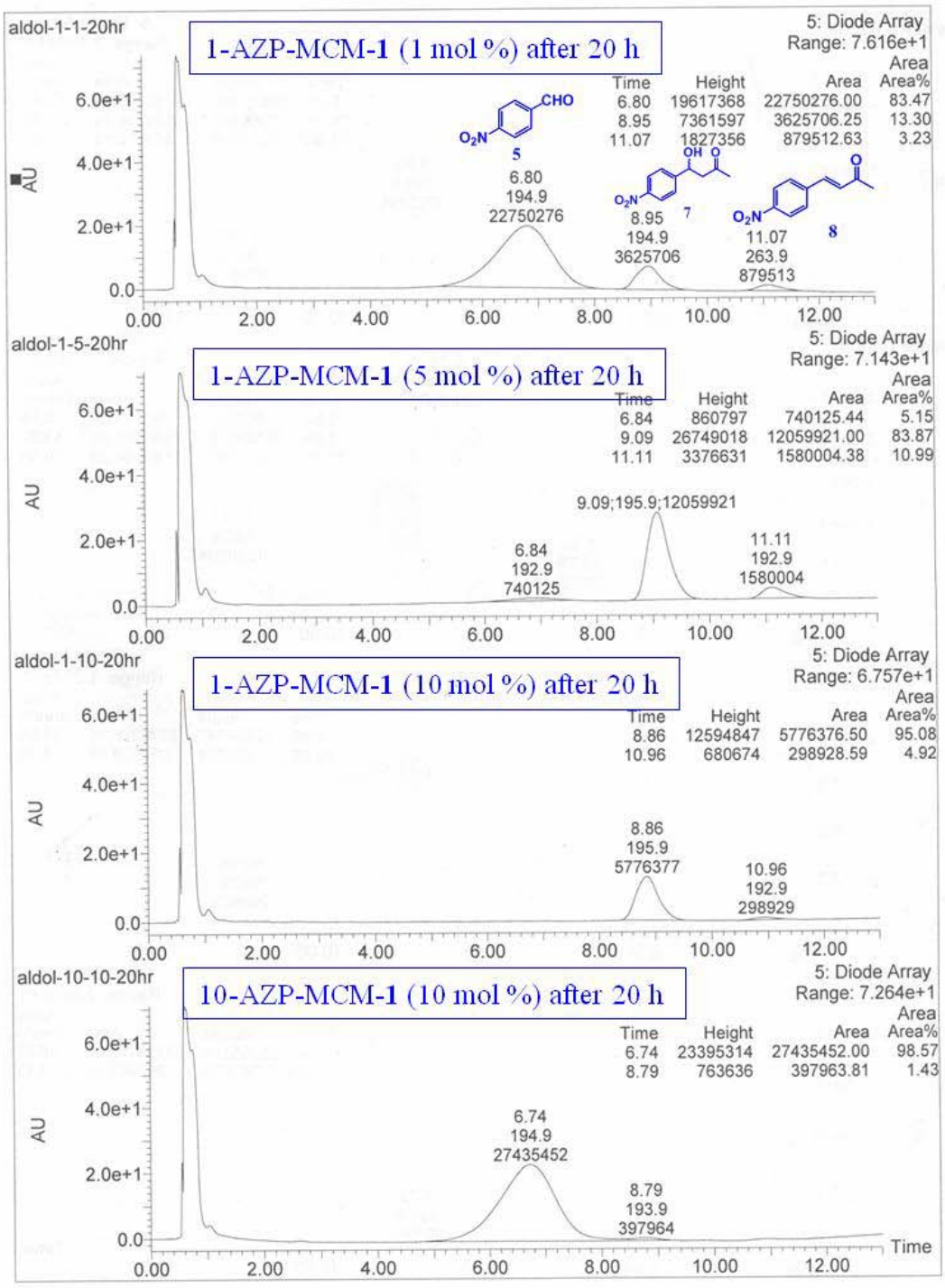
aldol-1-1-20hr
1-AZP-MCM-1 (1 mol %) after 20 h
5: Diode Array
Range: 7.616e+1
Time Height Area Area%
6.80 19617368 22750276.00 83.47
8.95 7361597 3625706.25 13.30
11.07 1827356 879512.63 3.23
6.80
194.9
22750276
8.95
194.9
3625706
11.07
263.9
879513
aldol-1-5-20hr
1-AZP-MCM-1 (5 mol %) after 20 h
5: Diode Array
Range: 7.143e+1
Time Height Area Area%
6.84 860797 740125.44 5.15
9.09 26749018 12059921.00 83.87
11.11 3376631 1580004.38 10.99
9.09;195.9;12059921
6.84
192.9
740125
11.11
192.9
1580004
aldol-1-10-20hr
1-AZP-MCM-1 (10 mol %) after 20 h
5: Diode Array
Range: 6.757e+1
Time Height Area Area%
8.86 12594847 5776376.50 95.08
10.96 680674 298928.59 4.92
8.86
195.9
5776377
10.96
192.9
298929
aldol-10-10-20hr
10-AZP-MCM-1 (10 mol %) after 20 h
5: Diode Array
Range: 7.264e+1
Time Height Area Area%
6.74 23395314 27435452.00 98.57
8.79 763636 397963.81 1.43
6.74
194.9
27435452
8.79
193.9
397964
AU
Time

LC-MS Profile (C): Aldol reactions (1st cycle)

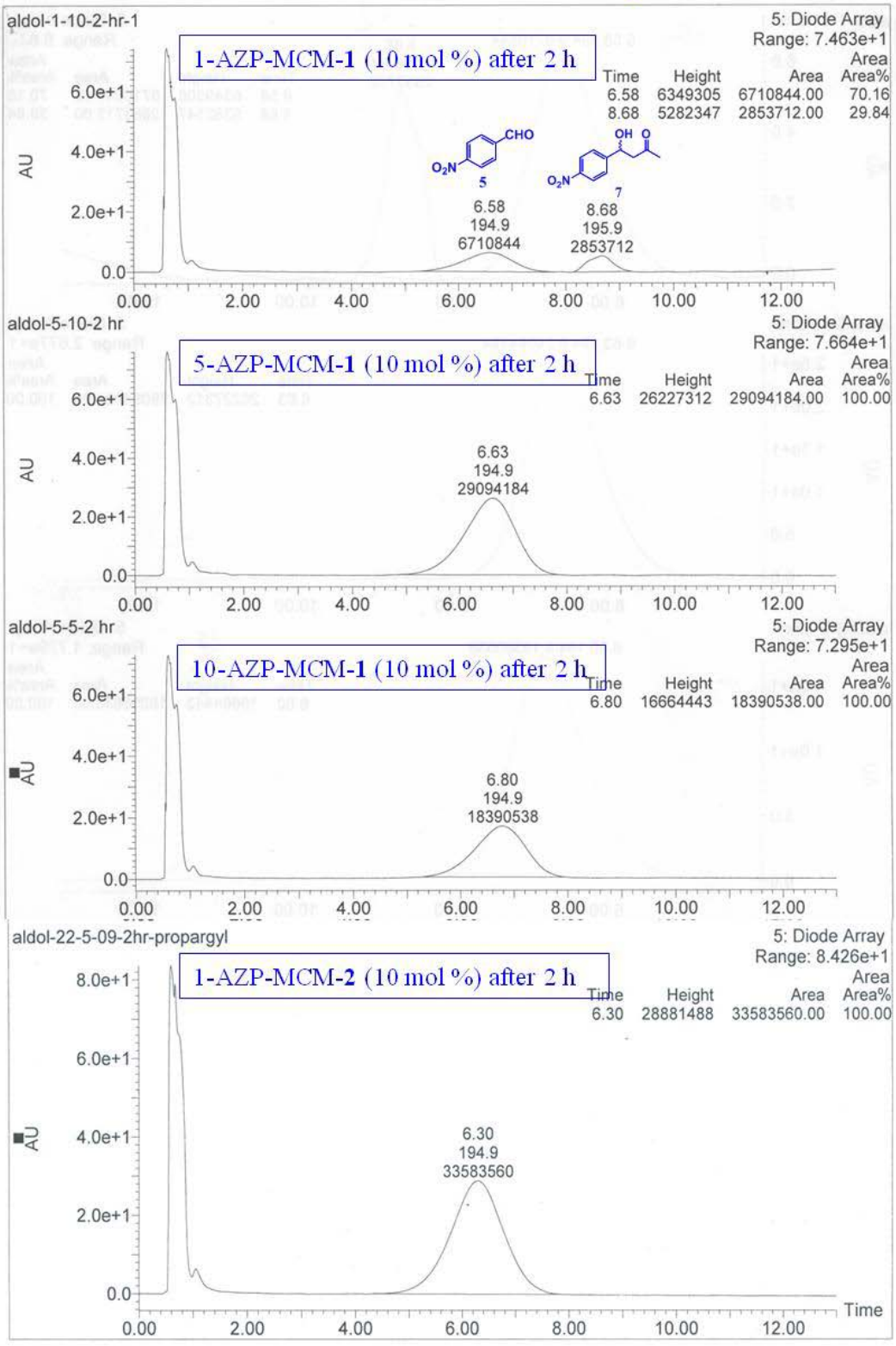

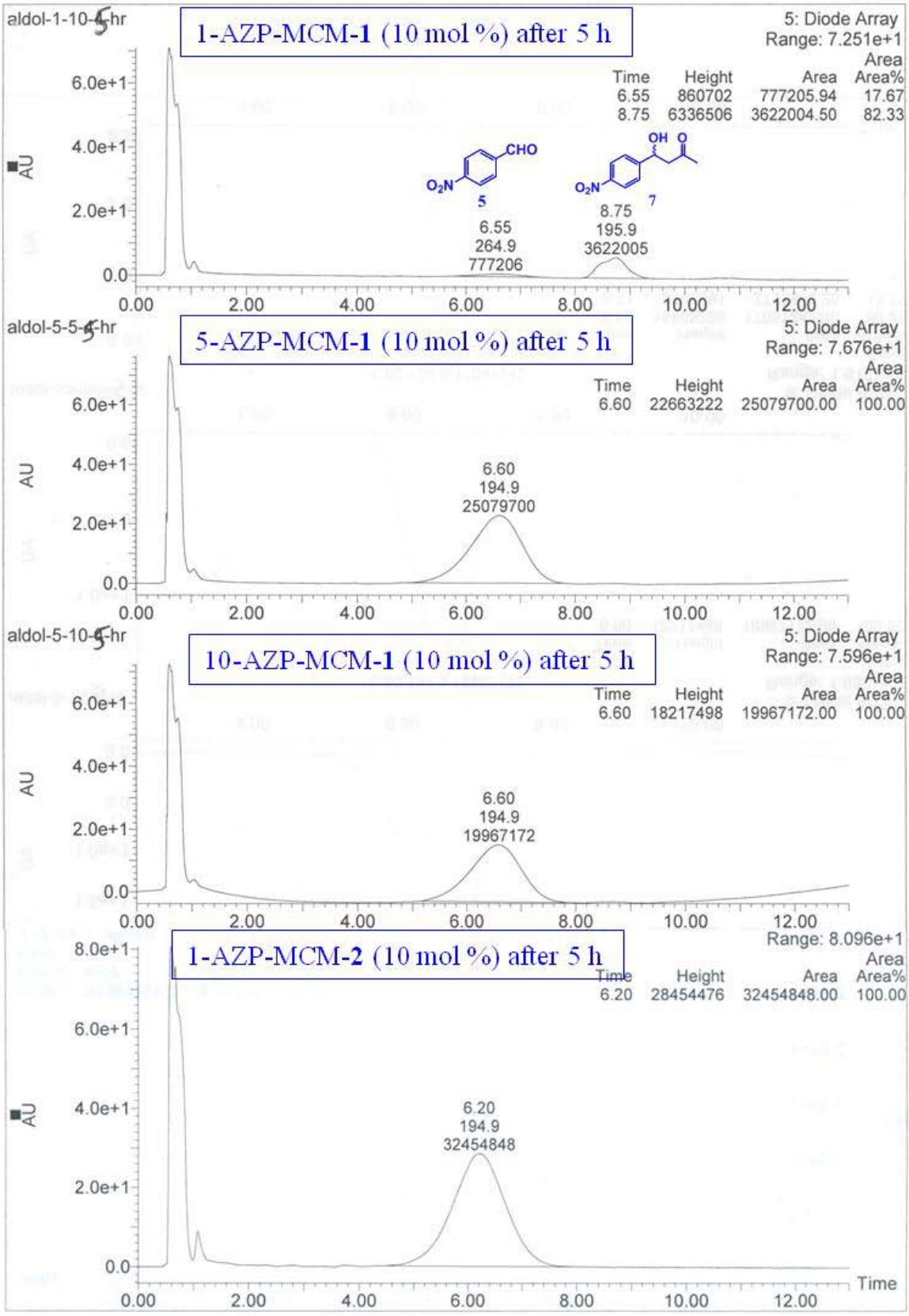
aldol-1-10-5-hr
1-AZP-MCM-1 (10 mol %) after 5 h
5: Diode Array
Range: 7.251e+1
Time Height Area Area%
6.55 860702 777205.94 17.67
8.75 6336506 3622004.50 82.33
CHO
O2N
5
OH O
O2N
7
6.55
264.9
777206
8.75
195.9
3622005
aldol-5-5-5-hr
5-AZP-MCM-1 (10 mol %) after 5 h
5: Diode Array
Range: 7.676e+1
Time Height Area Area%
6.60 22663222 25079700.00 100.00
6.60
194.9
25079700
aldol-5-10-5-hr
10-AZP-MCM-1 (10 mol %) after 5 h
5: Diode Array
Range: 7.596e+1
Time Height Area Area%
6.60 18217498 19967172.00 100.00
6.60
194.9
19967172
1-AZP-MCM-2 (10 mol %) after 5 h
Range: 8.096e+1
Time Height Area Area%
6.20 28454476 32454848.00 100.00
6.20
194.9
32454848
AU
Time
0.00
2.00
4.00
6.00
8.00
10.00
12.00

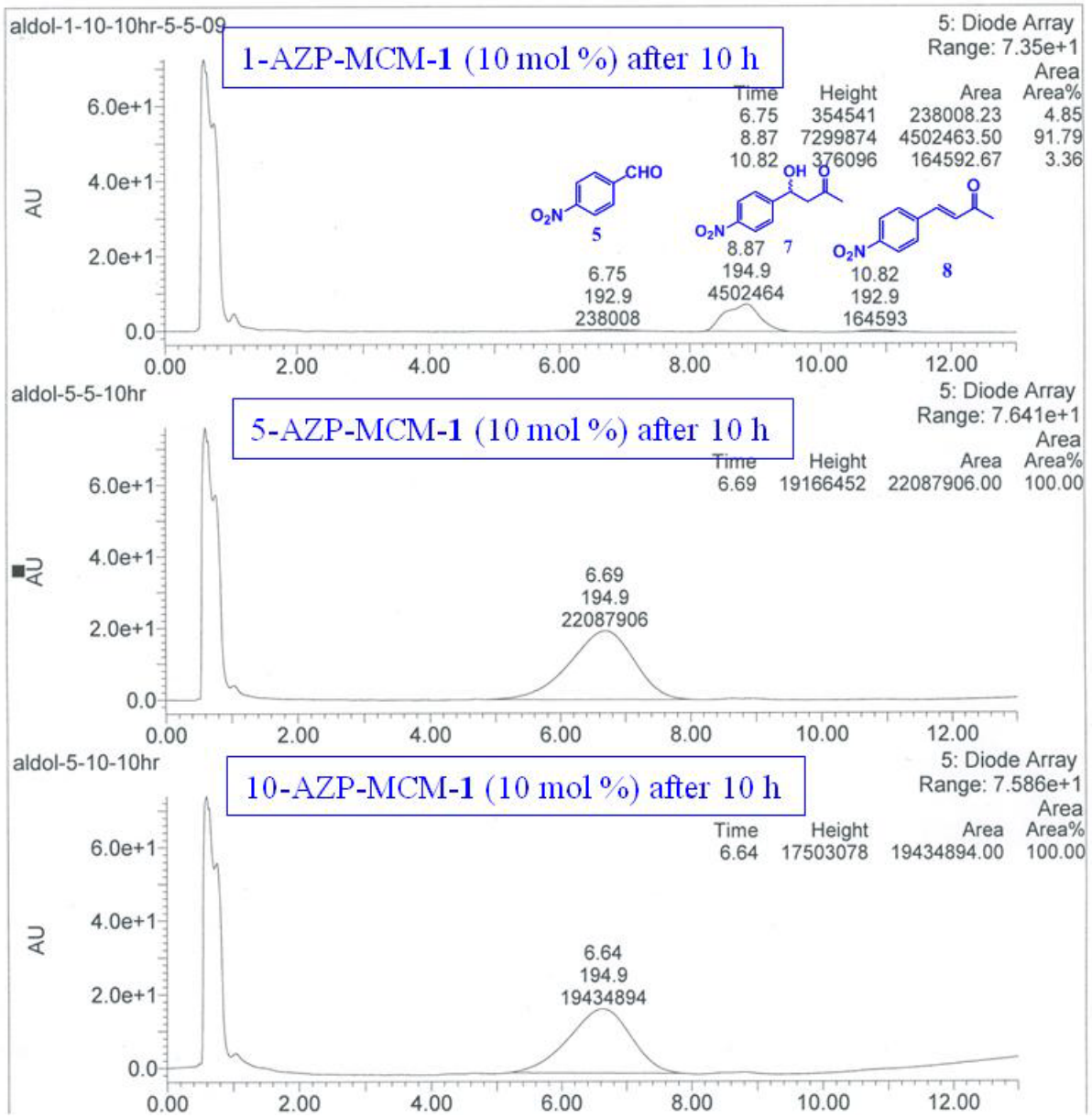
aldol-1-10-10hr-5-5-09
1-AZP-MCM-1 (10 mol %) after 10 h
5: Diode Array
Range: 7.35e+1
Time Height Area Area%
6.75 354541 238008.23 4.85
8.87 7299874 4502463.50 91.79
10.82 376096 164592.67 3.36
CHO
O2N
5
OH
O
O2N
7
O2N
O
8
6.75
192.9
238008
8.87
194.9
4502464
10.82
192.9
164593
AU
6.0e+1
4.0e+1
2.0e+1
0.0
0.00
2.00
4.00
6.00
8.00
10.00
12.00
aldol-5-5-10hr
5-AZP-MCM-1 (10 mol %) after 10 h
5: Diode Array
Range: 7.641e+1
Time Height Area Area%
6.69 19166452 22087906.00 100.00
6.69
194.9
22087906
aldol-5-10-10hr
10-AZP-MCM-1 (10 mol %) after 10 h
5: Diode Array
Range: 7.586e+1
Time Height Area Area%
6.64 17503078 19434894.00 100.00
6.64
194.9
19434894

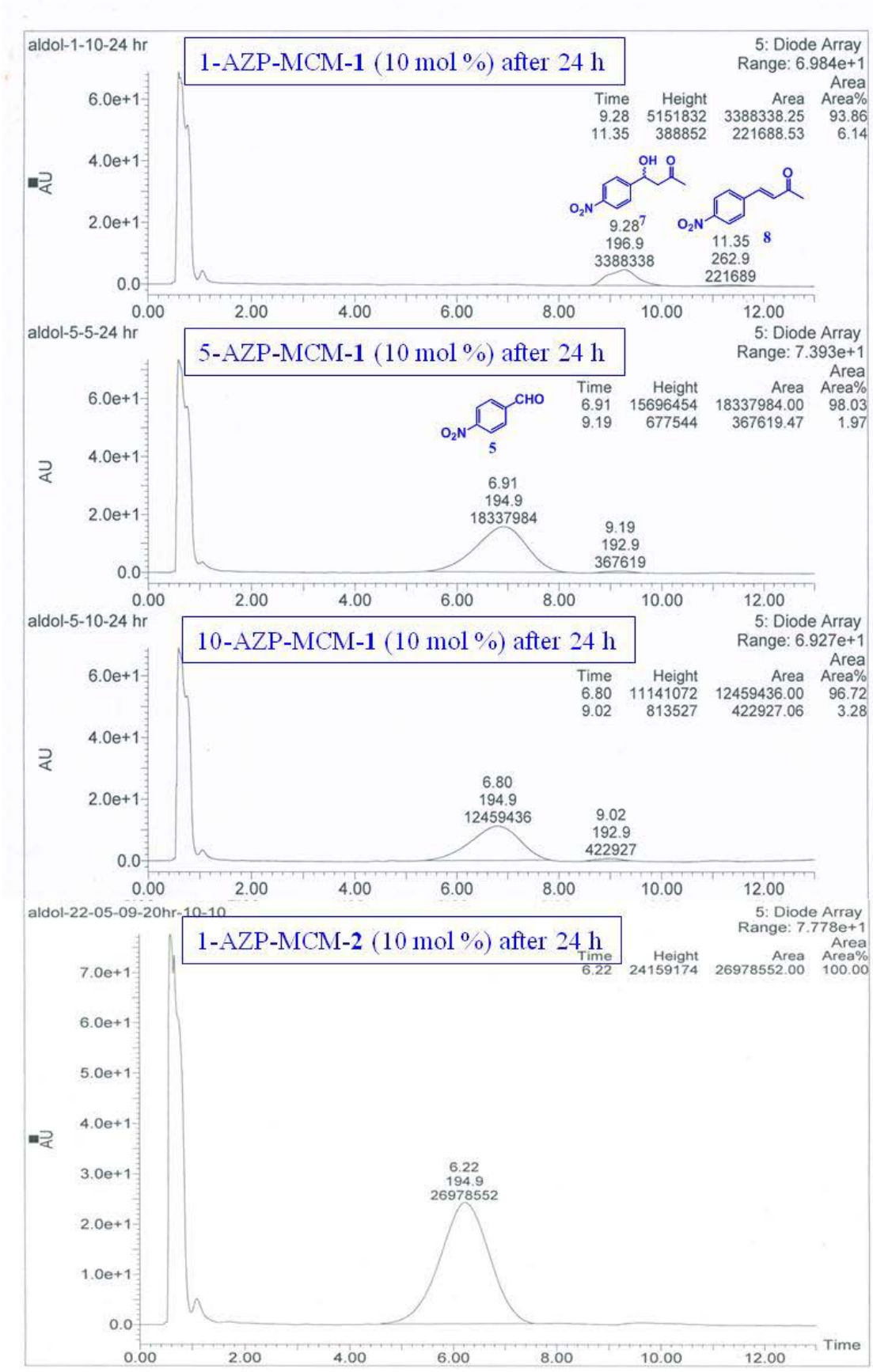
aldol-1-10-24 hr
1-AZP-MCM-1 (10 mol %) after 24 h
5: Diode Array
Range: 6.984e+1
Time Height Area Area%
9.28 5151832 3388338.25 93.86
11.35 388852 221688.53 6.14
9.28 7
196.9
3388338
11.35 8
262.9
221689
aldol-5-5-24 hr
5-AZP-MCM-1 (10 mol %) after 24 h
5: Diode Array
Range: 7.393e+1
Time Height Area Area%
6.91 15696454 18337984.00 98.03
9.19 677544 367619.47 1.97
5
6.91
194.9
18337984
9.19
192.9
367619
aldol-5-10-24 hr
10-AZP-MCM-1 (10 mol %) after 24 h
5: Diode Array
Range: 6.927e+1
Time Height Area Area%
6.80 11141072 12459436.00 96.72
9.02 813527 422927.06 3.28
6.80
194.9
12459436
9.02
192.9
422927
aldol-22-05-09-20hr-10-10
1-AZP-MCM-2 (10 mol %) after 24 h
5: Diode Array
Range: 7.778e+1
Time Height Area Area%
6.22 24159174 26978552.00 100.00
6.22
194.9
26978552
AU
Time

LC-MS Profile (D): Aldol reactions (3rd cycle)

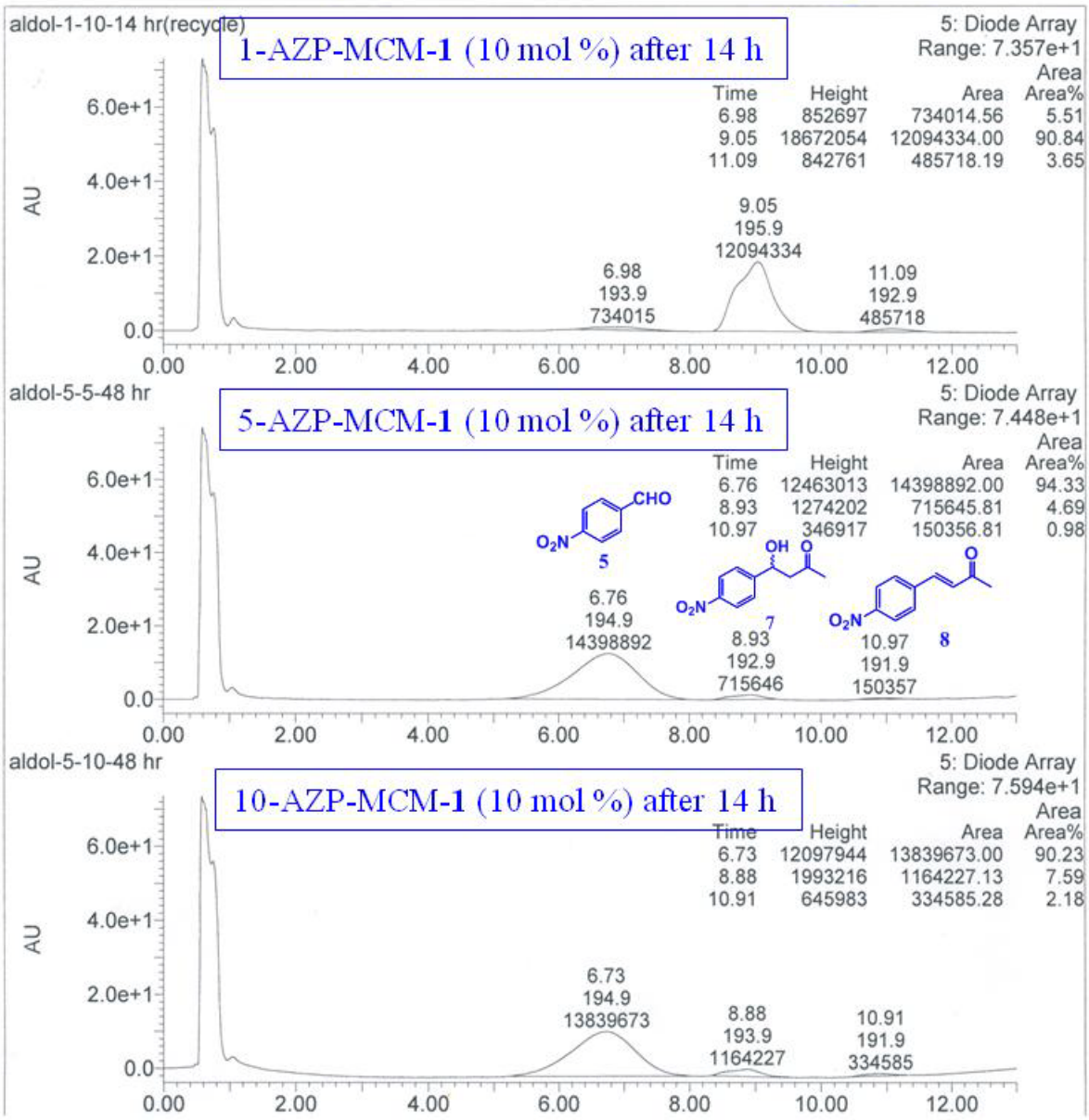

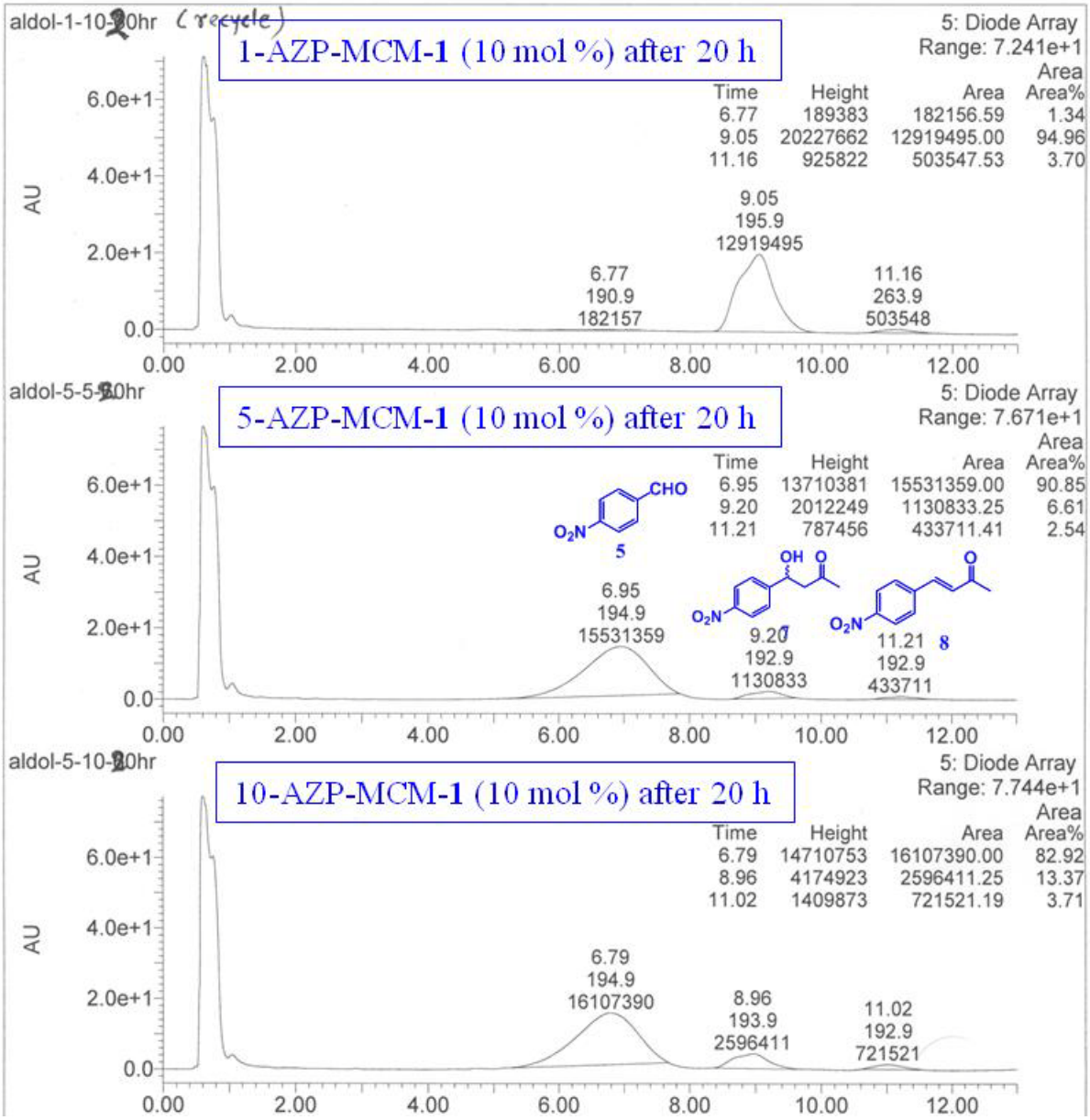
aldol-1-10-20hr (recycle)
1-AZP-MCM-1 (10 mol %) after 20 h
5: Diode Array
Range: 7.241e+1
Time Height Area Area%
6.77 189383 182156.59 1.34
9.05 20227662 12919495.00 94.96
11.16 925822 503547.53 3.70
9.05
195.9
12919495
6.77
190.9
182157
11.16
263.9
503548
AU
6.0e+1
4.0e+1
2.0e+1
0.0
0.00 2.00 4.00 6.00 8.00 10.00 12.00
aldol-5-5-20hr
5-AZP-MCM-1 (10 mol %) after 20 h
5: Diode Array
Range: 7.671e+1
Time Height Area Area%
6.95 13710381 15531359.00 90.85
9.20 2012249 1130833.25 6.61
11.21 787456 433711.41 2.54
CHO
O2N
5
OH O
O2N
7
O
O2N
8
6.95
194.9
15531359
9.20
192.9
1130833
11.21
192.9
433711
aldol-5-10-20hr
10-AZP-MCM-1 (10 mol %) after 20 h
5: Diode Array
Range: 7.744e+1
Time Height Area Area%
6.79 14710753 16107390.00 82.92
8.96 4174923 2596411.25 13.37
11.02 1409873 721521.19 3.71
6.79
194.9
16107390
8.96
193.9
2596411
11.02
192.9
721521

LC-MS Profile (E): Aldol reactions

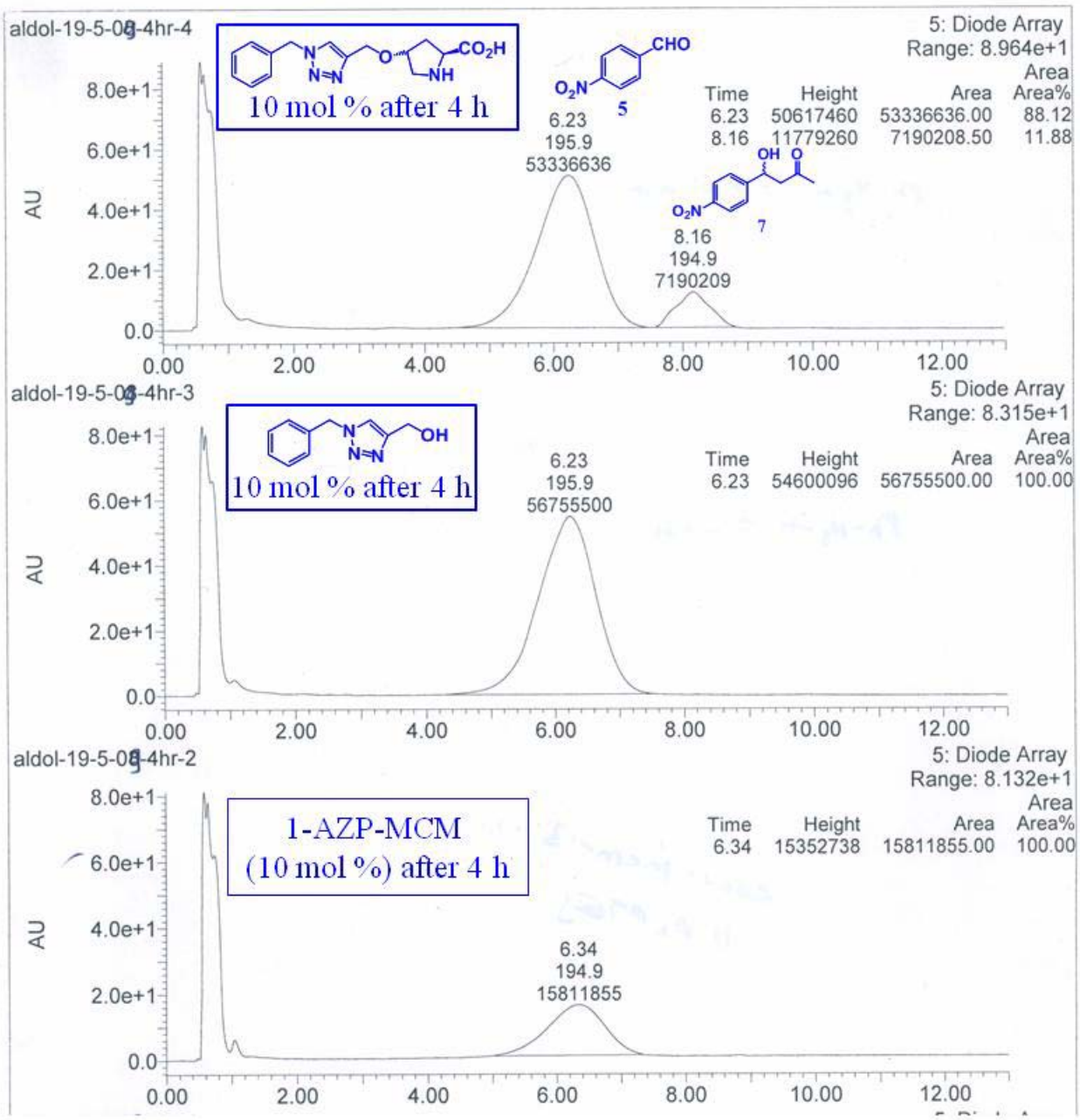

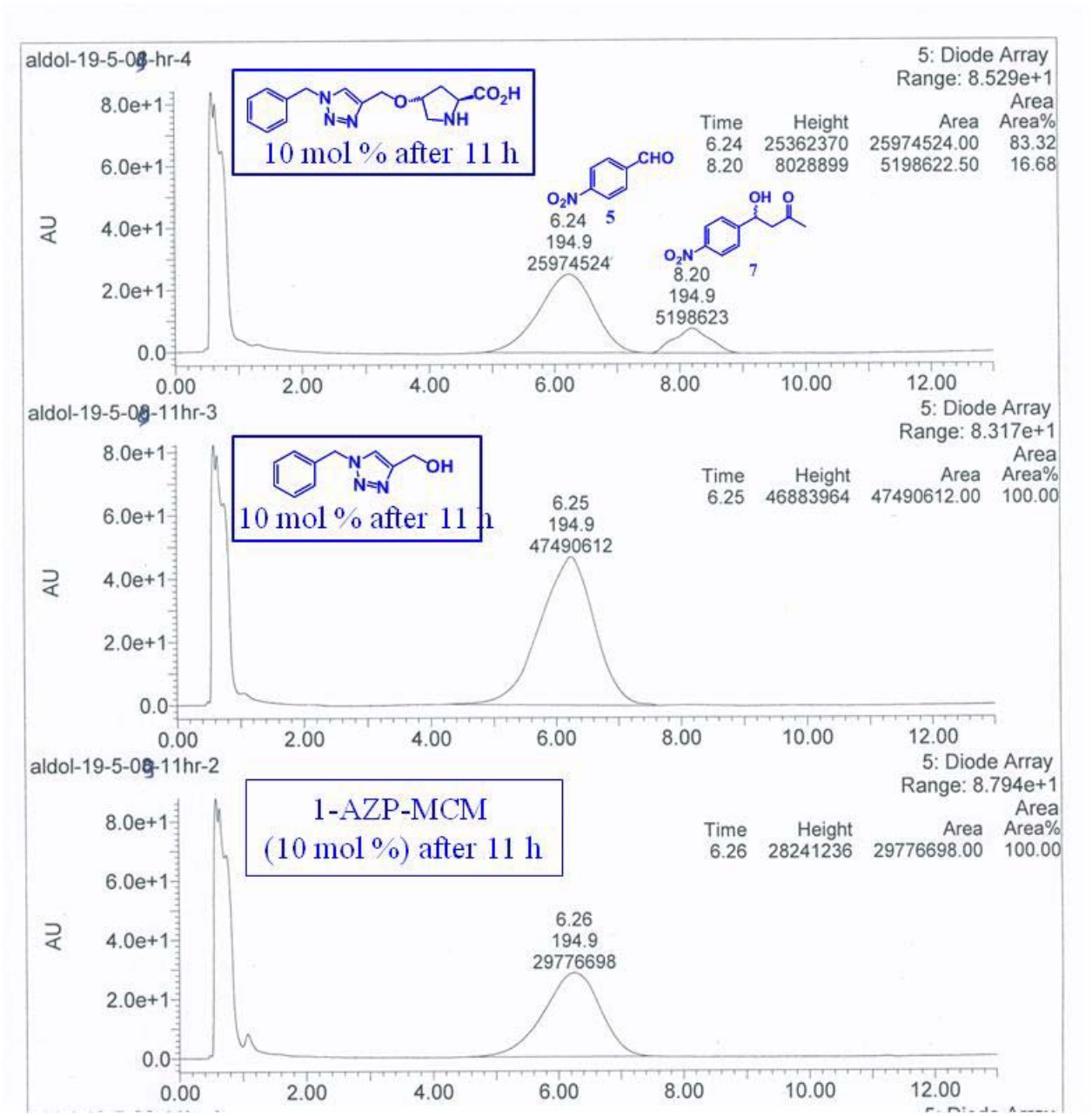
aldol-19-5-08-hr-4
5: Diode Array
Range: 8.529e+1
Area
Time Height Area Area%
6.24 25362370 25974524.00 83.32
8.20 8028899 5198622.50 16.68
10 mol % after 11 h
CHO
O_2N
6.24 5
194.9
25974524
OH O
O_2N
8.20 7
194.9
5198623
AU
8.0e+1
6.0e+1
4.0e+1
2.0e+1
0.0
0.00 2.00 4.00 6.00 8.00 10.00 12.00
aldol-19-5-08-11hr-3
5: Diode Array
Range: 8.317e+1
Area
Time Height Area Area%
6.25 46883964 47490612.00 100.00
OH
10 mol % after 11 h
6.25
194.9
47490612
aldol-19-5-08-11hr-2
5: Diode Array
Range: 8.794e+1
Area
Time Height Area Area%
6.26 28241236 29776698.00 100.00
1-AZP-MCM
(10 mol %) after 11 h
6.26
194.9
29776698

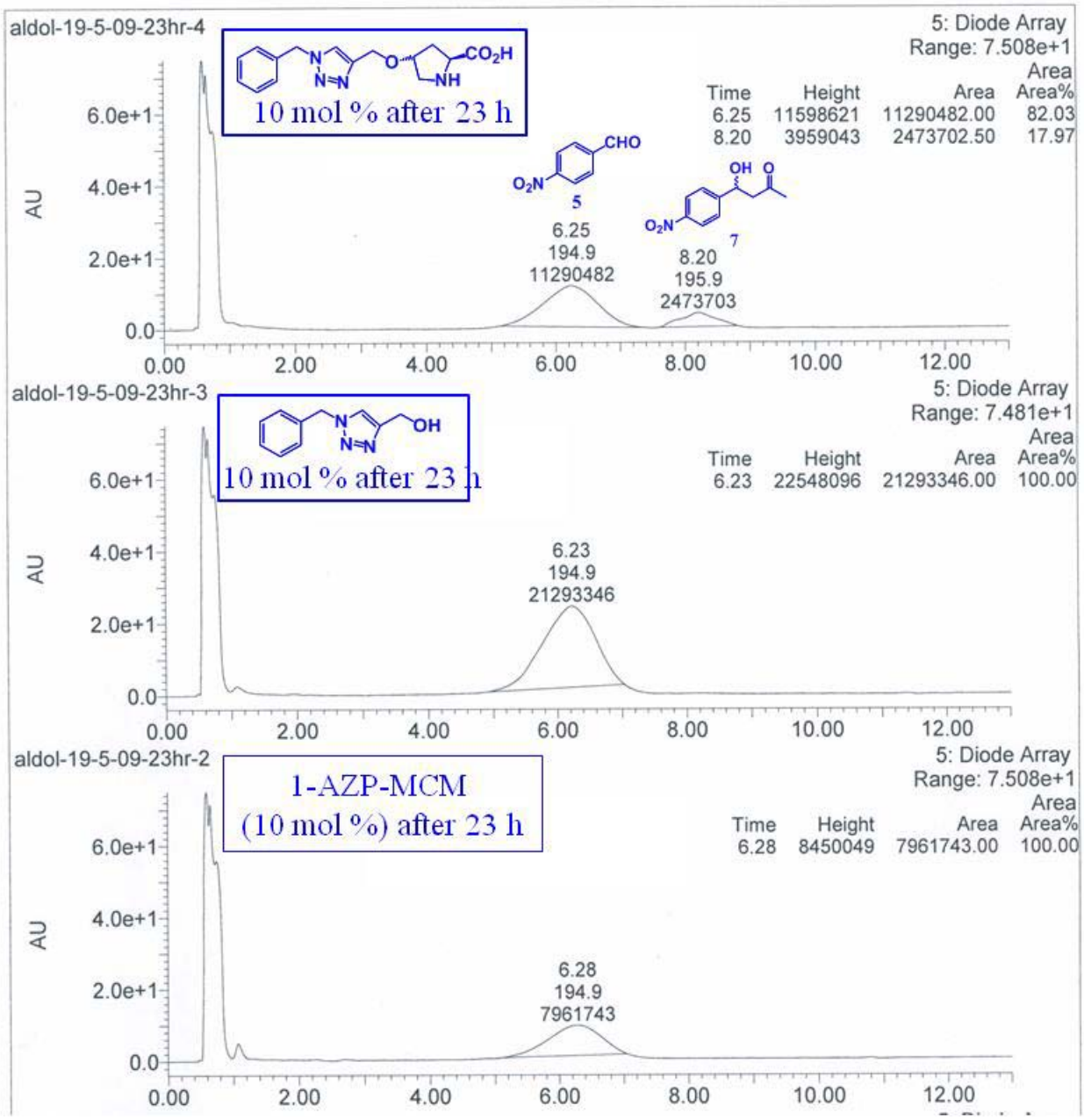
aldol-19-5-09-23hr-4
10 mol % after 23 h
5: Diode Array
Range: 7.508e+1
Time Height Area Area%
6.25 11598621 11290482.00 82.03
8.20 3959043 2473702.50 17.97
5
7
6.25
194.9
11290482
8.20
195.9
2473703
AU
aldol-19-5-09-23hr-3
10 mol % after 23 h
5: Diode Array
Range: 7.481e+1
Time Height Area Area%
6.23 22548096 21293346.00 100.00
6.23
194.9
21293346
aldol-19-5-09-23hr-2
1-AZP-MCM
(10 mol %) after 23 h
5: Diode Array
Range: 7.508e+1
Time Height Area Area%
6.28 8450049 7961743.00 100.00
6.28
194.9
7961743

Chiral HPLC: Aldol reactions

1-AZP-MCM-**1** (10 mol %) 1st Cycle

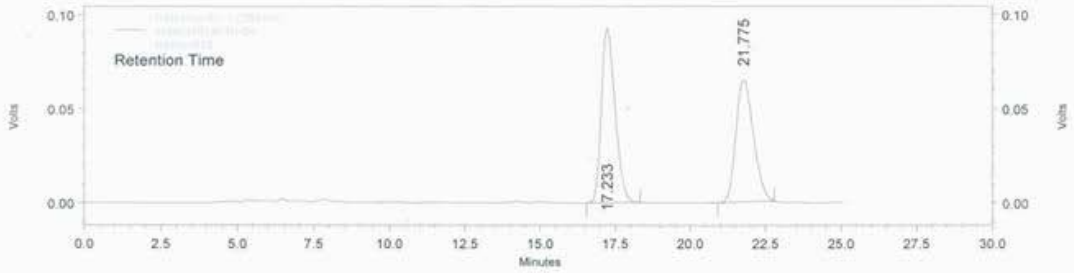

Detector A - 1
(254nm)

Pk #	Retention Time	Area	Area %	Height	Height Percent
1	17.233	2950286	53.000	92598	58.83
2	21.775	2616323	47.000	64807	41.17
Totals		5566609	100.000	157405	100.00

Grp Leader : Dr. S. Hotha
Column : ChiralPak AS-H
Mobile Phase : IPA: n-Hexane (30:70)
Wavelength : 254 nm
Flow Rate : 0.7mL/min(40Kgf)
Sample Con : 1.6mg/1ml Inj vol-10ul

1-AZP-MCM-**1** (10 mol %) 3rd Cycle

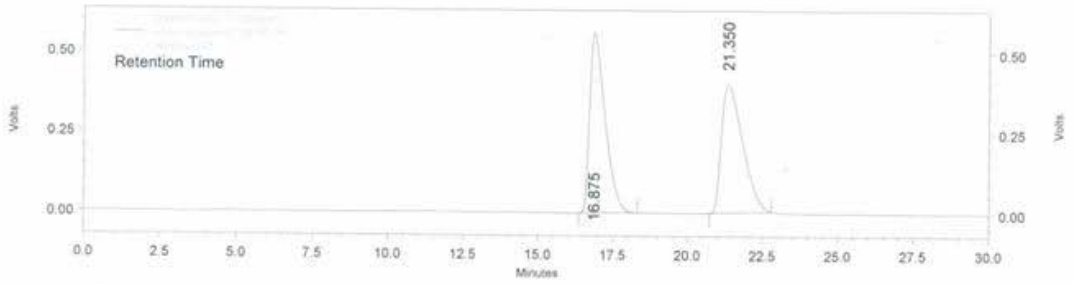

Detector A - 1
(254nm)

Pk #	Retention Time	Area	Area %	Height	Height Percent
1	16.875	20126194	50.533	561178	58.38
2	21.350	19701636	49.467	399995	41.62
Totals		39827830	100.000	961173	100.00

Grp Leader : Dr. S. Hotha
Column : ChiralPak AS-H
Mobile Phase : IPA: n-Hexane (30:70)
Wavelength : 254 nm
Flow Rate : 0.7mL/min(40Kgf)
Sample Con : 1.6mg/1ml Inj vol-10ul

5-AZP-MCM-**1** (10 mol %)

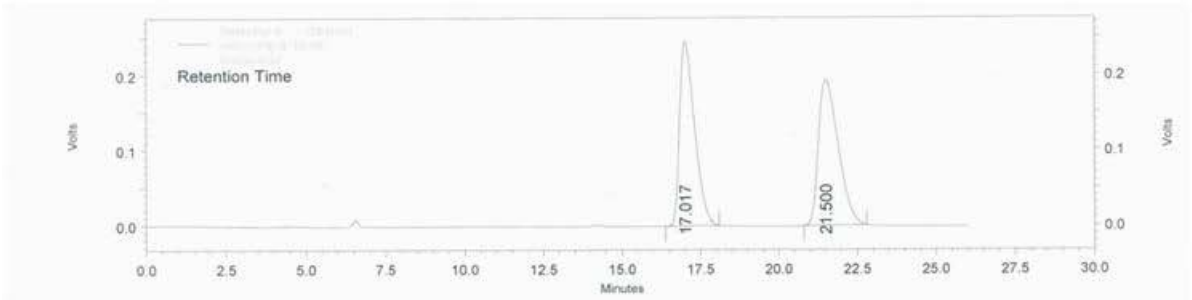

Detector A - 1 (254nm)

Pk #	Retention Time	Area	Area %	Height	Height Percent
1	17.017	8191569	49.052	246013	55.93
2	21.500	8508104	50.948	193834	44.07
Totals		16699673	100.000	439847	100.00

Grp Leader : Dr. S. Hotha
Column : ChiralPak AS-H
Mobile Phase : IPA: n-Hexane (30:70)
Wavelength : 254 nm
Flow Rate : 0.7mL/min(40Kgf)
Sample Con : 1.6mg/1ml Inj vol-10ul

10-AZP-MCM-**1** (10 mol %)

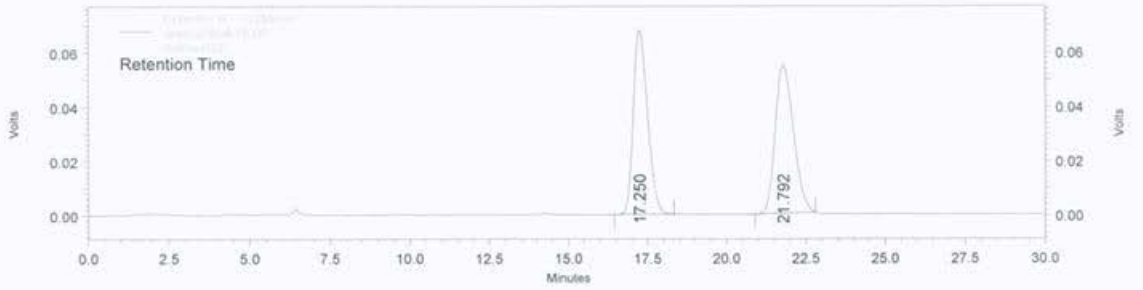

Detector A - 1 (254nm)

Pk #	Retention Time	Area	Area %	Height	Height Percent
1	17.250	2139665	49.419	68007	55.42
2	21.792	2189993	50.581	54711	44.58
Totals		4329658	100.000	122718	100.00

Grp Leader : Dr. S. Hotha
Column : ChiralPak AS-H
Mobile Phase : IPA: n-Hexane (30:70)
Wavelength : 254 nm
Flow Rate : 0.7mL/min(40Kgf)
Sample Con : 1.6mg/1ml Inj vol-10ul

Appendix III

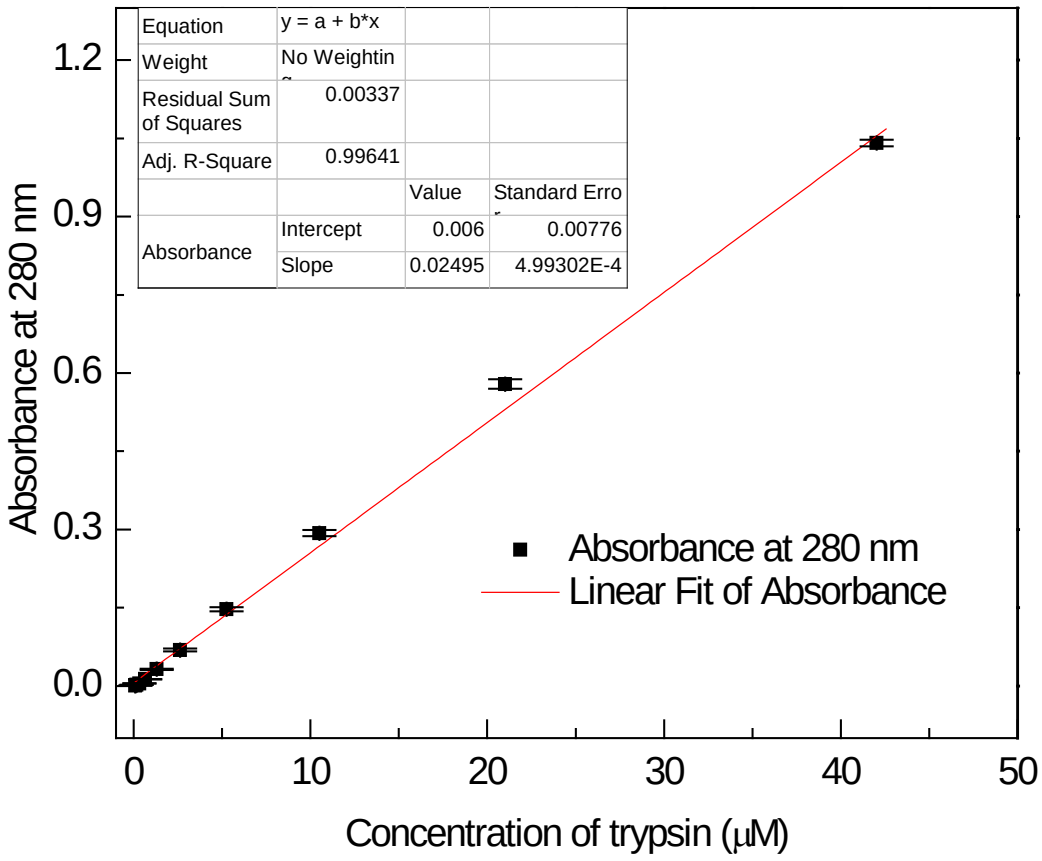

Figure C1: Calibration curve for tyrpsin in 100 mM, pH 7 phosphate buffer

Amount of trypsin immobilized on PHY-SBA-MSN was calculated according to the equation

y = a + b*x where a = 0.006 ± 0.0078, b = 0.02495 ± 0.000499 and R^2 = 0.9964 from Figure A1.

Total volume	Absorbance at 280 nm	Trypsin present in 2.1 mL (μmol)	% of trypsin immobilization	% of trypsin present in solution
2.1 mL	0.04339	3.15×10^{-3}	88	12

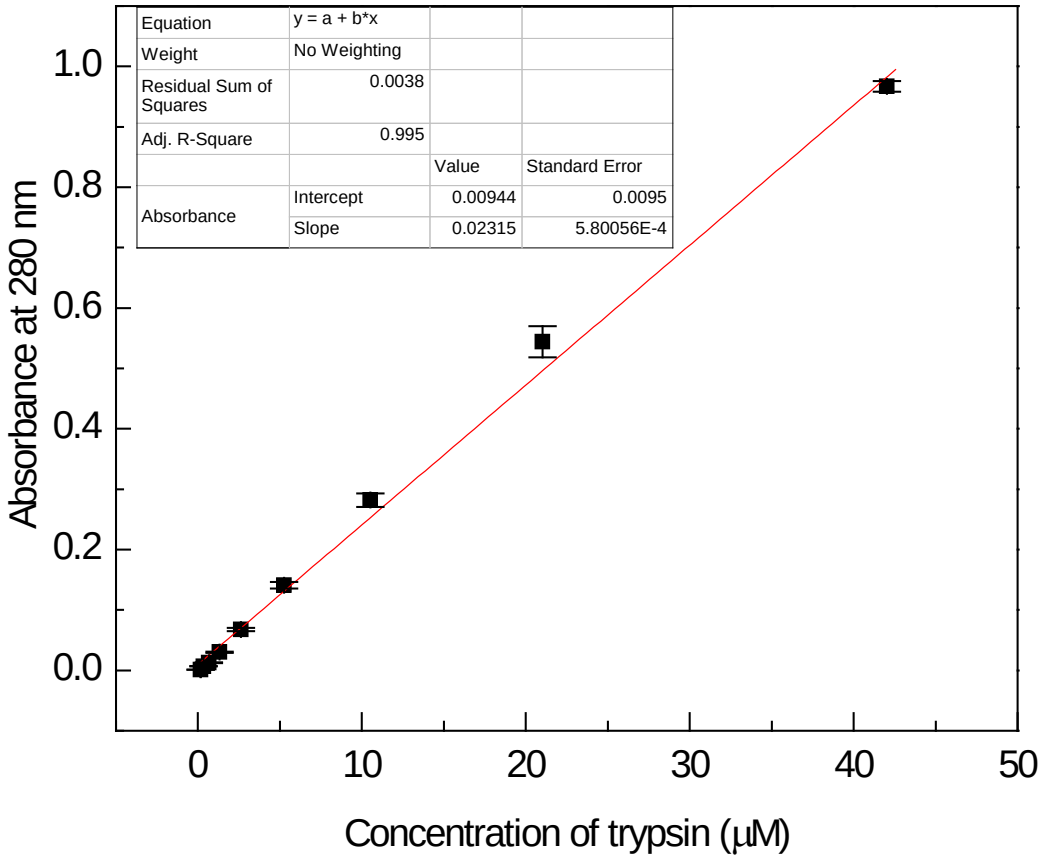

Figure C2: Calibration curve for tyrpsin in 10% PEG solution prepared in 50 mM, pH 8 tris buffer

Amount of trypsin leached from PEG-SBA-MSN during PEG solution treatment was calculated according to the equation y = a + b*x where a = 0.00944 ± 0.0095, b = 0.02315 ± 0.00058 and R^2 = 0.995 from Figure C2.

Total volume	Absorbance at 280 nm	Trypsin present in 1.5 mL (µmol)	% of trypsin leached (wrt 0.51 mg in AZP-SBA)
1.5 mL	0.305	0.0191	89

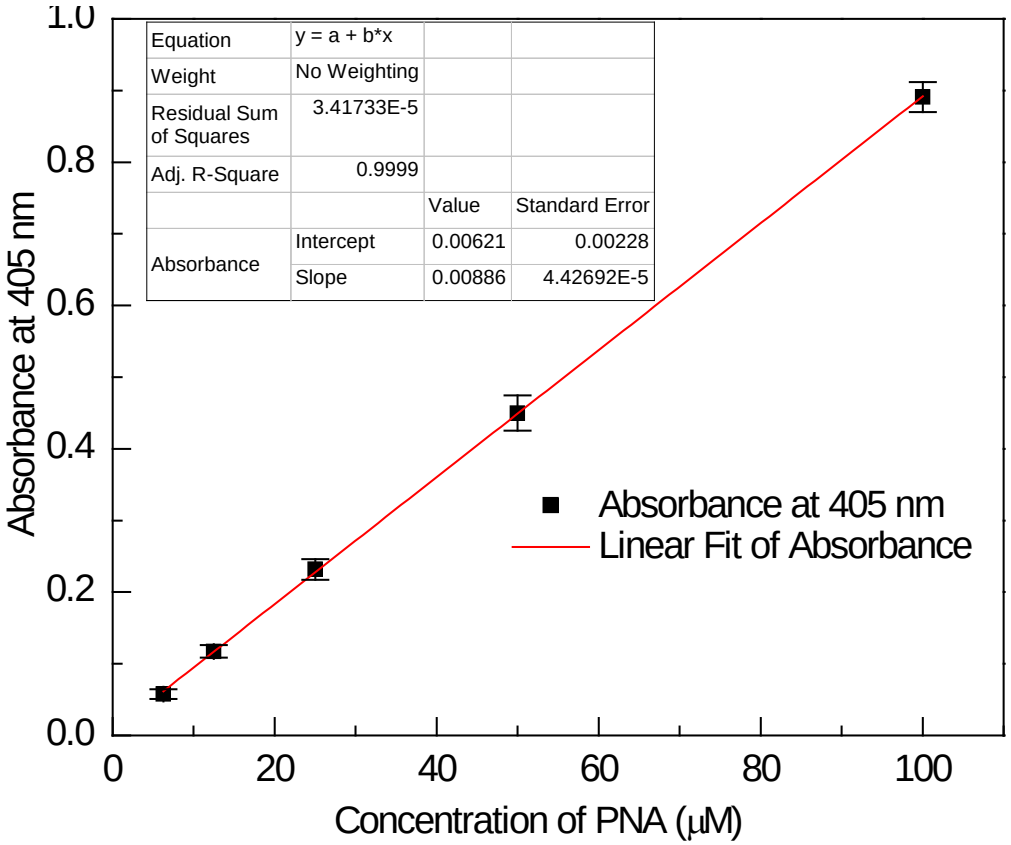

Figure C3: Calibration curve for p-nitroaniline (PNA) in 50 mM, pH 8 tris buffer.

List of Research Credentials, Awards and Conferences

List of Publications

1. "Clickable" SBA-15 mesoporous materials: synthesis, characterization and their reaction with alkynes.
   Bharmana Malvi, Bibhas R. Sarkar, Debasis Pati, Renny Mathew, T. G. Ajitkumar and Sayam Sen Gupta.
   J. Mater. Chem., 2009, **19**, 1409-1416.
2. One pot glucose detection by [Fe^{III}(biuret-amide)] immobilized on mesoporous silica nanoparticles: an efficient HRP mimic.
   Bharmana Malvi, Chakadola Panda, Basab B. Dhar, Sayam Sen Gupta.
   Chem. Commun., 2012, **48**, 5379-5381.
3. Encapsulation of enzyme in large mesoporous material with small mesoporous windows.
   Bharmana Malvi and Sayam Sen Gupta.
   Chem. Commun., 2012, **48**, 7853-7855.
4. Synthesis and characterization of poly-L-lysine grafted SBA-15 using NCA polymerization and click chemistry.
   Mrityunjoy Kar, **Bharmana Malvi**, Anindita Das, Suyana Panneri, Sayam Sen Gupta.
   J. Mater. Chem., 2011, **21**, 6690-6691
5. Functionalization of SBA-15 Mesoporous Materials using Thiol-Ene "Click" Michael Addition Reaction.
   Sushma Kumari, **Bharmana Malvi**, Anal Ganai, K. Vijayamohanan and Sayam Sen Gupta.
   J. Phy. Chem. C **115**, 17774-17781.

List of Manuscripts under preparation

1. Synthesis and Characterization of "Clickable" MCM-41 Mesoporous Materials for Site Isolation of Prolines
   Bharmana Malvi, Shivaji Thadke, Rajeesh P., Srinivas Hotha, Sayam Sen Gupta

Contributions to National/International Symposia/Conferences

1. *"Second International Conference on Multifunctional, Hybrid and Nanomaterials"* from 6-10 March 2011 held in Strasbourg, France.
   Poster presentation.
2. "*International Conference on Advanced Materials" (ICAM-2008)* held at Kottayam, Kerala during February 18-21, 2008
   Poster presentation
3. Symposium on *"Catalysis for Sustainable Energy and Chemicals"* organized by National Chemical Laboratory, Pune from 18-21 January 2009.
   Poster presentation
4. 11th CRSI National Symposium in Chemistry held at National Chemical Laboratory, Pune from 6-8 February 2009.
   Poster presentation

Awards

1. Won third prize in poster presentation at "*International Conference on Advanced Materials" (ICAM-2008)* held at Kottayam, Kerala during February 18-21, 2008.
2. Won best poster presentation award at *"National Science Day"* celebration event organized by National Chemical Laboratory, Pune from 27-28 February 2012